Master's thesis

NTNU
Norwegian University of Science and Technology
Faculty of Natural Sciences
Department of Chemical Engineering

Minadir Saracevic

NO to NO2 oxidation over Supported Cobalt Oxides Catalysts

Master's thesis in Chemical Engineering and Biotechnology
Supervisor: Magnus Rønning
July 2019

NTNU
Norwegian University of
Science and Technology

Minadir Saracevic

NO to NO2 oxidation over Supported Cobalt Oxides Catalysts

Master's thesis in Chemical Engineering and Biotechnology
Supervisor: Magnus Rønning
July 2019

Norwegian University of Science and Technology
Faculty of Natural Sciences
Department of Chemical Engineering

NTNU
Norwegian University of
Science and Technology

Abstract

The majority of the nitric acid demand goes to the production of ammonium nitrates, which is used in the production of fertilizers. Nitric acid production uses the Ostwald process, where one of the three reaction steps is the oxidation of NO to NO_2. This reaction step is a homogeneous gas phase reaction, which is not catalyzed. Introducing a suitable, cost-efficient catalyst could potentially increase the production rate, attain a more efficient heat recovery system, and reduce the capital costs of the process. Previous studies have shown that cobalt oxides (Co_3O_4) have promising activity for NO oxidation at three-digit ppm levels of NO. The aim of this thesis was to investigate supported cobalt oxide catalysts for NO oxidation in the Ostwald process at industrial conditions (10 % NO, 6 % O_2, 15 % H_2O, rest Ar, T = 350 °C) at atmospheric pressure.

There were 15 supported catalysts prepared by incipient wetness impregnation with weight percentages of 5, 10 and 20wt%Co on Al_2O_3, TiO_2, SiO_2, CeO_2, and ZrO_2. In addition, two Al_2O_3 promoted catalysts were made: 20wt%Co-0.5wt%Pt/Al_2O_3 and 20wt%Co-5wt%K/Al_2O_3. The characterization techniques used were as follows: Nitrogen adsorption/desorption, X-ray diffraction (XRD), and temperature programmed reduction (TPR). Activity measurements were performed in a packed bed reactor with GHSV = 43 400 h^{-1}. The NO conversion was measured in the temperature range 150-450 °C at atmospheric pressure both in dry and wet conditions. A sequence of dry-wet-dry conditions was run at 350 °C to stability test the catalysts.

In the absence of water, the catalytic activity increased as the cobalt loading was increased. In dry conditions at 350 °C, the rate of reaction was 5.5 µmol s^{-1} g_c^{-1} for 20Co/Al_2O_3, 5.1 µmol s^{-1} g_c^{-1} for 20Co/TiO_2, 10.9 µmol s^{-1} g_c^{-1} for 20Co/SiO_2, 12.7 µmol s^{-1} g_c^{-1} for 20Co/CeO_2 and 13.0 µmol s^{-1} g_c^{-1} for 20Co/ZrO_2. When steam was introduced into the feed, the NO conversion over the catalysts decreased due to the inhibition effect of water. The catalytic activity increased with cobalt loading in wet conditions for the catalysts supported on Al_2O_3, TiO_2, and SiO_2. In wet conditions at 350 °C, the rate of reaction was 1.6 µmol s^{-1} g_c^{-1} for 20Co/Al_2O_3, 1.2 µmol s^{-1} g_c^{-1} for 20Co/TiO_2 and 2.5 µmol s^{-1} g_c^{-1} for 20Co/SiO_2. The ceria supported catalysts were independent of the cobalt loading in wet conditions, where the 5 and 20wt%Co had a rate of reactions equal to 5.7 µmol s^{-1} g_c^{-1}. A similar trend was observed for the zirconia supported catalysts, where the 5 and 20wt%Co had a rate of reactions equal to 4.6 µmol s^{-1} g_c^{-1} and 5.0 µmol s^{-1} g_c^{-1}, respectively. The activity over the promoted catalysts showed to give no significant increase in NO oxidation. The results indicate that ceria supported catalyst with low cobalt loading has the potential to be a suitable, cost-efficient catalyst for NO oxidation in the Ostwald process at industrial conditions in nitric acid production.

Sammendrag

Flertallet av salpetersyrebehovet går til produksjon av ammoniumnitrater, som brukes i produksjon av gjødsel. Produksjon av salpetersyre benytter Ostwald prosessen, hvor en av de tre reaksjonstrinnene er oksidasjonen av NO til NO2. Dette reaksjonstrinnet er en homogen gassfasereaksjon, som ikke er katalysert. Innføring av en egnet, kostnadseffektiv katalysator kan mulig øke produksjonsraten, oppnå en mer effektiv varme gjenopprettingssystem og redusere kapitalkostnadene til prosessen. Tidligere studier har vist at koboltoksider (Co_3O_4) har lovende aktivitet for NO oksidasjon ved tresifret ppm nivå av NO. Målet med denne oppgaven var å undersøke koboltoksider på bærere for NO oksidasjon i Ostwald prosessen ved industrielle forhold (10 % NO, 6 % O_2, 15 % H_2O, resten Ar, T = 350 °C) ved atmosfærisk trykk.

Det var 15 katalysatorer som ble fremstilt ved "incipient wetness impregnation" med vektprosent 5, 10 og 20wt%Co på Al_2O_3, TiO_2, SiO_2, CeO_2 og ZrO_2 I tillegg ble det fremstilt to Al_2O_3 promoterte katalysatorer: 20wt%Co-0.5wt%Pt/Al_2O_3 og 20wt%Co-5wt%K/Al_2O_3. Karakteriseringsteknikkene som ble brukt var som følger: Nitrogen adsorpsjon/desorpsjon, røntgendiffraksjon (XRD) og temperaturprogrammert reduksjon (TPR). Aktivitetsmålinger ble utført i en reaktor med GHSV = 43 400 h^{-1}. NO omsetning ble målt i temperaturområdet 150-450 °C ved atmosfærisk trykk, både i tørre og våte forhold. En sekvens av tørr-våt-tørr forhold ble kjørt ved 350 °C for å stabilitets teste katalysatorene.

I fravær av vann økte den katalytiske aktivitet ettersom koboltmengden ble øket. Ved tørre forhold ved 350 °C var reaksjonsraten 5.5 µmol s^{-1} g_c^{-1} for 20Co/Al_2O_3, 5.1 µmol s^{-1} g_c^{-1} for 20Co/TiO_2, 10.9 µmol s^{-1} g_c^{-1} for 20Co/SiO_2, 12.7 µmol s^{-1} g_c^{-1} for 20Co/CeO_2 og 13.0 µmol s^{-1} g_c^{-1} for 20Co/ZrO_2. Når damp ble introdusert, reduserte NO omsetningen over katalysatorene på grunn av den inhiberende effekten av vann. Den katalytiske aktiviteten økte med koboltmengde i våte betingelser for katalysatorene med bærere på Al_2O_3, TiO_2 og SiO_2. Ved våte betingelser ved 350 °C var reaksjonsraten 1.6 µmol s^{-1} g_c^{-1} for 20Co/Al_2O_3, 1.2 µmol s^{-1} g_c^{-1} for 20Co/TiO_2 og 2.5 µmol s^{-1} g_c^{-1} for 20Co/SiO_2. Koboltoksider på ceria bærere var uavhengig av koboltmengden under våte betingelser, hvor 5 og 20wt%Co hadde en reaksjonsrate på 5.7 µmol s^{-1} g_c^{-1}. En lignende trend ble observert for koboldoksider på zirkonia bærere, hvor 5 og 20wt%Co hadde en reaksjonsrate på henholdsvis 4.6 µmol s^{-1} g_c^{-1} og 5.0 µmol s^{-1} g_c^{-1}. Aktiviteten over de promoterte katalysatorene gav ingen markant økning i NO oksidasjonen. Resultatene indikerer at koboltoksider på ceria bærer med lav koboltmengde har potensial til å være en egnet, kostnadseffektiv katalysator for NO oksidasjon i Ostwald prosessen ved industrielle forhold i salpetersyreproduksjon.

Preface

The master thesis marks the final chapter of the two-year master program Chemical Engineering and Biotechnology at the Norwegian University of Science and Technology (NTNU). This master thesis is a continuation of the specialization project written in autumn 2018 and was a part of the subject TKP 4580 Chemical Engineering, Specialization project. The thesis was written for the Catalysis group at the Department of Chemical Engineering at NTNU.

First, I would like to thank my supervisor Professor Magnus Rønning, for inspiring me to choose the research field of catalysis for this thesis. He guided me through the thesis and was always available to have valuable discussions. I appreciate the knowledge and experience I have obtained from this thesis.

Finally, I am very grateful to my co-supervisor Ata ul Rauf Salman for always being available to assist with the theoretical and experimental part of my thesis. I appreciate the time he has spent helping me throughout the entire work.

Contents

Abstract **i**

Sammendrag **iii**

Preface **v**

Table of Contents **ix**

List of Tables **xiii**

List of Figures **xix**

Abbreviations **xx**

Symbols **xxi**

1 Introduction **1**
1.1 Goal and approach 4

2 Literature Review **5**
2.1 Supported cobalt oxides catalysts 6

3 Theory **11**
3.1 Support materials 11
3.1.1 Aluminum oxide, Al_2O_3 12
3.1.2 Titanium dioxide, TiO_2 12
3.1.3 Cerium dioxide, CeO_2 13
3.1.4 Silicon dioxide, SiO_2 13
3.1.5 Zirconium dioxide, ZrO_2 14

3.2 Preparation of the catalyst . . . 14
3.2.1 Incipient wetness impregnation . . . 15
3.2.2 Calcination . . . 16
3.3 Characterization of the catalyst . . . 16
3.3.1 Nitrogen adsorption/desorption . . . 17
3.3.2 X-ray diffraction . . . 19
3.3.3 Temperature programmed reduction . . . 21

4 Experiment **23**
4.1 Catalyst preparation . . . 23
4.2 Characterization techniques . . . 24
4.2.1 X-ray diffraction . . . 25
4.2.2 Nitrogen adsorption/desorption . . . 25
4.2.3 Temperature programmed reduction . . . 25
4.3 Activity measurements . . . 26

5 Results and discussion **31**
5.1 Characterization . . . 31
5.1.1 Nitrogen adsorption/desorption . . . 31
5.1.2 X-ray diffraction . . . 32
5.1.3 Temperature programmed reduction . . . 38
5.2 NO oxidation activity measurements . . . 46
5.2.1 Blank run, supports and unsupported Co_3O_4 . . . 47
5.2.2 Supported cobalt oxides on alumina . . . 49
5.2.3 Promoted alumina supported cobalt oxides catalysts . . . 54
5.2.4 Supported cobalt oxides on titania . . . 59
5.2.5 Supported cobalt oxides on silica . . . 65
5.2.6 Supported cobalt oxides on ceria . . . 71
5.2.7 Supported cobalt oxides on zirconia . . . 76
5.3 Comparison between the supported cobalt oxide catalysts . . . 82

6 Conclusion **85**

7 Future work **87**

References **89**

Appendix A Catalyst synthesis calculations **97**

Appendix B Sample preparations **103**
B.1 Nitrogen adsorption/desorption sample weights 103
B.2 TPR sample weights 104
B.3 Activity measurements 105

Appendix C Nitrogen adsorption/desorption **107**

Appendix D X-ray diffraction **111**
D.1 Alumina supported catalysts 111
D.2 Titania supported catalysts 114
D.3 Silica supported catalysts 115
D.4 Ceria supported catalysts 117
D.5 Zirconia supported catalysts 118

Appendix E Activity measurements **121**
E.1 Alumina supported catalysts 121
E.2 Promoted catalysts 122
E.3 Titania supported catalysts 123
E.4 Silica supported catalysts 124
E.5 Ceria supported catalysts 125
E.6 Zirconia supported catalysts 126
E.7 Ceria support 127
E.8 Pure Cobalt Oxides 128

Appendix F Risk Assessment **129**

List of Tables

5.1 The BET surface area determined from BET adsorption, the average pore size from the BJH desorption and the cumulative pore volume from BJH desorption of the calcined supports. 32
5.2 A summation of the peak data used in the Scherrer equation and the crystallite size, particle size, and dispersion values of the Co_3O_4 on the various supported catalysts. K = 0.9, λ = 1.540 60 Å. 37
5.3 An overview of the results from the activity performance over the alumina supported catalysts in dry conditions. 51
5.4 An overview of the results from the activity performance over the alumina supported catalysts in wet conditions. 52
5.5 The average conversions from each period in the stability test of the alumina supported catalysts with the calculated regeneration and activity loss. 53
5.6 An overview of the results from the activity performance over the promoted catalysts and the $20Co/Al_2O_3$ in dry conditions. 56
5.7 An overview of the results from the activity performance over the promoted catalyst and the $20Co/Al_2O_3$ in wet conditions. 57
5.8 The average conversions from each period in the stability test of the promoted catalysts and $20Co/Al_2O_3$ with the calculated regeneration and activity loss. 59
5.9 An overview of the results from the activity performance over the TiO_2 supported catalysts in dry conditions. 61
5.10 An overview of the results from the activity performance over the TiO_2 supported catalysts in wet conditions. 63
5.11 The average conversions from each period in the stability test of the titania supported catalysts with the calculated regeneration and activity loss. . . . 64

5.12 An overview of the results from the activity performance over the SiO_2 supported catalysts in dry conditions. 67
5.13 An overview of the results from the activity performance over the SiO_2 supported catalysts in wet conditions. 69
5.14 The average conversions from each period in the stability test of the silica supported catalysts with the calculated regeneration and activity loss. . . . 70
5.15 An overview of the results from the activity performance over the CeO_2 supported catalysts in dry conditions. 72
5.16 An overview of the results from the activity performance over the CeO_2 supported catalysts in wet conditions. 74
5.17 The average conversions from each period in the stability test of the ceria supported catalysts with the calculated regeneration and activity loss. . . . 75
5.18 An overview of the results from the activity performance over the ZrO_2 supported catalysts in dry conditions. 77
5.19 An overview of the results from the activity performance over the ZrO_2 supported catalysts in wet conditions. 79
5.20 The average conversions from each period in the stability test of the zirconia supported catalysts with the calculated regeneration and activity loss. . 80
5.21 The particle size and dispersion of the cobalt oxides on the supported catalyst and the conversion, rate of reaction, and turnover frequency at 350 °C in both dry and wet conditions. 82

A.1 The chemical used in the synthesis and the calculated IWP of all the supports. 97
A.2 A summary of all the weights used to determine the synthesis calculations for the alumina supported catalysts 99
A.3 A summary of all the weights used to determine the synthesis calculations for the titania supported catalysts 99
A.4 A summary of all the weights used to determine the synthesis calculations for the silica supported catalysts 100
A.5 A summary of all the weights used to determine the synthesis calculations for the ceria supported catalysts 100
A.6 A summary of all the weights used to determine the synthesis calculations for the zirconia supported catalysts 101

B.1 The weights of the calcined supports before and after the vacuum procedure for nitrogen adsorption/desorption analysis 103
B.2 The weights of the various catalysts for TPR analysis 104
B.3 The weights of the catalysts and SiC for wet-TPR analysis 104
B.4 The amount of catalyst and SiC weight placed inside the reactor for the activity measurements of NO oxidation over supported cobalt oxide catalysts 105

B.5 The amount placed inside the reactor for the activity measurements of NO oxidation over SiC, CeO_2 and Co_3O_4 105

List of Figures

1.1 An illustration of the Ostwald process with the three main reactions steps. Adapted from [11]. 3

3.1 An illustration of the different steps involved by the incipient wetness impregnation of the supported catalysts [45]. 15
3.2 An illustration of multilayer adsorption as the relative pressure increases in a single cylindrical pore. Adapted from [46]. 17
3.3 The incoming X-rays are scattered by the atoms in lattice. Bragg's relation can be used to calculate the spacings between the lattice planes and used to identify the phases of the crystallites in the catalyst [33]. 20

4.1 An illustration of the several components involved in the installation of the reactor setup [12]. 27
4.2 A process flow diagram of the experimental setup used for NO oxidation activity measurements. The red lines indicate the heated gas lines. 1. Globe valve, 2. Reducing valve, 3. Gate valve, 4. Mass flow controller, 5. Check valve, 6. Three-way valve, 7. Water tank, 8. Liquid flow controller, 9. Evaporator, 10. Reactor, 11. Water condenser, 12. Fourier transform infrared analyzer. 28

5.1 The XRD patterns of the cobalt oxide supported on Al_2O_3 with metal loading of 5, 10, and 20wt%Co. 33
5.2 The XRD patterns of the promoted cobalt oxides supported on Al_2O_3 with metal loading of 20wt%Co and the 20Co/Al_2O_3 as a reference. 33
5.3 The XRD pattern of the cobalt oxides supported on TiO_2 with metal loading of 5, 10, and 20wt%Co. 34

5.4 The XRD pattern of the cobalt oxide supported on SiO_2 with metal loading of 5, 10, and 20wt%Co. 35
5.5 The XRD pattern of the cobalt oxides supported on CeO_2 with metal loading of 5, 10, and 20wt%Co. 35
5.6 The XRD pattern of the cobalt oxides supported on ZrO_2 with metal loading of 5, 10, and 20wt%Co. 36
5.7 The TPR-profiles of the cobalt oxides supported on Al_2O_3 with metal loading of 5, 10, and 20wt%Co. 39
5.8 The TPR-profiles of the promoted catalyst supported on Al_2O_3 with the $20Co/Al_2O_3$ as a reference. 40
5.9 The TPR-profiles of the cobalt oxides supported on TiO_2 with metal loading of 5, 10, and 20wt%Co. 41
5.10 The TPR-profiles of the cobalt oxides supported on SiO_2 with metal loading of 5, 10, and 20wt%Co. 42
5.11 The TPR-profiles of the cobalt oxides supported on CeO_2 with metal loading of 5, 10, and 20wt%Co. 43
5.12 The TPR-profiles of the cobalt oxides supported on ZrO_2 with metal loading of 5, 10, and 20wt%Co. 44
5.13 The wet-TPR profiles of the 20wt% supported on ZrO_2, CeO_2, Al_2O_3, and SiO_2. 45
5.14 The activity measurement of the gas phase conversion with 2.75 g SiC and the thermodynamic equilibrium. GHSV = 43 400 h^{-1}. Feed: 10 % NO, 6 % O_2, rest Ar. 47
5.15 The NO to NO_2 conversion over CeO_2 in dry and wet conditions. GHSV = 43 400 h^{-1}. Dry feed: 10 % NO, 6 % O_2, rest Ar. Wet feed: 10 % NO, 6 % O_2, 15 % H_2O, rest Ar. 48
5.16 The NO to NO_2 conversion over Co_3O_4 in dry and wet conditions. GHSV = 43 400 h^{-1}. Dry feed: 10 % NO, 6 % O_2, rest Ar. Wet feed: 10 % NO, 6 % O_2, 15 % H_2O, rest Ar. 49
5.17 The NO to NO_2 conversion over cobalt oxides supported on Al_2O_3 with metal loading of 5, 10, and 20wt%Co in dry conditions. GHSV = 43 400 h^{-1}. Feed: 10 % NO, 6 % O_2, rest Ar. 50
5.18 The NO to NO_2 conversion over cobalt oxides supported on Al_2O_3 with metal loading of 5, 10, and 20wt%Co in wet conditions. GHSV = 43 400 h^{-1}. Feed: 10 % NO, 6 % O_2, 15 % H_2O, rest Ar. 51
5.19 The stability tests at 350 °C for the cobalt oxides supported on Al_2O_3 with metal loading of 5, 10, and 20wt%Co. GHSV = 43 400 h^{-1}. Dry feed: 10 % NO, 6 % O_2, rest Ar. Wet feed: 10 % NO, 6 % O_2, 15 % H_2O, rest Ar. 53

5.20 The NO to NO_2 conversion over the promoted catalyst supported on Al_2O_3 with 20Co/Al_2O_3 as a reference in dry conditions. GHSV = 43 400 h^{-1}. Feed: 10 % NO, 6 % O_2, rest Ar. 55
5.21 The NO to NO_2 conversion over the promoted catalyst supported on Al_2O_3 with 20Co/Al_2O_3 as a reference in wet conditions. GHSV = 43 400 h^{-1}. Feed: 10 % NO, 6 % O_2, 15 % H_2O, rest Ar. 56
5.22 The stability tests at 350 °C for the promoted catalysts supported on Al_2O_3 with 20Co/Al_2O_3 as reference. GHSV = 43 400 h^{-1}. Dry feed: 10 % NO, 6 % O_2, rest Ar. Wet feed: 10 % NO, 6 % O_2, 15 % H_2O, rest Ar. 58
5.23 The NO to NO_2 conversion over cobalt oxides supported on TiO_2 with metal loading of 5, 10, and 20wt%Co in dry conditions. GHSV = 43 400 h^{-1}. Feed: 10 % NO, 6 % O_2, rest Ar. 60
5.24 The NO to NO_2 conversion over cobalt oxides supported on TiO_2 with metal loading of 5, 10, and 20wt%Co in wet conditions. GHSV = 43 400 h^{-1}. Feed: 10 % NO, 6 % O_2, 15 % H_2O, rest Ar. 62
5.25 The stability tests at 350 °C for the cobalt oxides supported on TiO_2 with metal loading of 5, 10, and 20wt%Co. GHSV = 43 400 h^{-1}. Dry feed: 10 % NO, 6 % O_2, rest Ar. Wet feed: 10 % NO, 6 % O_2, 15 % H_2O, rest Ar. 64
5.26 The NO to NO_2 conversion over cobalt oxides supported on SiO_2 with metal loading of 5, 10, and 20wt%Co in dry conditions. GHSV = 43 400 h^{-1}. Feed: 10 % NO, 6 % O_2, rest Ar. 66
5.27 The NO to NO_2 conversion over cobalt oxides supported on SiO_2 with metal loading of 5, 10, and 20wt%Co in wet conditions. GHSV = 43 400 h^{-1}. Feed: 10 % NO, 6 % O_2, 15 % H_2O, rest Ar. 68
5.28 The stability tests at 350 °C for the cobalt oxides supported on SiO_2 with metal loading of 5, 10, and 20wt%Co. GHSV = 43 400 h^{-1}. Dry feed: 10 % NO, 6 % O_2, rest Ar. Wet feed: 10 % NO, 6 % O_2, 15 % H_2O, rest Ar. 69
5.29 The NO to NO_2 conversion over cobalt oxides supported on CeO_2 with metal loading of 5, 10, and 20wt%Co in dry conditions. GHSV = 43 400 h^{-1}. Feed: 10 % NO, 6 % O_2, rest Ar. 71
5.30 The NO to NO_2 conversion over cobalt oxides supported on CeO_2 with metal loading of 5, 10, and 20wt%Co in wet conditions. GHSV = 43 400 h^{-1}. Feed: 10 % NO, 6 % O_2, 15 % H_2O, rest Ar. 73
5.31 The stability tests at 350 °C for the cobalt oxides supported on CeO_2 with metal loading of 5, 10, and 20wt%Co. GHSV = 43 400 h^{-1}. Dry feed: 10 % NO, 6 % O_2, rest Ar. Wet feed: 10 % NO, 6 % O_2, 15 % H_2O, rest Ar. 75
5.32 The NO to NO_2 conversion over cobalt oxides supported on ZrO_2 with metal loading of 5, 10, and 20wt%Co in dry conditions. GHSV = 43 400 h^{-1}. Feed: 10 % NO, 6 % O_2, rest Ar. 76

5.33 The NO to NO_2 conversion over cobalt oxides supported on ZrO_2 with metal loading of 5, 10, and 20wt%Co in wet conditions. GHSV = 43 400 h^{-1}. Feed: 10 % NO, 6 % O_2, 15 % H_2O, rest Ar. 78
5.34 The stability tests at 350 °C for the cobalt oxides supported on ZrO_2 with metal loading of 5, 10, and 20wt%Co. GHSV = 43 400 h^{-1}. Dry feed: 10 % NO, 6 % O_2, rest Ar. Wet feed: 10 % NO, 6 % O_2, 15 % H_2O, rest Ar. 80

C.1 The nitrogen adsorption/desorption isotherms and the pore size distribution of the calcined Al_2O_3 support 107
C.2 The nitrogen adsorption/desorption isotherms and the pore size distribution of the calcined TiO_2 support 108
C.3 The nitrogen adsorption/desorption isotherms and the pore size distribution of the calcined SiO_2 support 108
C.4 The nitrogen adsorption/desorption isotherms and the pore size distribution of the calcined CeO_2 support 109
C.5 The nitrogen adsorption/desorption isotherms and the pore size distribution of the calcined ZrO_2 support 109

D.1 The XRD pattern of the 5wt%Co/Al_2O_3 111
D.2 The XRD pattern of the 10wt%Co/Al_2O_3 112
D.3 The XRD pattern of the 20wt%Co/Al_2O_3 112
D.4 The 20wt%Co-0.5wt%Pt/Al_2O_3 113
D.5 The XRD pattern of the 20wt%Co-5wt%K/Al_2O_3 113
D.6 The XRD pattern of the 5wt%Co/TiO_2 114
D.7 The XRD pattern of the 10wt%Co/TiO_2 114
D.8 The XRD pattern of the 20wt%Co/TiO_2 115
D.9 The XRD pattern of the 5wt%Co/SiO_2 115
D.10 The XRD pattern of the 10wt%Co/SiO_2 116
D.11 The XRD pattern of the 20wt%Co/SiO_2 116
D.12 The XRD pattern of the 5wt%Co/CeO_2 117
D.13 The XRD pattern of the 10wt%Co/CeO_2 117
D.14 The XRD pattern of the 20wt%Co/CeO_2 118
D.15 The XRD pattern of the 5wt%Co/ZrO_2 118
D.16 The XRD pattern of the 10wt%Co/ZrO_2 119
D.17 The XRD pattern of the 20wt%Co/ZrO_2 119

E.1 The NO to NO_2 conversion over cobalt oxides supported on Al_2O_3 with metal loading of 5, 10, and 20wt%Co in dry conditions. GHSV = 43 400 h^{-1}. Feed: 10 % NO, 6 % O_2, rest Ar. 121

E.2 The NO to NO_2 conversion over cobalt oxides supported on Al_2O_3 with metal loading of 5, 10, and 20wt%Co in wet conditions. GHSV = 43 400 h^{-1}. Feed: 10 % NO, 6 % O_2, rest Ar. 122
E.3 The NO to NO_2 conversion over the promoted catalyst supported on Al_2O_3 with 20Co/Al_2O_3 as a reference in dry conditions. GHSV = 43 400 h^{-1}. Feed: 10 % NO, 6 % O_2, rest Ar. 122
E.4 The NO to NO_2 conversion over the promoted catalyst supported on Al_2O_3 with 20Co/Al_2O_3 as a reference in wet conditions. GHSV = 43 400 h^{-1}. Feed: 10 % NO, 6 % O_2, 15 % H_2O, rest Ar. 123
E.5 The NO to NO_2 conversion over cobalt oxides supported on TiO_2 with metal loading of 5, 10, and 20wt%Co in dry conditions. GHSV = 43 400 h^{-1}. Feed: 10 % NO, 6 % O_2, rest Ar. 123
E.6 The NO to NO_2 conversion over cobalt oxides supported on TiO_2 with metal loading of 5, 10, and 20wt%Co in wet conditions. GHSV = 43 400 h^{-1}. Feed: 10 % NO, 6 % O_2, rest Ar. 124
E.7 The NO to NO_2 conversion over cobalt oxides supported on SiO_2 with metal loading of 5, 10, and 20wt%Co in dry conditions. GHSV = 43 400 h^{-1}. Feed: 10 % NO, 6 % O_2, rest Ar. 124
E.8 The NO to NO_2 conversion over cobalt oxides supported on SiO_2 with metal loading of 5, 10, and 20wt%Co in wet conditions. GHSV = 43 400 h^{-1}. Feed: 10 % NO, 6 % O_2, rest Ar. 125
E.9 The NO to NO_2 conversion over cobalt oxides supported on CeO_2 with metal loading of 5, 10, and 20wt%Co in dry conditions. GHSV = 43 400 h^{-1}. Feed: 10 % NO, 6 % O_2, rest Ar. 125
E.10 The NO to NO_2 conversion over cobalt oxides supported on CeO_2 with metal loading of 5, 10, and 20wt%Co in wet conditions. GHSV = 43 400 h^{-1}. Feed: 10 % NO, 6 % O_2, rest Ar. 126
E.11 The NO to NO_2 conversion over cobalt oxides supported on ZrO_2 with metal loading of 5, 10, and 20wt%Co in dry conditions. GHSV = 43 400 h^{-1}. Feed: 10 % NO, 6 % O_2, rest Ar. 126
E.12 The NO to NO_2 conversion over cobalt oxides supported on ZrO_2 with metal loading of 5, 10, and 20wt%Co in wet conditions. GHSV = 43 400 h^{-1}. Feed: 10 % NO, 6 % O_2, rest Ar. 127
E.13 The NO to NO_2 conversion over CeO_2 in dry and wet conditions. GHSV = 43 400 h^{-1}. Dry feed: 10 % NO, 6 % O_2, rest Ar. Wet feed: 10 % NO, 6 % O_2, 15 % H_2O, rest Ar. 127
E.14 The NO to NO_2 conversion over Co_3O_4 in dry and wet conditions. GHSV = 43 400 h^{-1}. Dry feed: 10 % NO, 6 % O_2, rest Ar. Wet feed: 10 % NO, 6 % O_2, 15 % H_2O, rest Ar. 128

Abbreviations

Abbreviations	Description
BET	Brunauer-Emmett-Teller
BJH	Barret-Joyner-Halenda
CEM	Controlled evaporator mixer
FTS	Fischer-Tropsch synthesis
FT-IR	Fourier transform infrared
FWHM	Full width half maximum
GHSV	Gas hourly space velocity
IWI	Incipient wetness impregnation
IWP	Incipient wetness point
LFC	Liquid flow controller
MFC	Mass flow controller
MS	Mass spectrometer
OSC	Oxygen storage capacity
PBR	Packed bed reactor
SCR	Selective catalytic reduction
TCD	Thermal conductivity detector
TOF	Turnover frequency
TPR	Temperature programmed reduction
TWCs	Three-way catalysts
XRD	X-ray diffraction

Symbols

Symbol	Unit	Description
$\langle L \rangle$	nm	Crystallite size from the Scherrer equation
β	radian/°	Width of the peak at half height
$\Delta_r H_{298}$	$kmol\,mol^{-1}$	Reaction entalpy, 298 K
θ	°	Angle
λ	nm	Wavelength of the X-rays
σ	-	Surface tension of liquid nitrogen
A_p	cm^2	Pore area
C	-	Constant for BET equation
d	nm	Distance between the lattice planes
D	%	Dispersion
$d(Co^0)$	nm	Particle size of Co^0
$d(Co_3O_4)$	nm	Particle size of Co_3O_4
g_c	g	Mass of the catalyst
k	$kmol\,s^{-1}\,m^{-3}\,atm^{-3}$	Reaction rate coefficient
K	-	Shape factor
M_w	$g\,mol^{-1}$	Molar weight
n	-	Integer number in Bragg's relation
$n_{NO,in}$	mol	Moles of NO in the inlet feed
$n_{NO,out}$	mol	Moles of NO in the outlet feed
$n_{NO_2,out}$	mol	Moles of NO_2 in the outlet feed
$NO_{conversion}$	%	Conversion of NO in the reactor
P	atm	Pressure
P_0	atm	Saturation pressure
p_{NO}	atm	Partial pressure of NO
p_{NO_2}	atm	Partial pressure of NO_2
r	$mol\,s^{-1}\,g_c^{-1}$	Rate of reaction
r_k	cm	Radius of the inner capillary
r_{NO}	$kmol\,s^{-1}\,m^{-3}$	Gas phase rate of reaction for NO
r_{NO_2}	$\mu mol\,s^{-1}\,g_c^{-1}$	Catalytic rate of reaction for NO_2
r_p	cm	Pore radius
T	°C	Temperature
T_k	K	Absolute temperature
t	cm	Thickness of the adsorption layer
V	cm^3	Volume
V_a	cm^3	Volume of N_2 adsorbed

V_m	cm^3	Volume adsorbed at monolayer coverage
V_{ma}	$cm^3\,mol^{-1}$	Molar volume of liquid nitrogen
$\dot{V}_{NO_2,out}$	$cm^3\,min^{-1}$	Volumetric flow rate of NO2
V_p	cm^3	Pore volume
V_{PT}	cm^3	Total pore volume of the support material
w_t	*%*	Metal loading based on weight
x_m	-	Metal loading fraction

Chapter 1

Introduction

The modern society has faced several challenges these past decades, and one that has yet to be solved is the issue of global warming. Since the early 60s, the ppm levels of CO_2 has been drastically increased due largely to the growth of the population and industrialization. CO_2 emissions are considered to be one of the main greenhouse gases to influence climate change [1]. The world population as of 2019 has reached over 7.7 billion and by 2037 is it estimated to reach beyond 9 billion [2]. Economic growth gives rise to higher standards of living and more availability of energy for the consumer. The total energy consumption in 2017 was over 13700 Mtoe, where oil, gas, and coal represented 81 % of the energy sources consumed [3]. Rapid growth in the global population combined with the increase in energy consumption and climate change emphasizes the significance of the situation at hand.

Challenges as a consequence of the population growth and climate change will be the future availability of fresh water and food supply. One of the primary food supply sources comes from agriculture, where it is desirable to have a healthy and strong growth of the crops. To accomplish this, the soil needs to contain essential minerals and nutrients. Phosphorus (P), potassium (K) and nitrogen (N) are the three main nutrients required to sustain crop growth. Sources of potassium and phosphorus mainly come from salts and minerals, while the nitrogen source comes in the form of nitrates and ammonium [4] [5]. Fertilizers are added to replace the minerals and nutrients removed from the soil, which are vital to have a healthy and arable land for maintaining high yield and productivity of the crops [6]. Fertilizers will become more important as food production has to keep up with the increasing population and for the soil to remain fertile.

The nitrates are derived from nitric acid, where the catalytic combustion of ammonia with

oxygen under pressure oxidizes towards NO and NO_2, and after that, the NO_2 is absorbed into water to form the acid. This process is referred to as the Ostwald process, developed by Wilhelm Ostwald in 1901 and is a common commercial production process for nitric acid today [5][7]. The Haber-Bosch process, where ammonia is synthesized from nitrogen and hydrogen, was developed by Fritz Haber and further improved by Carl Bosch in the early 20th century. The Haber-Bosch process made the ammonia economically feasible to manufacture, which paved the way for the Ostwald process [7]. Nitric acid is used as an intermediate to produce ammonium nitrate (NH_4NO_3), which is primarily used to produce fertilizers [8]. In 2017, about 75 % of the global nitric acid demand went to the production of ammonium nitrates [9]. Further development and optimization of the Ostwald process will become more critical as the demand for fertilizers may be more crucial in the future. From an environmental perspective, a more effective production process may introduce a better heat recovery of the system, which indirectly could contribute to fewer emissions from energy sources.

The overall reaction of the Ostwald process is exothermic and is shown in Equation 1.1 [10].

$$NH_3 + 2\,O_2 \longrightarrow HNO_3 + H_2O \qquad \Delta_r H_{298} = -330\,\mathrm{kJ/mol} \tag{1.1}$$

The Ostwald process is described by three main reaction steps: the catalytic combustion of ammonia (NH_3), the oxidation of nitrogen monoxide (NO) and the absorption of nitrogen dioxide (NO_2) in water. These three chemical reaction steps are shown in Equation 1.2, Equation 1.3, and Equation 1.4, respectively [10].

$$4\,NH_3 + 5\,O_2 \longrightarrow 4\,NO + 6\,H_2O \qquad \Delta_r H_{298} = -907\,\mathrm{kJ/mol} \tag{1.2}$$

$$2\,NO + O_2 \longrightarrow 2\,NO_2 \qquad \Delta_r H_{298} = -113.8\,\mathrm{kJ/mol} \tag{1.3}$$

$$3\,NO_2 + H_2O \longrightarrow 2\,HNO_3 + NO \qquad \Delta_r H_{298} = -37\,\mathrm{kJ/mol} \tag{1.4}$$

In the first reaction step, catalytic combustion of NH_3 with O_2 oxidizes the ammonia into NO over a Pt-Rh catalyst gauze. The maximum conversion of the reaction step reaches up to 98 % and is highly exothermic and rapid. It is favored by having low pressure and high temperature [11]. The second reaction step a homogeneous gas phase reaction, where NO oxidizes to NO_2 and the produced gas is in equilibrium with its dimer dinitrogen tetroxide N_2O_4 [11]. The oxidation of NO to NO_2 is a third order reaction and is shown in Equation 1.5 [10][11].

$$r_{NO} = -k \cdot p_{NO}^2 \cdot p_{O_2} \tag{1.5}$$

where k is the reaction rate coefficient, p_{NO} is the partial pressure of NO and p_{O_2} is the partial pressure of O_2. The reaction given in Equation 1.5 is inverse dependent on the temperature, where decreasing the temperature causes the rate coefficient to increase [12].

By using Le Chatelier's principle, the third order reaction is favored by high pressure and is also thermodynamically and kinetically favored by low temperature [12]. In the last reaction step, nitric acid is formed by the absorption of NO_2 into the water and is favored by high pressure. Different reactions occur in the liquid phase and the gas phase, where the last reaction step is a simplification of what occurs but sufficient enough to describe the phenomena [10]. Figure 1.1 illustrates the Ostwald process with the three reaction steps:

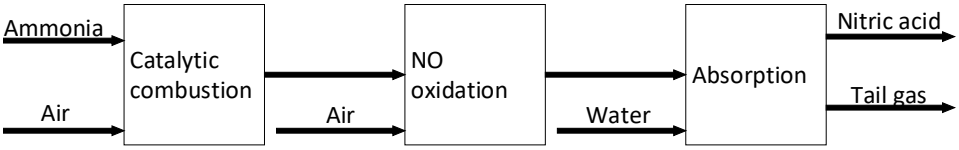

Figure 1.1: An illustration of the Ostwald process with the three main reactions steps. Adapted from [11].

The Ostwald process has reactions steps that benefit the pressure conditions differently, where the catalytic combustion of NH_3 is favored by low pressure, and the absorption of NO_2 is favored by high pressure. The production plant could be ran using a single pressure design, where the process operates at a high-pressure range (7-12 bar). The higher pressure reduces the equipment size, which could reduce the capital cost of the process plant. This design also results in a higher catalyst temperature, which enables more efficient energy recovery [10]. Another way to operate the Ostwald process is to optimize the different reaction steps by introducing a dual-pressure design. There would be two different pressures ranges, where the NH_3 combustion operates a lower pressure range (4-5 bar) and the absorption of NO_2 operates at a higher pressure range (10-15 bar) [10]. Operating at two different pressures gives overall higher conversion efficiency, but the downside is that it results in a more substantial investment cost. The design choice will depend on the production capacity, feasibility, and profitability of the nitric acid production plant [10].

The homogeneous gas phase reaction of NO to NO_2 is currently a non-catalyzed process. Introducing a reactor with a suitable catalyst could optimize the NO oxidation to maximize the amount of NO_2 going into the absorption column to form nitric acid. The overall conversion effectiveness would increase, and it could achieve a more efficient heat recovery system of the process [10]. Investigating new cost-efficient catalysts are necessary to find for the NO to NO_2 oxidation process. Noble metals are known for being active on supported catalysts for various applications and processes but are expensive and scarce. Less expensive materials such as supported cobalt oxide catalysts are potential alternatives to replace the more costly noble metals. Utilizing a reactor with a cost-efficient catalyst would decrease the size of the unit, reducing the investment cost, and potentially achieve

a more effective production process.

1.1 Goal and approach

In this work, the goal was to investigate cobalt oxides supported on gamma-aluminium oxide (γ-Al_2O_3), titanium dioxide (TiO_2), cerium dioxide (CeO_2), silicon dioxide (SiO_2) and zirconium dioxide (ZrO_2) for the NO oxidation to NO_2 in the Ostwald process at industrial conditions in nitric acid production. In total there were 17 catalysts, where two of them were promoted. There were three different supported cobalt oxides catalysts on each support material by varying the metal loading of cobalt at 5, 10, and 20wt%Co. Two catalysts were made which were promoted on 20wt%Co/γ-Al_2O_3, one promoted with 0.5wt%Pt and the other one promoted with 5wt%K. The non-promoted and promoted catalysts supported on Al_2O_3, which are five catalysts in total, were made and investigated in the specialization project in autumn 2018. Only characterization techniques were performed on these alumina catalysts during the specialization project. Hence, activity measurements were performed on these in this thesis, and the results were compared with the other supported cobalt oxide catalysts.

The characterization techniques used to understand the activity measurements were as follows: Nitrogen adsorption/desorption, X-ray diffraction (XRD), and temperature programmed reduction (TPR). The activity measurements of NO oxidation over the supported cobalt oxides catalysts were run at process conditions resembling the Ostwald process at industrial conditions (10 % NO, 6 % O_2, 15 % H_2O, rest Ar, T = 350 °C). The activity measurements were performed in a packed bed reactor and ran in dry conditions (10 % NO, 6 % O_2, rest Ar) and wet conditions (10 % NO, 6 % O_2, 15 % H_2O, rest Ar). The activity was measured at atmospheric pressure with the temperature ranging between 150-450 °C. Stability tests of the catalysts were performed at 350 °C by introducing a sequence of dry, wet, and then dry conditions with a measuring duration of 2 hours in each step.

Chapter 2

Literature Review

In recent decades, the focus on reducing greenhouse gas emissions into the atmosphere has been steadily increasing, where researchers are trying to find methods that could be applied to reduce both the local and global emissions. One way to approach the matter in hand is to look into existing processes in industry and automotive vehicles that release pollution into the atmosphere and see if it can be improved upon. Introducing new materials into existing technologies may result in more energy efficient solutions which could potentially reduce the gas emission output from the processes. Research regarding the usage of cobalt oxides in various applications has shown that the material may be used as catalysts, solid oxide fuel cells, electrode materials, and so on [13]. In several processes, the cobalt material works as an oxidation agent, where the transition metal oxide Co_3O_4 (Co^{3+}/Co^{2+}) exhibited a high ability to oxide compounds such as CO and NH3 [14][15][16]. The cobalt oxides may potentially be a suitable catalyst in other reactions involving oxidation reactions. In the Fischer-Tropsch synthesis (FTS), the cobalt material is used as a catalyst in the process. The cobalt may be supported on various support materials such as Al_2O_3, TiO_2, and ZrO_2. In the FTS, the cobalt is active in its metal state Co^0 in the supported cobalt catalyst [17][18].

As previously mentioned, cobalt has the potential to be utilized into different solutions, but one of the interesting properties regarding this material is its ability to oxidize NO to NO_2. The use of cobalt oxides for NO oxidation has been previously studied regarding NO in three digit ppm levels, where pollution of NOx from diesel engines is one of the areas where the cobalt material could potentially be implemented [19][20]. These studies showed that Co_3O_4 exhibited high catalytic activity towards NO oxidation. The high catalytic activity for NO oxidation at ppm levels of NO shows that Co_3O_4 could potentially be a used a catalyst for the NO to NO_2 oxidation step in the Ostwald process. It remains

to be seen how the cobalt oxides will perform when the concentration of NO is increased up to 10 % in the feed stream and how the characteristics of the catalyst such as crystallite size, dispersion, reducibility, and loading impact the NO to NO_2 oxidation.

The cobalt oxides can either be unsupported or supported catalysts, where in this work the latter is primarily considered. Different support materials may be used, but for the present work supports such as Al_2O_3, TiO_2, CeO_2, ZrO_2, and SiO_2 were impregnated to achieve supported cobalt oxides catalysts. These supports have shown potential candidates as support materials for the NO oxidation. Thus, literature regarding these types of catalysts in NO to NO_2 oxidation was further investigated.

2.1 Supported cobalt oxides catalysts

Kim et al. studied several different supported cobalt oxides catalysts for NO oxidation with supports such as SiO_2, ZrO_2, TiO_2, and CeO_2 [21]. The inlet reactants consisted of 500 ppm NO and 5 % O_2 in N_2 with a total flow rate of $200\,cm^3\,min^{-1}$. There were two types of 10wt%Co/CeO2 catalysts, which were prepared, one had a high surface area ($230\,m^2\,g^{-1}$) and the other with a low surface area ($66\,m^2\,g^{-1}$). The activity measurements of these two catalysts show that the low surface catalyst had significant lower catalytic activity for NO oxidation compared to the high surface one, which shows that it may be beneficial to utilize a high surface catalyst to increase the NO conversion. In terms of catalytic performance based upon which support was used, the following order shows decreasing catalytic activity for NO oxidation from their results: CeO_2(High surface) > SiO_2 > CeO_2(Low surface) > ZrO_2 > TiO_2 [21]. This order may give an indication towards which supported catalysts could potentially have higher catalytic performance when introduced to the process conditions in nitric acid production. The NO oxidation experiments performed by Kim et al. ran in the absence of water, where the activity may differ when exposed to water in Ostwald process conditions.

Weiss et al. studied the catalytic NO oxidation rate with Co_3O_4 supported on SiO_2 and rhodium (Rh) supported on Al_2O_3. They showed that the NO turnover rate increased with larger cluster sizes of cobalt oxides [22]. On larger oxide clusters, the vacancies needed for O_2 activation were more abundant compared to small clusters, where the larger cluster delocalized electrons better than the small ones. The metal and oxide clusters bound oxygen more strongly on small clusters, which gave fewer concentrations of vacant sites that bind O_2 in kinetically relevant steps and decreased the NO oxidation rates [22]. They also suggested that the high NO oxidation turnover rates on Co_3O_4 dependent on the ability of Co^{3+} to undergo one-electron reductions, where the cobalt oxides have reduction-oxidation cycles between Co^{3+} and Co^{2+} [22]. These results from Weiss et al. indicate which cat-

alyst characteristics may be important to investigate to understand further how it affects the NO to NO_2 oxidation. The reduction of the supported cobalt oxides may also depend on which support material is used, where finding a suitable support can be one of several factors which could increase the reducibility of the Co_3O_4. Also, using supported cobalt oxide catalyst with reduction promoters may potentially influence the NO oxidation rates and increase the NO conversion levels.

Noble metals such as Pt and Ru have shown to exhibit high NO conversions in the presence of three-digit ppm levels of NO in dry conditions [23][24]. Salman et al. investigated the effects of implementing a platinum catalyst supported on γ-Al_2O_3 under Ostwald process conditions [12]. The catalyst, 1wt% Pt/Al_2O_3, was tested with a feed composition consisting of 10 % NO, 6 % O_2, 15 % H_2O, and rest Ar to replicate the gas composition from the ammonia combustion step outlet. The inlet gas flow was at $200\,\mathrm{N\,cm^3\,min^{-1}}$, which corresponds a GHSV equal to $43\,400\,\mathrm{h^{-1}}$. The NO conversion level reached up to 30 % at approximately 420 °C. It was reported that the NO conversion curves with the presence and absence of water to be near identical, indicating that the catalyst was unaffected by the introduction of water into the inlet feed [12]. The water resistance of platinum could potentially be interesting to implement in the case of supported cobalt oxide catalyst, where platinum promotion could decrease the effects of water deactivation in wet conditions.

Noble metals are known to be beneficial promoters on supported catalysts, but it is desired to find alternative promoters that could contribute to the supported cobalt oxide catalysts. Wang et al. showed that promoting the cobalt oxides on TiO_2 support with potassium increased the NO conversion [25]. The support material, $K_2Ti_2O_5$, was synthesized by melting K_2CO_3 and TiO_2 together at 850 °C and crushing it into powder. After that, the support was soaked in $Co(NO_3)_2$ at a set time duration to achieve the desired metal loading of cobalt. The inlet feed gas composition into the reactor consisted of 700 ppm NO, 10 % O_2 and rest with He. The catalytic performance of the potassium promoted catalyst showed higher NO conversion than platinum supported both on Al_2O_3 and TiO_2. In addition, a potassium promoted catalyst was made by incipient wetness impregnation, but the NO conversion was significantly decreased as a result. These findings illustrate the possibility of utilizing potassium as a promoter in supported cobalt oxide catalysts, potentially reducing the necessity of noble metals. The authors also reported the effects on NO conversion by increasing the metal loading of cobalt metal on TiO_2. It was reported that NO conversion increased as the metal loading of cobalt increases until an insignificant increase in conversion levels above 20wt% Co as the support surface reached saturation of cobalt [25].

Yung et al. studied the NO to NO_2 oxidation on cobalt-based catalysts supported on ZrO_2 and TiO_2 [26]. Both sol-gel and incipient wetness impregnation (IWI) techniques were

used to prepare the catalysts at 10wt% Co loading. The calcination temperature in post-synthesis varied between 300, 400, 500, and 600 °C to investigate its effects on catalytic performance. The inlet gas flow rate was set to 45 $cm^3 min^{-1}$(STP) and consisted of 1000 ppm NO, 10 % O_2 and rest He. At 300 °C calcination temperature, the TiO_2 supported catalysts synthesized by both techniques achieved high NO conversions. As the calcination temperature increased, the catalysts made by sol-gel had a more significant decrease in NO conversion compared to the catalysts made by the IWI technique. This showed that the supported catalysts prepared by IWI achieved more thermally stable catalysts for NO oxidation. For the 10wt% Co/ZrO2 catalysts synthesized with IWI, it could be observed that the initial NO conversion at lower temperatures was increased as the calcination temperature decreased, which was the similar case with the TiO_2 supported catalysts. The calcination temperature impacted the NO conversion considerably at the temperature range before the conversions reached thermodynamic equilibrium. This indicates the importance of catalyst preparation has on the catalytic performance of the supported catalysts. These experimental results from Yung et al. showed that the choice of the synthesizing method and calcination temperature could be an important part of achieving a high NO conversion level [26].

Irfan et al. developed several different types of supported catalysts for NO to NO_2 oxidation, where these were investigated to find a suitable catalyst in the fast selective catalytic reduction (SCR) process [27]. The supported catalyst Co_3O_4/TiO_2, $CuOx/TiO_2$, $MnOx/TiO_2$, and Co_3O_4/SiO_2 were prepared by impregnation method and contained typically 20wt% of metal loading [27]. The total gas flow rate at the inlet was set to 1500 $cm^3 min^{-1}$ and consisted of 150 ppm NO, 10 % O_2, 8 % H_2O, and N_2 balance. The Co_3O_4 based catalysts outperformed both the copper and manganese oxide catalysts, where maximum NO conversion of $CuOx/TiO_2$ and $MnOx/TiO_2$ at 350 °C were approximately 34 and 32 %, respectively. For Co_3O_4/TiO_2 the NO conversion reached above 40 % at 350 °C, while for the Co_3O_4/SiO_2 catalyst it reached 69 % at a lower temperature of 300 °C. This showed that cobalt oxides supported on SiO_2 had higher catalytic activity than the cobalt oxides supported on TiO_2. The authors also performed activity measurements on the unsupported metal oxides to determine which metal oxide had higher activity towards NO oxidation. The activity measurements of the NO oxidation showed that unsupported Co_3O_4 exhibited the highest maximum conversion, followed by MnOx and CuOx. This showed that Co_3O_4 has a high NO to NO_2 oxidation potential at low concentrations of NO and had higher catalytic activity than MnOx and CuOx at given process conditions. These activity experiments were run with 8 % H_2O, where both the supported and unsupported cobalt oxides had higher catalytic activity than the other support metal oxides catalyst in the presence of water [27].

Yu et al. studied cobalt oxides supported on various metal-doped ceria catalysts for NO to

NO_2 oxidation [28]. The citric sol-gel method was utilized to prepare a series of CeO_2 supports doped with 20 mol% of M (M = Zr^{4+}, Sn^{4+}, and Ti^{4+}). These support materials were loaded with cobalt oxides by a one-step sol-gel method to achieve $Co_3O_4/Ce_{0.8}M_{0.2}O_2$. The inlet gas feed consisted of 390 ppm NO, 8 % O_2, N_2 balance, and the flow rate into the reactor was set to 100 $cm^3\,min^{-1}$. Regarding the NO activity of supported cobalt oxide catalysts, the one with non-doped ceria support, Co-CeO_2, had the highest maximum conversion. The activity of the other catalysts was decreasing and was in the following order: Co-Ce > Co-Ce-Zr > Co-Ce-Sn > Co-Ce-Ti. The H_2-TPR of the catalysts showed that the peak corresponding to the reduction of Co^{3+} to Co^{2+} at lower temperatures might increase the catalytic activity, which was in agreement with the activity results of the supported cobalt oxides catalysts [28]. If the NO oxidation is dependent on the initial reducibility of the Co_3O_4, it can be interestingly to see if this relationship can be observed on the NO oxidation over supported cobalt oxides catalyst in Ostwald process conditions.

Chapter 3

Theory

3.1 Support materials

In heterogeneous catalysis, the supported catalysts represent the largest group and are of major economic importance in refinery technology and the chemical industry [29]. Supported catalysts usually consist of at least two components, the active components, and a high surface area support material. The active components are applied to the surface of a porous support, which mostly is inert solids. The supports primary function is to increase the surface area of the active components, where the active phase is highly dispersed on a stable support surface [29]. In addition, the support stabilizes the active components to reduce sintering, i.e., reducing the growth of the particle size of the active metals [29][30].

Choosing a support will depend on how it impacts the catalytic activity, selectivity, regenerability, stability, and costs of the supported catalyst. Likewise, catalyst deactivation is an essential factor when investigating a suitable support material for the given process. For the support to remain a porous, high surface area material, the solid has to be stable towards the process temperature. Adequate thermal stability is necessary to minimize the degradation of the support and to avoid the transition into a less desired phase of the support. The mechanical strength may be of high importance if the catalyst is exposed to conditions that stress the material, where the physical structure may degrade due to either the process conditions or reactor configurations [29][30].

A vast range of different supports is used from metal oxides such as alumina, silica, and titania to activated carbon, ceramics, clays, and zeolites. The chemical and physical aspects of the supports and their effects give an indication on which may be suitable candidates to be used in the supported catalysts [29]. In this work, Al_2O_3, TiO_2, CeO_2, SiO_2, and ZrO_2

were used as supports, and their properties were further looked into.

3.1.1 Aluminum oxide, Al_2O_3

Alumina, Al_2O_3, is a good catalyst support because of the ability to disperse the support phase, high thermal stability, and moderate price. The ability to disperse the active components is due to the acid-basic character of the alumina surface. The material has stable OH groups at the surface, the high polarity of the surface acid-base pairs and Lewis acidity, which gives sites for cationic, anionic, and metallic species to attach into [31]. The formation of mixed metal-support compounds can occur during the catalyst preparation, where there is a high potential for mixed oxide formation during calcination. For cobalt supported on alumina, the metal-support interaction may be strong due to the formation of irreducible cobalt phases. Diffusion of Co^{2+} may occupy tetrahedral sites of the alumina support, which leads to the formation of Co^{2+} with O−Al ligands [32].

The alumina material may transition into various types of alumina polymorphs, such as γ, δ, θ, η, and α-Al_2O_3. These transitions occur during heat treatment, where the alumina is exposed at a specific elevated temperature for the given phase transition [31]. Among these various types of alumina phases, the γ-Al_2O_3 is the most commonly used in supported catalysts. The γ-Al_2O_3 has a high surface area (50-300 $m^2\,g^{-1}$) and mesopores size ranging between 5 and 15 nm with a pore volume of about 0.6 $cm^3\,g^{-1}$ [33]. The material has a high thermal and mechanical stability and with its properties making it suitable as a support material for various applications such as hydrotreating, reforming, methanol synthesis, dehydration, hydrogenation and so forth [33].

3.1.2 Titanium dioxide, TiO_2

Titania, TiO_2, is known to be used in several applications such as in solar cells and photocatalyst due to its electronic and optical properties and as semiconductor because of its wide band gap (3.2 eV) under ultraviolet light. Titania is also used as a support for metal oxides in heterogeneous catalysis since it is known to have favorable properties such as low pressure drop, thermal shock resistance, chemical durability, high structural strength, and low manufacturing cost [34].

The TiO_2 can exist in three crystallite forms such as anatase, rutile, and brookite, but the latter is rarely used and there is no interest for most applications. The structure of the anatase phase consists of zigzag chains of octahedral molecules linked to each other, but for the rutile phase, it consists of linear chains of opposite edge-shared octahedral structure [34]. The transitional phase from anatase to rutile occurs between 600-700 °C, where the transition often leads to extensive sintering and a loss of specific surface area by a factor up

to ten [29][34]. Among the crystallite forms, the anatase phase is most used as support for metal oxides due to its high surface area, strong interaction with the metal nanoparticles and acid-base property [34][35]. The specific surface area of TiO_2 is between 40-200 $m^2\,g^{-1}$, and the structure of the material is mesoporous [34][29].

3.1.3 Cerium dioxide, CeO_2

Ceria, CeO_2, is known for being used as a non-inert support or as a catalyst, especially it is of importance in the construction of the three-way catalysts (TWCs). The CeO_2 crystallizes as the fluorite structure, where eight equivalent neighbor oxygen anions are coordinated around each cerium cation at the corners of a cube and each anion coordinated by four cations to form a tetrahedron [36]. Mesoporous CeO_2 has been reported to have a specific surface area above $200\,m^2\,g^{-1}$ after being calcined at 300-400 °C [37]. Another reported a calcined CeO_2 support to have obtained a surface area of $100\,m^2\,g^{-1}$ with a total pore volume of $0.33\,cm^3\,g^{-1}$ and a mesopore size distribution between 8-15 nm [38].

The cerium material is known for its oxygen storage capacity (OSC), where it has the ability shuttle between Ce(III) and Ce(IV) states [36]. This fast and reversible Ce^{4+}/Ce^{3+} redox cycling enables CeO_2 to release and store lattice oxygen [39]. It was reported that cobalt supported on cerium oxides have shown to enhance the redox process of Ce^{4+}/Ce^{3+}, where the effects increased with metal loading of cobalt [40]. As most support act as inert materials, addition redox contribution from the cerium support could be beneficial in a redox reaction system.

3.1.4 Silicon dioxide, SiO_2

The silica, SiO_2, as a support have a unique advantage, where its properties such as pore size, particle size, and surface area are easily adjusted to comply for the requirements to the given application [33]. The surface area of silica could potentially be large, where the specific surface area of SiO_2 could reach up to $1000\,m^2\,g^{-1}$. However, the disadvantage of silica is the low thermal stability of the material. It is used as the catalyst support in processes which operate at low temperatures, about below 300 °C. Silica is used as a support in applications such as polymerization, hydration, and oxidation [33].

Silica used as a support for catalysts is commonly the amorphous form of SiO_2, where the material may be produced by the sol-gel process, precipitation or flame hydrolysis [41]. The surface is covered by OH groups and is relatively neutral in acid-base chemistry. The Brønsteds sites at the surface are weakly acidic, and silica is known to be an inert support material [41][42]. The formation of volatile hydroxides may occur in the presence of steam at elevated temperatures, limiting the hydrothermal stability of the SiO_2 as a

support [33][41].

3.1.5 Zirconium dioxide, ZrO_2

Zirconia, ZrO_2, as a catalyst support has several benefits such as high thermal stability and have both acid and base properties. Although the acidic and basic properties are found at the surface, their strength is weak, but these acidic and basic sites work both independently and cooperatively at the surface of the oxides [41][43]. This characterizes the ZrO_2 as an acid-base bifunctional oxide. Another advantage of zirconia as a support is that it is stable under oxidizing and reducing atmospheres, which is beneficial in various applications [43].

For zirconia, a total of three crystalline modifications are known. The monoclinic modification is stable at room temperature and up to 1200 °C. The tetragonal modification is preferred above 1200 °C, whereas the cubic modification is stable over 1900 °C [43][41]. The zirconia is referred to as an inert support material due to the monoclinic phase being reported as inactive [41]. Furthermore, a metastable tetragonal form of zirconia is possible and is stable up to 650 °C. Impurities and crystallite size effects have been proposed to explain the possibility of having the metastable modification at low temperatures. The downside of using zirconia as a support is the low surface area, where the surface area is between 40-100 $m^2\,g^{-1}$ when calcined at 600 °C [43].

3.2 Preparation of the catalyst

In the preparation of supported catalysts, the preparation methods are primarily divided into dry and wet methods. The coprecipitation method is utilized when the materials used are cheap, and the aim is to yield a porous material with a high surface area and obtain optimum catalytic activity per unit volume. If the catalyst preparation involves expensive precursors, such as noble metals, and is it desired to deposit the active phase as nanometer-sized particles on the support material, then either impregnation or precipitation from solution are the preferred methods [33].

The incipient wetness impregnation was used to prepare the various support cobalt catalysts. The preparation method is a well established and relatively simple method, where it can be scaled up and produced for industrial applications. Cobalt and platinum are expensive metals, and it is desired to have it well dispersed at the support surface with minimal loss of the active metals. By utilizing incipient wetness impregnation, the active phase of the metals are at the surface of the support, and by varying the precursor concentration, the desired metal loading can be controlled.

3.2.1 Incipient wetness impregnation

Impregnation involves bringing the precursor solution into the pore space of the support. Before the impregnation, the support has been either dried or calcined to remove any volatile impurities or residual moisture to reduce the risk of pore blockage after the synthesis of the supported catalyst. A solution containing the selected precursor with volume, V, is added into support with a pore volume, V_{PT}. The amount of precursor solution is equal to the volume of pores in the support, $V=V_{PT}$, such that there is no excess solution remaining outside the pore space. Hence, this method is referred to as the ”dry” or ”incipient wetness” impregnation [41].

After the impregnation, the solvent from the pores is evaporated by drying the catalyst. This is accomplished by heating it above the boiling point of the solvent, either under a gas flow or under static conditions. As the solvent evaporates from the pores, the precursor concentration increases and leads to saturation and crystallization of the precursor [44]. An illustration of the different steps involved in the incipient wetness impregnation can be seen in Figure 3.1 [45]:

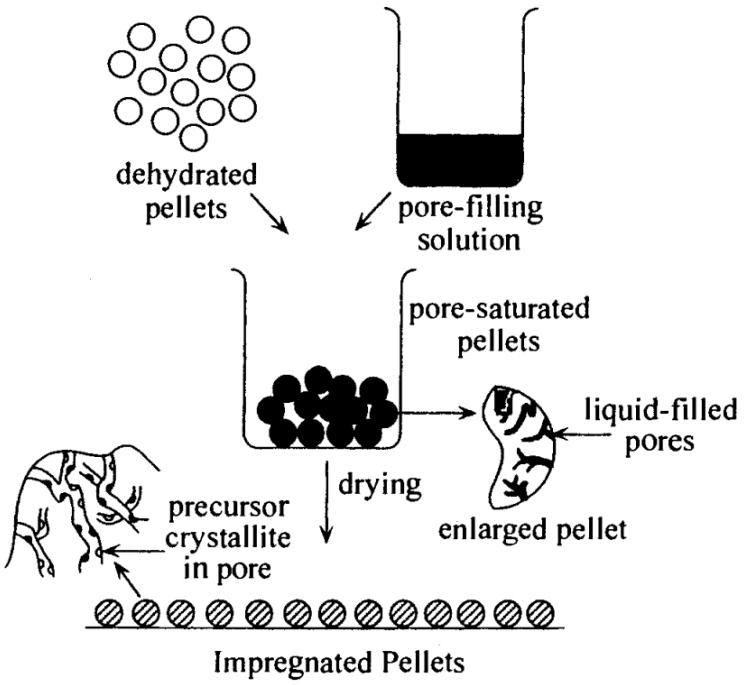

Figure 3.1: An illustration of the different steps involved by the incipient wetness impregnation of the supported catalysts [45].

During the impregnation, the solid-liquid interface replaces the solid-gas interface, which generally causes a decrease in the free enthalpy of the system, and heat is being released. Usually, this has little effect on the impregnation but may become an issue for some specific cases. If the precursor solubility is inverse temperature depended (i.e., retrograde solubility), the solution may reach saturation due to the increase in temperature from the heat being released. Another situation may be that a solution contains an unstable mixture of metal precursors, where the precipitation of a mixed compound is poorly distributed on the support surface due to the temperature rise [41].

The air present in the pores before catalyst synthesis is being entrapped as the precursor solution is impregnating the support. Inside the pores, a part of the air is imprisoned as bubbles and compressed under the effect of the capillary forces. The pressure of these air bubbles may reach tens of bars, which may cause the walls of the pore in contact with the bubbles to break down. The high pressure causes the air to dissolve into the solution and escapes progressively from the pores of the catalyst [41].

3.2.2 Calcination

Calcination involves the thermal treatment of the catalyst after the synthesis or to pretreat the support before the impregnation. The technique is performed by introducing a gas flow through the catalyst at an elevated temperature, where solid-state reactions occur. Nitrates, oxalates, acetates, chlorides, or other anions are burnt or decomposed during these reactions and removed from the supported catalyst [44]. Among several gas options, air could be used as the gas flow to enable oxidation to occur at the elevated temperature. This will yield the oxidation state of all elements present to reach their desired values [41]. The anions of the precursor salt have to be chosen such that it may be removed during the calcination of the catalyst. Choosing the temperature for the calcination depends on the active phases and the support material. In the case of cobalt oxides, the temperature should be elevated to achieve the desired oxidation state but need to avoid deactivation of the active phase such as sintering and to avoid the transition to a less desired phase of the support [41].

3.3 Characterization of the catalyst

In this section, the theory regarding nitrogen adsorption/desorption, X-ray diffraction, and temperature programmed reduction are described.

3.3.1 Nitrogen adsorption/desorption

Nitrogen adsorption is a characterization technique used to determine the surface area of the supported catalysts. The surface area is calculated by determining the number of physisorbed nitrogen molecules to form a monolayer coverage at the surface of the material. A nitrogen molecule, N_2, occupies at the surface $0.162\,nm^2$ at $-196\,°C$, which is used to in the calculation of the surface area [33]. However, some challenges are present when utilizing nitrogen adsorption. The physisorbed nitrogen can form several layers of molecules when the gas is introduced to the sample surface, where multilayer of N_2 takes place. Figure 3.2 illustrates multilayer adsorption as the relative pressure increases in a single cylindrical pore [46]:

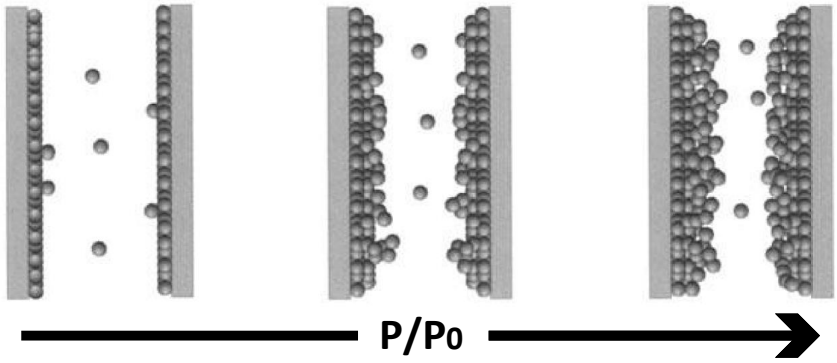

Figure 3.2: An illustration of multilayer adsorption as the relative pressure increases in a single cylindrical pore. Adapted from [46].

If there are small and narrow pores present, the nitrogen may also condense [33]. Equation 3.1 shows the Brunauer-Emmett-Teller (BET) isotherm used to describe the adsorption isotherm of physisorbed species [47]:

$$\frac{P}{V_a(P_0-P)} = \frac{(C-1)P}{V_m \cdot C \cdot P_0} + \frac{1}{V_m \cdot C} \tag{3.1}$$

where P is the partial pressure of N_2, V_a is the volume of N_2 adsorbed at pressure P, P_0 is the saturation pressure at a given temperature, V_m is the volume of N_2 adsorbed at monolayer coverage, and C is a constant [41][47]. The BET isotherm model is based upon various assumptions and is valid under the following conditions [33]:

- Regardless of the layer, the rate of adsorption and desorption are equal
- At the first layer, the molecules adsorb on equivalent adsorption sites

- Past the first adsorption layer, a new adsorption layer can only adsorb on adsorption sites constituted by the previous layer
- The interaction between the adsorbates are ignored
- The adsorption-desorption conditions for all layers, except for the first, are the same.
- The adsorption energy for the molecules equals the condensation energy in the second layer and above.
- The multilayer thickness grows to infinite when the saturation pressure is reached (P=P_0).

To make sure that nitrogen is the adsorbed gas at the surface of the material during the BET experiment, the sample needs to be degassed before the analysis. Therefore, the sample is exposed to vacuum at an elevated temperature to remove the adsorbed gas before conducting the experiment.

In order to determine the surface area, the relation between $P/V_a(P_0 - P)$ and P/P_0 needs to be linear when using the BET isotherm [41]. The linear relation is generally restricted in the range of P/P_0 between 0.05-0.30 in the BET isotherm, where P/P_0 equal to 0.30 the monolayer is assumed to be filled. Beyond this point, the second layer of adsorbed nitrogen starts to form, and subsequently, multilayer formation occurs. Therefore, the range of P/P_0 between 0.05-0.3 in the BET isotherm is used in the calculation of the surface area of the material [33][41]. The surface area determined by this technique is referred to as the BET surface area. With the assumptions used in this model, it is expected that the calculated surface area may vary up to 20 % from the actual surface area of the material. A comparison between surface area should thus be between ones that have been determined by the BET isotherm and with the same assumption in this model [41].

In order to determine the pore size distribution, the Barret-Joyner-Halenda (BJH) method was utilized. The principle behind this method is to fill the pores of a porous material with nitrogen until the pressure ratio (P/P_0) has reached equal to 1, where at this point it is assumed that the pores are filled. Thereafter, the pressure was reduced in several steps, and the volume of desorbed nitrogen gas was measured in each of the steps. The thickness of the adsorbed gas layer, t, will also be affected by the pressure reduction steps [48]. Equation 3.2 shows how the pore volume for step n can be calculated [48]:

$$V_{P_n} = \frac{{r_{P_n}}^2}{(r_{k_n} + \Delta t_n)^2} \cdot \Delta V_n - \frac{{r_{P_n}}^2}{(r_{k_n} + \Delta t_n)^2} \cdot \Delta t_n \cdot \sum_{j=1}^{n-1} \frac{r_P - t_r}{r_P} \cdot A_{P_j} \tag{3.2}$$

where V_{P_n} is the pore volume in step n, r_{P_n} is the pore radius in step n, Δt_n is the reduction in thickness of the adsorption layer in step n, ΔV_n is the volume of desorbed gas in step n,

r_{k_n} is the radius of the inner capillary in step n, A_p is the pore area, and t_r is the thickness of the physically adsorbed layer at the corresponding value of P/P_0 [48].

To determine the pore radius, the Kelvin equation is used with the assumption that the pores are cylindrical. Also, the amount of adsorbate and gas phase in equilibrium was assumed to follow two mechanisms. For the first mechanism, the physical adsorption occurs on the pore walls. For the second one, the capillary condensation occurs in the inner capillary volume [48]. In order to obtain a relationship between P/P_0 and r_k, the Kelvin equation shown below is used [48]:

$$log\left(\frac{P}{P_0}\right) = \frac{-2\sigma V_{ma}}{8.316 \cdot 10^7 \cdot 2.303 \cdot T_k \cdot r_k} = \frac{-4.14}{r_k} \tag{3.3}$$

where σ is surface tension of liquid nitrogen, V_{ma} is the molar volume of liquid nitrogen, r_k is the radius of the capillary in cm, T_k is the absolute temperature in K and $8.316 \cdot 10^7$ is the gas constant in ergs per degree [48]. The equation $r_p = r_k + t$ is also used to have a relation between the pressure ratio and the r_p [48]. The thickness, t, as a function of the relative pressure may be determined by using the t-plot method [46][47][48][49].

3.3.2 X-ray diffraction

X-ray diffraction (XRD) is a technique applied in catalyst characterization to identify the crystallite phase inside the catalyst and to get an indication of the crystallite size [33]. The material is irradiated by the X-rays and are scattered by the crystallite phases in the catalyst. Figure 3.3 illustrates how the crystal planes diffract the X-rays and how it derives the lattice spacing by using Bragg's relation as shown in Equation 3.4 [33]:

$$n\lambda = 2dsin\theta; \quad n = 1, 2, ... \tag{3.4}$$

where λ is the wavelength of the X-rays, d is the distance between the lattice planes, θ is the angle between the irradiating X-ray and the lattice plane and n is an integer [33].

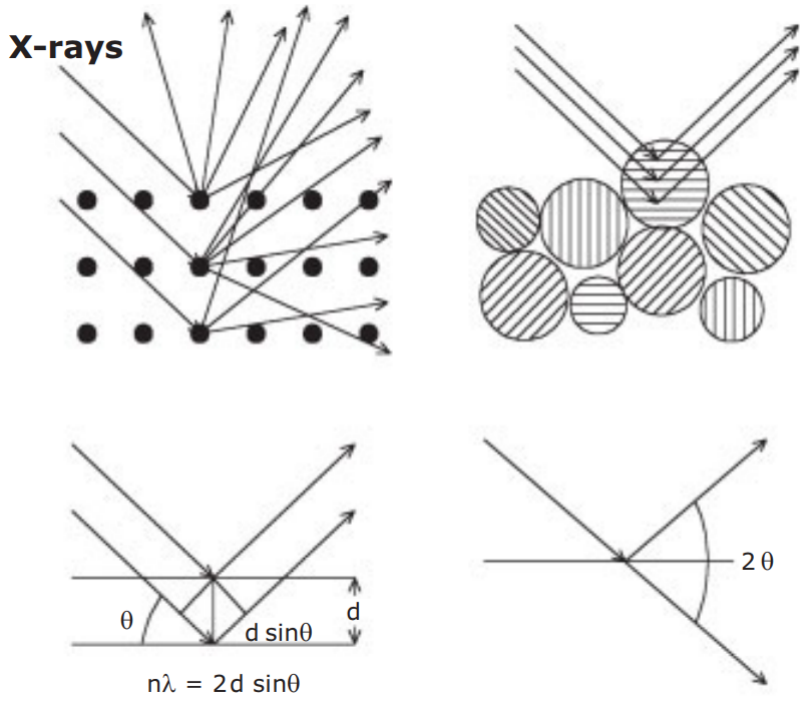

Figure 3.3: The incoming X-rays are scattered by the atoms in lattice. Bragg's relation can be used to calculate the spacings between the lattice planes and used to identify the phases of the crystallites in the catalyst [33].

The Scherrer equation shown below can be used to calculate the average size of the crystallite phases [33]:

$$\langle L \rangle = \frac{K\lambda}{\beta cos\theta} \tag{3.5}$$

where $\langle L \rangle$ is a measure of the particle dimension in the direction perpendicular to the reflecting plane which may be referred to as the crystallite size, K is the shape factor, β is the width of the peak at half height in radians (FWHM), and θ is the angle between the incoming X-ray and the plane [33]. The Scherrer equation is used to calculate the average crystallite size by using the diffraction pattern from the X-rays of the crystallite phases present in the material. The value of the shape factor K depends on the shape of the crystallite. By default, the value may be set equal to 1, but having an indication on the shape can change the value used. The shape factor value was set to be equal to 0.9, which assumes that the crystallite sizes are spherical [50].

The average spherical particle size of Co_3O_4 can be estimated by using a geometric factor

equal to 4/3, which is multiplied with the crystallite size given from the Scherrer equation as shown in Equation 3.6 [51]:

$$d(Co_3O_4) = \frac{4}{3} \cdot \langle L \rangle (Co_3O_4) \tag{3.6}$$

where d(Co_3O_4) is the particle size of Co_3O_4 and $\langle L \rangle (Co_3O_4)$ is the crystallite size of Co_3O_4. With the particle size of the Co_3O_4, the particle size of metallic cobalt (Co^0) can be estimated by using Equation 3.7 [51]:

$$d(Co^0) = d(Co_3O_4) \cdot 0.75 \tag{3.7}$$

where d(Co^0) is the particle size of Co^0. The ratio given in the equation is based upon the relative molar volumes between Co^0 and Co_3O_4 [51]. The ratio is not valid if the cobalt oxide particles crack such as during hydrogen reduction. In that case, the equation given cannot be used [51]. The dispersion, D, is the total number of metal atoms on the surface divided by the total number of metals atom on the surface and bulk, as shown in Equation 3.8 [41]:

$$D = \frac{\text{Total number of metal atoms on the surface}}{\text{Total number of metal atoms on the surface and bulk}} \tag{3.8}$$

The dispersion of cobalt may be calculated by using the particle size of the metallic cobalt, as shown in Equation 3.9 [51]:

$$D[\%] = \frac{96}{d(Co^0)} \tag{3.9}$$

where D is the dispersion in percentage. The equation is based upon the assumption that the site density of cobalt is equal to $14.6\,\text{atoms}\,\text{nm}^{-2}$ and that the particles are spherical and uniform [51]. By combining Equation 3.7 and 3.9 and isolating the dispersion gives the following equation:

$$D[\%] = \frac{96}{0.75 \cdot d(Co_3O_4)} \tag{3.10}$$

The equation above was used to calculate the dispersion of the cobalt oxides particles at the support surface. It was based on the assumption that the number of cobalt atoms at the particle surface remains the same between its metallic form and metal oxide.

3.3.3 Temperature programmed reduction

To determine at which temperatures the metal oxides in the catalyst reduces, the temperature programmed reduction (TPR) technique can be utilized. This is achieved by introducing the catalyst sample to a flow of reducing agent while the temperature is increased linearly over time. The reducing agent often consists of argon, which is an inert gas, with some percentage of a reducing gas such as carbon monoxide (CO) or hydrogen (H_2) [41]. Equation 3.11 shows an example of a complete reduction of a metal oxide species with

hydrogen:

$$M_yO_x + xH_2 \longrightarrow yM + xH_2O \tag{3.11}$$

In order to determine the gas consumption of hydrogen, the outlet gas composition can be measured by using a thermal conductivity detector (TCD) or a mass spectrometer (MS) [33]. From the measurements, the degree of reduction and average oxidation state of the metal species after reduction can be determined [41]. The information attained from the TPR-profile may be used in other characterization techniques such as chemisorption, where it is desired to know at which temperature the metal oxide transition into its metallic state.

Chapter 4

Experiment

4.1 Catalyst preparation

Before the impregnation procedure, the various supports were calcined to thermal stress the material to avoid blockage of pores after the supported catalysts have been impregnated and calcined. The supported catalysts need to be sieved in the correct fraction range to minimize mass transfer limitations and back pressure to build up when the activity measurements are performed. To mitigate these issues, the various supports were sieved between the range 53 - 90 µm before the impregnation procedure. In the case of CeO_2, the support was sieved between 38 - 53 µm as there was limited sieve fraction higher than 53 µm. Before the supports were calcined, the materials were sieved in the correct range to maximize the yield of desired sieve fraction after the calcination. For TiO_2, SiO_2, and CeO_2, the supports were calcined at 500 °C for 2 hours with a ramp rate of $10\,^{\circ}\mathrm{C}\,\mathrm{min}^{-1}$ under a gas flow of air. For ZrO_2, the support was calcined under a gas flow of air at 600 °C for 2 hours with a ramp rate of $10\,^{\circ}\mathrm{C}\,\mathrm{min}^{-1}$. In the case of Al_2O_3, the support was previously calcined at 750 °C for 2 hours with the same ramp rate as the other supports.

Each of the supports was impregnated with various concentrations of metal precursor solution to vary the metal loading of cobalt on the supported catalyst. Before the precursor solution could be made, the amount of pore volume in each support material needs to be determined before the impregnation, i.e., determining the incipient wetness point (IWP) of the supports. The IWP of each support was determined experimentally by weighing an amount of the support and measuring how much deionized water was required until the pore volume was filled up. The pores were considered to be filled when the supports went from a dry to a wet surface. Thereafter, the pore volume, V_{PT}, before each impregnation could be calculated. An amount of precursor salt, cobalt(II) nitrate hexahydrate

($Co(NO_3)_2{\cdot}6H_2O$), was weighted depending on the desired metal loading of cobalt and mixed with deionized water such that V = V_{PT}. The water contribution from the hydrate was taken into account when adding the required amount of deionized water into the precursor solution. The precursor solution was stirred until no undissolved cobalt nitrate was observed, and a clear solution was achieved. The calcined support was impregnated by adding dropwise of the precursor solution into the material.

To remove the water after the impregnation, the sample was dried overnight in a ventilated oven at 120 °C. The sample was stirred with a glass rod every 15 min for the first hour and afterward every 30 min for the second hour until it was left to dry. After the drying procedure, the sample was calcined at 300 °C for 16 hours with a ramp rate of 2 °C min^{-1} and afterward at 500 °C for 2 hours with a ramp rate of 10 °C min^{-1}. After the calcination, the supported catalyst was sieved to get the fraction between 53 - 90 µm, except for cobalt oxides supported on CeO_2 which was sieved to get the fraction between 38 - 53 µm. For 20wt%Co on CeO_2 and ZrO_2, the impregnation procedure had to be done twice due to the low IWP of the supports. The added amount of deionized water was not sufficient enough to dissolve the cobalt nitrate in the precursor solution. The impregnation of these catalysts was done by first impregnating it with the half amount of cobalt nitrate required for 20wt%Co, then let it dry in the oven and subsequently impregnate it again to achieve the desired metal loading. After that, the procedure was the same as the other support catalysts.

In total there was 12 supported catalyst made during the master thesis, with metal loading of 5, 10 and 20wt%Co on TiO_2, CeO_2, SiO_2, and ZrO_2. The five cobalt oxides supported on $\gamma - Al_2O_3$, which were made in the project prior to the master thesis, were made under similar procedures and conditions as in this work. For the non-promoted catalysts on alumina with 5, 10 and 20wt%Co/Al_2O_3 will be referred to as 5Co/Al_2O_3, 10Co/Al_2O_3, and 20Co/Al_2O_3, respectively. This was also implemented for the cobalt oxides supported on TiO_2, CeO_2, SiO_2, and ZrO_2. The catalyst with 0.5wt%Pt promoted on 20wt%Co/Al_2O_3 will be referred to as 20Co-Pt/Al_2O_3. For the catalyst with 5wt%K promoted on 20wt%Co/Al_2O_3 will be referred to as 20Co-K/Al_2O_3.

All information regarding the calculation and values used for the impregnation can be found in Appendix A. The risk assessment of the experimental work during the thesis can be found in Appendix F.

4.2 Characterization techniques

In the following section, the process conditions and procedures of the characterization techniques used during this work are described.

4.2.1 X-ray diffraction

To perform the XRD-analysis of the catalysts, the Bruker D8 DaVinci X-ray diffractometer was utilized. The anode material of the X-ray tube consisted of Cu, and the XRD-unit have Kα1 and Kα2 equal to 1.54060 and 1.54439 Å, respectively. The X-ray generator was at 40 kV and 40 mV with a wavelength equal set to 1.54060 Å. The catalysts were analyzed using a low crystallinity program to avoid the diffraction patterns to be to be distorted due to the cobalt content. The same program was used on all of the catalysts, which was a low crystallinity program measuring between 15-75° for a 60 min duration with a fixed split opening set equal to 0.3°. The XRD patterns of the catalysts can be seen in Appendix D. It should be noted that when the XRD patterns were presented in the results and discussion chapter, the background noise was subtracted from the XRD patterns.

4.2.2 Nitrogen adsorption/desorption

Nitrogen adsorption was performed to determine the BET surface area of the samples, while nitrogen desorption was utilized to determine the pore size distribution of the samples. In this work, only the calcined support materials were analyzed. The nitrogen adsorption and desorption were performed by using the Micromeritics TriStar II 3020 at $-196\,^{\circ}\mathrm{C}$. A total of 88 P/P_0 points were analyzed for each support, which includes the points used both in the nitrogen adsorption and desorption. The points were more concentrated at the start of the adsorption curve and around saturation pressure to attain more reliable data. The BET isotherms and pore size distribution plots are given in Appendix C.

Before the analysis, the samples were degassed to remove the adsorbed gases on the surface of the supports. About 200 mg of the support was added into an analysis glass and degassed overnight at 200 °C in vacuum by using the unit VacPrep 061 by Micromeritics. The sample mass of each analysis is given in Appendix B.

4.2.3 Temperature programmed reduction

The TPR experiments were performed to determine at which temperatures hydrogen reduces on the supported catalysts. The unit used to perform the experiments was the Altamira BenchCat Hybrid. The TPR instrument used a U-tube shaped quartz glass, where 100 mg of the sample was placed between two plugs of quartz wool to keep it in place. The procedure of the TPR analysis consisted in total of four steps. In the first step, the sample is pre-treated by introducing a flow of inert gas (He, Ar) with $50\,\mathrm{cm^3\,min^{-1}}$ at 150 °C for 30 min with a ramp rate of $10\,^{\circ}\mathrm{C\,min^{-1}}$. Thereafter, the second step cooled down the sample to 40 °C under a gas flow of inert gas. The third one was the reduction step, in which the sample was heated up to 800 °C with a ramp rate of $10\,^{\circ}\mathrm{C\,min^{-1}}$ under a gas flow of argon with 7 % of hydrogen (7 %H_2/Ar). In the final step, a pulse calibration with five

injections of the 7 %H_2/Ar gas was performed. The sample mass of each analysis is given in Appendix B.

In addition to the regular TPR-experiments, there were performed wet-TPR experiments by introducing steam with hydrogen diluted in argon. These experiments were performed at the same reactor setup used for the activity measurements of the NO oxidation. The catalyst bed was prepared by mixing 500 mg of the catalyst with 2.75 g of silicon carbide (SiC). To minimize back pressure build-up, the SiC was sieved in the fraction between 53 - 90 µm. Thereafter, the catalyst mixture was placed between two plugs of quartz wool in the reactor to keep the catalyst bed in place. The procedure for wet-TPR consisted of three steps. The first step was the pre-treatment of the catalyst by having a gas flow of argon with 200 $cm^3\,min^{-1}$ at 150 °C for 30 min with a ramp rate of 10 $°C\,min^{-1}$. In the second step, the catalyst bed was cooled down to 120 °C under a gas flow of argon. In the last step, the reduction of the catalyst was performed by introducing a gas consisting of 5 % H_2, 6 % H_2O, and rest Ar with 200 $cm^3\,min^{-1}$. The catalyst bed was heated from 120 to 500 °C with a ramp rate of 5 $°C\,min^{-1}$. The outlet gases from the reactor were analyzed by using a mass spectrometer by Pfeiffer Vacuum. The sample mass of each analysis is given in Appendix B.

4.3 Activity measurements

The activity measurements of the NO to NO_2 oxidation were performed by using a packed bed reactor (PBR). The reactor was made out of stainless steel, and it was a tubular and vertical reactor with a length and inner diameter equal to 8 and 0.97 cm, respectively. To minimize the temperature gradients along the axial direction of the reactor, it was installed between two blocks made out of aluminum. In each of the aluminum blocks, there were placed two cartridge heaters to generate heat to increase the temperature inside the reactor during the activity measurements. The thermocouple was installed from the top of the reactor and measured the temperature of the catalyst bed. An illustration of the reactor setup can be seen in Figure 4.1:

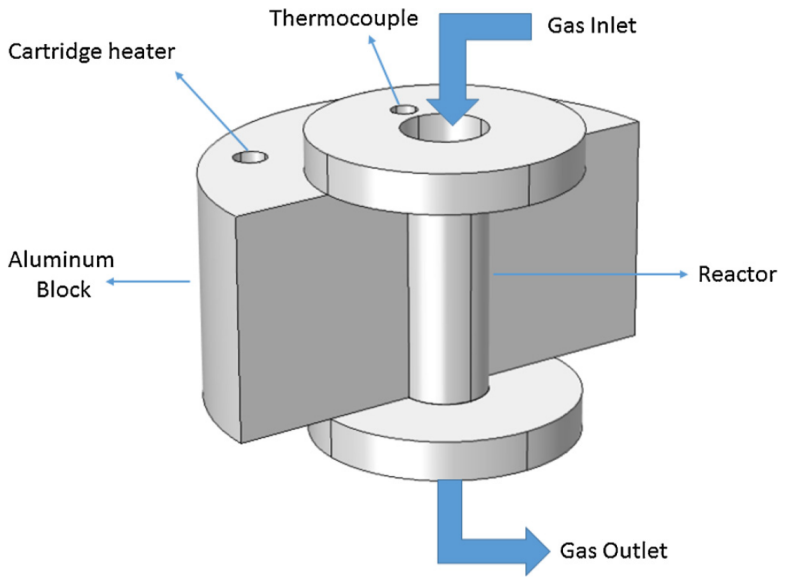

Figure 4.1: An illustration of the several components involved in the installation of the reactor setup [12].

Before installing the reactor, it needs to be filled with the desired catalyst. To prepare the catalyst bed, 500 mg of catalyst and 2.75 g of SiC are mixed together. The SiC material acts as an inert packing material and minimizes the temperature gradient along the axial direction of the reactor. The catalyst and SiC were sieved before they were mixed to get the fraction between 53 - 90 µm. The sieve fraction minimizes potential back pressure build-up during the experiments and to attain a homogeneous mixture. The reactor was prepared by having the catalyst mixture placed between two plugs of quartz wool inside the reactor so that it remains as a static catalyst bed.

A process flow diagram of the experimental setup used for activity measurements of NO oxidation can be seen in Figure 4.2:

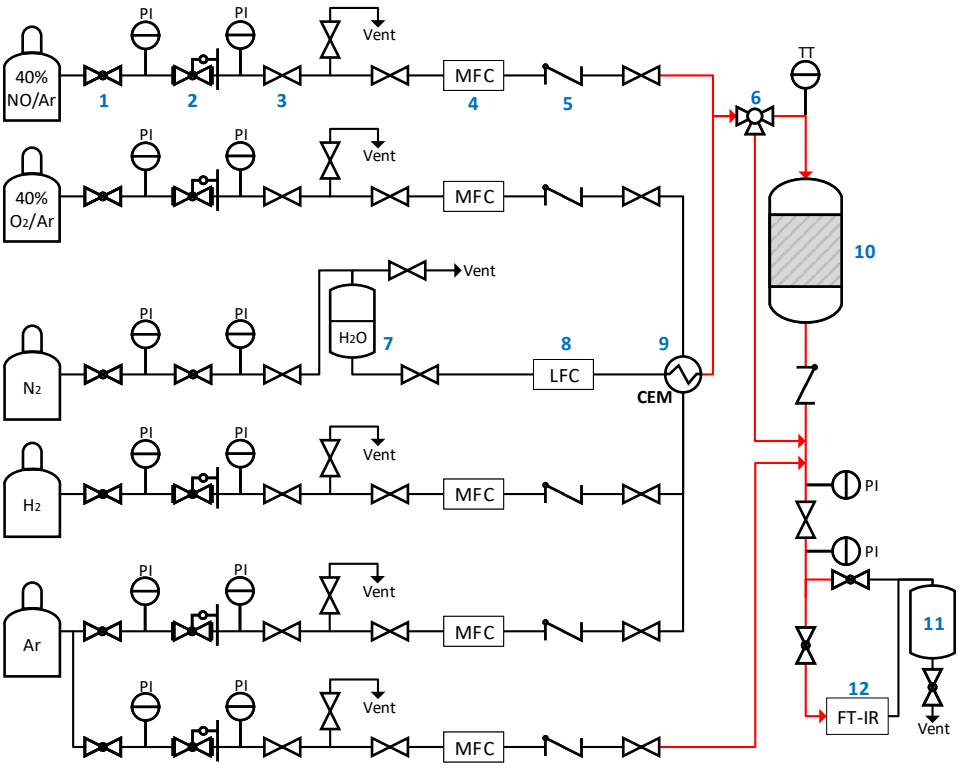

Figure 4.2: A process flow diagram of the experimental setup used for NO oxidation activity measurements. The red lines indicate the heated gas lines. 1. Globe valve, 2. Reducing valve, 3. Gate valve, 4. Mass flow controller, 5. Check valve, 6. Three-way valve, 7. Water tank, 8. Liquid flow controller, 9. Evaporator, 10. Reactor, 11. Water condenser, 12. Fourier transform infrared analyzer.

Mass flow controllers (MFC) were used to control each of the gas flows separately before it was mixed at the inlet of the reactor. After the MFCs, the gas lines are being heated up to 200 °C, which is illustrated as red lines in Figure 4.2. The water feed was controlled by a liquid flow controller (LFC) and led to a controlled evaporator mixer (CEM), where the water and the gases, except for NO, went through the evaporator and steam was produced as illustrated in the figure above. The water comes from a tank that was pressurized with nitrogen gas. The gases are mixed at the reactor inlet to reduce the effects of the homogeneous gas phase reaction in gas lines before reaching the reactor. The total inlet gas feed was set equal to 200 $cm^3 min^{-1}$, which corresponds to a GHSV equal to 43 400 h^{-1}. The reactor operated at atmospheric pressure during the activity measurements. The outlet gas from the reactor was diluted with 800 $cm^3 min^{-1}$ of argon to minimize further gas phase reaction contributions and to cool down the gas before it was analyzed at 191 °C. The instrument used to analyze the composition of the outlet gas was a Fourier transform infrared analyzer (FT-IR) by MKS, which was calibrated at 191 °C and 1 atm.

Before starting the activity measurements for the dry runs, the catalysts were activated by feeding the reactor with a gas flow of argon with 10 % O_2 at 500 °C for 1 hour with a ramp rate of 10 °C min^{-1}. Thereafter, the activity measurements for the dry run was initiated by having a gas composition of 10 % NO, 6 % O_2 and rest Ar fed at the reactor inlet and measuring the activity between 150-450 °C with a ramp rate set to 5 °C min^{-1}. After the dry run, the wet run was started by using the same temperature range of 150-450 °C with the ramp rate set to 5 °C min^{-1}, but the gas composition fed to the reactor consisted of 10 % NO, 6 % O_2, 15 % H_2O and rest Ar. After running both the dry and wet run, a stability test of the same catalyst sample was performed at 350 °C to investigate the stability of the catalyst, and the effects water has on the catalyst deactivation. The stability procedure was a sequence of dry, wet, dry conditions where each of the conditions ran for 2 hours.

In addition to the supported catalysts, the supports were run to investigate the potential catalytic contribution to the NO oxidation. Previous tests showed that both an empty reactor and one filled with 2.75 g SiC have equal gas phase conversion across the temperature range of 150-450 °C under the same conditions given for the activity measurements. As the gas phase conversion at a given temperature was constant for the experiments, the total NO conversions from the activity measurements are used when presenting the results and when using the conversions for the calculations. The sample mass used in the activity measurements of the NO oxidation is given in Appendix B.

The NO to NO_2 stoichiometry is equal to 1:1 by using the oxidation reaction given in Equation 1.3 and gives the molar balance shown in Equation 4.1:

$$n_{\mathrm{NO},in} = n_{\mathrm{NO_2},out} + n_{\mathrm{NO},out} \tag{4.1}$$

where $n_{NO,in}$ is moles of NO in the inlet gas, $n_{NO_2,out}$ is moles of NO_2 in the outlet gas and $n_{NO,out}$ is moles of NO in the outlet gas. In order to determine the conversion of NO to NO_2, the equation shown below was used [12]:

$$NO_{Conversion}[\%] = \frac{n_{\mathrm{NO_2},out}}{n_{\mathrm{NO},in}} \cdot 100 \tag{4.2}$$

where $NO_{Conversion}$ is the conversion of NO to NO_2. To compare the catalytic activity between the supported catalysts, the turnover frequency (TOF) was calculated to determine the number of moles reacted per active site per unit of time. Equation 4.3 shows the formula for calculating the TOF for the supported catalyst:

$$TOF = \frac{r \cdot M_w}{x_m \cdot D} \tag{4.3}$$

where r is the rate of reaction, M_w is the molar weight of the active metal, x_m is the fraction of active metal, and D is the dispersion of the active component. The rate of reaction was calculated by using the equation given below:

$$r_{NO_2}[\mu mol\, s^{-1}\, g_c^{-1}] = \frac{\dot{V}_{NO_2,out}[cm^3\, min^{-1}]}{g_c} \cdot \frac{10^6}{60 \cdot 24 \cdot 1000} \tag{4.4}$$

where r_{NO_2} is the rate of NO_2 production, $\dot{V}_{NO_2,out}$ is the volumetric flow rate of NO_2 in the outlet gas, and g_c is mass of the catalyst. The rate of reactions presented and used in the TOF values were based upon the catalytic NO conversion and not the total NO conversion. This was achieved by taking the total NO conversion from the activity measurements and subtracting it with the gas phase conversion at a given temperature of interest to determine the rate of reaction. Thus, the rate of reaction and TOF values were based upon the catalytic contribution from the catalysts.

Chapter 5

Results and discussion

5.1 Characterization

In this section, the characterization results of the catalysts and supports are shown and discussed. In the first part, the BET surface area and pore size distribution of the calcined supports are compared and discussed. Thereafter, the X-ray diffractions are shown to identify the oxidation state present at the supported catalysts and to determine the particle size and dispersion of the cobalt oxides. In the third part, the TPR-profiles of the supported catalysts are presented to investigate the reducibility of the supported cobalt oxides. The characterization techniques were used to distinguish the difference between the supported catalysts and to determine which properties may impact the NO to NO_2 oxidation.

The catalysts supported on alumina were prepared and characterized in the previous specialization project, TKP 4580. The XRD and TPR-profiles of these supported catalysts are presented and discussed in this thesis to have the opportunity to compare between the various supported catalysts [52].

5.1.1 Nitrogen adsorption/desorption

It is desired for the supports to be thermally stable and to avoid any phase transitions to occur under the given process conditions. One way to indicate if the phase of the support may have changed was by looking into the BET surface area of the calcined supports. Table 5.1 shows the BET surface area determined from BET adsorption, the average pore size from the BJH desorption and the cumulative pore volume from BJH desorption of the calcined supports:

Table 5.1: The BET surface area determined from BET adsorption, the average pore size from the BJH desorption and the cumulative pore volume from BJH desorption of the calcined supports.

Support	BET surface area $[m^2\,g^{-1}]$	Pore size [nm]	Pore volume $[cm^3\,g^{-1}]$
SiO_2	153	12.7	0.61
Al_2O_3	152	15.8	0.79
TiO_2	129	10.9	0.43
CeO_2	122	5.2	0.23
ZrO_2	84	11.9	0.34

The BET surface area of the calcined supports seemed to be in the expected range. The surface area of the SiO_2 was the highest among the supports and was equal to $153\,m^2\,g^{-1}$, followed by Al_2O_3, TiO_2, CeO_2, and ZrO_2. For the γ-Al_2O_3, the support was calcined up to 750 °C. The phase transition into α-Al_2O_3 start at 900 °C and has a low surface area at 3-5 $m^2\,g^{-1}$, which indicate that alumina remained in the γ-phase [53][33]. For the remaining supports, the calcination temperature was up to 500 °C, which should not be sufficient enough for a potential phase transition of the supports. For further confirmation, the XRD may be used to identify the phase of selected supports. The research by Kim et al. showed that the surface area of the ceria support impacted the NO oxidation over the supported cobalt oxides, where higher surface area increased the NO conversion at three digit ppm levels of NO [21]. Having a higher surface area may be beneficial for the NO oxidation. At the end of the chapter, the catalytic activity of the supported catalysts are compared, and it can be seen if having a higher surface area may be beneficial.

From Table 5.1, it can be seen that as the average pore size of the support decreases, the cumulative pore volume follows the same trend except for the TiO_2 support. This may be due to the pore volume getting more even contribution from a wider pore width range, which can be seen from the pore size distribution given in Appendix C. The average pore size and pore volume trend observed are not necessarily a general correlation, where a boundless combination of various support properties may give different trends than observed in this case.

5.1.2 X-ray diffraction

The XRD of the supported catalysts were used to identify the oxidation state of cobalt and to check if the phase of selected supports has remained in its desired state. In addition, the crystallite size, particle size, and dispersion of the cobalt oxides were determined by using the XRD patterns of the catalysts. Figure 5.1 shows the XRD of the cobalt oxides supported on Al_2O_3 with metal loading at 5, 10, and 20wt%Co:

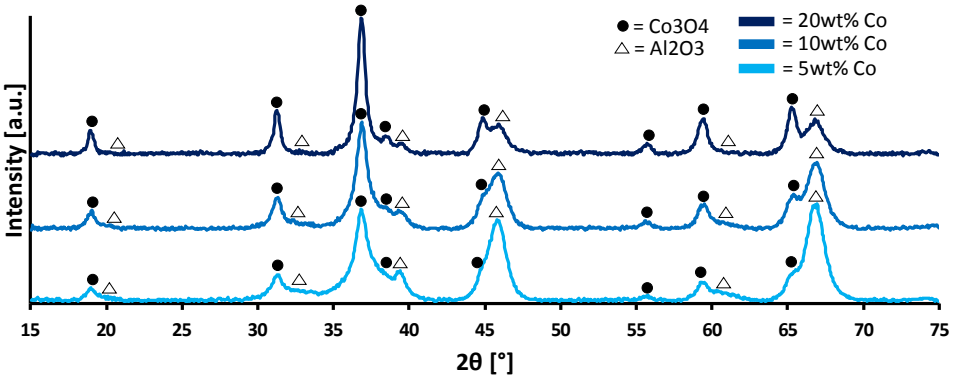

Figure 5.1: The XRD patterns of the cobalt oxide supported on Al_2O_3 with metal loading of 5, 10, and 20wt%Co.

From Figure 5.1, it can be seen that the cobalt oxides supported on alumina are in the form of Co_3O_4. The calcination temperature at 500 °C was sufficient enough to remove the nitrates after the catalyst preparation and to generate the desired oxidation state of the cobalt oxides. The specific peaks for Co_3O_4 at 18.7, 31.3, 36.8, 55.7, and 59.7° become more distinctive as the metal loading of Co increases. The specific peaks for Al_2O_3 at 45.9 and 66.9° can be seen to become less distinct as the percentage of the support decreases. The peaks from both Co_3O_4 and Al_2O_3 are overlapping excepts for cobalt oxide peak at 55.7°. This specific peak was chosen to be used to calculate the crystallite size of the cobalt oxides present on the alumina support [52].

Figure 5.2 shows the XRD of the promoted cobalt oxides supported on Al_2O_3 with metal loading of 20wt%Co and the 20Co/Al_2O_3 as a reference:

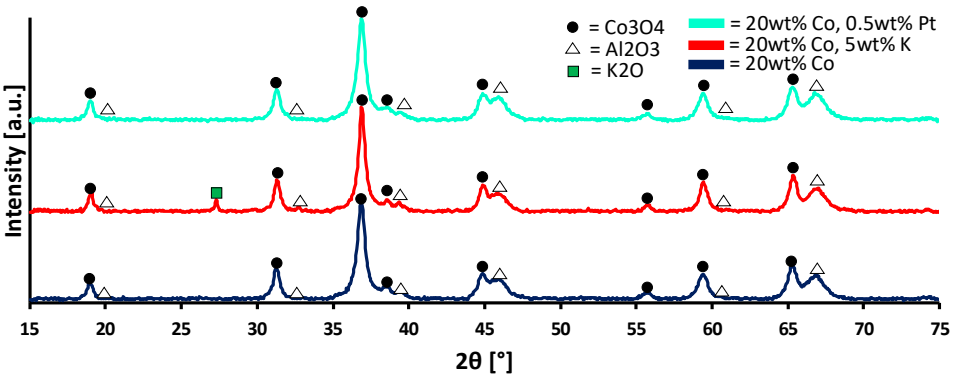

Figure 5.2: The XRD patterns of the promoted cobalt oxides supported on Al_2O_3 with metal loading of 20wt%Co and the 20Co/Al_2O_3 as a reference.

As seen from Figure 5.2, the catalyst promoted with 0.5wt%Pt was not sufficient enough to give a distinctive peak in the XRD pattern. In regards to the catalyst promoted with 5wt%K, a specific peak at 27.3° for K_2O could be seen. It should be noted that that potassium oxide did not have an exact match, where matching peak for K_2O was shifted 0.3-0.4 ° to the right of the peak present in the XRD pattern. The potassium may have reacted with cobalt or alumina to form a compound different from K_2O. Another scenario may be that leftover nitrates from catalyst preparation were still present, but were not likely as the calcination went up to 500 °C [52].

Figure 5.3 shows the XRD of the cobalt oxides supported on TiO_2 with metal loading at 5, 10, and 20wt%Co:

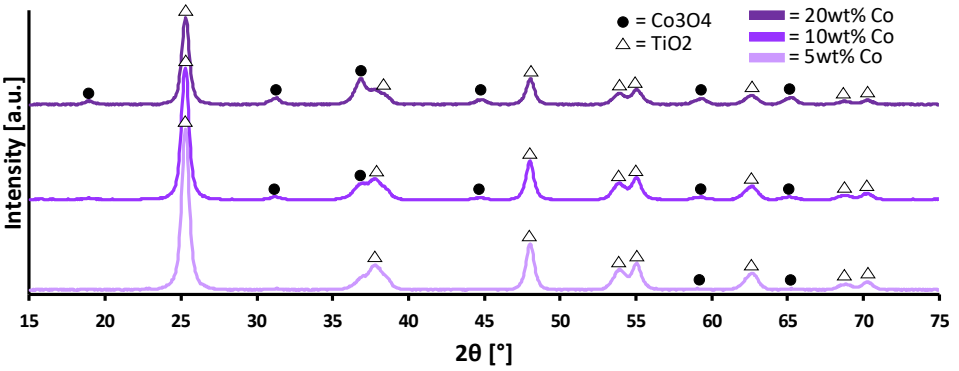

Figure 5.3: The XRD pattern of the cobalt oxides supported on TiO_2 with metal loading of 5, 10, and 20wt%Co.

As seen from the figure above, the catalyst preparation of TiO_2 catalyst yielded the cobalt oxide as Co_3O_4. The distinctive peaks of the cobalt oxides were challenging to detect for the 5wt%Co. The peak at 18.9° was only visible for the 20wt%Co and the ones at 31.2 and 44.8° were detected for the 10 and 20wt%Co. The two peaks at 59.3 and 65.4° were detected for all three catalysts, but the intensity at these peaks was low. This would indicate that the cobalt oxides were well dispersed into the support material and that the crystallite size of these oxides was small. The peaks at 59.3° were chosen for the calculation of the crystallite size of the cobalt oxides as these did not interfere with the TiO_2 peaks and to use the same peak across the supported catalysts. The peaks for the TiO_2 detected that the support remained as anatase, where the support did not phase transition into rutile during the calcination procedure.

Figure 5.4 shows the XRD of the cobalt oxides supported on SiO_2 with metal loading at 5, 10, and 20wt%Co:

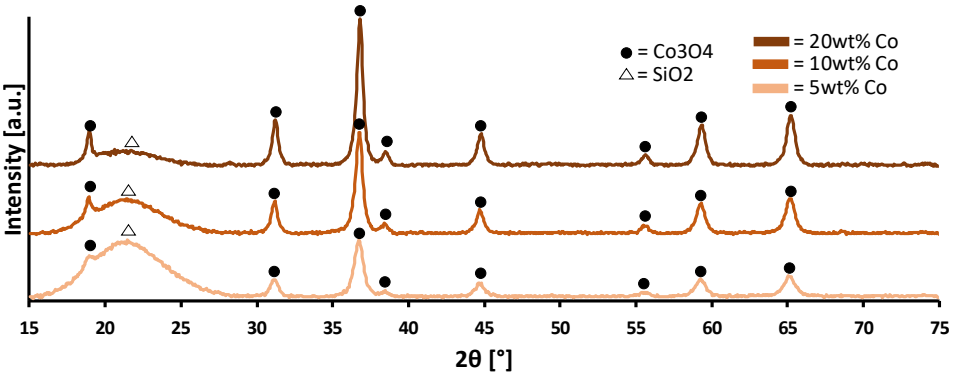

Figure 5.4: The XRD pattern of the cobalt oxide supported on SiO_2 with metal loading of 5, 10, and 20wt%Co.

All of the peaks of the cobalt oxides with 5, 10, and 20wt%Co are present in Figure 5.4. The intensity of these peaks become more prominent as the cobalt loading increases. There was only one peak that represented the silica, which had several SiO_2 contributions around 22°. This peak can be seen to decrease in intensity as the metal loading of cobalt increases. Choosing the peak to calculate the Co_3O_4 crystallite size was more flexible compared to the previous XRD patterns since there little to no overlapping from the support. It was decided to chose the peak at 59.3° for the crystallite size calculation since there was no overlapping with the other peaks and to continue using the same Co_3O_4 peak across the supported catalyst.

Figure 5.5 shows the XRD of the cobalt oxides supported on CeO_2 with metal loading at 5, 10, and 20wt%Co:

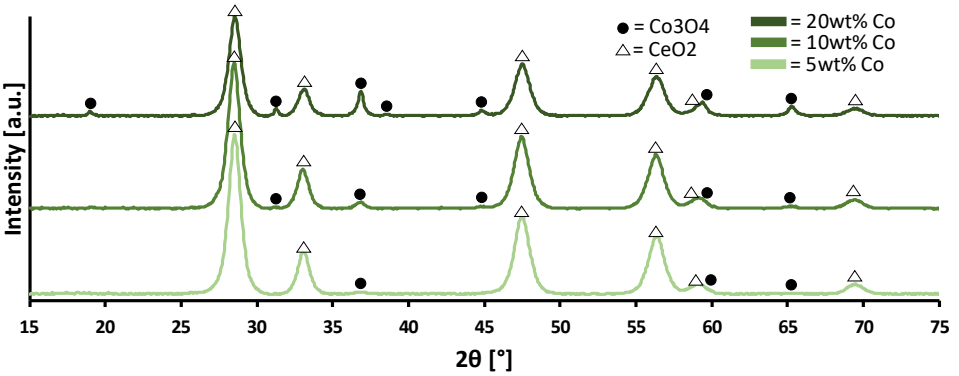

Figure 5.5: The XRD pattern of the cobalt oxides supported on CeO_2 with metal loading of 5, 10, and 20wt%Co.

From Figure 5.5, the peaks of Co_3O_4 were detected at 19.0, 31.2, 36.8, 38.5, 44.8, 59.3, and 65.2° for the catalyst with 20wt%Co. For the 10wt%Co, there was no peak detected at 19°. For the 5wt%Co, there was no detection of Co_3O_4 at 19, 38.5, and 44.8°. When choosing the peak to be used for the crystallite size calculation of the cobalt oxides, one of the peaks detected for the 5wt%Co was picked. The most prominent of the three peaks detected was the one at 36.8°, and there was no overlapping from ceria. The support may be reduced if there are low oxygen pressures at temperatures above 685 °C [36]. The XRD patterns detected that the support had the stoichiometry as CeO_2, which was expected as the calcination temperature did not exceed above 500 °C under the gas flow of air.

Figure 5.6 shows the XRD of the cobalt oxides supported on ZrO_2 with metal loading at 5, 10, and 20wt%Co:

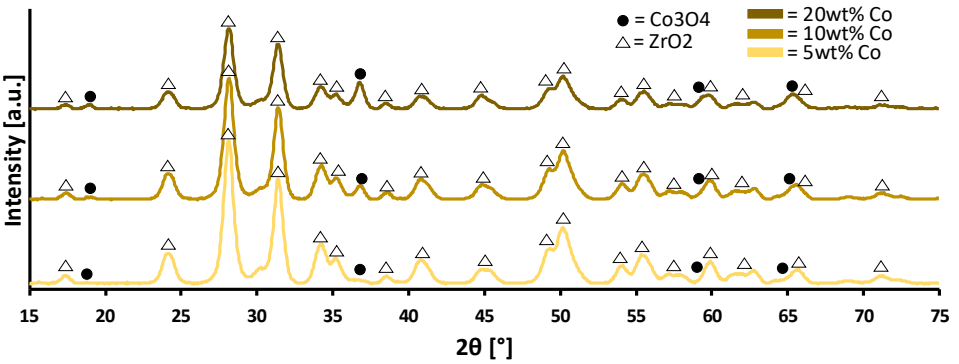

Figure 5.6: The XRD pattern of the cobalt oxides supported on ZrO_2 with metal loading of 5, 10, and 20wt%Co.

From the figure above, it can be seen that the zirconia has several peaks in the XRD pattern, far more than the supports previously shown. The intensity of the ZrO_2 peaks was decreased as the metal loading of cobalt was increased. The cobalt oxides in the form of Co_3O_4 was detected at 19.0, 36.7, 59.5, and 65.4° in the XRD patterns. These Co_3O_4 peaks did not have a significant increase in peak intensity except for the one at 36.7°. A challenge arises when the peak for crystallite size calculation needs to be chosen for the cobalt oxides, as all of the peaks are overlapping each other in various degrees. The one that seemed to most distinct for the Co_3O_4 was at approximately 36.7° and was chosen to determine the crystallite size of the cobalt oxides on zirconia.

To estimate the average crystallite size of the cobalt oxides, the Scherrer equation given in Equation 3.5 was used on the chosen peaks of Co_3O_4 from the XRD patterns for each of the supports. Subsequently, the particle size and dispersion of the cobalt oxides was calculated

by using Equation 3.6 and Equation 3.10, respectively. Table 5.2 shows the peak data used in the Scherrer equation and the crystallite size, particle size, and dispersion values of the Co_3O_4 on the various supported catalysts.

Table 5.2: A summation of the peak data used in the Scherrer equation and the crystallite size, particle size, and dispersion values of the Co_3O_4 on the various supported catalysts. K = 0.9, λ = 1.540 60 Å.

Catalyst	2θ [°]	β [°]	$\langle L \rangle (Co_3O_4)$ [a] [nm]	$d(Co_3O_4)$ [b] [nm]	D [c] [%]
$5Co/Al_2O_3$	59.39	0.78	12	16	8.2
$10Co/Al_2O_3$	59.44	0.75	12	16	7.8
$20Co/Al_2O_3$	59.38	0.67	14	18	7.1
$20Co\text{-}Pt/Al_2O_3$	59.39	0.69	15	20	6.5
$20Co\text{-}K/Al_2O_3$	59.41	0.57	16	21	6.0
$5Co/SiO_2$	59.24	0.72	13	17	7.5
$10Co/SiO_2$	59.26	0.63	15	20	6.6
$20Co/SiO_2$	59.31	0.60	15	20	6.3
$5Co/TiO_2$	59.02	0.93	10	13	9.7
$10Co/TiO_2$	59.36	0.93	10	13	9.7
$20Co/TiO_2$	59.29	0.83	11	15	8.7
$5Co/ZrO_2$	36.70	0.88	10	13	10.1
$10Co/ZrO_2$	36.78	0.57	15	19	6.6
$20Co/ZrO_2$	36.75	0.65	13	17	7.4
$5Co/CeO_2$	36.79	0.71	12	16	8.1
$10Co/CeO_2$	36.79	0.67	13	17	7.6
$20Co/CeO_2$	36.83	0.40	21	28	4.6

[a] $\langle L \rangle = \frac{K\lambda}{\beta cos\theta}$ [b] $d(Co_3O_4) = \frac{4}{3} \cdot \langle L \rangle (Co_3O_4)$ [c] $D = \frac{96}{0.75 \cdot d(Co_3O_4)}$

The overall trend observed in Table 5.2 was when the metal loading of cobalt increased, the crystallite size of the Co_3O_4 was increased. The same behavior was observed by Xiong et al., where increasing the metal loading of cobalt on alumina support caused the crystallite size of cobalt oxides to increase [54]. Higher amounts of the active metals present at the surface of the support contribute to particle growth of the cobalt oxides. As a consequence, the cobalt oxides available on the surface of the particles divided by the total amount in the particle decreases as the particles of Co_3O_4 increases, i.e., the dispersion value decreases as observed in the table above. One exception from this observation was with $10Co/ZrO_2$, where the crystallite size was the largest among the zirconia catalysts.

From the XRD-patterns it was shown that the zirconia support peaks were overlapping with the peaks from the cobalt oxides. This may have contributed to give an inaccurate representation of the crystallite size when using the Scherrer equation, where the shape of the Co_3O_4 peak was not ideal. Another explanation may be that the support structure of the support on 10Co/ZrO_2 differed from the rest of the zirconia supported catalysts, where the physical structure of the support may have changed. A decrease in surface area of the support may have contributed to the size enlargement of the crystallites. Smaller pore size and pore volume could potentially force the cobalt oxides particles to grow at the outer surface of the support. The latter could be the probable cause for the 20Co/CeO_2, where a sudden increase in crystallite size could be due to the restricted pore size and volume for ceria support. It could also be due to the impregnation procedure for this catalyst, as it was impregnated twice which could forced cobalt oxides to accumulate outside the pores after the second impregnation due to the pores being filled up from the first impregnation.

For the cobalt oxides supported on Al_2O_3, SiO_2, and TiO_2, the crystallite sizes were calculated from the Co_3O_4 peaks at approximately 59° in the XRD patterns. For the remaining catalysts supported on ZrO_2 and CeO_2, the Co_3O_4 peaks chosen for the calculation differed, where the peaks at approximately 37° were used. This was not an optimal procedure, as the crystallite size may differ depending on which peak was used. A more optimal approach would have been to calculate the crystallite size of several Co_3O_4 peaks and take the average value. In this case, it was was not a viable option since, on several occasions, the Co_3O_4 are overlapping with the peaks from the support material, and some Co_3O_4 peaks are not detected for the catalysts with lower metal loading of cobalt.

5.1.3 Temperature programmed reduction

To determine the reduction potential of the supported catalysts, TPR experiments were performed. Figure 5.7 shows the TPR-profiles for the cobalt oxides supported on Al_2O_3 with metal loading of 5, 10, and 20wt%Co:

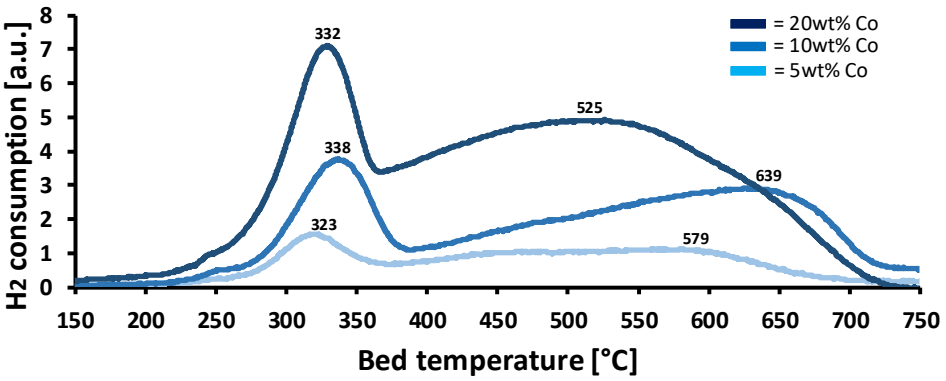

Figure 5.7: The TPR-profiles of the cobalt oxides supported on Al_2O_3 with metal loading of 5, 10, and 20wt%Co.

From the TPR-profiles in the figure above, it can be observed two reduction peaks for each of the catalysts. The two reduction peaks and their respective temperature ranges are similar to previous TPR studies on cobalt oxides supported on γ-Al_2O_3 [55][56]. For complete reduction to metallic cobalt, the two peaks suggest that the cobalt oxides, Co_3O_4, undergo reduction to Co^0 in two steps. In the first peak, the Co_3O_4 was reduced to CoO, followed by a further reduction to Co^0 in the second peak as seen in Equation 5.1 and 5.2 [57]:

$$Co_3O_4 + H_2 \longrightarrow 3\,CoO + H_2O \tag{5.1}$$

$$CoO + H_2 \longrightarrow Co + H_2O \tag{5.2}$$

At the first reduction peaks of the non promoted alumina catalysts, the measured temperature ranged between 323-338 °C, where increasing the metal loading of cobalt did not have a significant effect on the reduction temperature of these peaks. This was not the case for the second reduction peaks, where it was observed that increasing the metal loading of cobalt on alumina impacted the reduction temperature. The second reduction peak for 5wt%Co was more or less flat between 450-600 °C with the largest H_2 consumption at 579 °C. As the metal loading was increased to 10wt%Co, the second peak had a reduction temperature of 639 °C. Increasing the metal loading to 20wt%Co lowered the reduction temperature to 525 °C, which would suggest that increasing cobalt loading on alumina reduces the reduction temperature of the second peak. As reported by Tsakoumis et al., during catalyst preparation, the formation of irreducible cobalt phases may occur due to the strong metal-support interaction between the cobalt and alumina [32]. Less fraction of the irreducible phases are present as the metal loading of cobalt was increased on the alumina support, and more of the cobalt oxides are reducible. From the TPR-profiles, it can be observed that the first peaks start to reduce above 200 °C. As the Co content decreases, it would seem that the reduction temperature was delayed, indicating that the cobalt oxides

start to reduce at lower temperatures with increasing metal loading of cobalt [52].

Two $20Co/Al_2O_3$ catalysts were promoted, one with 0.5wt%Pt and the second one with 5wt%K. The TPR-profiles of the promoted Al_2O_3 catalysts and the $20Co/Al_2O_3$ as a reference are shown in Figure 5.8:

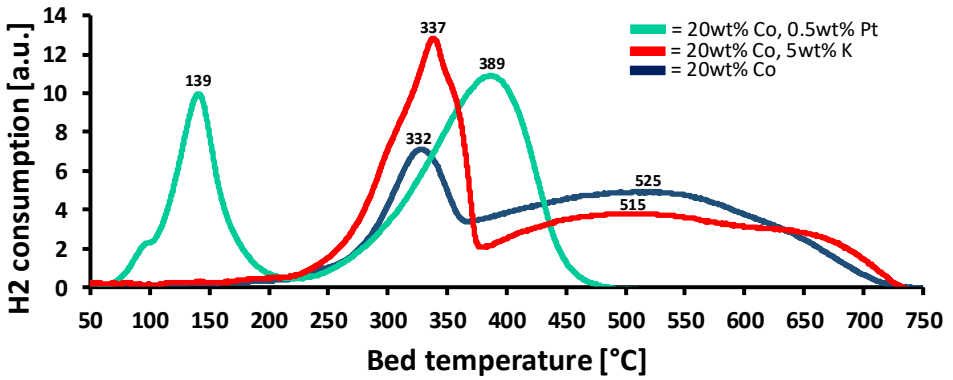

Figure 5.8: The TPR-profiles of the promoted catalyst supported on Al_2O_3 with the $20Co/Al_2O_3$ as a reference.

From Figure 5.8, it can be observed two reduction peaks for the Pt promoted catalyst. The first reduction peak temperature was at 139 °C, and the second reduction peak temperature was at 389 °C. The first peak was suggested to be the reduction of PtO_2 to the metallic Pt. From the second peak, it can be observed that adding the catalyst with Pt promoted the reducibility of the cobalt oxides, where the reduction to Co^0 lowered the reduction peak temperature from 525 to 389 °C. Similar trends were observed in previous work involving the reduction of cobalt oxides supported on alumina, which was promoted with platinum [58][59]. Looking into the potassium promoted catalyst, the two reduction peaks had an insignificant change in the peak temperatures. The H_2 consumption was increased in the first reduction peak while it was lowered in the second reduction peak. The potassium could have promoted the reducibility of the cobalt oxides in the first peak. Another possibility may be that the reduction to Co^0 was shifted towards lower temperature as observed with the Pt promoted catalyst. Chemisorption experiments from the project prior to the master thesis showed that the dispersion of Co^0 increased when the potassium was added, indicating that it potentially promoted the reducibility towards Co^0 [52].

Figure 5.9 shows the TPR-profiles for the cobalt oxides supported on TiO_2 with metal loading of 5, 10, and 20wt%Co:

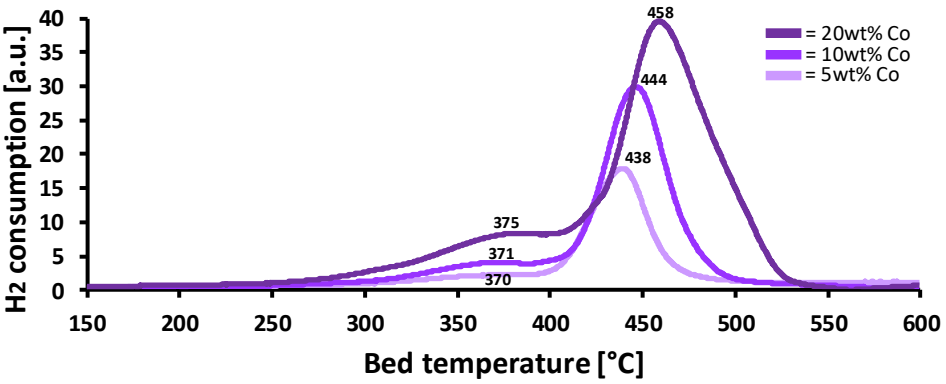

Figure 5.9: The TPR-profiles of the cobalt oxides supported on TiO_2 with metal loading of 5, 10, and 20wt%Co.

Two reduction peaks are observed for the TiO_2 catalysts in the figure above. The first reduction peaks measured a temperature range between 370-375 °C. Similar to the cobalt oxides supported on Al_2O_3, the metal loading had an insignificant effect on the first peak temperatures. However, for the second peaks, it can be observed that increasing the metal loading of cobalt increased the reduction peak temperatures, where it went from 438 °C for 5wt%Co to 458 °C for 20wt%Co. A similar trend has been previously reported, where it was suggested that when reducing the concentration of cobalt at the support surface, the reduction temperature was also reduced. It was stated it was due to the homogeneous distribution of the cobalt oxides both inside and outside of the pores of the TiO_2 support [60]. Another explanation may be that the reduction of the second peaks was kinetically limited due to the high heating rate of 10 °C min^{-1} during the TPR experiments. The reducibility from CoO to Co^0 seemed to be similar between the catalysts, where the left shoulder of the second peaks ascend approximately with similar H_2 consumption at given temperatures. As the cobalt oxides reduce, the concentration of metallic cobalt increases at the outer layer of the crystallites. The oxygen transport from the cobalt oxides in the center and towards the outer surface of the crystallites may have kinetically limited the reduction. By using a lower heating rate in the TPR experiments, the second reduction peak temperatures may have been more similar.

The first peak for $20Co/TiO_2$ starts to reduce above 250 °C, followed by the lower Co content catalysts, which start to reduce approximately up to 300 °C. This was higher compared to the alumina catalysts, indicating that the cobalt oxides on TiO_2 are harder to reduce. This could be explained by the metal-support interaction, where cobalt oxides supported on TiO_2 may have stronger interactions compared to the alumina catalysts. From the XRD results, the TiO_2 had among the smallest particles size of the cobalt oxides. Well-dispersed and small cobalt oxide particles could have contributed to the lower reduction potential of

Co_3O_4. The second reduction peaks were remarkably larger compared to the first reduction peaks, which was also the case for previous TPR studies of cobalt oxides on TiO_2 [61][62]. This observation may be due to the increased reducibility from CoO to Co^0 on TiO_2 at lower reduction temperature as seen by the high H_2 consumption in the second peaks. Another possibility may be that some of the Co_3O_4 reduction to CoO occurred at higher temperatures, contributing to more intensive H_2 consumption at the higher temperature range.

Figure 5.10 shows the TPR-profiles for the cobalt oxides supported on SiO_2 with metal loading of 5, 10, and 20wt%Co:

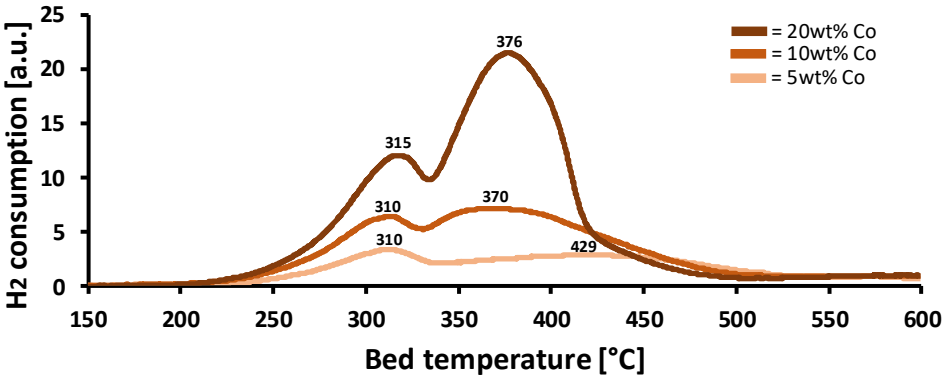

Figure 5.10: The TPR-profiles of the cobalt oxides supported on SiO_2 with metal loading of 5, 10, and 20wt%Co.

Similar to previously supported catalysts, two reduction peaks are observed in Figure 5.10. The first reduction peak temperatures were between 310-315 °C, where the metal loading had a minimal effect on the peak temperatures. This was also observed for the second reduction peaks where it varied between 370-376 °C. It should be noted that for 5Co/SiO2, the second reduction peak temperature was at 429 °C, but it was overall flat across the second peak. The H_2 consumption increased with Co loading for the two reduction peaks but was more dominant for the second reduction peaks. It would seem that the reducibility to Co^0 increased with the Co loading. Khodakov et al. studied the reducibility of cobalt oxides supported on silica, and it was suggested that the effect of metal-support interaction played a role in the reducibility of the cobalt particles. The smaller cobalt particles have stronger metal-support interactions compared to larger cobalt particles, where the stronger interaction for smaller particles stabilized the oxides particles and clusters in the silica [63]. It would seem to be the case, as the particle size of cobalt oxides increased with Co loading on SiO_2, although the particle size from 10 to 20wt%Co was minimally increased as seen from the XRD results. The first reduction peaks start to reduce the Co_3O_4 above

200 °C. It was similar to the alumina catalysts, but the H_2 consumption at the first peaks for the silica catalysts has higher intensity, which indicates that a higher amount of bulk Co_3O_4 have been reduced.

Figure 5.11 shows the TPR-profiles for the cobalt oxides supported on CeO_2 with metal loading of 5, 10, and 20wt%Co:

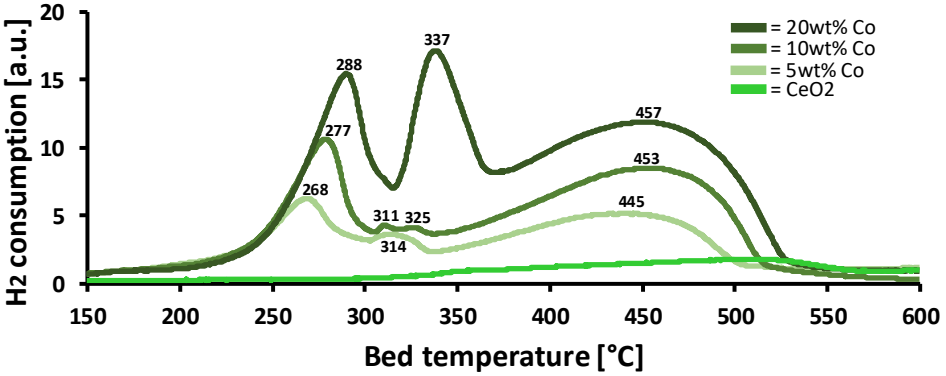

Figure 5.11: The TPR-profiles of the cobalt oxides supported on CeO_2 with metal loading of 5, 10, and 20wt%Co.

The catalysts shown in Figure 5.11 have three reduction peaks. Luo et al. had s similar observation for the hydrogen reduction of mesoporous Co_3O_4/CeO2 catalysts [64]. In their studies, it was suggested that the first reduction peaks measured between 268-288 °C correlate to the reduction of Co^{3+} to Co^{2+} at the interface between Co_3O_4 and CeO_2 [64]. The interaction between the cobalt oxides and ceria increased the reducibility of Co_3O_4, which can be observed by the lower reduction temperatures of the first peaks compared to Al_2O_3, TiO_2, and SiO_2 supported catalysts. In the second reduction peaks between 311-337 °C, it was suggested that the reduction of independent Co_3O_4 that are weakly interacting with the CeO_2 support goes directly to Co^0 [64]. From the figure above, it can be seen that the H_2 consumption for the second peak was significantly increased when the metal loading of cobalt went from 10 to 20wt%Co. From characterizations results given in section 5.1.1 and 5.1.2, it was shown that the calcined CeO_2 support had an average pore size diameter of 5.2 nm and that the average crystallite size of Co_3O_4 increased from 13 to 21 nm when the cobalt loading was increased from 10 to 20wt%Co. In comparison, the crystallite size from 5 to 10wt%Co only increased from 12 to 13 nm. These results indicate high crystallite growth of cobalt oxides outside of the pores in CeO_2 when the cobalt loading was increased to 20wt%Co. Thus, the higher fraction of Co_3O_4 at 20wt%Co that are weakly interacting with the support could have contributed to the high H_2 consumption observed at 337 °C. For the third peaks ranging between 445-457 °C, it was suggested that Co^{2+}

interacting with CeO_2 reduces to Co^0 [64]. Also, it can be seen from the TPR-profiles that the reduction of the first peaks start above 200 °C and was independent of the cobalt loading.

A TPR experiment was run for pure CeO_2, which can be seen in Figure 5.11. Above 300 °C, the H_2 consumption seems to be increasing until a peak was reached around 525 °C. Luo et al. suggested that the oxygen species at the surface are being reduced up to the given peak temperature [64]. This indicates that the CeO_2 may not be a inert support and could potentially contribute to the oxidation of NO to NO_2.

Figure 5.12 shows the TPR-profiles for the cobalt oxides supported on ZrO_2 with metal loading of 5, 10, and 20wt%Co:

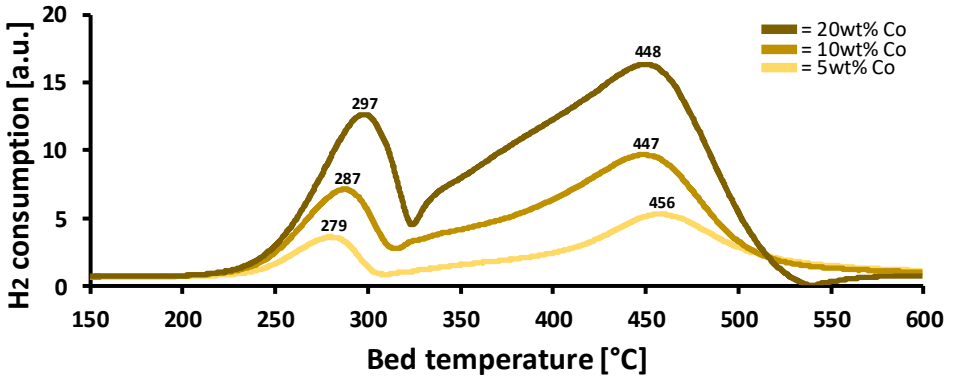

Figure 5.12: The TPR-profiles of the cobalt oxides supported on ZrO_2 with metal loading of 5, 10, and 20wt%Co.

From the figure above, it can be observed a two-step reduction of the cobalt oxides supported on zirconia. The first reduction peaks were measured between 279-297 °C and the second reduction peaks were measured between 448-456 °C. Similar to the CeO_2 supported catalyst, the reduction of the first peaks start above 200 °C, the first peak temperatures increase with cobalt loading and the measured temperature range are close with the first reduction peaks of CeO_2 supported catalysts. The first peak temperatures were lower compared to Al_2O_3, TiO_2, and SiO_2 supported catalysts, which indicate increased reducibility of cobalt oxides when supported on ZrO_2. The ZrO_2 material has weak acidic and basic properties at the surface, which could have contributed to weaker metal-support interaction and more reducibility of the cobalt oxides compared to Al_2O_3, TiO_2 and SiO_2. For the second peaks, it can be observed that the peak temperatures are more or less independent of the cobalt loading. The temperature reduced from 456 to 447 °C when the cobalt loading increased from 5 to 10wt%Co, which could be due to the increase of crystal-

lite size of the cobalt oxides. Larger particles could have contributed to weaker interaction with the support and increased the reducibility of the CoO. The TPR-profiles in Figure 5.12 were similar with previous studies on cobalt oxides supported on ZrO_2 [65][66].

The NO oxidation in nitric acid production occurs with the presence of water in the feed. To determine the effects of adding steam at the reactor inlet has on the reducibility of the cobalt oxides, wet-TPR experiments were performed on selected catalysts. The 20wt%Co catalysts supported on ZrO_2, CeO_2, Al_2O_3 and SiO_2 were tested with the presence of 6 % H_2O and 5 % H_2 in balance Ar and TPR-profiles are shown in Figure 5.13. Because of time limitations, the wet TPR experiment for TiO_2 catalyst was not performed and therefore not present in the figure below.

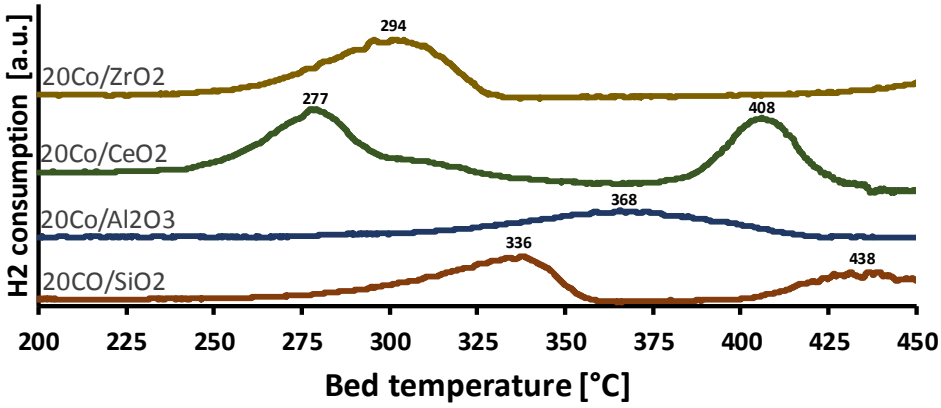

Figure 5.13: The wet-TPR profiles of the 20wt% supported on ZrO_2, CeO_2, Al_2O_3, and SiO_2.

Looking into the wet-TPR profiles, it can be observed that the start reduction for the catalysts has been delayed. For 20Co/ZrO_2, the first peak started to reduce just before 250 °C, but the peak temperature had an insignificant change. As water is a product in hydrogen reduction reaction, the increase of the partial pressure of steam may have inhibited the reducibility of the cobalt oxides. The reduction of CoO started at 325 °C in dry-TPR, but it can be seen that it was delayed to 425 °C in wet-TPR. In the case of 20Co/CeO_2, the first peak started to reduce above 225 °C in wet-TPR compared to 200 °C in dry conditions. The first peak temperature decreased from 288 to 277 °C in wet conditions. The compositions of the wet gas feed contained 5 % H_2 while it was 7 % H_2 in dry conditions. The lower partial pressure of hydrogen and the inhibition due to the presence of steam may have caused less fraction of the Co_3O_4 to be reduced at CeO_2 support. It should be noted that the ramp rate during wet-TPR was 5 °C min^{-1} compared to the 10 °C min^{-1} for the dry-TPR experiment. This may have caused the first peak temperature to be lowered due to more of the Co_3O_4 was reduced at lower temperatures. The second peak for CeO_2 was

delayed to 408 from 337 °C in the presence of steam.

For 20C/Al_2O_3 shown in Figure 5.13, it can be seen that the reduction of Co_3O_4 started around 275 °C, which was a significant increase from 200 °C in dry TPR. The first reduction peak shifted from 332 to 368 °C, which would indicate that the presence of steam lowered the reducibility of the cobalt oxides supported on Al_2O_3. For 20Co/SiO_2, the initial reduction went from 200 to 250 °C and the first peak temperature was shifted from 315 to 336 °C. For the second peak, the temperature was shifted from 376 to 438 °C. These results indicate that with the presence of steam, the reduction potential for the cobalt oxides reduced for all of the catalysts in Figure 5.13. In addition, the wet conditions for the NO oxidation have 15 % H_2O, which could further affect the reducibility of the cobalt oxides. As previously mentioned, Weiss et al. suggested that the NO oxidation depended on the reducibility of the Co_3O_4, where the cobalt oxides have reduction-oxidation cycles between Co^{3+} and Co^{2+} [22]. Based on the TPR-profiles, it is excepted that the NO conversion will be affected by the presence of steam in wet conditions during the NO oxidation to NO_2. Based on the comparison between dry and wet-TPR, it can be expected that the NO conversion starts at higher temperatures in wet conditions compared to the activity measurements in dry conditions due to the lower reducibility of cobalt oxides in the presence of steam. The research from Yu et al. on NO oxidation over supported cobalt oxides showed that the catalytic activity increased when the peak correlated to the reduction of Co^{3+} started at lower temperatures [28]. In the results of the activity measurements of the NO oxidation, the NO conversion curves were studied to see if the same correlation between the reduction of Co^{3+} from TPR experiments and the catalytic activity over the supported catalysts could be seen both in dry and wet process conditions.

5.2 NO oxidation activity measurements

In this section, the NO oxidation activity measurements of the catalysts are presented and discussed. In the first part, the activity measurement of a blank run was shown to determine the gas phase contribution during NO oxidation. In addition, activity measurements of the supports were investigated to determine if the materials were inert or contributed to the NO conversion. Furthermore, the activity measurement of unsupported Co_3O_4 was shown to determine the catalytic activity from pure cobalt oxides. After that, the activity measurements and stability tests of the cobalt oxides supported on given supports were presented and discussed. In the last part, the characterization and activity results are compared to determine which supported catalysts exhibit the highest NO conversion and to determine any trends between activity and catalyst characteristics.

There were different back-pressure contributions in the activity measurements, depending

on the catalysts used. To improve the comparison between the results, all of the NO conversion curves of the catalysts were adjusted such that the curves begin approximately from the same conversion level as the gas phase contribution at 150 °C. Unaltered raw data can be found in Appendix E.

5.2.1 Blank run, supports and unsupported Co_3O_4

The NO oxidation to NO_2 is a homogeneous gas phase reaction in nitric acid production. Looking into the reaction given in Equation 1.5, the rate coefficient is reverse dependent on the temperature, which means the reaction is favored by low temperature. Also, the reaction is favored by high pressure. In order to determine the gas phase contribution, activity measurements of NO oxidation were performed where the reactor was filled with 2.75 g of SiC. Figure 5.14 shows the activity measurements of the gas phase conversion with SiC and the thermodynamic equilibrium:

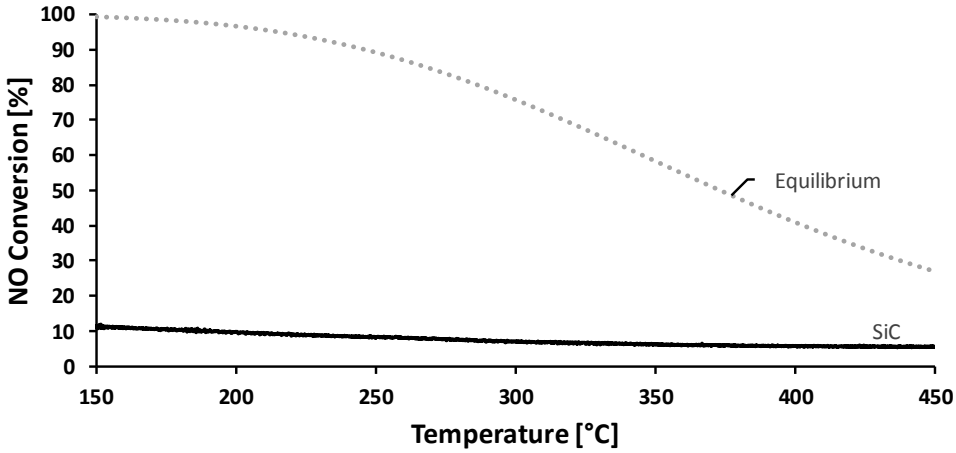

Figure 5.14: The activity measurement of the gas phase conversion with 2.75 g SiC and the thermodynamic equilibrium. GHSV = 43 400 h^{-1}. Feed: 10 % NO, 6 % O_2, rest Ar.

From the figure above, the gas phase conversion went from 11.1 % at 150 °C to 5.3 % at 450 °C. The inverse dependency on the temperature in the gas phase reaction showed that the conversion curve reduced as the temperature was increased. It was also performed a run in wet conditions where the feed contained 15 % H_2O, but it gave no change in the gas phase conversion. This blank run with only SiC showed in Figure 5.14 was given as the baseline for gas phase contribution in all of the activity measurements of the catalysts, where it diminished between the gas phase conversion and the conversion due to the catalytic activity from the supported catalysts.

The support materials are commonly considered as inert in supported catalysts. The supports Al_2O_3, TiO_2, ZrO_2, and SiO_2 have been previously run in the same reactor setup and did not give additional catalytic activity for the NO oxidation, where it followed the gas phase conversion as shown in Figure 5.14. However, this was not the case when NO oxidation activity measurement was run with calcined CeO_2 support. Figure 5.15 shows the activity measurements of the NO oxidation over 500 mg CeO_2 and 2.75 SiC in dry and wet conditions:

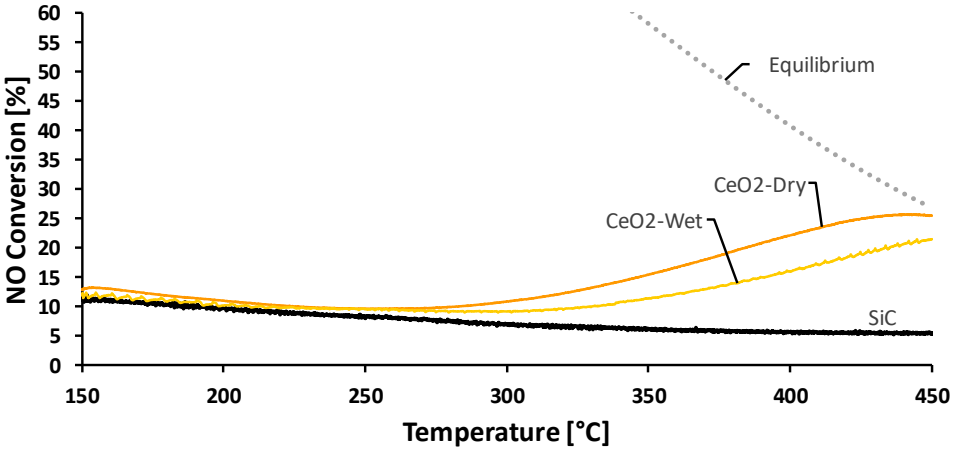

Figure 5.15: The NO to NO_2 conversion over CeO_2 in dry and wet conditions. GHSV = 43 400 h^{-1}. Dry feed: 10 % NO, 6 % O_2, rest Ar. Wet feed: 10 % NO, 6 % O_2, 15 % H_2O, rest Ar.

From Figure 5.15, it can be seen that the CeO_2 support has catalytic activity towards NO oxidation. In dry conditions, the maximum conversion was 26 % at 441 °C. In wet conditions, the maximum conversion was 21 % at 450 °C. In dry conditions at 350 °C, the NO conversion and rate of reaction were 15 % and 2.6 µmol s^{-1} g_c^{-1}, respectively. In wet conditions at 350 °C, the conversion and rate of reaction were 11 % and 1.4 µmol s^{-1} g_c^{-1}, respectively. In the figure above, it can be observed that the catalytic activity started above 250 °C in dry conditions and around 300 °C in wet conditions. From the TPR-profile of CeO_2, the H_2 reduction started at around 300 °C and showed that the support might have the potential for reduction to oxidize the NO to NO_2. These results indicated that the CeO_2 acted as a non-inert support and could potentially contribute to the NO oxidation together with supported cobalt oxides.

The active components in the supported catalysts are the cobalt oxides, Co_3O_4. Activity measurements of unsupported Co_3O_4 were performed to see if the catalytic performance may be improved by supporting the cobalt oxides at given support material. Figure 5.16 shows the activity measurements of the NO oxidation over 500 mg Co_3O_4 and 2.75 g SiC

in dry and wet conditions:

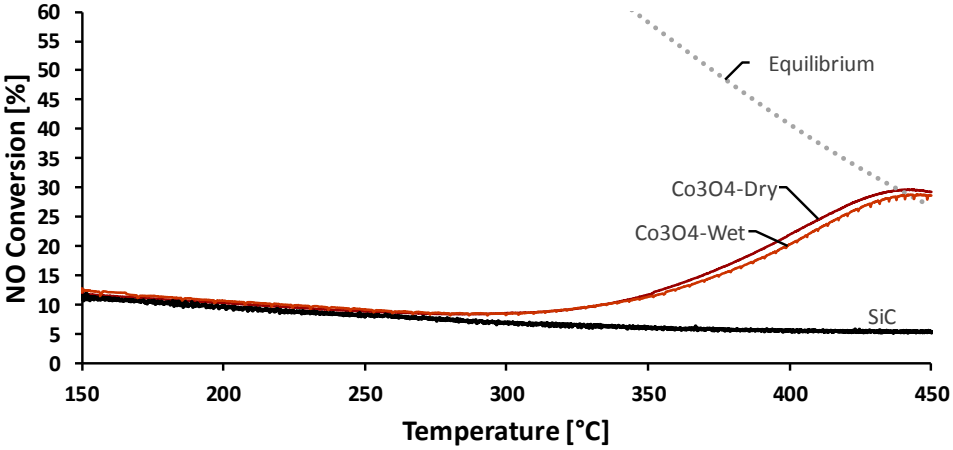

Figure 5.16: The NO to NO_2 conversion over Co_3O_4 in dry and wet conditions. GHSV = 43 400 h^{-1}. Dry feed: 10 % NO, 6 % O_2, rest Ar. Wet feed: 10 % NO, 6 % O_2, 15 % H_2O, rest Ar.

From Figure 5.16, it can be seen that the presence of steam in the wet conditions did not have a significant effect on the conversion levels. The maximum conversion in dry condition was 30 % at 443 °C and in wet conditions the maximum conversion was 29 % at 443 °C. In dry conditions at 350 °C, the conversion and rate of reaction were 12 % and 1.6 µmol s^{-1} g_c^{-1}, respectively. In wet conditions at 350 °C, the conversion and rate of reaction were 11 % and 1.5 µmol s^{-1} g_c^{-1}, respectively. Compared to CeO_2, the unsupported Co_3O_4 was outperformed in dry conditions at 350 °C, but the conversion and rate of reaction at 350 °C were similar in wet conditions. Using pure unsupported Co_3O_4 did not seem to give a significant high NO conversion levels at lower temperatures. In the results of the NO oxidation activity measurements of the supported catalysts, it can be seen if supporting the cobalt oxides contributes to increased catalytic activity.

5.2.2 Supported cobalt oxides on alumina

Figure 5.17 shows the activity measurements of NO oxidation over the cobalt oxides supported on Al_2O_3 with metal loading of 5, 10, and 20wt%Co in dry conditions:

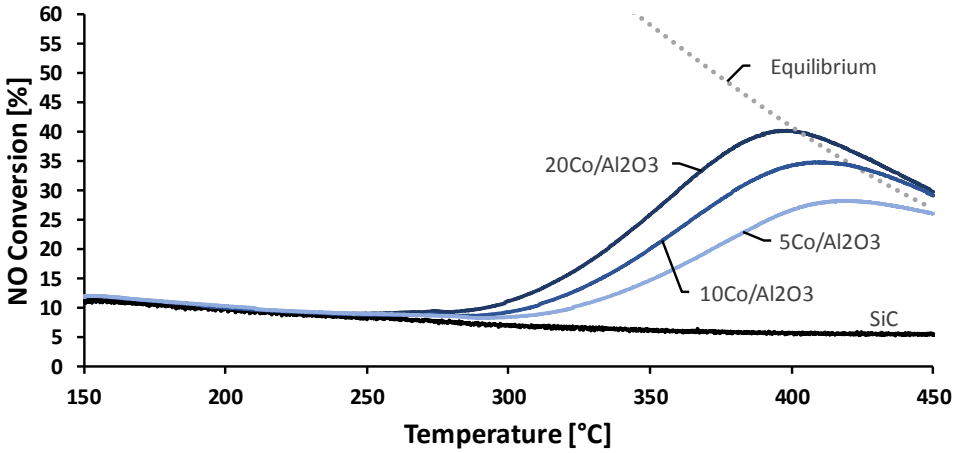

Figure 5.17: The NO to NO_2 conversion over cobalt oxides supported on Al_2O_3 with metal loading of 5, 10, and 20wt%Co in dry conditions. GHSV = 43 400 h^{-1}. Feed: 10 % NO, 6 % O_2, rest Ar.

From Figure 5.17, it can be seen that the conversion increased with cobalt loading, where $20Co/Al_2O_3$ had the highest activity across the temperature range. The slope of the curves was increasing with cobalt loading, and the initial catalytic activity of the curves seem to begin at different temperatures. From the TPR-profiles of the alumina supported catalysts, it was shown that the temperature of the initial reduction of Co_3O_4 was shifted to lower temperatures with increasing cobalt loading. It would indicate that the NO conversion was affected by the reducibility of the cobalt oxides and the number of Co_3O_4 available at the surface of the alumina support. It can be observed that the conversion curves go beyond the equilibrium line, which should not be possible as that is the thermodynamic equilibrium. Experimental errors such as increased pressure in the reactor due to back pressure build up, and imprecise temperature measurement of the catalyst bed could have caused the conversion curve to exceed the equilibrium line.

Table 5.3 shows the maximum conversion with the respective temperature and the conversion, rate of reaction, and turnover frequency at 350 °C of the NO conversion curves given in Figure 5.17:

Table 5.3: An overview of the results from the activity performance over the alumina supported catalysts in dry conditions.

Catalyst	20Co	10Co	5Co
Maximum conversion [%]	40	35	28
Respective temperature [°C]	398	410	417
Conversion at 350 °C [%]	26	20	15
Rate of reaction [$\mu mol\,s^{-1}\,g_c^{-1}$]	5.5	3.9	2.4
Turnover frequency [s^{-1}]	0.023	0.029	0.034

From the table above, the 20Co/Al_2O_3 had the highest conversion of 40 % at 398 °C. As the cobalt loading decreased, the maximum conversion declined, and the respective temperature was shifted towards higher temperatures. The 20Co/Al_2O_3 had 26 % conversion at 350 °C with a rate of reaction equal to 5.5 $\mu mol\,s^{-1}\,g_c^{-1}$, which was the largest among the three alumina supported catalysts. In regards to the TOF values, it can be seen to increase as the cobalt loading decreased. The TOF values, which determine the number of molecules reacted per active site per unit of time, were more optimal as the metal loading of cobalt was decreased. However, the performance of the low Co content catalysts supported on Al_2O_3 in terms of conversion and rate of reaction at 350 °C was low compared to the performance of the 20Co/Al_2O_3 catalysts.

Figure 5.18 shows the activity measurements of NO oxidation over the cobalt oxides supported on Al_2O_3 with metal loading of 5, 10, and 20wt%Co in wet conditions:

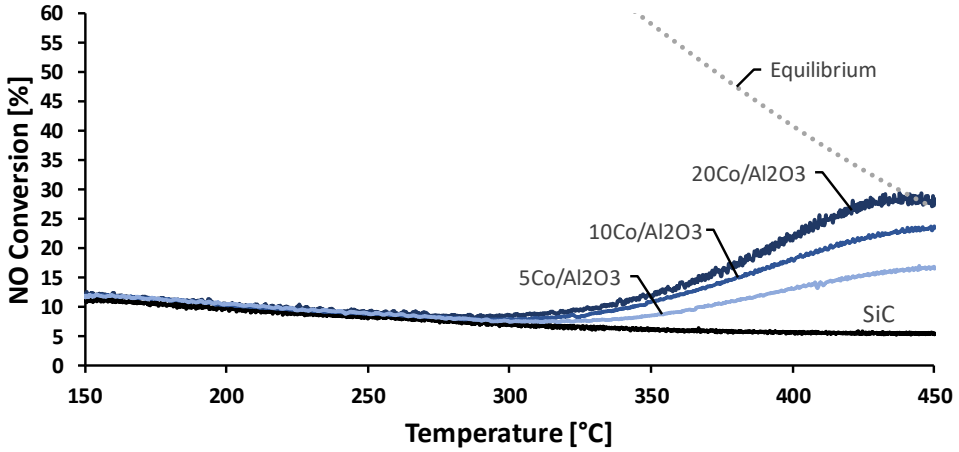

Figure 5.18: The NO to NO_2 conversion over cobalt oxides supported on Al_2O_3 with metal loading of 5, 10, and 20wt%Co in wet conditions. GHSV = 43 400 h^{-1}. Feed: 10 % NO, 6 % O_2, 15 % H_2O, rest Ar.

From the figure above, it can be seen that the NO conversion increases with cobalt loading, where 20Co/Al_2O_3 achieved the highest conversion among the alumina supported catalysts. The difference in the conversion curves in wet conditions was similar to the trend of the conversions curves in dry conditions. A difference between dry and wet conditions was that the catalytic activity initiated at different temperatures. In dry conditions, the catalytic activity started above 250 °C, while in wet conditions it was shifted towards 300 °C. From the wet-TPR experiment for 20Co/Al_2O_3, it was shown that the initial reduction of Co_3O_4 was shifted to a higher temperature with the presence of steam. The lower reducibility of the cobalt oxides may have decreased the slope of the curves due to the presence of steam. As a consequence, the NO conversion was limited by the equilibrium before reaching any high levels.

Table 5.4 shows the maximum conversion with the respective temperature and the conversion, rate of reaction, and turnover frequency at 350 °C of the NO conversion curves given in Figure 5.18:

Table 5.4: An overview of the results from the activity performance over the alumina supported catalysts in wet conditions.

Catalyst	20Co	10Co	5Co
Maximum conversion [%]	30	24	17
Respective temperature [°C]	438	450	445
Conversion at 350 °C [%]	12	11	8
Rate of reaction [$\mu mol\, s^{-1}\, g_c^{-1}$]	1.6	1.3	0.7
Turnover frequency [s^{-1}]	0.006	0.010	0.010

From Table 5.4, the 20Co/Al_2O_3 achieved the highest maximum conversion of 30 % at 438 °C, while 5Co/Al_2O_3 only reached maximum conversion of 17 % at 445 °C. The conversion at 350 °C for 10 and 20wt%Co were close, with only one percentage point difference. Still, the 20wt%Co performed better in regards to the given conversion levels and rate of reaction. Looking into the TOF values, it can be noted that as the cobalt loading decreased the TOF was increased. However, for 5 and 10wt%Co the TOF values were equal $0.010\, s^{-1}$. The difference between the TOF values was less compared to the ones given in dry conditions.

Figure 5.19 shows the stability tests for the cobalt oxides supported on Al_2O_3 with metal loading of 5, 10, and 20wt%Co:

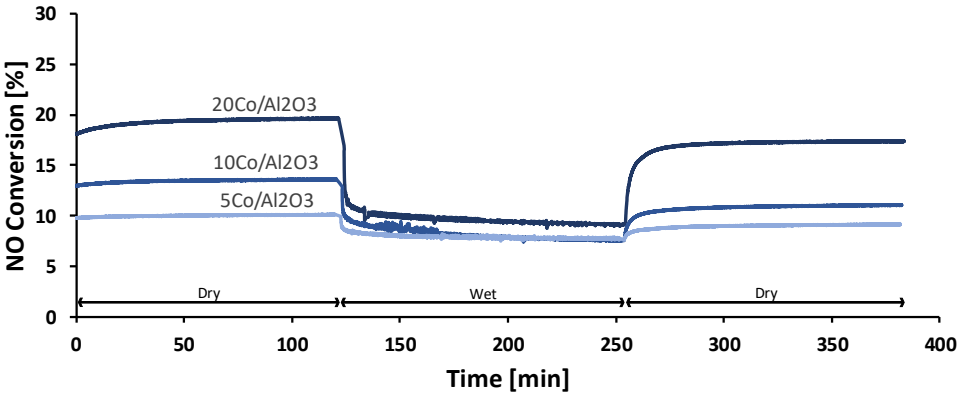

Figure 5.19: The stability tests at 350 °C for the cobalt oxides supported on Al_2O_3 with metal loading of 5, 10, and 20wt%Co. GHSV = 43 400 h^{-1}. Dry feed: 10 % NO, 6 % O_2, rest Ar. Wet feed: 10 % NO, 6 % O_2, 15 % H_2O, rest Ar.

The stability test above shows a sequence of three periods, which ran at 350 °C. The first period was in dry conditions for 2 hours, followed by wet conditions for 2 hours and the final period in dry conditions for an additional 2 hours. The conversion level in the first dry run seemed to be stable, indicating no significant deactivation of the catalysts. When wet conditions were introduced, it can be observed that the presence of steam caused immediate activity loss of the catalysts. As the stability tests in wet conditions were going on, it can be seen to deactivate the catalytic activity with time. When the second dry run began, the conversion levels increased and were stable for the remaining time. Table 5.5 shows the average conversion values in each of the periods with the regeneration and activity loss of the alumina supported catalysts.

Table 5.5: The average conversions from each period in the stability test of the alumina supported catalysts with the calculated regeneration and activity loss.

Catalyst	1st Dry [%]	Wet [%]	2nd Dry [%]	Regeneration [a] [%]	Activity loss [b] [%]
20Co	19	10	17	88	51
10Co	13	8	11	80	41
5Co	10	8	9	90	22

[a] Regeneration = 2nd Dry / 1st Dry [b] Activity loss = 1 - Wet / 1st Dry

From Table 5.5, the regeneration after the catalysts experienced wet conditions affected the most for the 10Co/Al_2O_3, where the regeneration was equal to 80 %. For 5Co/Al_2O_3 and 20Co/Al_2O_3, the regeneration was equal to 90 and 88 %, respectively. The activity loss due to the presence of steam had the most inhibition effect on the conversion as the cobalt

loading increased. For $20Co/Al_2O_3$ the activity loss was at 51 %, while for $5Co/Al_2O_3$ it was equal to 22 %. It should be noted that only 2 hours in each of the periods can only indicate the initial deactivation and activity loss of the supported catalysts. For more thorough stability testing, the time duration must be increased to ensure steady-state values are achieved. Nevertheless, the short time period of 2 hours in each period was sufficient enough to indicate the initial deactivation and activity loss of supported catalysts by introducing steam into the feed.

By looking into the activity measurements performed both in dry and wet conditions, the $20Co/Al_2O_3$ had the highest maximum conversion at the lowest respective temperature and had the best conversion and rate of reaction at 350 °C among the alumina support catalysts. The increased reducibility of the Co_3O_4 with cobalt loading seemed to have increased the NO conversion. These results may indicate that the reducibility of the cobalt oxides played an important part in NO oxidation over the alumina supported catalysts. The $5Co/Al_2O_3$ had the highest TOF values in both dry and wet conditions but had the lowest conversions and rate of reactions compared to the other two supported catalysts. From the stability test, it was shown that $20Co/Al_2O_3$ outperformed the two other in terms of conversion levels, but had the highest activity loss due to the presence of steam. After the wet period, the $10Co/Al_2O_3$ had the least regeneration among the catalysts, followed by $20Co/Al_2O_3$ and $5Co/Al_2O_3$.

5.2.3 Promoted alumina supported cobalt oxides catalysts

Two $20Co/Al_2O_3$ catalysts were promoted, one with 0.5wt% Pt and the second one with 5wt% K. These catalysts were made to investigate if adding promoters could potentially increase the NO oxidation. Figure 5.20 shows the activity measurements of NO oxidation over the promoted catalyst supported on Al_2O_3 with $20Co/Al_2O_3$ as a reference in dry conditions:

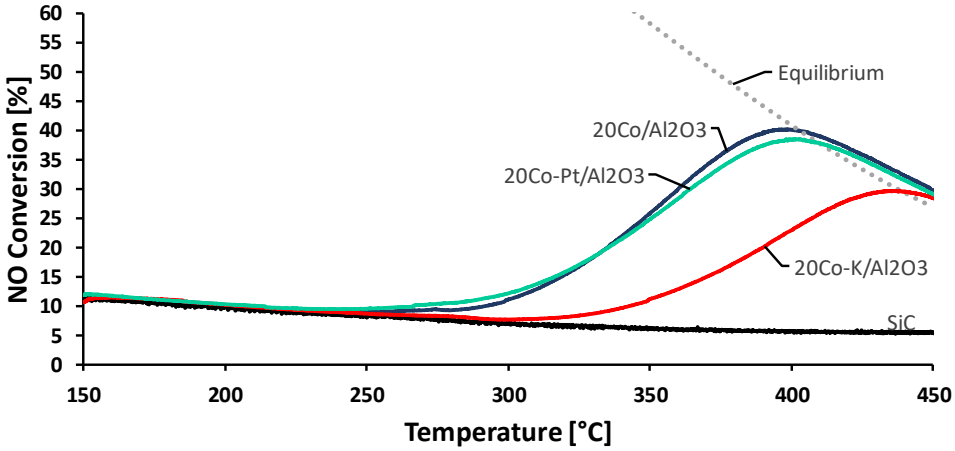

Figure 5.20: The NO to NO_2 conversion over the promoted catalyst supported on Al_2O_3 with $20Co/Al_2O_3$ as a reference in dry conditions. GHSV = 43 400 h^{-1}. Feed: 10 % NO, 6 % O_2, rest Ar.

From Figure 5.20, the conversion curve for the Pt promoted and the reference catalyst was similar across the temperature range. The Pt promoted had initially higher conversion at lower temperatures, but was taken by the $20Co/Al_2O_3$ towards 350 °C. From the TPR-profiles, it was shown that the initial Co_3O_4 reduction was more or less unaffected by the Pt promotion, where the Pt may have mainly contributed to have increased reduction towards Co^0 and not any significant change in the reduction of Co^{3+}. In the case of the K promoted catalyst, the conversion was greatly affected by the addition of potassium at the support surface. From the TPR-profile, it was shown that the initial reduction of the first peak correlated to the reduction of Co^{3+} was shifted towards lower temperatures compared to the reference catalyst. Looking into the conversion curve for the K promoted catalyst, it indicates that the reduction of Co^{3+} was reduced and not increased. The presence of potassium at the surface may have blocked the active cobalt oxides sites, causing the overall lower conversion across the measured temperature range. Same as the alumina supported catalysts, the curves are overshooting the equilibrium line in Figure 5.20, which could be due to inaccurate measurements of the actual temperature and back pressure build up.

Table 5.6 shows the maximum conversion with the respective temperature and the conversion, rate of reaction, and turnover frequency at 350 °C of the NO conversion curves given in Figure 5.20:

Table 5.6: An overview of the results from the activity performance over the promoted catalysts and the $20Co/Al_2O_3$ in dry conditions.

Catalyst	20Co	20Co-Pt	20Co-K
Maximum conversion [%]	40	38	30
Respective temperature [°C]	398	403	437
Conversion at 350 °C [%]	26	25	11
Rate of reaction [$\mu mol\,s^{-1}\,g_c^{-1}$]	5.5	5.2	1.4
Turnover frequency [s^{-1}]	0.023	0.024	0.007

From Table 5.6, the $20Co/Al_2O_3$ had the highest maximum conversion of 40 % at 398 °C, but was similar with the Pt promoted catalyst which had maximum conversion of 38 % at 403 °C. For the $20Co/Al_2O_3$, the conversion, rate of reaction, and TOF at 350 °C were equal to 26 %, 5.5 $\mu mol\,s^{-1}\,g_c^{-1}$, and 0.023 s^{-1}, respectively. The activity performance of the Pt promoted was slightly lower than the $20Al_2O_3$ at 350 °C but was more or less the same. The K promoted at 350 °C was significantly worse compared to the $20Co/Al_2O_3$, which indicate that the potassium deactivated the catalytic performance of the $20Co/Al_2O_3$.

Figure 5.21 shows the activity measurements of NO oxidation over the promoted catalyst supported on Al_2O_3 with $20Co/Al_2O_3$ as a reference in wet conditions:

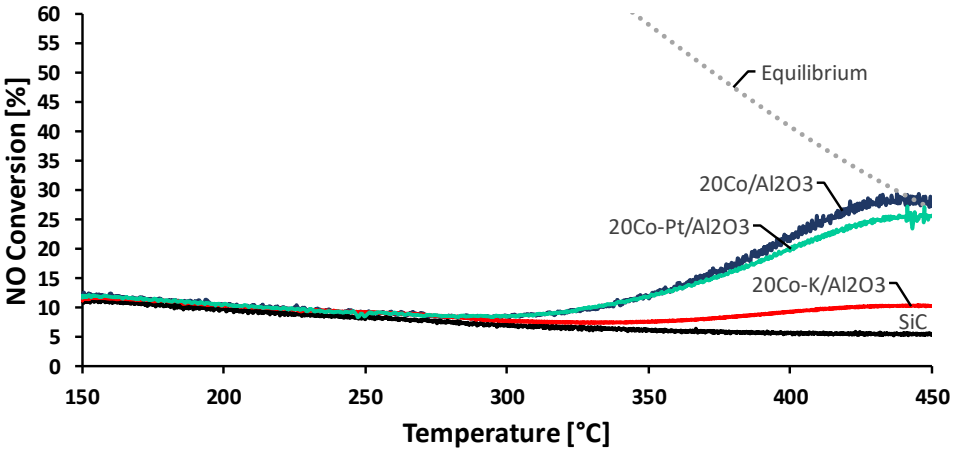

Figure 5.21: The NO to NO_2 conversion over the promoted catalyst supported on Al_2O_3 with $20Co/Al_2O_3$ as a reference in wet conditions. GHSV = 43 400 h^{-1}. Feed: 10 % NO, 6 % O_2, 15 % H_2O, rest Ar.

From the figure above, it can be observed that conversion curves follow the same trend as

the ones given in dry conditions. The conversion curves of the Pt promoted catalyst and the 20Co/Al_2O_3 are similar until the Pt promoted catalyst was outperformed above 375 °C. The conversion curve of the K promoted catalyst was considerably lower in wet conditions, where there was almost no catalytic activity up to 350 °C. Even up to 450 °C, the K promoted catalyst had small catalytic activity. The presence of steam has shifted the initial catalytic activity towards higher temperatures similar to the affected reducibility of cobalt oxides observed in the wet-TPR profiles. The slopes were also decreased in the presence of steam, similar to the observations of the alumina supported catalysts in wet conditions. This would result in the conversion curves reaching the thermodynamic equilibrium before achieving any high maximum conversions.

Table 5.7 shows the maximum conversion with the respective temperature and the conversion, rate of reaction, and turnover frequency at 350 °C of the NO conversion curves given in Figure 5.21:

Table 5.7: An overview of the results from the activity performance over the promoted catalyst and the 20Co/Al_2O_3 in wet conditions.

Catalyst	20Co	20Co-Pt	20Co-K
Maximum conversion [%]	29	27	10
Respective temperature [°C]	438	441	450
Conversion at 350 °C [%]	12	12	7
Rate of reaction [$\mu mol\, s^{-1}\, g_c^{-1}$]	1.6	1.6	0.4
Turnover frequency [s^{-1}]	0.006	0.007	0.002

From Table 5.7, the 20Co/Al_2O_3 had the largest maximum conversion of 29 % at 438 °C, followed closely by the Pt promoted catalyst with maximum conversion of 27 % at 441 °C. The K promoted catalyst had the maximum conversion of 10 % at 450 °C. At 350 °C, the conversion, rate of reaction, and the TOF were the same for both the Pt promoted catalyst and 20Co/Al_2O_3 in wet conditions. However, at 350 °C the K promoted catalyst had only 7 % total conversion, where 6.1 percentage points of the conversion correlated to gas phase contribution, which gave only 0.9 % catalytic conversion. Hence, the low rate of reaction and TOF value from the K promoted catalyst in wet conditions.

Figure 5.22 shows the stability tests of the promoted catalyst supported on Al_2O_3 with 20Co/Al_2O_3 as a reference:

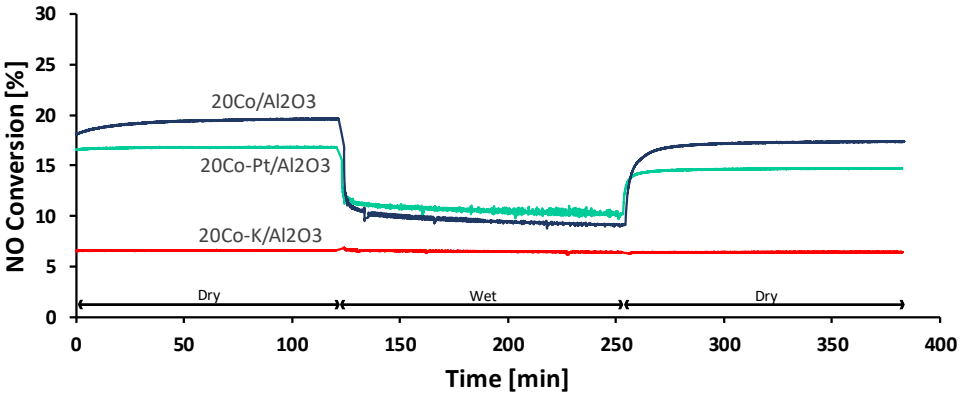

Figure 5.22: The stability tests at 350 °C for the promoted catalysts supported on Al_2O_3 with $20Co/Al_2O_3$ as reference. GHSV = 43 400 h^{-1}. Dry feed: 10 % NO, 6 % O_2, rest Ar. Wet feed: 10 % NO, 6 % O_2, 15 % H_2O, rest Ar.

The stability tests shown in Figure 5.22 were performed at 350 °C with a sequence of dry, wet, and then again dry conditions, where each period had a time duration of 2 hours. In the first dry run, it can be seen that the conversions were stable across the time duration with a gradual increase for the $20Co/Al_2O_3$. When steam was introduced, it can be seen to give activity loss for both the Pt promoted catalyst and $20Co/Al_2O_3$. Interestingly, the Pt promoted catalyst performed better in wet conditions compared to $20Co/Al_2O_3$ even when it had less catalytic activity in dry conditions. Salman et al. reported that a Pt/Al_2O_3 catalyst had insignificant changes in NO conversion between dry and wet feed under Ostwald process conditions [12]. Promoting the $20Co/Al_2O_3$ with platinum may have contributed to the catalyst to be more resistant towards the presence of steam, as observed from the conversions in wet conditions in Figure 5.22. In the second dry run, the conversions increased in the absence of steam and were stable during the time duration of the run for the Pt promoted catalyst and $20Co/Al_2O_3$. For the K promoted catalyst, it can be observed to more or less no change between dry and wet conditions due to being purely gas phase contribution and no catalytic activity at 350 °C. Table 5.8 shows the average conversion values in each of the periods with the regeneration and activity loss of the promoted catalysts and $20Co/Al_2O_3$.

Table 5.8: The average conversions from each period in the stability test of the promoted catalysts and $20Co/Al_2O_3$ with the calculated regeneration and activity loss.

Catalyst	1st Dry [%]	Wet [%]	2nd Dry [%]	Regeneration [a] [%]	Activity loss [b] [%]
20Co	19	10	17	88	51
20Co-Pt	17	11	15	87	37
20Co-K	7	6	6	97	2

[a] Regeneration = 2nd Dry / 1st Dry [b] Activity loss = 1 - Wet / 1st Dry

When it comes to the regeneration, it was similar between the Pt promoted catalyst and $20CO/Al_2O_3$. However, in regards to the activity loss due to the presence of steam, it can be seen that it went from 51 to 37 % when promoting the $20Co/Al_2O_3$ with 0.5wt%Pt. This indicates that promoting a supported cobalt oxide catalyst with platinum could potentially be a method to reduce the inhibition effects of water during NO oxidation. Still, each of the periods only lasted for 2 hours, which was not sufficient enough to make any conclusions in regards to long terms effects. Nevertheless, promoting with platinum may have the potential to improve the catalytic activity of NO oxidation in Ostwald process conditions. For the K promoted catalyst, it can be seen to have high regeneration and low activity loss. As the conversion in each period was mostly gas phase contribution, these calculated values do not give any valid information. The catalyst was not active at 350 °C, which shows that promoting the catalyst with potassium did not improve the catalytic activity of the cobalt oxides.

5.2.4 Supported cobalt oxides on titania

Figure 5.23 shows the activity measurements of NO oxidation over the cobalt oxides supported on TiO_2 with metal loading of 5, 10, and 20wt%Co in dry conditions:

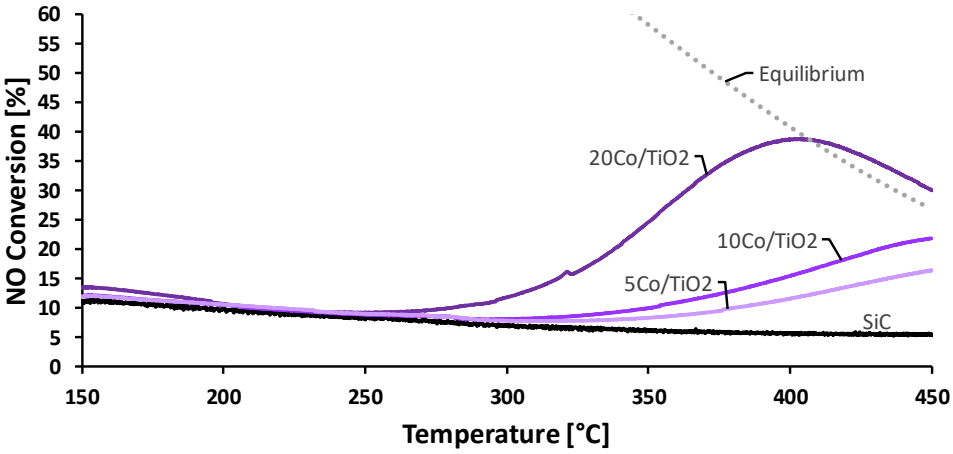

Figure 5.23: The NO to NO_2 conversion over cobalt oxides supported on TiO_2 with metal loading of 5, 10, and 20wt%Co in dry conditions. GHSV = 43 400 h^{-1}. Feed: 10 % NO, 6 % O_2, rest Ar.

From the figure above, it can be seen that the conversion was increased with cobalt loading, where the 20Co/TiO_2 had the highest conversion across the temperature range. The initial catalytic activity of the catalysts started at different temperatures, where the temperature was increased with decreasing cobalt loading. In the TPR-profiles of the TiO_2 support catalysts, the initial reduction of Co_3O_4 for 20Co/TiO_2 started around 250 °C and for the two other catalysts it started around 300 °C. This was the case when looking into the initial catalytic activity of the catalysts, where it started at the same temperatures as the initial reduction of the cobalt oxides in the TPR-profiles. This shows that the NO conversion at the TiO_2 supported catalysts are dependent on the reduction of the Co_3O_4. The slope of the conversion curve increases with cobalt loading, which may indicate that the NO oxidation was increased due to more active sites at the support surface. Similar to previous activity measurements, the equilibrium line was exceeded due to inaccurate measurements of the actual temperature and back pressure contributions.

Table 5.9 shows the maximum conversion with the respective temperature and the conversion, rate of reaction, and turnover frequency at 350 °C of the NO conversion curves given in Figure 5.23:

Table 5.9: An overview of the results from the activity performance over the TiO_2 supported catalysts in dry conditions.

Catalyst	20Co	10Co	5Co
Maximum conversion [%]	39	22	16
Respective temperature [°C]	403	450	450
Conversion at 350 °C [%]	25	10	8
Rate of reaction [$\mu mol\,s^{-1}\,g_c^{-1}$]	5.1	1.1	0.6
Turnover frequency [s^{-1}]	0.017	0.006	0.007

The 20Co/TiO_2 achieved the highest maximum conversion of 39 % at 403 °C, as shown in Table 5.9. As the cobalt loading decreased, the maximum conversion decreased with the respective temperature shifted towards higher values. At 350 °C, the 20Co/TiO_2 had a conversion, rate of reaction and TOF equal to 25 %, 5.1 $\mu mol\,s^{-1}\,g_c^{-1}$ and 0.017 s^{-1}, respectively. The 5Co/TiO_2 and 10Co/TiO_2 had significantly lower activity performance at 350 °C due to the initial catalytic activity starting after 300 °C. This impacted the conversions at 350 °C, which were only 10 and 8 % for 10Co/TiO_2 and 5Co/TiO_2, respectively. The total conversions at 350 °C caused the catalytic performance to be small at this point, which can be seen by the low rate of reactions of these two catalysts. The TOF values increased with cobalt loading, which could have been caused by the low catalytic activity in relation to the number of cobalt oxides available at the support surface for 5 and 10wt%Co.

Figure 5.24 shows the activity measurements of NO oxidation over the cobalt oxides supported on TiO_2 with metal loading of 5, 10, and 20wt%Co in wet conditions:

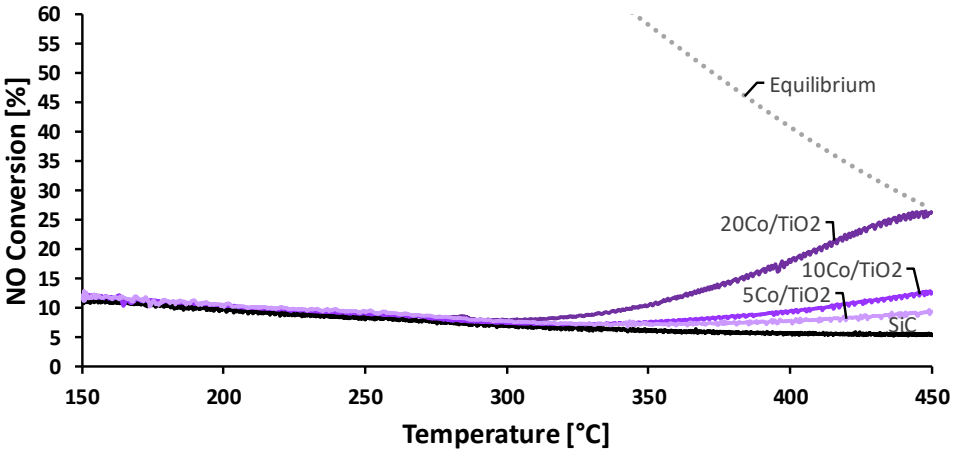

Figure 5.24: The NO to NO_2 conversion over cobalt oxides supported on TiO_2 with metal loading of 5, 10, and 20wt%Co in wet conditions. GHSV = 43 400 h^{-1}. Feed: 10 % NO, 6 % O_2, 15 % H_2O, rest Ar.

From Figure 5.24, it can be seen that the conversion of the titania supported catalysts increased with cobalt loading, where it followed the same trend as the alumina supported catalysts in wet conditions. The presence of steam shifted the initial catalytic activity of the catalysts towards higher temperatures. A wet-TPR of the 20Co/TiO_2 was not performed, but looking into the figure above, it would suggest that the initial reduction of Co_3O_4 has been shifted to higher temperatures. The conversion curve for 20Co/TiO_2 started to increase around 300 °C in wet conditions, which was a 50 °C increase from dry conditions. Likewise, the initial catalytic activity for 5Co/TiO_2 and 10Co/TiO_2 went from 300 °C to around 350 °C when water was introduced into the feed. Having water present in the feed also reduced the slopes the conversion curves, which may indicate to decreased reducibility of the cobalt oxides. As a consequence, the maximum conversion hit the equilibrium line before reaching high values, which was the case for 20Co/TiO_2. For 5Co/TiO_2 and 10Co/TiO_2, the late initial catalytic activity and gradual increase of the conversion resulted in small maximum conversions at high temperatures.

Table 5.10 shows the maximum conversion with the respective temperature and the conversion, rate of reaction, and turnover frequency at 350 °C of the NO conversion curves given in Figure 5.24

Table 5.10: An overview of the results from the activity performance over the TiO_2 supported catalysts in wet conditions.

Catalyst	20Co	10Co	5Co
Maximum conversion [%]	26	13	9
Respective temperature [°C]	448	450	450
Conversion at 350 °C [%]	10	7	7
Rate of reaction [$\mu mol\,s^{-1}\,g_c^{-1}$]	1.2	0.4	0.3
Turnover frequency [s^{-1}]	0.004	0.002	0.004

From the table above, it can be seen that the maximum conversion increased with cobalt loading, where it went from 9 % for 5Co/TiO_2 to 26 % for 20Co/TiO_2. The temperatures associated with the maximum conversions were at 450 °C with a minor decrease for the 20Co/TiO_2. The conversion curves did not reach the equilibrium line before reaching 450 °C, except for 20Co/TiO_2 where it just reached the thermodynamic equilibrium at around 450 °C. At 350 °C, the 20Co/TiO_2 had the highest conversion of 10 % and rate of reaction equal to 1.2 $\mu mol\,s^{-1}\,g_c^{-1}$. For the catalysts with 5 and 10wt%Co, the conversions at 350 °C were equal to 7 %, which gave a low rate of reactions. Similar to the K promoted catalyst, only 0.9 percentage points of the total conversion of 7 % correlates to the catalytic activity of the cobalt oxides. Introducing water into the feed may have affected the reducibility of the cobalt oxides to the point that it gave no significant catalytic activity at 350 °C for 5Co/TiO_2 and 10Co/TiO_2. Looking into the TOF values, it did not have any significant changes with cobalt loading.

Figure 5.25 shows the stability tests for the cobalt oxides supported on TiO_2 with metal loading of 5, 10, and 20wt%Co:

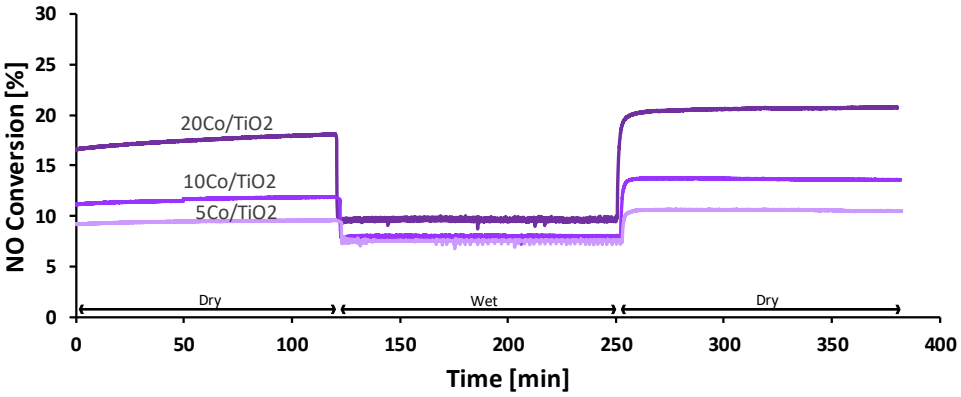

Figure 5.25: The stability tests at 350 °C for the cobalt oxides supported on TiO_2 with metal loading of 5, 10, and 20wt%Co. GHSV = 43 400 h^{-1}. Dry feed: 10 % NO, 6 % O_2, rest Ar. Wet feed: 10 % NO, 6 % O_2, 15 % H_2O, rest Ar.

The stability tests of the titania supported catalysts were performed at 350 °C by running a sequence consisting of three periods. In the first period, the catalyst were run in dry conditions for 2 hours. After that, the catalyst were introduced to wet conditions with a hold time of 2 hours. Lastly, the catalysts were introduced to dry conditions for an additional 2 hours. As seen from the figure above, the catalysts were stable and gradually increasing the conversion in the first dry run. After introducing water, it can be seen that the conversion immediately loses activity. However, the conversions during wet conditions were quite stable and did not decrease the conversion during the time duration when in the presence of steam. When the second dry run started, it can be observed that the catalyst gained activity after being exposed to steam during wet conditions. Table 5.11 shows the average conversion values in each of the periods with the regeneration and activity loss of the titania supported catalysts.

Table 5.11: The average conversions from each period in the stability test of the titania supported catalysts with the calculated regeneration and activity loss.

Catalyst	1st Dry [%]	Wet [%]	2nd Dry [%]	Regeneration [a] [%]	Activity loss [b] [%]
20Co	18	10	21	117	46
10Co	12	8	14	117	32
5Co	9	8	11	112	21

[a] Regeneration = 2nd Dry / 1st Dry [b] Activity loss = 1 - Wet / 1st Dry

From Table 5.11, the conversions from first to second dry run were increased after being through wet conditions for 2 hours. Looking into the regeneration, it can be seen that the

presence of steam did not deactivate the catalysts, but instead increased the catalytic activity of the supported cobalt oxides. Reconstruction of the cobalt species at the support surface could have occurred during the presence of steam, where it was favored for the NO oxidation. The Hüttig temperature of cobalt, at the point where the cobalt atoms at the surface become mobile, is 253 °C [67]. As the stability tests were occurring at 350 °C, there may be a possibility for the cobalt oxides to have sintered, where the crystallite size of the cobalt oxides could have increased. Larger crystallite sizes may have caused the reducibility of the cobalt oxides to be increased, which is beneficial for the NO oxidation as previously discussed. It should be noted that the conversion during the first dry period had a gradual increase before the wet conditions, where adding water into the feed may have just accelerated the sintering process. When it comes to the activity loss, it can be seen in Table 5.11 that it was increased with cobalt loading, which was the same case for the alumina supported catalysts.

Among the titania supported catalysts, it was shown that 20Co/TiO_2 had the highest catalytic performance both in dry and wet conditions. The higher reduction potential of Co_3O_4 for the 20Co/TiO_2 compared to 10Co/TiO_2 and 5Co/TiO_2 would show to be beneficial for the NO oxidation. From the stability tests, it was shown that the titania supported catalysts were stable in the presence of steam and had the potential to increase the catalytic activity due to the possible reconstruction of the cobalt oxides at the surface of the support. However, the activity loss increased with metal loading when steam was introduced into the feed with 5Co/TiO_2 being the least affected.

5.2.5 Supported cobalt oxides on silica

Figure 5.26 shows the activity measurements of NO oxidation over the cobalt oxides supported on SiO_2 with metal loading of 5, 10, and 20wt%Co in dry conditions:

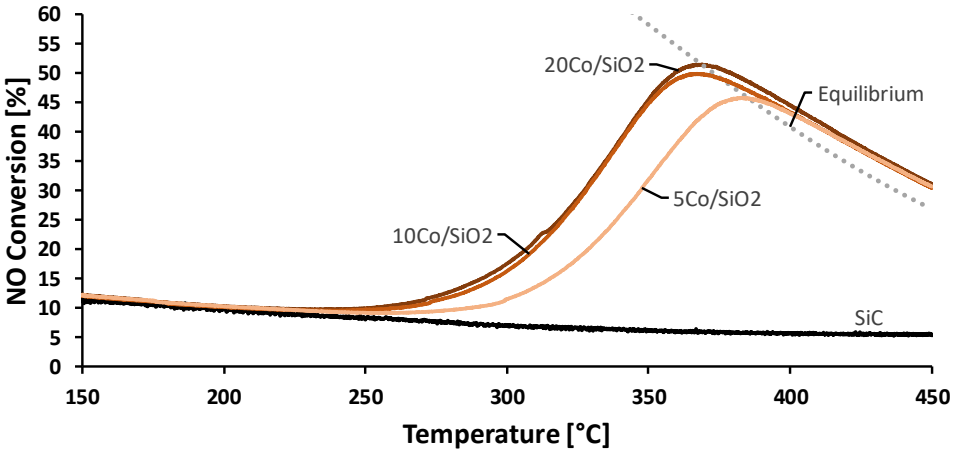

Figure 5.26: The NO to NO_2 conversion over cobalt oxides supported on SiO_2 with metal loading of 5, 10, and 20wt%Co in dry conditions. GHSV = 43 400 h^{-1}. Feed: 10 % NO, 6 % O_2, rest Ar.

From Figure 5.26, the conversion curves for 20Co/SiO_2 and 10Co/SiO_2 were near identical across the temperature range with a slight difference in the maximum conversions. The 5Co/SiO_2 had less initial catalytic activity, where the NO conversion started around 250 °C. From the TPR-profiles, the reduction of Co_3O_4 at 20Co/SiO_2 and 10Co/SiO_2 started after 200 °C while for 5Co/SiO_2 it began just before 250 °C. Since 5Co/SiO_2 had lower reducibility of the Co_3O_4, the catalytic activity started at higher temperatures compared to the two other catalysts. As a consequence, the conversion curve was lower across the temperature range. The crystallite size of Co_3O_4 was 15 nm for both 20Co/SiO_2 and 10Co/SiO_2, while for 5Co/SiO_2 it was only 13 nm. As previously discussed, the metal-support interaction may have stabilized the smaller cobalt particles which may have impacted the reducibility of Co_3O_4 for 5Co/SiO_2 [63]. Similar to previous activity measurements in dry conditions, the equilibrium line was exceeded most likely due to imprecise measurements of the actual temperature values, and back pressure build up because of the catalytic bed.

Table 5.12 shows the maximum conversion with the respective temperature and the conversion, rate of reaction, and turnover frequency at 350 °C of the NO conversion curves given in Figure 5.26:

Table 5.12: An overview of the results from the activity performance over the SiO_2 supported catalysts in dry conditions.

Catalyst	20Co	10Co	5Co
Maximum conversion [%]	51	50	46
Respective temperature [°C]	369	367	383
Conversion at 350 °C [%]	45	45	32
Rate of reaction [$\mu mol\,s^{-1}\,g_c^{-1}$]	10.9	10.8	7.1
Turnover frequency [s^{-1}]	0.051	0.096	0.112

From Table 5.12, the maximum conversion for 20Co/SiO_2 and 10Co/SiO_2 were 51 % at 369 °C and 50 % at 367 °C, respectively. At 350 °C, the 20Co/SiO_2 had a conversion of 45 % and rate of reaction equal to 10.9 $\mu mol\,s^{-1}\,g_c^{-1}$, which was near identical with 10Co/SiO_2. The metal loading difference between these two catalysts had insignificant impact on the catalytic activity of the catalysts in dry conditions. For 5Co/SiO_2, it achieved a maximum conversion of 46 % at 383 °C. At 350 °C it had a conversion of 32 % and rate of reaction equal to 7.1 $\mu mol\,s^{-1}\,g_c^{-1}$. Looking into the TOF values, it can be seen to increase when the cobalt loading was decreased. The ratio between catalytic activity and the amount of cobalt present at the surface would seem to more optimized with decreasing cobalt loading. However, the difference in TOF values between 10 and 20wt%Co was larger compared to the difference between 5 and 10wt%Co. Since the conversions are the same at 350 °C for 10 and 20wt%Co, the TOF for 10Co/SiO_2 was approximate twice the value due to the having half the amount of cobalt loading and similar dispersion values.

Figure 5.27 shows the activity measurements of NO oxidation over the cobalt oxides supported on SiO_2 with metal loading of 5, 10, and 20wt%Co in wet conditions:

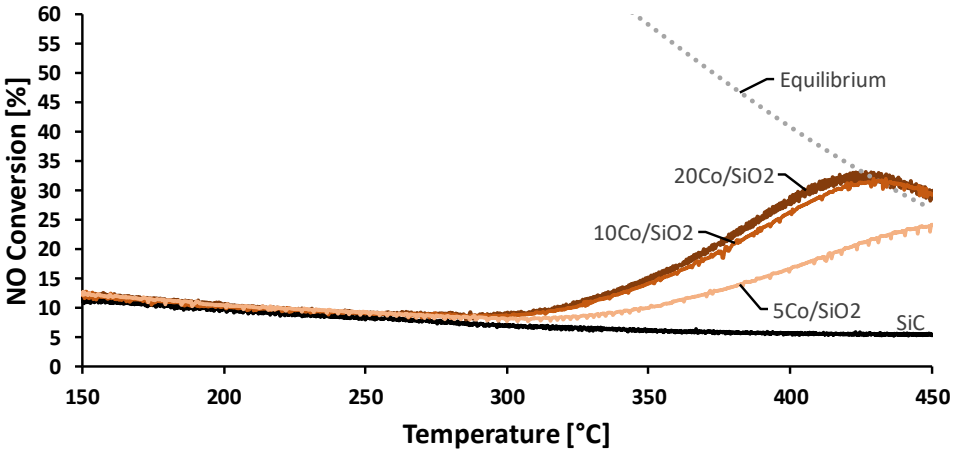

Figure 5.27: The NO to NO_2 conversion over cobalt oxides supported on SiO_2 with metal loading of 5, 10, and 20wt%Co in wet conditions. GHSV = 43 400 h^{-1}. Feed: 10 % NO, 6 % O_2, 15 % H_2O, rest Ar.

From Figure 5.27 it can be seen that the conversion curves follow a similar trend as observed in dry conditions, where 10Co/SiO_2 and 20Co/SiO_2 have equal catalytic contribution across the temperature range while 5Co/SiO_2 had the least catalytic performance. The initial catalytic activity for 10Co/SiO_2 and 20Co/SiO_2 started before 300 °C, which was an increase of about 50 °C from dry conditions. A similar case was observed with 5Co/SiO_2, where the initial catalytic activity had approximately been shifted 50 °C and started around 300 °C in wet conditions. The wet-TPR of 20Co/SiO_2 showed that the reduction of Co_3O_4 was shifted from 200 °C when in the absence of steam to above 250 °C when in the presence of steam. The slopes of the conversion curves were observed to be decreased in wet conditions, and with the combination of starting the catalytic activity at higher temperatures, the maximum conversion did not reach any high values before reaching the thermodynamic equilibrium. It was also observed that the equilibrium line was exceeded in wet conditions, which could be due to the imprecise measurement of the actual temperature or increased pressure because of the catalyst bed.

Table 5.13 shows the maximum conversion with the respective temperature and the conversion, rate of reaction, and turnover frequency at 350 °C of the NO conversion curves given in Figure 5.27:

Table 5.13: An overview of the results from the activity performance over the SiO_2 supported catalysts in wet conditions.

Catalyst	20Co	10Co	5Co
Maximum conversion [%]	33	32	24
Respective temperature [°C]	427	434	450
Conversion at 350 °C [%]	15	14	10
Rate of reaction [$\mu mol\,s^{-1}\,g_c^{-1}$]	2.5	2.2	1.1
Turnover frequency [s^{-1}]	0.012	0.020	0.017

From Table 5.13, it can seen that in wet conditions the $20Co/SiO_2$ had the highest maximum conversion of 33 % at 427 °C, but was closely followed by $10Co/SiO_2$ which had maximum conversion of 32 % at 434 °C. The $5Co/SiO_2$ did not perform to the same extent, which had a maximum conversion of 24 % at 450 °C. At 350 °C, the $20Co/SiO_2$ had the highest conversion of 15 % and rate of reaction equal to 2.5 $\mu mol\,s^{-1}\,g_c^{-1}$. The $10Co/SiO_2$ had similar catalytic performance, which caused the TOF values to be close to twice the value compared to one for $20Co/SiO_2$ as both catalysts have similar dispersion values. The smaller catalytic activity over $5Co/SiO_2$ at 350 °C gave lower TOF value than for $10Co/SiO_2$, which could be caused by the higher activity loss in wet conditions compared to the other 5wt%Co catalysts.

Figure 5.28 shows the stability tests for the cobalt oxides supported on SiO_2 with metal loading of 5, 10, and 20wt%Co:

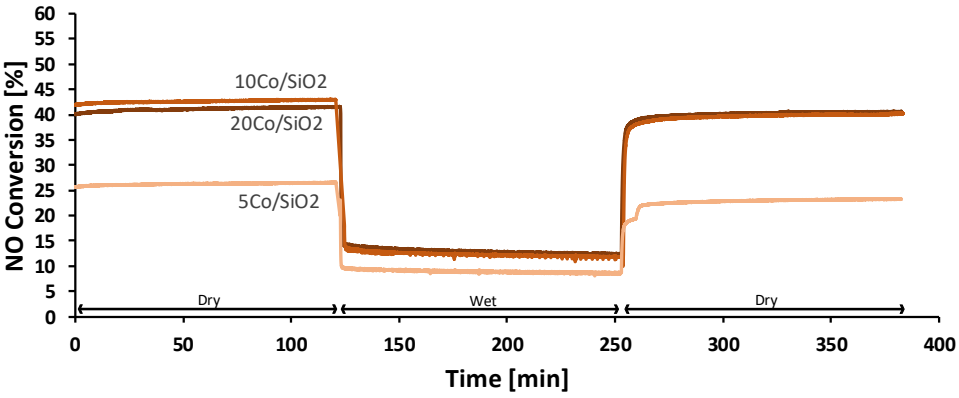

Figure 5.28: The stability tests at 350 °C for the cobalt oxides supported on SiO_2 with metal loading of 5, 10, and 20wt%Co. GHSV = 43 400 h^{-1}. Dry feed: 10 % NO, 6 % O_2, rest Ar. Wet feed: 10 % NO, 6 % O_2, 15 % H_2O, rest Ar.

The stability tests shown in Figure 5.28 were run by having a sequence of dry, wet, and

then dry conditions where each period lasted for 2 hours. In the first dry period, it can be seen that the activity of the catalysts was stable with no sign of initial deactivation. When the wet conditions were introduced, the conversions quickly dropped but became stable with a gradual decline during the wet run. After going into the second dry period, the conversions increased and were stable for the remaining time duration. Table 5.14 shows the average conversion values in each of the periods with the regeneration and activity loss of the silica supported catalysts.

Table 5.14: The average conversions from each period in the stability test of the silica supported catalysts with the calculated regeneration and activity loss.

Catalyst	1st Dry [%]	Wet [%]	2nd Dry [%]	Regeneration [a] [%]	Activity loss [b] [%]
20Co	41	13	40	98	69
10Co	43	12	40	93	71
5Co	26	9	23	87	66

[a] Regeneration = 2nd Dry / 1st Dry [b] Activity loss = 1 - Wet / 1st Dry

The regeneration of the silica supported catalysts was increasing as the metal loading of cobalt was increased. The 20Co/SiO_2 catalyst had a high regeneration, where it was equal to 98 %. In comparison, the 5Co/SiO_2 had a regeneration equal to 87 %. The mesoporous silica is known for having limited hydrothermal stability, where hydrolysis of the silica surface may have occurred during wet conditions [33][68][69]. The presence of high-temperature steam may potentially have caused structural destruction of the mesoporous silica [68]. The surface of the support may have been less exposed to steam with increasing metal loading of cobalt, which may have limited the deactivation of the silica support as the surface was more covered with cobalt oxides. For the Al_2O_3 and TiO_2 supported catalysts, the activity loss increased with cobalt loading, which was not as apparent for the case of the silica supported catalysts where the activity loss was more independent on the cobalt loading.

The results from activity measurements in both dry and wet conditions showed that 20Co/SiO_2 had the highest conversion levels and rate of reactions, but the 10Co/SiO_2 had near identical values with an only slight difference in the catalytic performance. The increased reduction potential of the Co_3O_4 for the 20Co/SiO_2 compared the two other silica supported catalysts would suggest to the cause for increased NO oxidation. From the stability tests, it was shown that 20Co/SiO_2 had the least deactivation of the catalyst after being in wet conditions for 2 hours. Nevertheless, it only indicates the initial deactivation and could be further deactivated if the time duration was prolonged. The activity loss was the least for the 5Co/SiO_2, but the value was similar for the other two catalysts.

5.2.6 Supported cobalt oxides on ceria

Figure 5.29 shows the activity measurements of NO oxidation over the cobalt oxides supported on CeO_2 with metal loading of 5, 10, and 20wt%Co in dry conditions:

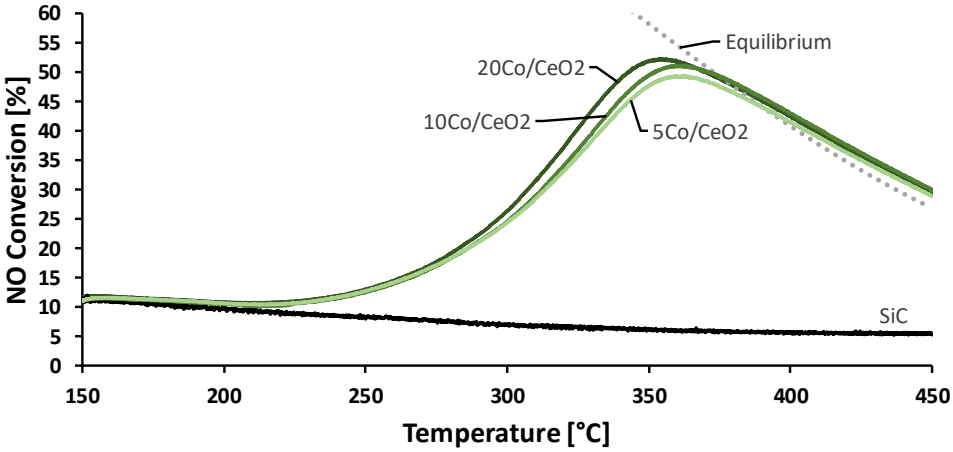

Figure 5.29: The NO to NO_2 conversion over cobalt oxides supported on CeO_2 with metal loading of 5, 10, and 20wt%Co in dry conditions. GHSV = 43 400 h^{-1}. Feed: 10 % NO, 6 % O_2, rest Ar.

From the figure above, it can be seen that the initial catalytic activities were equal between the ceria supported catalysts, where it was independent of the metal loading of cobalt. Around 300 °C and beyond it can be observed that the conversion curves increased with cobalt loading. Although the difference between the conversion curves was small, the increased amount of cobalt oxides present at the surface of the support could have contributed to higher maximum conversion as the cobalt loading was increased. From the TPR-profiles, the initial reduction of Co_3O_4 for all three catalysts began above 200 °C, which can be seen to be a similar case with NO oxidation in dry conditions. As the reducibility of the Co^{3+} were equal between the ceria supported catalysts, it resulted in similar catalytic activity for NO oxidation. Similar to previous activity measurements, the equilibrium line was exceeded due to inaccurate measurement of the actual temperature and back pressure build up from the catalyst bed.

Table 5.15 shows the maximum conversion with the respective temperature and the conversion, rate of reaction, and turnover frequency at 350 °C of the NO conversion curves given in Figure 5.29:

Table 5.15: An overview of the results from the activity performance over the CeO_2 supported catalysts in dry conditions.

Catalyst	20Co	10Co	5Co
Maximum conversion [%]	52	51	49
Respective temperature [°C]	354	361	362
Conversion at 350 °C [%]	52	49	48
Rate of reaction [$\mu mol\,s^{-1}\,g_c^{-1}$]	12.7	12.0	11.6
Turnover frequency [s^{-1}]	0.081	0.093	0.168

From Table 5.15, it can be shown that 20Co/CeO_2 had the highest maximum conversion of 52 % at 354 °C, but was closely followed by 10Co/CeO_2 and 5Co/CeO_2. The temperature associated with the maximum conversion was increasing from 354 to 362 °C going from 20 to 5wt%Co, which was a small difference. Looking into the activity at 350 °C, it can be observed that the 20Co/CeO_2 had a conversion of 52 % and a rate of reaction equal to 12.7 $\mu mol\,s^{-1}\,g_c^{-1}$. The two other catalysts had similar activity at 350 °C, with a small difference in the performance. The TOF values increased with cobalt loading, which can be expected as the performance of the catalysts was similar at the given temperature. The TOF value close to doubled going from 10 to 5wt%Co as the dispersion values were similar and reducing the cobalt amount in half. This was not the case going from 20 to 10wt% because of the vast difference in dispersion values due to the significant crystallite growth going from 10 to 20wt%Co.

Figure 5.30 shows the activity measurements of NO oxidation over the cobalt oxides supported on CeO_2 with metal loading of 5, 10, and 20wt%Co in wet conditions:

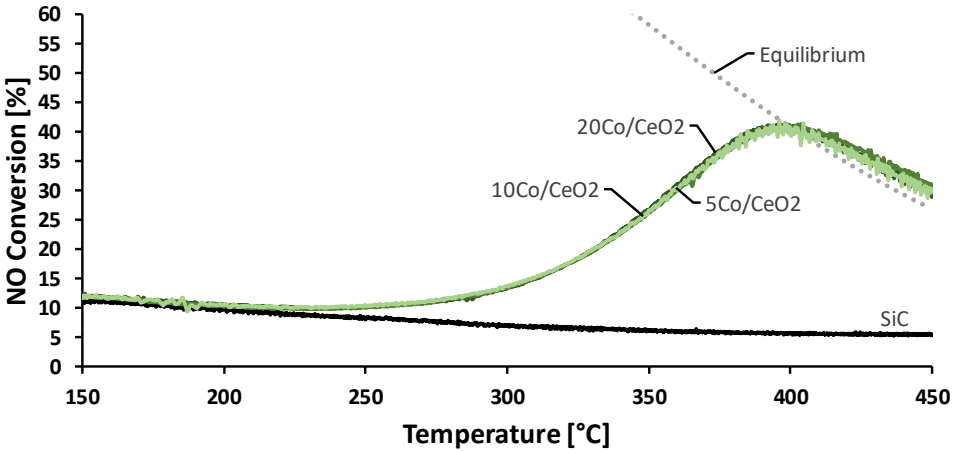

Figure 5.30: The NO to NO_2 conversion over cobalt oxides supported on CeO_2 with metal loading of 5, 10, and 20wt%Co in wet conditions. GHSV = 43 400 h^{-1}. Feed: 10 % NO, 6 % O_2, 15 % H_2O, rest Ar.

From Figure 5.30, the conversion curves were near identical across the temperature range in wet conditions. For the alumina and titania supported catalysts, the conversion level increased as the metal loading of cobalt was increased. This was not the case for the ceria supported catalysts as the NO conversion was independent of the cobalt loading. The TPR-profiles of the ceria supported catalysts showed that in the absence of water, the reducibility of Co^{3+} did not change with cobalt loading, which would seem to be the same case when exposed to water. The initial catalytic activity went from 200 °C in dry conditions to around 225 °C in wet conditions, which was in agreement with the observation in the wet-TPR of the 20Co/CeO_2. Introducing water into the feed affected the slopes of the conversions curves, where the reducibility of the Co_3O_4 may have been decreased. The inhibition effects of water shifted the maximum conversion to higher temperatures and did not reach the same conversion levels as in dry conditions as the equilibrium line was reached. Similar to the activity measurements in dry conditions, the equilibrium line was exceeded.

Table 5.16 shows the maximum conversion with the respective temperature and the conversion, rate of reaction, and turnover frequency at 350 °C of the NO conversion curves given in Figure 5.30:

Table 5.16: An overview of the results from the activity performance over the CeO_2 supported catalysts in wet conditions.

Catalyst	20Co	10Co	5Co
Maximum conversion [%]	41	41	42
Respective temperature [°C]	396	404	396
Conversion at 350 °C [%]	27	26	27
Rate of reaction [$\mu mol\, s^{-1}\, g_c^{-1}$]	5.7	5.6	5.7
Turnover frequency [s^{-1}]	0.036	0.043	0.083

From the table above it can be seen that all three catalysts are nearly indistinguishable in terms of maximum conversions and the conversion and rate of reactions at 350 °C. The $10Co/CeO_2$ had maximum conversion at 404 °C, which was higher compared to the other two catalysts which had maximum conversion at 396 °C. From Figure 5.30, it can be seen the conversion curves were fluctuating, which was caused by the process controller of the water going into the evaporator. Thus, the catalytic performances of the ceria supported catalysts can be considered to be identical as it is within experimental error. The maximum conversion of $20Co/CeO_2$ was 41 % at 396 °C, which was similar to the two other catalysts. At 350 °C, the conversion and rate of reaction had an insignificant change as the cobalt loading was increased. The TOF values can be seen to increase as the metal loading of cobalt was decreased, which may be expected as the catalytic performance of the catalysts was almost identical.

Figure 5.31 shows the stability tests for the cobalt oxides supported on CeO_2 with metal loading of 5, 10, and 20wt%Co:

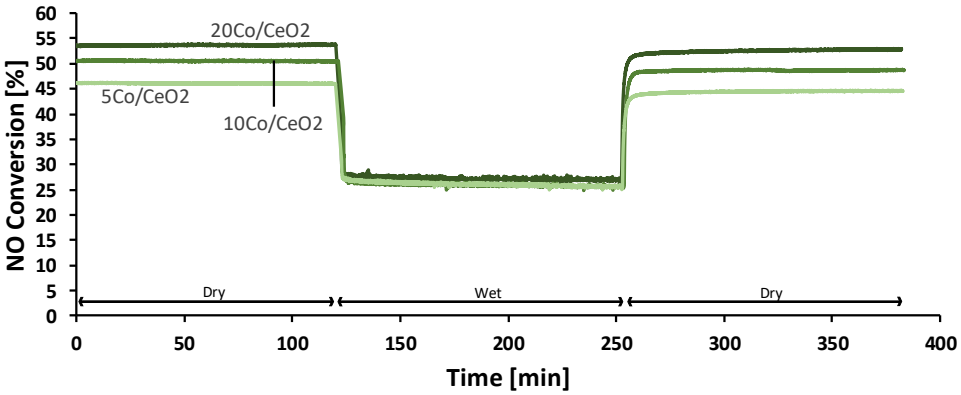

Figure 5.31: The stability tests at 350 °C for the cobalt oxides supported on CeO_2 with metal loading of 5, 10, and 20wt%Co. GHSV = 43 400 h^{-1}. Dry feed: 10 % NO, 6 % O_2, rest Ar. Wet feed: 10 % NO, 6 % O_2, 15 % H_2O, rest Ar.

The stability tests of the ceria supported catalysts were run by having a sequence of dry, wet, and dry conditions, where each period lasted for a time duration of 2 hours. In the first dry run, it can be seen that the conversions of the catalysts were stable, which would suggest that the cobalt remains in its active oxidation state of Co_3O_4. After being introduced to wet conditions, the activity loss due to the presence of steam could be observed. Nevertheless, the conversions were stable in wet conditions with minimal deactivation of the catalysts. During the second dry period, it can be seen that the conversions increased and were stable for the remaining time duration. Table 5.17 shows the average conversion values in each of the periods with the regeneration and activity loss of the ceria supported catalysts.

Table 5.17: The average conversions from each period in the stability test of the ceria supported catalysts with the calculated regeneration and activity loss.

Catalyst	1st Dry [%]	Wet [%]	2nd Dry [%]	Regeneration [a] [%]	Activity loss [b] [%]
20Co	54	27	52	98	49
10Co	51	26	49	96	49
5Co	46	26	44	97	44

[a] Regeneration = 2nd Dry / 1st Dry [b] Activity loss = 1 - Wet / 1st Dry

From the table above it can be seen that the regeneration for the 20Co/CeO_2 was 98 %, which indicates resistance towards initial water deactivation. The two other catalysts also showed good regeneration with only 1-2 percentage points lower than for the 20Co/CeO_2. For the 5Co/CeO_2, it had the least activity loss and was equal to 44 %. The activity loss

of $20Co/CeO_2$ and $10Co/CeO_2$ were identical and were equal to 49 %. The activity loss for the ceria supported catalysts were similar, but compared to the other supported cobalt oxides catalysts, the ceria supported ones had decent conversions in wet conditions.

In dry conditions, the $20Co/CeO_2$ had the highest catalytic performance compared to the two other ceria supported catalysts, but the $5Co/CeO_2$ had the highest TOF value. However, in wet conditions, the catalytic performance was near identical for all three catalysts. As the TOF value in wet conditions was the highest for $5Co/CeO_2$, it performed better having identical catalytic activity and yet having the least amount of cobalt loading out of the three catalysts. Compared to the alumina, titania and silica supported catalysts, it was shown that all three ceria supported catalysts had better catalytic activity both in dry and wet conditions. From the stability tests, it was shown that the three catalysts had almost no deactivation after being exposed to water and had acceptable activity loss considering that the conversion remained adequate even in wet conditions at 350 °C.

5.2.7 Supported cobalt oxides on zirconia

Figure 5.32 shows the activity measurements of NO oxidation over the cobalt oxides supported on ZrO_2 with metal loading of 5, 10, and 20wt%Co in dry conditions:

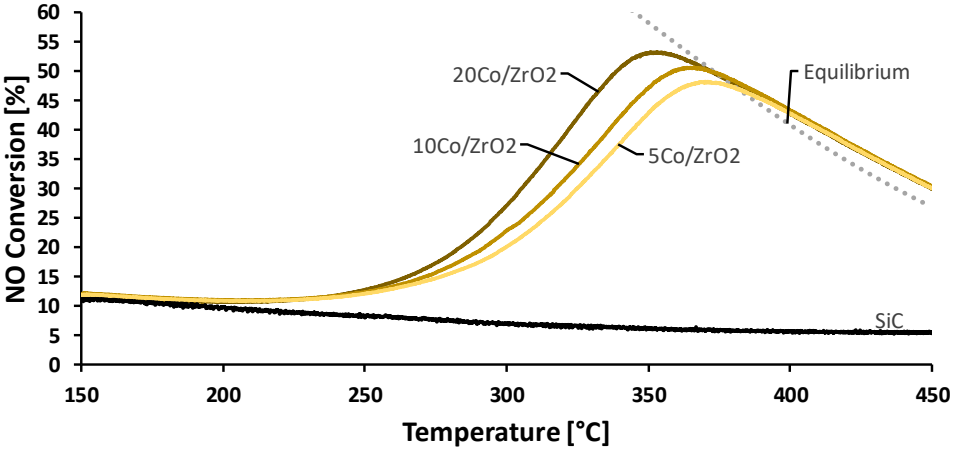

Figure 5.32: The NO to NO_2 conversion over cobalt oxides supported on ZrO_2 with metal loading of 5, 10, and 20wt%Co in dry conditions. GHSV = 43 400 h^{-1}. Feed: 10 % NO, 6 % O_2, rest Ar.

The conversion curves of the zirconia supported catalysts can be seen to be increasing as the cobalt loading was increased, where the $20Co/ZrO_2$ achieved the highest activity across the temperature range. The initial activity of the catalysts can be seen to start from the same point, which was around 200 °C. As the temperature increased, the conversion curves differed between the catalysts, where increasing the cobalt loading increased the

slopes of the conversion curves. The reduction potential of the Co_3O_4 may be the cause of the difference in the activity. From the TPR-profiles, it was shown for the zirconia supported catalysts that the Co_3O_4 started to reduce above 200 °C. However, as the cobalt loading was increased, the reducibility of the cobalt oxides was also increased. Looking into Figure 5.32, the increased reducibility of the cobalt oxides due to the increase in cobalt loading resulted in higher activity towards NO oxidation in dry conditions. As previous activity measurements in dry conditions, the equilibrium line was exceeded most likely due to inaccurate temperature measurements and back pressure contribution due to the catalyst bed.

Table 5.18 shows the maximum conversion with the respective temperature and the conversion, rate of reaction, and turnover frequency at 350 °C of the NO conversion curves given in Figure 5.32:

Table 5.18: An overview of the results from the activity performance over the ZrO_2 supported catalysts in dry conditions.

Catalyst	20Co	10Co	5Co
Maximum conversion [%]	53	51	48
Respective temperature [°C]	351	366	370
Conversion at 350 °C [%]	53	47	43
Rate of reaction [$\mu mol\,s^{-1}\,g_c^{-1}$]	13.0	11.4	10.2
Turnover frequency [s^{-1}]	0.052	0.102	0.120

It can be seen from the table that the 20Co/ZrO_2 had the highest maximum conversion of 53 % at 351 °C. For 5Co/ZrO_2, the maximum conversion was 48 % and the respective temperature was at 370 °C. As the cobalt loading decreased, the maximum conversion decreased, and the respective temperature was shifted to higher values. At 350 °C, the 20Co/ZrO_2 had the highest catalytic activity with a conversion of 53 % and the rate of reaction equal to 13.0 $\mu mol\,s^{-1}\,g_c^{-1}$. As cobalt loading decreased, the catalytic performance followed as seen by the 5Co/ZrO_2 having a conversion equal to 43 % and a rate of reaction equal to 10.2 $\mu mol\,s^{-1}\,g_c^{-1}$. Looking into the relationship between catalytic activity and the amount of cobalt, it can be seen that the 5Co/ZrO_2 had a TOF value equal to 0.120 s^{-1}, which was the highest among the zirconia supported catalysts. As the cobalt loading was increased, the TOF value was decreased, which was the observation with the alumina, silica, and ceria supported catalysts.

Figure 5.33 shows the activity measurements of NO oxidation over the cobalt oxides supported on ZrO_2 with metal loading of 5, 10, and 20wt%Co in wet conditions:

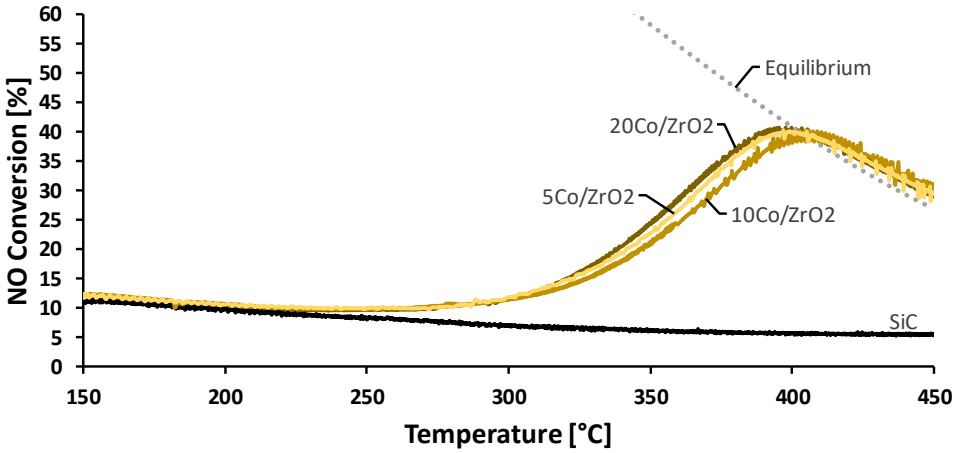

Figure 5.33: The NO to NO_2 conversion over cobalt oxides supported on ZrO_2 with metal loading of 5, 10, and 20wt%Co in wet conditions. GHSV = 43 400 h^{-1}. Feed: 10 % NO, 6 % O_2, 15 % H_2O, rest Ar.

From Figure 5.33, the conversion curve of all the three catalysts have the same initial catalytic activity, where it started above 225 °C. As the temperature rises above 300 °C, it can be seen that the conversion curves start to differentiate between one another, where the 20Co/ZrO_2 had the highest conversion across the temperature range. The initial activity went from around 200 to 225 °C when water was introduced into the feed. From the wet-TPR of 20Co/ZrO_2, the initial reduction of Co^{3+} began above 225 °C, which was in agreement with the initial activity observed in Figure 5.33. This showed that the reducibility of the cobalt oxides decreased when exposed to water, shifting the initial reduction temperature towards higher values. The slopes of the conversion curves can be seen to have decreased due to the presence of steam in the feed. However, the catalytic activity was similar with only small differences between the conversion curves. It would suggest that the zirconia supported catalysts in wet conditions were not entirely dependent on the cobalt loading, which was the opposite case with alumina and titania supported catalysts. Interestingly, the 20Co/ZrO_2 and 5Co/ZrO_2 were almost identical in the catalytic activity, while the 10Co/ZrO_2 had the least activity out of the three zirconia supported catalysts. From the XRD-results, the crystallite size of the 10Co/ZrO_2 was the largest out of the three catalysts. Having lower dispersion value could have caused less exposure of the active sites at the surface, which may have given a small decrease in activity during wet conditions. Nevertheless, the catalytic performance of these catalysts was similar across the temperature range in wet conditions. As in dry conditions, the equilibrium line was crossed due to inaccurate measurements of the actual temperature and potential increase in back pressure build at higher temperatures.

Table 5.19 shows the maximum conversion with the respective temperature and the conversion, rate of reaction, and turnover frequency at 350 °C of the NO conversion curves given in Figure 5.33:

Table 5.19: An overview of the results from the activity performance over the ZrO_2 supported catalysts in wet conditions.

Catalyst	20Co	10Co	5Co
Maximum conversion [%]	41	40	40
Respective temperature [°C]	395	406	397
Conversion at 350 °C [%]	24	21	23
Rate of reaction [$\mu mol\,s^{-1}\,g_c^{-1}$]	5.0	4.1	4.6
Turnover frequency [s^{-1}]	0.020	0.037	0.054

From the table above, the $20Co/ZrO_2$ had the highest maximum conversion of 41 % at 395 °C. As the cobalt loading decreased there was an insignificant change in the maximum conversions, where there was only one percentage point difference for the 5 and 10wt%Co. The temperature associated with the maximum conversion was 406 °C for $10Co/ZrO_2$ and 397 °C for $5Co/CeO_2$, where it may indicate that in wet conditions the reducibility of the cobalt oxides affected the most for the 10wt%Co catalyst. At 350 °C, the $20Co/ZrO_2$ achieved the highest conversion of 24 % and a rate of reaction equal to $5.0\,\mu mol\,s^{-1}\,g_c^{-1}$. Closely followed by the $5Co/ZrO_2$, which had conversion of 23 % and a rate of reaction equal to $4.6\,\mu mol\,s^{-1}\,g_c^{-1}$ at 350 °C. The $10Co/ZrO_2$ at the least catalytic activity among the zirconia supported catalysts with a conversion of 21 % and a rate of reaction equal to $4.1\,\mu mol\,s^{-1}\,g_c^{-1}$ at 350 °C. The TOF value can be seen to increase as the cobalt was decreased, going from $0.020\,s^{-1}$ at 20wt%Co to $0.054\,s^{-1}$ at 5wt%Co, which was the similar case with the ceria supported catalysts in wet conditions.

Figure 5.34 shows the stability tests for the cobalt oxides supported on ZrO_2 with metal loading of 5, 10, and 20wt%Co:

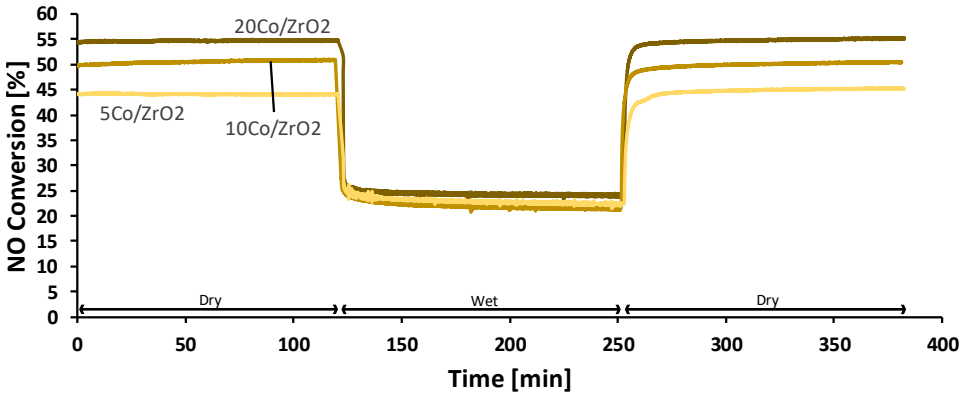

Figure 5.34: The stability tests at 350 °C for the cobalt oxides supported on ZrO_2 with metal loading of 5, 10, and 20wt%Co. GHSV = 43 400 h^{-1}. Dry feed: 10 % NO, 6 % O_2, rest Ar. Wet feed: 10 % NO, 6 % O_2, 15 % H_2O, rest Ar.

The stability tests of the zirconia supported catalysts were performed by having a sequence consisting of dry, wet, and then dry conditions for a time duration of 2 hours in each of the periods at 350 °C. During the first dry period, the conversions were stable for the time duration, which indicates that the cobalt oxides remained in its active oxide state of Co_3O_4. Immediate activity loss of the catalysts could be seen in the presence of steam, but the conversions were stable during wet conditions. As the water was removed from the feed, it can be seen that the conversion increased with almost no sign of deactivation from being exposed to water. Table 5.20 shows the average conversion values in each of the periods with the regeneration and activity loss of the zirconia supported catalysts.

Table 5.20: The average conversions from each period in the stability test of the zirconia supported catalysts with the calculated regeneration and activity loss.

Catalyst	1st Dry [%]	Wet [%]	2nd Dry [%]	Regeneration [a] [%]	Activity loss [b] [%]
20Co	55	24	55	100	56
10Co	51	22	50	99	57
5Co	44	23	45	102	48

[a] Regeneration = 2nd Dry / 1st Dry [b] Activity loss = 1 - Wet / 1st Dry

From Table 5.20, the 5Co/ZrO_2 gained catalytic activity after being exposed to wet conditions, where it achieved a regeneration value of 102 %. The 20Co/ZrO_2 was not deactivated after being exposed to water, where it had a regeneration value of 100 %. The 10Co/ZrO_2 achieved a regeneration value of 99 %, which was almost no deactivation after being in wet conditions for 2 hours. The activity loss was the least for 5Co/ZrO_2 with a 48 % loss in

conversion going from dry to wet conditions. As the cobalt loading increased, the activity loss was increased. The 20Co/ZrO_2 had an activity loss of 56 %, followed by 10Co/ZrO_2 with a one percentage point difference. Still, the conversions at 350 °C remained between 22-24 % when in the presence of steam which shows potential for NO oxidation.

In dry conditions, the 20Co/ZrO_2 had the highest maximum conversion at the lowest respective temperature and had the most catalytic activity at 350 °C, but TOF value decreased as the cobalt loading increased. The reducibility of the cobalt oxides supported on zirconia increased with cobalt loading, where the NO conversion levels in dry conditions increased with cobalt loading. In the presence of steam, the activity difference between the catalysts became less distinguishable, where the catalytic performance became less dependent on the cobalt loading. The 20Co/ZrO_2 had slightly better conversion and rate of reaction than 5Co/ZrO_2 at 350 °C, but the 5wt%Co catalyst had the least activity loss among the zirconia catalysts and was the only one which gained activity after being exposed to water in the stability test.

5.3 Comparison between the supported cobalt oxide catalysts

The results were in this section compared to determine which catalysts had the most catalytic activity and which characteristics impact the NO conversion. Table 5.21 shows the particle size and dispersion of the cobalt oxides on the supported catalysts and the conversion, rate of reaction, and turnover frequency at 350 °C in both dry and wet conditions.

Table 5.21: The particle size and dispersion of the cobalt oxides on the supported catalyst and the conversion, rate of reaction, and turnover frequency at 350 °C in both dry and wet conditions.

Catalyst	d(Co_3O_4)	D	Conversion		Rate of reaction		TOF	
			Dry	Wet	Dry	Wet	Dry	Wet
	[nm]	[nm]	[%]		[$\mu mol\, s^{-1}\, g_c^{-1}$]		[s^{-1}]	
5Co/Al_2O_3	16	8.2	15	8	2.4	0.7	0.034	0.010
10Co/Al_2O_3	16	7.8	20	11	3.9	1.3	0.029	0.010
20Co/Al_2O_3	18	7.1	26	12	5.5	1.6	0.023	0.006
20Co-Pt/Al_2O_3	20	6.5	25	12	5.2	1.6	0.024	0.007
20Co-K/Al_2O_3	21	6.0	11	7	1.4	0.4	0.007	0.002
5Co/TiO_2	13	9.7	8	7	0.6	0.3	0.007	0.004
10Co/TiO_2	13	9.7	10	7	1.1	0.4	0.006	0.002
20Co/TiO_2	15	8.7	25	10	5.1	1.2	0.017	0.004
5Co/SiO_2	17	7.5	32	10	7.1	1.1	0.112	0.017
10Co/SiO_2	20	6.6	45	14	10.8	2.2	0.096	0.020
20Co/SiO_2	20	6.3	45	15	10.9	2.5	0.051	0.012
5Co/CeO_2	16	8.1	48	27	11.6	5.7	0.168	0.083
10Co/CeO_2	17	7.6	49	26	12.0	5.6	0.093	0.043
20Co/CeO_2	28	4.6	52	27	12.7	5.7	0.081	0.036
5Co/ZrO_2	13	10.1	43	23	10.2	4.6	0.120	0.054
10Co/ZrO_2	19	6.6	47	21	11.4	4.1	0.102	0.037
20Co/ZrO_2	17	7.4	53	24	13.0	5.0	0.052	0.020

Looking into the NO conversion at 350 °C, the following order shows decreasing conversion and rate of reaction over the catalysts in both dry and wet conditions based upon which support was used: $CeO_2 > ZrO_2 > SiO_2 > Al_2O_3 > TiO_2$. There was one exception from the given order, where at 20wt%Co in dry conditions the zirconia supported catalyst had one percentage point higher in conversion than the ceria supported one and subsequently having a higher rate of reaction. In terms of the initial reduction from Co^{3+} to Co^{2+} and the

first reduction peak temperature given in the TPR-profiles, the following order shows the decreasing reducibility of Co_3O_4 on the supported catalyst: $CeO_2 > ZrO_2 > SiO_2 > Al_2O_3 > TiO_2$. The two orders show that there was a correlation between the reducibility of Co^{3+} to Co^{2+} and the catalytic activity over the supported cobalt oxide catalysts. These trends are in agreement with the observation by Yu et al., whereby lowering the peak temperature correlated to the reduction from Co^{3+} to Co^{2+} increased the catalytic activity for NO oxidation. As previously mentioned, Weiss et al. suggested that high NO oxidation turnover rates depended on the ability of the cobalt oxides to undergo one-electron reductions from Co^{3+} to Co^{2+} [22]. This may seem to be the case, where increasing the reducibility of the Co^{3+} to Co^{2+} increased NO conversion over the supported catalysts. From the TPR-profiles, the 20Co-Pt/Al_2O_3 increased the reducibility from Co^{2+} to Co^0, but the catalytic activity between 20Co-Pt/Al_2O_3 and 20Co/Al_2O_3 were near identical. Based on this observation, it may indicate that the reduction from Co^{3+} to Co^{2+} plays a more critical role in increasing the NO oxidation.

For the non promoted catalysts, it can be seen from Table 5.21 that increasing the metal loading of cobalt increases, in general, the conversion in dry conditions to a varying degree depending on which support was used. However, it wet conditions it can be seen that the conversions over the cobalt oxides supported on ceria were independent of the cobalt loading. A similar case may be observed with the zirconia supported catalysts, although there were small differences in conversions between the catalysts. For most of the catalysts, it can be seen that a decrease in the dispersion, which means an increase in cobalt oxide particles, gives a higher rate of reactions. Weiss at al. suggested that larger cluster sizes of cobalt oxides increased the NO conversion due to the increased vacancies needed for O_2 activation, whereby having smaller clusters bound the oxygen more strongly which gave fewer concentrations of the vacant sites that bind the O_2 in kinetically relevant steps [22]. For the ceria supported catalysts, this was not the case as the rate of reaction in wet conditions was independent of the dispersion values. Ceria is known for its oxygen storage capacity, which may have played a role when introduced to wet conditions [36]. For the promoted catalysts, the change in particle size and dispersion did not give any significant contribution to the catalytic activity. The surface area of the calcined supported were decreasing in the following order: $SiO_2 > Al_2O_3 > TiO_2 > CeO_2 > ZrO_2$. Comparing the order with catalytic activity over the supported catalysts, there was no obvious trend to be observed. The results suggest that the reducibility of the cobalt oxides played a more central role rather than the surface area of the supports. In terms of TOF values given in Table 5.21, it can be for the most catalysts to be increasing as the cobalt loading decreases. For the titania supported catalysts, the activity for 5 and 10wt%Co were low compared to the 20wt%Co, which results in the TOF values to deviate from the general trend observed across the supported catalysts.

The NO oxidation did not seem to deactivate the catalyst during dry conditions as seen by the stable conversion levels during the stability tests of the catalysts. It could perhaps be due to the oxygen available in the feed, where reduction-oxidation cycles between Co^{3+} and Co^{2+} may occur where the oxygen oxidizes the cobalt to the desired oxidation state of Co_3O_4. When steam was introduced in the stability tests, it can be seen that conversion decreased due to the inhibition of water. The decrease in conversion may be due to water adsorption on the active sites, where it may have decreased the availability of cobalt oxides sites for the NO oxidation [70][71]. As soon as the water was removed from the feed by going into the second dry period in the stability tests, it can be seen that the conversions were promptly increased. The activity loss was in general increasing with metal loading of cobalt, where the 5wt%Co catalysts usually had the least activity loss going from dry to wet conditions.

The ceria supported catalysts showed to be the most catalytic active towards NO conversions, followed by the zirconia supported catalysts. However, the regeneration of the zirconia supported catalysts were slightly higher compared to the ceria supported catalysts. The stability tests were run for a total time duration of 6 hours, where each period lasted for 2 hours in the sequence of dry-wet-dry conditions. The regeneration of the catalysts only indicates initial deactivation due to the presence of steam. It may be possible that if the time duration was extended, the deactivation of the catalysts could have been more significant for the ceria supported catalysts. Thus, the zirconia supported catalysts may have been more active than the ceria supported catalysts if the time duration was extended.

Chapter 6

Conclusion

The supported cobalt oxides catalysts were successfully synthesized on supports such as Al_2O_3, TiO_2, SiO_2, CeO_2, and ZrO_2. From nitrogen adsorption, the following shows the decreasing order of the BET surface area of the calcined supports: $SiO_2 > Al_2O_3 > TiO_2 > CeO_2 > ZrO_2$. The XRD confirmed that the cobalt oxides were present as Co_3O_4. The TPR-profiles indicated to a two-step reduction profile of the cobalt oxides, going from Co^{3+} to Co^{2+} and followed by Co^{2+} to Co^0. Based on the TPR-profiles, the following shows the decreasing order of reducibility for Co^{3+} to Co^{2+} over the supported catalysts: $CeO_2 > ZrO_2 > SiO_2 > Al_2O_3 > TiO_2$. In general, the dispersion decreased and particle size of Co_3O_4 increased as the cobalt loading was increased. The particle size and dispersion of the cobalt oxides were estimated by using the patterns from XRD.

Activity measurements of NO oxidation over the supported catalysts were performed at industrial conditions (10 % NO, 6 % O_2, 15 % H_2O, rest Ar) between 150-450 °C to investigate a suitable, cost-efficient catalyst to potentially replace the homogeneous gas phase reaction in nitric acid production. The supported catalysts were tested in the absence and in the presence of water to investigate the effects of introducing steam into the inlet feed. In dry conditions it was seen that the catalytic activity increased with cobalt loading, where the ones with 20wt%Co had the highest conversions at 350 °C. In the absence of water at 350 °C, the rate of reactions was 5.5 $\mu mol\,s^{-1}\,g_c^{-1}$ for $20Co/Al_2O_3$, 5.1 $\mu mol\,s^{-1}\,g_c^{-1}$ for $20Co/TiO_2$, 10.9 $\mu mol\,s^{-1}\,g_c^{-1}$ for $20Co/SiO_2$, 12.7 $\mu mol\,s^{-1}\,g_c^{-1}$ for $20Co/CeO_2$, and 13.0 $\mu mol\,s^{-1}\,g_c^{-1}$ for $20Co/ZrO_2$. In wet conditions, it could be seen that the conversion decreased due to the presence of water. For the catalysts supported on Al_2O_3, TiO_2, and SiO_2, the catalytic activity increased with metal loading in wet conditions. At 350 °C in the presence of water, the rate of reaction was 1.6 $\mu mol\,s^{-1}\,g_c^{-1}$ for $20Co/Al_2O_3$, 1.2 $\mu mol\,s^{-1}\,g_c^{-1}$ for $20Co/TiO_2$, and 2.5 $\mu mol\,s^{-1}\,g_c^{-1}$ for $20Co/SiO_2$. How-

ever, for the ceria supported catalysts it was shown that the catalytic activity in wet conditions was independent of the cobalt loading, where the rate of reaction was 5.7 $\mu mol\,s^{-1}\,g_c^{-1}$ for both 5 and 20wt%Co. The catalytic activity over the zirconia supported catalysts also showed to be less dependent of cobalt loading in wet conditions at 350 °C, where the rate of reaction was 4.6 $\mu mol\,s^{-1}\,g_c^{-1}$ for 5Co/ZrO_2 and 5.0 $\mu mol\,s^{-1}\,g_c^{-1}$ for 20Co/ZrO_2. In terms of conversion and rate of reaction at 350 °C, the following order shows the decreasing catalytic performance over the supported catalysts: $CeO_2 > ZrO_2 > SiO_2 > Al_2O_3 > TiO_2$. It can be seen that the NO oxidation correlated with the ability of the cobalt oxides to reduce from Co^{3+} to Co^{2+}, which indicate the importance of choosing a support to increase the reducibility of the cobalt oxides.

The Pt promoted catalyst, 20Co-Pt/Al_2O_3, did not give any significant catalytic activity. From TPR-experiments, it was shown it promoted the reducibility of Co^{2+} to Co^0 but it would seem that the NO oxidation was unaffected. However, it was more resistant towards water deactivation, where the activity loss due to the presence of water was less affected for the platinum promoted catalyst. Promoting the catalyst with potassium, 20Co-K/Al_2O_3, significantly reduced the catalytic activity towards NO oxidation, which showed that adding potassium into the precursor solution before the impregnation of the support did not give any desired effects.

Stability tests of the supported catalysts were performed at 350 °C with a sequence consisting of three periods with 2 hours time duration in each of them: dry, wet, and then dry conditions. All of the catalysts experienced activity loss due to the presence of water as it went from dry to wet conditions, where the titania supported catalysts were the least affected by the inhibition effects of water. Going from the first to the second dry period after being exposed to water, it was shown that the titania supported catalysts gained activity. Water deactivation did not affect for the zirconia supported catalysts, where the catalysts were more or less fully regenerated after being exposed to water. The ceria supported catalysts had regeneration above 96 %, which indicated high resistance towards initial water deactivation. For the remaining Al_2O_3 and SiO_2 supported catalysts, the regeneration was 80-90 % and 87-98 %, respectively.

In terms of catalytic activity at industrial conditions, it was shown that the cobalt oxides supported on ceria had the highest conversions and rate of reactions towards NO oxidation. It showed to have excellent resistance towards initial water deactivation, and the conversions were independent of cobalt loading in wet conditions. The 5Co/CeO_2 had higher TOF value and the least activity loss due to the presence of water, which makes it a more efficient catalyst in terms of cobalt loading. Cobalt oxides supported on ceria with low metal loading of cobalt have the potential to be a suitable, cost-efficient catalyst for NO oxidation at industrial conditions in nitric acid production.

Chapter 7

Future work

The Pt promoted catalyst was activated in an oxidizing atmosphere to ensure Co_3O_4 at the surface of the support. The catalytic activity may be improved by introducing hydrogen over the Pt promoted catalyst, where it may be possible to reduce the platinum oxide to metallic platinum while the cobalt oxides remained in its desired state of Co_3O_4.

The platinum promoted catalyst showed to be more resistance towards water deactivation than the same non-promoted supported catalyst. Further investigation should be considered, where promising catalysts such as ceria supported cobalt oxide catalysts may be promoted with platinum to increase resistance towards water deactivation.

The ceria supported cobalt oxides catalysts had the highest catalytic activity and were independent of the metal loading of cobalt in the wet conditions. Further research of these catalysts should be considered, where the cobalt loading could be lowered until the desired catalytic activity is reached with acceptable resistance towards water deactivation.

The stability tests of the catalysts indicate the initial deactivation of the catalytic activity when exposed to water. The total time duration of each test was run for 6 hours, where 2 hours were spent in the presence of water. In order to determine long term effects of water deactivation, the test needs to be continued until a steady-state conversion is observed. These results may change the perception of which supported catalysts perform better for NO oxidation at industrial conditions.

The reduction of the cobalt oxides seemed to be important for the NO oxidation. Further research should be considered to understand how metal-support interactions and reduction potential of Co_3O_4 impact the catalytic activity for NO oxidation at industrial conditions.

References

[1] E. S. R. Laboratory, *Trends in Atmospheric Carbon Dioxide*. 2019, Accessed 21.04.19. [Online]. Available: https://www.esrl.noaa.gov/gmd/ccgg/trends/full.html.

[2] Worldometers, *World Population Projections*. 2019, Accessed 21.04.19. [Online]. Available: https://www.worldometers.info/world-population/.

[3] Enerdata, *Total energy consumption*. 2018, Accessed 21.04.19. [Online]. Available: https://yearbook.enerdata.net/total-energy/world-consumption-statistics.html.

[4] N. Goverment, *Plant nutrients in the soil*. 2018, Accessed 28.06.19. [Online]. Available: https://www.dpi.nsw.gov.au/agriculture/soils/improvement/plant-nutrients.

[5] S. norske leksikon, *Fullgjødsel*. 2016, Accessed 21.04.19. [Online]. Available: https://snl.no/fullgj%C3%B8dsel.

[6] Yara, *Basic agronomy facts*. 2018, Accessed 28.06.19. [Online]. Available: https://www.yara.com/crop-nutrition/why-fertilizer/basic-agronomy-facts/.

[7] E. Britannica, *Nitric Acid*. 2018, Accessed 24.04.19. [Online]. Available: https://www.britannica.com/science/nitric-acid.

[8] J. G. Speight, "Chapter Three - Industrial Inorganic Chemistry", J. G. Speight, Ed., pp. 111–169, 2017. [Online]. Available: http://www.sciencedirect.com/science/article/pii/B9780128498910000035.

[9] A. M. Research, *Global Nitric Acid Market Size 2017*. 2018, Accessed 24.04.19. [Online]. Available: https://www.adroitmarketresearch.com/industry-reports/nitric-acid-market.

[10] J. A. Moulijn, M. Makkee, and A. E. V. Diepen, *Chemical Process Technology*, 2nd ed. UK: Wiley, 2013.

[11] M. Thieman, E. Scheibler, and K. W. Wiegand, "Nitric Acid, Nitrous Acid, and Nitrogen Oxides", *Ullmann's Encyclopedia of Industrial Chemistry*, vol. 24, pp. 177–225, 2000. [Online]. Available: https://onlinelibrary.wiley.com/doi/abs/10.1002/14356007.a17_293.

[12] A. U. R. Salman, B. C. Enger, X. Auvray, R. Lødeng, M. Menon, D. Waller, and M. Rønning, "Catalytic oxidation of NO to NO_2 for nitric acid production over a Pt/Al_2O_3 catalyst", *Applied Catalysis A: General*, vol. 564, pp. 142–146, 2018. [Online]. Available: http://www.sciencedirect.com/science/article/pii/S0926860X18303429.

[13] T. Takami, *Functional Cobalt Oxides: Fundamentals, properties, and applications*, 1st ed. US: Pan Stanford, 2014.

[14] K. Schmidt-Szałowski, K. Krawczyk, and J. Petryk, "The properties of cobalt oxide catalyst for ammonia oxidation", *Applied Catalysis A: General*, vol. 175, no. 1, pp. 147–157, 1998. [Online]. Available: http://www.sciencedirect.com/science/article/pii/S0926860X98002063.

[15] H.-K. Lin, H.-C. Chiu, H.-C. Tsai, S.-H. Chien, and C.-B. Wang, "Synthesis, Characterization and Catalytic Oxidation of Carbon Monoxide over Cobalt Oxide", *Catalysis Letters*, vol. 88, no. 3, pp. 169–174, 2003. [Online]. Available: https://doi.org/10.1023/A:1024013822986.

[16] S. Royer and D. Duprez, "Catalytic Oxidation of Carbon Monoxide over Transition Metal Oxides", *ChemCatChem*, vol. 3, no. 1, pp. 24–65, 2011. [Online]. Available: https://onlinelibrary.wiley.com/doi/abs/10.1002/cctc.201000378.

[17] Z. Li, M. Si, L. Xin, R. Liu, R. Liu, and J. Lü, "Cobalt catalysts for Fischer–Tropsch synthesis: The effect of support, precipitant and pH value", *Chinese Journal of Chemical Engineering*, vol. 26, no. 4, pp. 747–752, 2018. [Online]. Available: http://www.sciencedirect.com/science/article/pii/S1004954117310182.

[18] K. Shimura, T. Miyazawa, T. Hanaoka, and S. Hirata, "Fischer–Tropsch synthesis over TiO2 supported cobalt catalyst: Effect of TiO2 crystal phase and metal ion loading", *Applied Catalysis A: General*, vol. 460-461, pp. 8–14, 2013. [Online]. Available: http://www.sciencedirect.com/science/article/pii/S0926860X13002147.

[19] B. W.-L. Jang, J. J. Spivey, M. C. Kung, and H. H. Kung, "Low-temperature NOx removal for flue gas cleanup", *Energy & Fuels*, vol. 11, no. 2, pp. 299–306, 1997. DOI: 10.1021/ef960138w.

[20] Y. Huang, D. Gao, Z. Tong, J. Zhang, and H. Luo, "Oxidation of NO over cobalt oxide supported on mesoporous silica", *Journal of Natural Gas Chemistry*, vol. 18, no. 4, pp. 421–428, 2009. [Online]. Available: http://www.sciencedirect.com/science/article/pii/S1003995308601358.

[21] D. S. Kim, Y. H. Kim, J. E. Yie, and E. D. Park, "No oxidation over supported cobalt oxide catalysts", *Korean Journal of Chemical Engineering*, vol. 27, no. 1, pp. 49–54, 2010. [Online]. Available: https://doi.org/10.1007/s11814-009-0290-8.

[22] B. M. Weiss, N. Artioli, and E. Iglesia, "Catalytic NO oxidation pathways and redox cycles on dispersed oxides of rhodium and cobalt", *ChemCatChem*, vol. 4, no. 9, pp. 1397–1404, [Online]. Available: https://onlinelibrary.wiley.com/doi/abs/10.1002/cctc.201200050.

[23] L. Li, Q. Shen, J. Cheng, and Z. Hao, "Catalytic oxidation of NO over TiO_2 supported platinum clusters I. Preparation, characterization and catalytic properties", *Applied Catalysis B: Environmental*, vol. 93, no. 3, pp. 259–266, 2010. [Online]. Available: http://www.sciencedirect.com/science/article/pii/S0926337309003919.

[24] L. Li, L. Qu, J. Cheng, J. Li, and Z. Hao, "Oxidation of nitric oxide to nitrogen dioxide over Ru catalysts", *Applied Catalysis B: Environmental*, vol. 88, no. 1, pp. 224–231, 2009. [Online]. Available: http://www.sciencedirect.com/science/article/pii/S0926337308003834.

[25] Q. Wang, S. Y. Park, L. Duan, and J. S. Chung, "Activity, stability and characterization of NO oxidation catalyst Co/KxTi_2O_5", *Applied Catalysis B: Environmental*, vol. 85, no. 1, pp. 10–16, 2008. [Online]. Available: http://www.sciencedirect.com/science/article/pii/S0926337308002385.

[26] M. M. Yung, E. M. Holmgreen, and U. S. Ozkan, "Cobalt-based catalysts supported on titania and zirconia for the oxidation of nitric oxide to nitrogen dioxide", *Journal of Catalysis*, vol. 247, no. 2, pp. 356–367, 2007. [Online]. Available: http://www.sciencedirect.com/science/article/pii/S0021951707000644.

[27] M. F. Irfan, J. H. Goo, and S. D. Kim, "Co_3O_4 based catalysts for NO oxidation and NOx reduction in fast SCR process", *Applied Catalysis B: Environmental*, vol. 78, no. 3, pp. 267–274, 2008. [Online]. Available: http://www.sciencedirect.com/science/article/pii/S0926337307003050.

[28] Y. Yu, L. Zhong, J. Ding, W. Cai, and Q. Zhong, "Cobalt supported on metal-doped ceria catalysts (M = Zr, Sn and Ti) for NO oxidation", *RSC Adv.*, vol. 5, pp. 23 193–23 201, 30 2015. DOI: 10.1039/C4RA15439H. [Online]. Available: http://dx.doi.org/10.1039/C4RA15439H.

[29] J. Hagen, *Industrial Catalysis: A Practical Approach*, 2nd ed. Germany: Wiley-VCH, 2006.

[30] J. T. Richardson, *Principles of Catalyst Development (Fundamental and Applied Catalysis)*, 1st ed. US: Springer, 1989.

[31] G. Busca, "Chapter Three - Structural, Surface, and Catalytic Properties of Aluminas", Advances in Catalysis, vol. 57, F. C. Jentoft, Ed., pp. 319–404, 2014. [Online]. Available: http://www.sciencedirect.com/science/article/pii/B9780128001271000035.

[32] N. E. Tsakoumis, M. Rønning, Ø. Borg, E. Rytter, and A. Holmen, "Deactivation of cobalt based Fischer–Tropsch catalysts: A review", *Catalysis Today*, vol. 154, no. 3, pp. 162–182, 2010, Eleventh International Symposium on Catalyst Deactivation , Delft(The Netherlands,) October 25-28, 2009. [Online]. Available: http://www.sciencedirect.com/science/article/pii/S0920586110002282.

[33] I. Chorkendorff and J. W. Niemantsverdriet, *Concepts of Modern Catalysis and Kinetics*, 3rd ed. Germany: Wiley-VCH, 2017.

[34] N. M. J. Samira Bagheri and S. B. A. Hamid, "Titanium Dioxide as a Catalyst Support in Heterogeneous Catalysis", *The Scientific World Journal*, vol. 2014, pp. 1–21, 15 2014. [Online]. Available: https://doi.org/10.1155/2014/727496.

[35] T. Fröschl, U. Hörmann, P. Kubiak, G. Kučerová, M. Pfanzelt, C. K. Weiss, R. J. Behm, N. Hüsing, U. Kaiser, K. Landfester, and M. Wohlfahrt-Mehrens, "High surface area crystalline titanium dioxide: Potential and limits in electrochemical energy storage and catalysis", *Chem. Soc. Rev.*, vol. 41, pp. 5313–5360, 15 2012. [Online]. Available: http://dx.doi.org/10.1039/C2CS35013K.

[36] T. Montini, M. Melchionna, M. Monai, and P. Fornasiero, "Fundamentals and Catalytic Applications of CeO_2-Based Materials", *Chemical Reviews*, vol. 116, no. 10, pp. 5987–6041, 2016. [Online]. Available: https://doi.org/10.1021/acs.chemrev.5b00603.

[37] S. Velu, M. Kapoor, S. Inagaki, and K. Suzuki, "Vapor phase hydrogenation of phenol over palladium supported on mesoporous CeO_2 and ZrO_2", *Applied Catalysis A: General*, vol. 245, no. 2, pp. 317–331, 2003. [Online]. Available: http://www.sciencedirect.com/science/article/pii/S0926860X02006555.

[38] Z.-Y. Yuan, V. Idakiev, A. Vantomme, T. Tabakova, T.-Z. Ren, and B.-L. Su, "Mesoporous and nanostructured CeO_2 as supports of nano-sized gold catalysts for low-temperature water-gas shift reaction", *Catalysis Today*, vol. 131, no. 1, pp. 203–210, 2008, Recent advances in catalysis - selected papers from APCAT 4 (Singapore, 6-8 December 2006). [Online]. Available: http://www.sciencedirect.com/science/article/pii/S0920586107006232.

[39] Z. Liu, J. Li, M. Buettner, R. V. Ranganathan, M. Uddi, and R. Wang, "Metal–Support Interactions in CeO_2- and SiO_2-Supported Cobalt Catalysts: Effect of Support Morphology, Reducibility, and Interfacial Configuration", *ACS Applied Materials & Interfaces*, vol. 11, no. 18, pp. 17 035–17 049, 2019. [Online]. Available: https://doi.org/10.1021/acsami.9b02455.

[40] J. Liu, Z. Zhao, J. Wang, C. Xu, A. Duan, G. Jiang, and Q. Yang, "The highly active catalysts of nanometric CeO_2-supported cobalt oxides for soot combustion", *Applied Catalysis B: Environmental*, vol. 84, no. 1, pp. 185–195, 2008. [Online].

Available: http://www.sciencedirect.com/science/article/pii/S0926337308001227.

[41] G. Ertl, H. Knözinger, F. Schüth, and J. Weitkamp, *Handbook of Heterogeneous Catalysis*, 2nd ed. Germany: Wiley-VCH, 2008, vol. 1.

[42] H. E. Bergna and W. O. Roberts, *Colloidal Silica: Fundamentals and Applications*, 1st ed. US: CRC press, 2005.

[43] T. Yamaguchi, "Application of ZrO_2 as a catalyst and a catalyst support", *Catalysis Today*, vol. 20, no. 2, pp. 199–217, 1994. [Online]. Available: http://www.sciencedirect.com/science/article/pii/0920586194800030.

[44] K. P. de Jong, *Synthesis of Solid Catalysts*, 1st ed. Germany: Wiley-VCH, 2009.

[45] C. H. Bartholomew and R. J. Farrauto, *Fundamentals of Industrial Catalytic Processes*, 2nd ed. US: Wiley-AIChE, 2006.

[46] S. Lowell, J. E. Shields, M. A. Thomas, and M. Thommes, *Characterization of Porous Solids and Powders: Surface Area, Pore Size and Density*, 1st ed. Dordrecht: Springer Netherlands, 2004.

[47] O. Tronstad, "Overflate og porefordelingsmålinger", *Institutt for industriell kjemi*, NTH, 1992.

[48] E. P. Barrett, L. G. Joyner, and P. P. Halenda, "The Determination of Pore Volume and Area Distributions in Porous Substances. I. Computations from Nitrogen Isotherms", *Journal of the American Chemical Society*, vol. 73, no. 1, pp. 373–380, 1951. [Online]. Available: https://doi.org/10.1021/ja01145a126.

[49] A. Galarneau, F. Villemot, J. Rodriguez, F. Fajula, and B. Coasne, "Validity of the t-plot Method to Assess Microporosity in Hierarchical Micro/Mesoporous Materials", *Langmuir*, vol. 30, no. 44, pp. 13 266–13 274, 2014. [Online]. Available: https://doi.org/10.1021/la5026679.

[50] N. Tamura and P. U. Gilbert, "Chapter Twenty-One - X-Ray Microdiffraction of Biominerals", in *Research Methods in Biomineralization Science*, ser. Methods in Enzymology, J. J. D. Yoreo, Ed., vol. 532, Academic Press, 2013, pp. 501–531. [Online]. Available: http://www.sciencedirect.com/science/article/pii/B9780124166172000217.

[51] Ø. Borg, S. Eri, E. A. Blekkan, S. Storsæter, H. Wigum, E. Rytter, and A. Holmen, "Fischer–Tropsch synthesis over γ-alumina-supported cobalt catalysts: Effect of support variables", *Journal of Catalysis*, vol. 248, no. 1, pp. 89–100, 2007. [Online]. Available: http://www.sciencedirect.com/science/article/pii/S0021951707001042.

[52] M. Saracevic, "NO TO NO_2 OXIDATION OVER SUPPORTED COBALT OXIDE CATALYSTS", Specialization Project, Department of Chemical Engineering, Trondheim, 2018.

[53] I. B. B. Sathyaseelan and K. Sivakumar, "Phase Transition Behavior of Nanocrystalline Al_2O_3 Powders", *Soft Nanoscience Letters*, vol. 3, no. 4, pp. 69–74, 2013. [Online]. Available: http://dx.doi.org/10.4236/snl.2013.34012.

[54] H.-f. Xiong, Y.-h. Zhang, J.-l. Li, and Y.-y. Gu, "Effect of cobalt loading on reducibility, dispersion and crystallite size of Co/Al_2O_3 fischer-tropsch catalyst", *Journal of Central South University of Technology*, vol. 11, no. 4, pp. 414–418, 2004. [Online]. Available: https://doi.org/10.1007/s11771-004-0086-2.

[55] G. Jacobs, P. M. Patterson, T. K. Das, M. Luo, and B. H. Davis, "Fischer–Tropsch synthesis: Effect of water on Co/Al_2O_3 catalysts and XAFS characterization of reoxidation phenomena", *Applied Catalysis A: General*, vol. 270, no. 1, pp. 65–76, 2004. [Online]. Available: http://www.sciencedirect.com/science/article/pii/S0926860X04003758.

[56] B. Jongsomjit and J. G. Goodwin, "Co-support compound formation in Co/Al_2O_3 catalysts: Effect of reduction gas containing CO", *Catalysis Today*, vol. 77, no. 3, pp. 191–204, 2002. [Online]. Available: http://www.sciencedirect.com/science/article/pii/S0920586102002456.

[57] J. Martens, H. V. '. Blik, and R. Prins, "Characterization of supported cobalt and cobalt-rhodium catalysts: II. Temperature-Programmed Reduction (TPR) and Oxidation (TPO) of $CoTiO_2$ and $Co-RhTiO_2$", *Journal of Catalysis*, vol. 97, no. 1, pp. 200–209, 1986. [Online]. Available: http://www.sciencedirect.com/science/article/pii/0021951786900503.

[58] G. Jacobs, T. K. Das, P. M. Patterson, J. Li, L. Sanchez, and B. H. Davis, "Fischer–tropsch synthesis XAFS: XAFS studies of the effect of water on a Pt-promoted Co/Al_2O_3 catalyst", *Applied Catalysis A: General*, vol. 247, no. 2, pp. 335–343, 2003. [Online]. Available: http://www.sciencedirect.com/science/article/pii/S0926860X03001078.

[59] C. L. Bianchi, "TPR and XPS Investigations of Co/Al_2O_3 Catalysts Promoted with Ru, Ir and Pt", *Catalysis Letters*, vol. 76, no. 3, pp. 155–159, 2001. [Online]. Available: https://doi.org/10.1023/A:1012289211065.

[60] M. Khosravi-Nikou and A. Bahrami, "A New Method for Synthesis of Cobalt-based Nano-catalyst on Titania for Fischer-Tropsch Reaction", *Energy Sources, Part A: Recovery, Utilization, and Environmental Effects*, vol. 37, no. 19, pp. 2041–2046, 2015. [Online]. Available: https://doi.org/10.1080/15567036.2011.604372.

[61] L. Qiu, Y. Wang, D. Pang, F. Ouyang, C. Zhang, and G. Cao, "Characterization and Catalytic Activity of Mn−Co/TiO_2 Catalysts for NO Oxidation to NO_2 at Low Temperature", *Catalysts*, vol. 6, no. 1, 2016. [Online]. Available: https://www.mdpi.com/2073-4344/6/1/9.

[62] J. Li, G. Lu, G. Wu, D. Mao, Y. Guo, Y. Wang, and Y. Guo, "Effect of TiO_2 crystal structure on the catalytic performance of Co_3O_4/TiO_2 catalyst for low-temperature CO oxidation", *Catal. Sci. Technol.*, vol. 4, pp. 1268–1275, 5 2014. [Online]. Available: http://dx.doi.org/10.1039/C3CY01004J.

[63] A. Khodakov, J. Lynch, D. Bazin, B. Rebours, N. Zanier, B. Moisson, and P. Chaumette, "Reducibility of Cobalt Species in Silica-Supported Fischer–Tropsch Catalysts", *Journal of Catalysis*, vol. 168, no. 1, pp. 16–25, 1997. [Online]. Available: http://www.sciencedirect.com/science/article/pii/S0021951797915736.

[64] J.-Y. Luo, M. Meng, X. Li, X.-G. Li, Y.-Q. Zha, T.-D. Hu, Y.-N. Xie, and J. Zhang, "Mesoporous Co_3O_4–CeO_2 and Pd/Co_3O_4–CeO_2 catalysts: Synthesis, characterization and mechanistic study of their catalytic properties for low-temperature CO oxidation", *Journal of Catalysis*, vol. 254, no. 2, pp. 310–324, 2008. [Online]. Available: http://www.sciencedirect.com/science/article/pii/S0021951708000146.

[65] H. Song, L. Zhang, and U. Ozkan, "Fuel Cell Grade Hydrogen Production from the Bio-Ethanol Steam Reforming over Co-based Catalysts: An Investigation of Reaction Networks and Active Sites", Jan. 2006.

[66] J.-G. Chen and Y.-H. Sun, "The structure and reactivity of coprecipitated Co-ZrO_2 catalysts for Fischer-Tropsch synthesis", in *Natural Gas Conversion VII*, ser. Studies in Surface Science and Catalysis, X. Bao and Y. Xu, Eds., vol. 147, Elsevier, 2004, pp. 277–282. [Online]. Available: http://www.sciencedirect.com/science/article/pii/S0167299104800648.

[67] B. Davis and M. L. Occelli, *Advances in Fischer-Tropsch Synthesis, Catalysts, and Catalysis*, 1st ed., ser. Chemical Industries. US: CRC Press, 2009.

[68] F. Zhang, Y. Yan, H. Yang, Y. Meng, C. Yu, B. Tu, and D. Zhao, "Understanding Effect of Wall Structure on the Hydrothermal Stability of Mesostructured Silica SBA-15", *The journal of physical chemistry. B*, vol. 109, pp. 8723–32, Jun. 2005. DOI: 10.1021/jp044632+.

[69] J. Choi, Y. Han, S. Park, J. Park, and H. Kim, "Pore Characteristics and Hydrothermal Stability of Mesoporous Silica: Role of Oleic Acid", *Journal of Nanomaterials*, vol. 2014, pp. 1–8, Jul. 2014. DOI: 10.1155/2014/580347.

[70] A. Jha, D.-W. Jeong, Y.-L. Lee, I. W. Nah, and H.-S. Roh, “Enhancing the catalytic performance of cobalt oxide by doping on ceria in the high temperature water–gas shift reaction”, *RSC Adv.*, vol. 5, pp. 103 023–103 029, 125 2015. [Online]. Available: http://dx.doi.org/10.1039/C5RA22704F.

[71] Y. Li and W. Shen, “Morphology-dependent nanocatalysts: Rod-shaped oxides”, *Chem. Soc. Rev.*, vol. 43, pp. 1543–1574, 5 2014. [Online]. Available: http://dx.doi.org/10.1039/C3CS60296F.

Appendix A

Catalyst synthesis calculations

In total there were 17 catalysts made by incipient wetness impregnation. Table A.1 shows the chemical used in the synthesis and the calculated IWP of all the supports:

Table A.1: The chemical used in the synthesis and the calculated IWP of all the supports.

Chemical	Supplier	CAS-number	Purity [%]	M_w [$g\,mol^{-1}$]	IWP
$Co(NO_3)_2 \cdot 6H_2O$	Sigma-Aldrich	10026-22-9	≤ 100	291.03	-
$Pt(IV)NO_3$ sol	Alfa-Aesar	10102-09-7	Pt 15 w/w	-	-
$K(NO_3)$	Sigma-Aldrich	7757-79-1	-	101.10	-
γ-Al_2O_3	Sasol-Puralox	1344-28-1	≤ 100	-	1.32
TiO_2	Alfa Aesar	1317-70-0	≤ 99	-	1.128
SiO_2	Alfa Aesar	7631-86-9	> 95	-	1.539
CeO_2	Rhodia	1306-38-3	≤ 100	-	0.619
ZrO_2	Thermo Fisher	1314-23-4	> 95	-	0.781

Below shows an example calculation of the alumina supported catalysts with 5wt%Co:

$$\text{Total amount of catalyst} = 5g \tag{A.1}$$

$$Co\,[g] = 0.05 \cdot 5g = 0.25g \tag{A.2}$$

$$\gamma - Al_2O_3\,[g] = (1 - 0.05) \cdot 5g = 4.75g \tag{A.3}$$

$$Co\,[moles] = \frac{0.25\,g}{58.9332\,g/moles} = 0.0042421\,moles \tag{A.4}$$

$$\mathrm{Co(NO_3)_2 \cdot 6H_2O}\,[g] = 0.0042421\,moles \cdot 291.03\,g/moles = 1.235\,g \tag{A.5}$$

$$\mathrm{H_2O_{IWP}}\,[g] = 1.32 \cdot 4.75\,g = 6.27\,g \tag{A.6}$$

$$\mathrm{H_2O_{Co(NO_3)_2 \cdot 6H_2O}}\,[g] = 6 \cdot 0.004221\,moles \cdot 18\,g/moles = 0.45815\,g \tag{A.7}$$

$$\mathrm{H_2O_{Deionized\ water}}\,[g] = 6.27 - 0.45815 = 5.81g \tag{A.8}$$

Below shows how the platinum promoted cobalt oxide catalyst was calculated (20 wt%Co, 0.5 wt%Pt /$\gamma - \mathrm{Al_2O_3}$:

$$\text{Total amount of catalyst} = 5g \tag{A.9}$$

$$Co\,[g] = 0.20 \cdot 5g = 1g \tag{A.10}$$

$$Pt\,[g] = 0.005 \cdot 5g = 0.025g \tag{A.11}$$

$$\gamma - \mathrm{Al_2O_3}\,[g] = (1 - 0.20 - 0.025) \cdot 5g = 3.975g \tag{A.12}$$

$$Co\,[moles] = \frac{1\,g}{58.9332\,g/moles} = 0.0169684\,moles \tag{A.13}$$

$$\mathrm{Co(NO_3)_2 \cdot 6H_2O}\,[g] = 0.0169684\,moles \cdot 291.03\,g/moles = 4.9383\,g \tag{A.14}$$

$$Pt_{\text{nitrate solution}}\,[g] = \frac{0.025\,g}{0.15} = 0.166667\,g \approx 0.166667\,ml \tag{A.15}$$

$$\mathrm{H_2O_{IWP}}\,[g] = 1.32 \cdot 3.975\,g = 5.247\,g \tag{A.16}$$

$$\mathrm{H_2O_{Co(NO_3)_2 \cdot 6H_2O}}\,[g] = 6 \cdot 0.0169684\,moles \cdot 18\,g/moles = 1.832583\,g \tag{A.17}$$

$$\mathrm{H_2O_{Pt/nitrate\ solution}}\,[g] = (1 - 0.15) \cdot 0.166667\,g = 0.141667\,g \tag{A.18}$$

$$\mathrm{H_2O_{Deionized\ water}}\,[g] = 5.247 - 1.832583 - 0.141667 = 3.27275g \tag{A.19}$$

Below shows how the potassium promoted cobalt oxide catalyst was calculated (20 wt%Co, 5 wt%K /$\gamma - \mathrm{Al_2O_3}$:

$$\text{Total amount of catalyst} = 5g \tag{A.20}$$

$$Co\,[g] = 0.20 \cdot 5g = 1g \tag{A.21}$$

$$K\,[g] = 0.05 \cdot 5g = 0.25g \tag{A.22}$$

$$\gamma - \mathrm{Al_2O_3}\,[g] = (1 - 0.20 - 0.25) \cdot 5g = 3.75g \tag{A.23}$$

$$Co\,[moles] = \frac{1\,g}{58.9332\,g/moles} = 0.0169684\,moles \tag{A.24}$$

$$\mathrm{Co(NO_3)_2 \cdot 6H_2O}\,[g] = 0.0169684\,moles \cdot 291.03\,g/moles = 4.9383\,g \tag{A.25}$$

$$K\,[moles] = \frac{0.25\,g}{39.0983\,g/moles} = 0.006394\,moles \tag{A.26}$$

$$\mathrm{KNO_3}\,[g] = 0.006394\,moles \cdot 101.1\,g/moles = 0.646448\,g \tag{A.27}$$

$$H_2O_{IWP}\,[g] = 1.32 \cdot 3.75\,g = 4.95\,g \tag{A.28}$$

$$H_2O_{Co(NO_3)_2 \cdot 6H_2O}\,[g] = 6 \cdot 0.0169684\,moles \cdot 18\,g/moles = 1.832583\,g \tag{A.29}$$

$$H_2O_{\text{Deionized water}}\,[g] = 4.95 - 1.832583 - 0.141667 = 3.11742g \tag{A.30}$$

Table A.2 shows a summary of the weights of the different calculations steps involving for synthesis of the alumina supported catalysts.

Table A.2: A summary of all the weights used to determine the synthesis calculations for the alumina supported catalysts

Catalyst	5wt%Co [g]	10wt%Co [g]	20wt%Co [g]	20wt%Co, 0.5wt%Pt [g]	20wt%Co, 5wt%K [g]
$Co(NO_3)_2 \cdot 6H_2O$	1.2346	2.4692	4.9383	4.9383	4.9383
$Pt(NO_3)_4$ solution	-	-	-	0.1667	-
KNO_3	-	-	-	-	0.6464
$\gamma - Al_2O_3$	4.75	4.50	4.00	3.975	3.75
H_2O(IWP)	6.27	5.94	5.28	5.247	4.95
Water formed	0.4581	0.9163	1.8326	1.9743	1.8326
Deionized water	5.8119	5.0237	3.4474	3.2727	3.1174

Table A.3 shows a summary of the weights of the different calculations steps involving the synthesis of the titania supported catalysts.

Table A.3: A summary of all the weights used to determine the synthesis calculations for the titania supported catalysts

Catalyst	5wt%Co [g]	10wt%Co [g]	20wt%Co [g]
$Co(NO_3)_2 \cdot 6H_2O$	1.2346	2.4692	4.9383
TiO_2	4.75	4.50	4.00
H_2O(IWP)	5.36	5.07	4.5107
Water formed	0.4581	0.9163	1.8326
Deionized water	4.8983	4.1583	2.6781

Table A.4 shows a summary of the weights of the different calculations steps involving the synthesis of the silica supported catalysts.

Table A.4: A summary of all the weights used to determine the synthesis calculations for the silica supported catalysts

Catalyst	5wt%Co [g]	10wt%Co [g]	20wt%Co [g]
$Co(NO_3)_2 \cdot 6H_2O$	1.1111	2.2222	4.4444
SiO_2	4.275	4.05	3.60
H_2O(IWP)	6.58	6.23	5.54
Water formed	0.4123	0.8247	1.6493
Deionized water	6.1648	5.4062	3.8893

Table A.5 shows a summary of the weights of the different calculations steps involving the synthesis of the ceria supported catalysts.

Table A.5: A summary of all the weights used to determine the synthesis calculations for the ceria supported catalysts

Catalyst	5wt%Co	10wt%Co	20wt%Co	
			First	Second
	[g]	[g]	[g]	
$Co(NO_3)_2 \cdot 6H_2O$	1.2346	2.4692	2.4692	2.4692
CeO_2	4.75	4.50	4.00	-
H_2O(IWP)	2.94	2.79	2.48	2.48
Water formed	0.4581	0.9163	0.9163	0.9163
Deionized water	2.4820	1.8691	1.5596	1.5596

Table A.6 shows a summary of the weights of the different calculations steps involving the synthesis of the zirconia supported catalysts.

Table A.6: A summary of all the weights used to determine the synthesis calculations for the zirconia supported catalysts

Catalyst	5wt%Co	10wt%Co	20wt%Co	
			First	Second
	[g]	[g]	[g]	
$Co(NO_3)_2 \cdot 6H_2O$	0.7407	1.4815	1.4815	1.4815
ZrO_2	2.85	2.70	2.40	-
H_2O(IWP)	2.23	2.11	1.87	1.87
Water formed	0.2749	0.5498	0.5498	0.5498
Deionized water	1.9510	1.5590	1.3246	1.3246

Appendix B

Sample preparations

B.1 Nitrogen adsorption/desorption sample weights

Table B.1 shows the weights of the calcined supports before and after the vacuum procedure for nitrogen adsorption/desorption analysis:

Table B.1: The weights of the calcined supports before and after the vacuum procedure for nitrogen adsorption/desorption analysis

Calcined support	Weight before vacuum [g]	Weight after vacuum [g]
Al_2O_3	0.2022	0.1882
TiO_2	0.2100	0.2019
SiO_2	0.2066	0.1991
CeO_2	0.2009	0.1933
ZrO_2	0.2022	0.1969

B.2 TPR sample weights

Table B.2 shows the amount of catalyst placed inside the U-tube reactor for TPR analysis:

Table B.2: The weights of the various catalysts for TPR analysis

Support	5wt%Co [g]	10wt%Co [g]	20wt%Co [g]
Al_2O_3	0.1000	0.1079	0.1052
TiO_2	0.1071	0.1076	0.1076
SiO_2	0.1107	0.1062	0.1086
CeO_2	0.1049	0.1024	0.1055
ZrO_2	0.1056	0.1100	0.0988
	20wt%Co-0.5wt%Pt [g]		20wt%Co-5wt%K [g]
Al_2O_3	0.1060		0.1065

In addition, TPR-experiment of pure CeO_2 was performed with a sample weight of 0.0968 g.

Table B.3 shows the amount of catalyst and SiC placed inside the reactor for wet-TPR analysis:

Table B.3: The weights of the catalysts and SiC for wet-TPR analysis

Catalyst	Sample [g]	SiC [g]
20wt%Co/Al_2O_3	0.5030	2.7561
20wt%Co/SiO_2	0.5018	2.7534
20wt%Co/CeO_2	0.5018	2.7570
20wt%Co/ZrO_2	0.5011	2.7522

B.3 Activity measurements

Table B.4 shows the amount of catalyst and SiC weight placed inside the reactor for the activity measurements of NO oxidation over supported cobalt oxide catalysts:

Table B.4: The amount of catalyst and SiC weight placed inside the reactor for the activity measurements of NO oxidation over supported cobalt oxide catalysts

Support	Type	5wt%Co [g]	10wt%Co [g]	20wt%Co [g]
Al_2O_3	Catalyst	0.5048	0.5015	0.5062
	SiC	2.7546	2.7514	2.7543
TiO_2	Catalyst	0.5027	0.5045	0.5030
	SiC	2.7532	2.7537	2.7555
SiO_2	Catalyst	0.5054	0.5045	0.5006
	SiC	2.7547	2.7540	2.7514
CeO_2	Catalyst	0.5092	0.5040	0.5025
	SiC	2.7538	2.7552	2.7528
ZrO_2	Catalyst	0.5027	0.5043	0.5013
	SiC	2.7528	2.7531	2.7547
		20wt%Co-0.5wt%Pt [g]		20wt%Co-5wt%K [g]
Al_2O_3	Catalyst	0.5022		0.5036
	SiC	2.7529		2.7536

Table B.5 shows the amount placed inside the reactor for the activity measurements of NO oxidation over SiC, CeO_2 and Co_3O_4:

Table B.5: The amount placed inside the reactor for the activity measurements of NO oxidation over SiC, CeO_2 and Co_3O_4

Type	Sample [g]	SiC [g]
SiC	-	2.7512
CeO_2	0.5030	2.7515
Co_3O_4	0.5016	2.7519

Appendix C

Nitrogen adsorption/desorption

Figure C.1 shows the nitrogen adsorption/desorption isotherms and the pore size distribution of the calcined Al_2O_3 support:

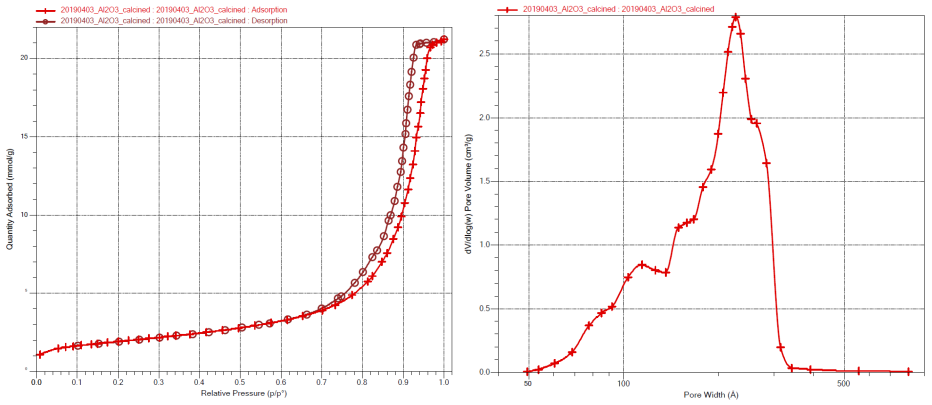

Figure C.1: The nitrogen adsorption/desorption isotherms and the pore size distribution of the calcined Al_2O_3 support

Figure C.2 shows the nitrogen adsorption/desorption isotherms and the pore size distribution of the calcined TiO_2 support:

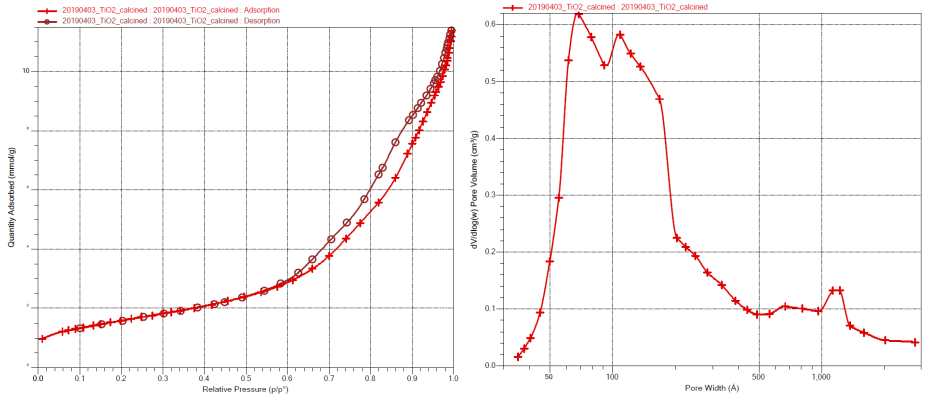

Figure C.2: The nitrogen adsorption/desorption isotherms and the pore size distribution of the calcined TiO_2 support

Figure C.3 shows the nitrogen adsorption/desorption isotherms and the pore size distribution of the calcined SiO_2 support:

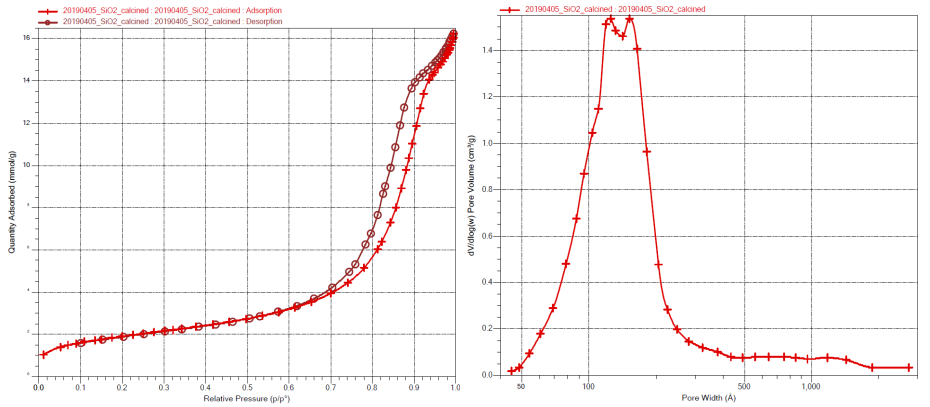

Figure C.3: The nitrogen adsorption/desorption isotherms and the pore size distribution of the calcined SiO_2 support

Figure C.4 shows the nitrogen adsorption/desorption isotherms and the pore size distribution of the calcined CeO_2 support:

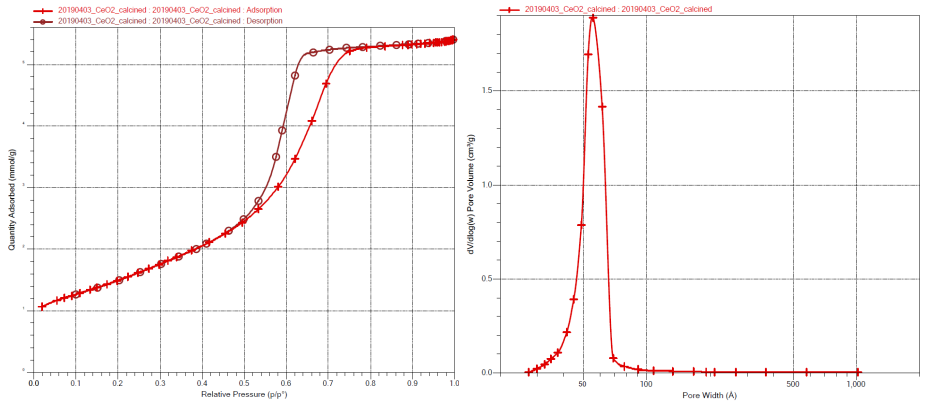

Figure C.4: The nitrogen adsorption/desorption isotherms and the pore size distribution of the calcined CeO_2 support

Figure C.5 shows the nitrogen adsorption/desorption isotherms and the pore size distribution of the calcined ZrO_2 support:

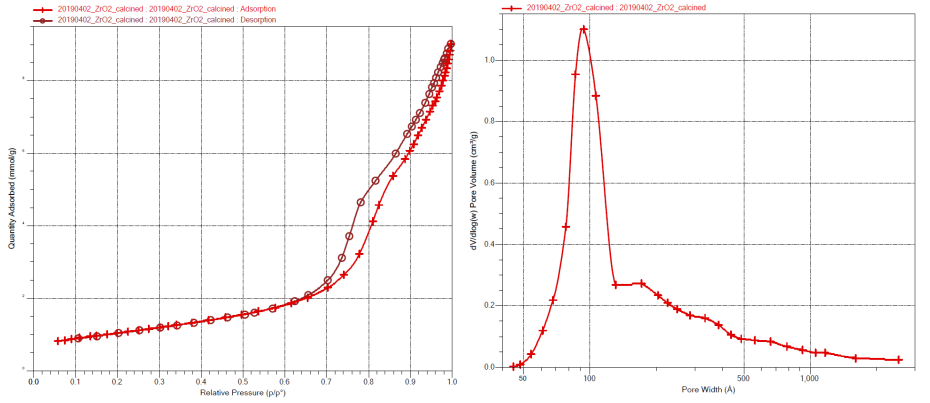

Figure C.5: The nitrogen adsorption/desorption isotherms and the pore size distribution of the calcined ZrO_2 support

Appendix D

X-ray diffraction

D.1 Alumina supported catalysts

Figure D.1 shows the XRD pattern of the 5wt%Co/Al_2O_3:

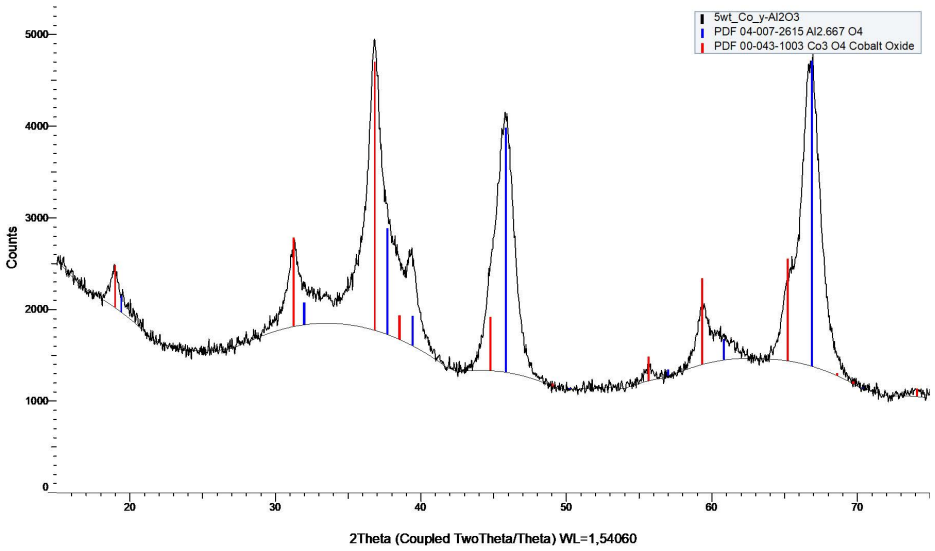

Figure D.1: The XRD pattern of the 5wt%Co/Al_2O_3

Figure D.2 shows the XRD pattern of the 10wt%Co/Al_2O_3:

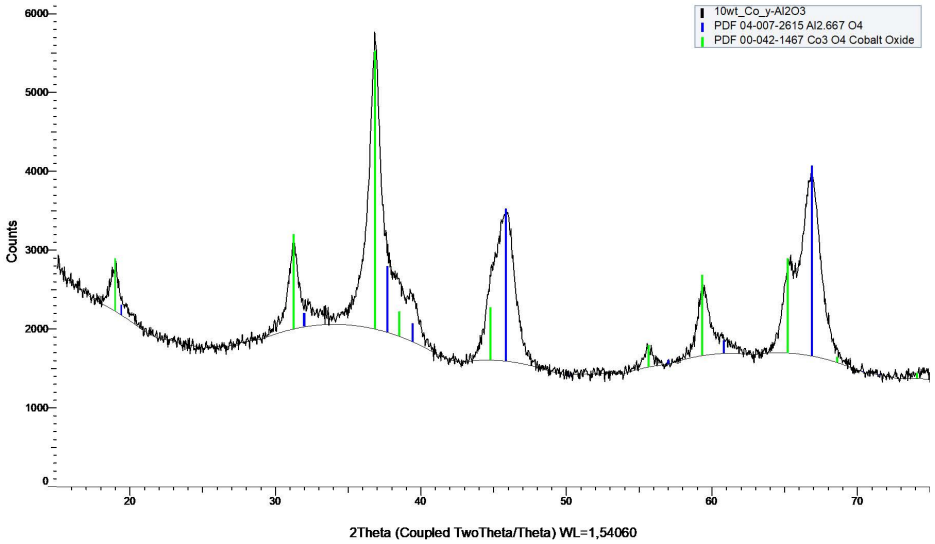

Figure D.2: The XRD pattern of the 10wt%Co/Al_2O_3

Figure D.3 shows the XRD pattern of the 20wt%Co/Al_2O_3:

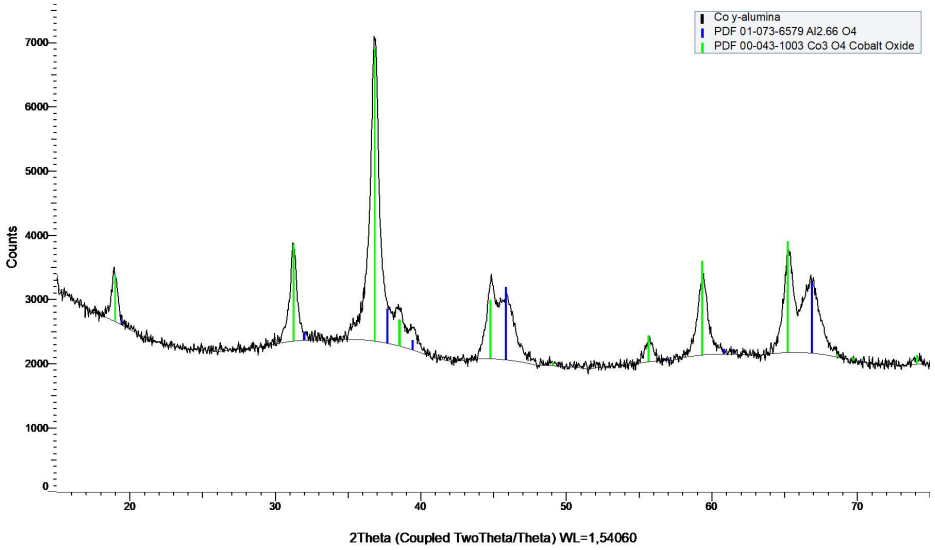

Figure D.3: The XRD pattern of the 20wt%Co/Al_2O_3

Figure D.4 shows the XRD pattern of the 20wt%Co-0.5wt%Pt/Al_2O_3:

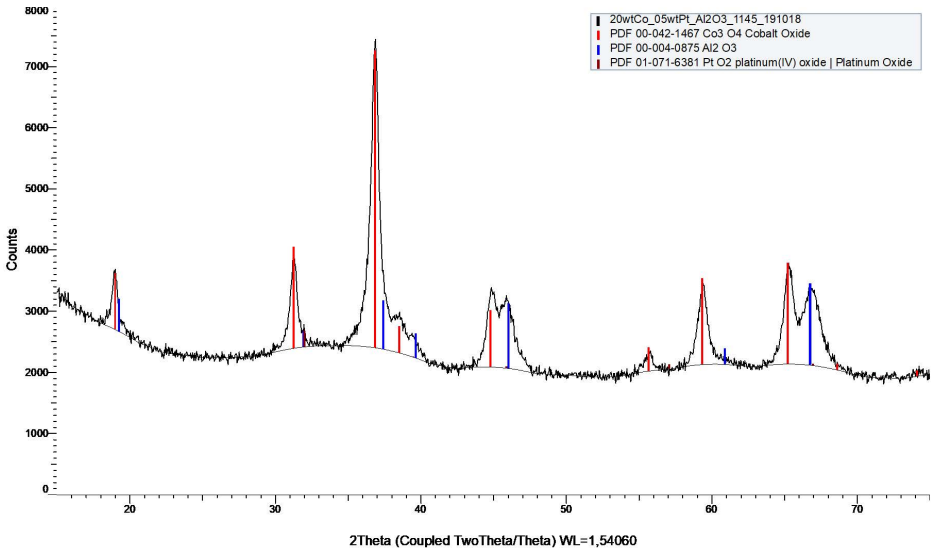

Figure D.4: The 20wt%Co-0.5wt%Pt/Al_2O_3

Figure D.5 shows the XRD pattern of 20wt%Co-5wt%K/Al_2O_3:

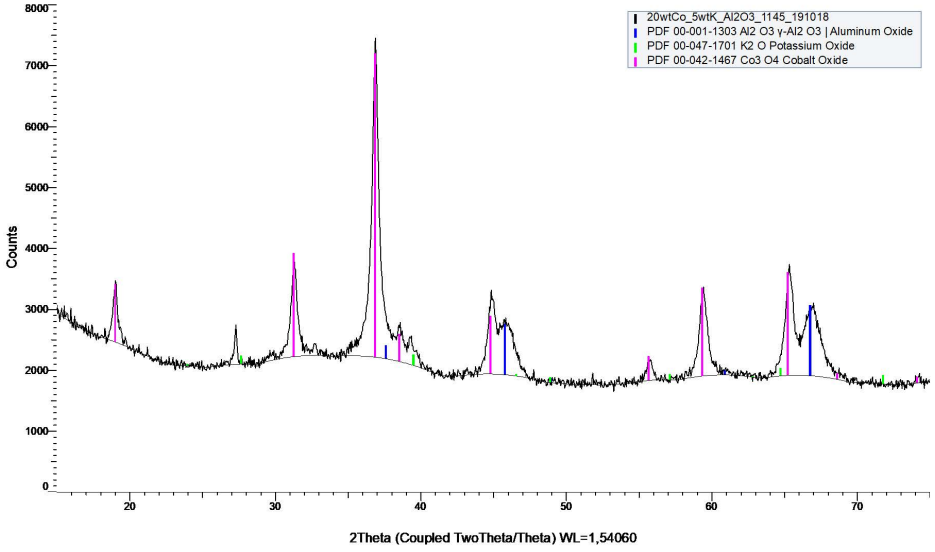

Figure D.5: The XRD pattern of the 20wt%Co-5wt%K/Al_2O_3

D.2 Titania supported catalysts

Figure D.6 shows the XRD pattern of the 5wt%Co/TiO_2:

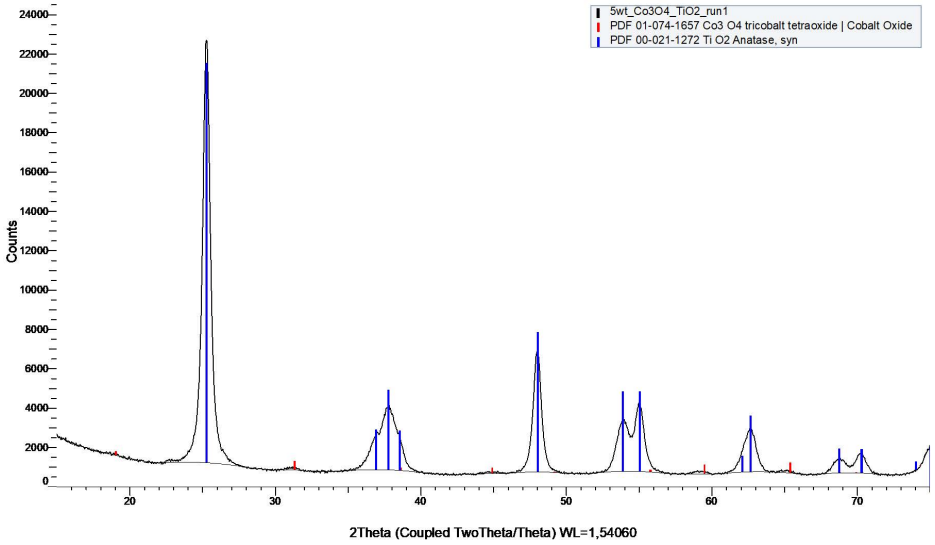

Figure D.6: The XRD pattern of the 5wt%Co/TiO_2

Figure D.7 shows the XRD pattern of the 10wt%Co/TiO_2:

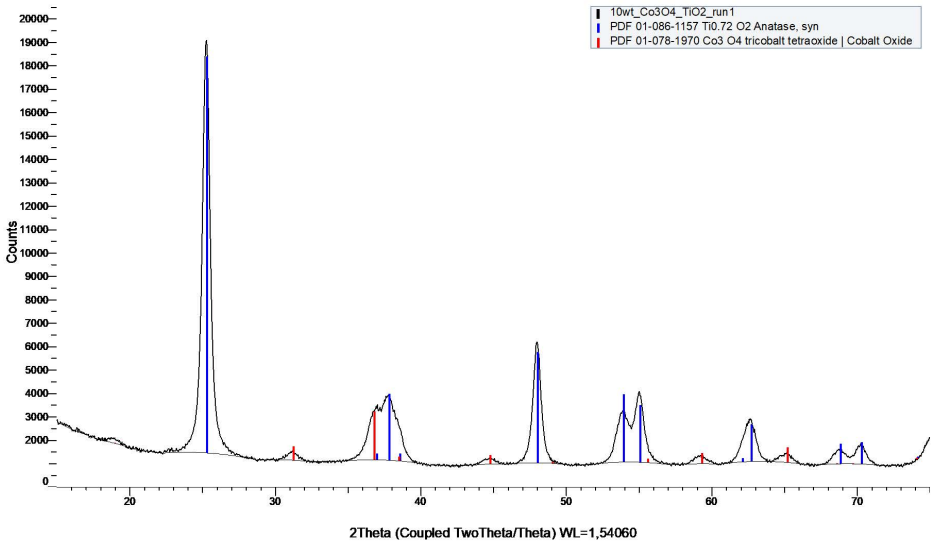

Figure D.7: The XRD pattern of the 10wt%Co/TiO_2

Figure D.8 shows the XRD pattern of the 20wt%Co/TiO_2:

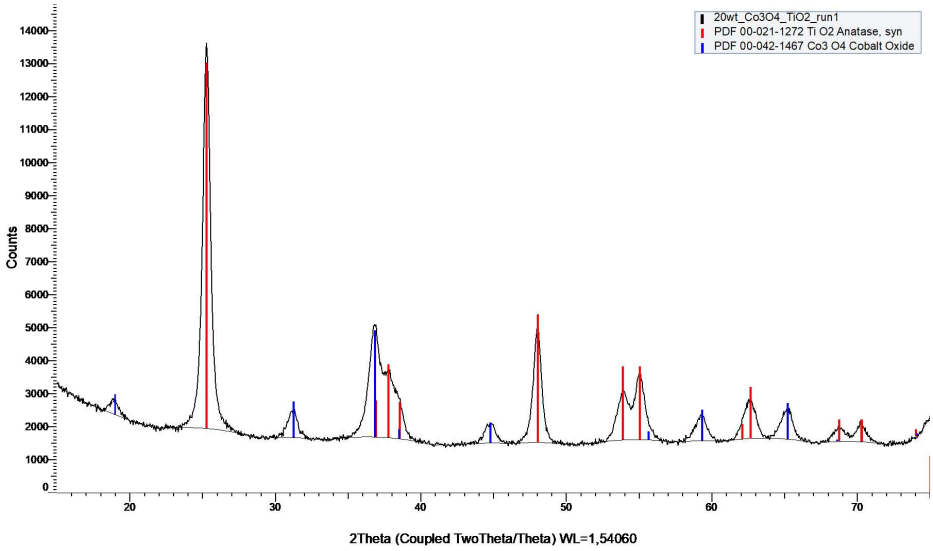

Figure D.8: The XRD pattern of the 20wt%Co/TiO_2

D.3 Silica supported catalysts

Figure D.9 shows the XRD pattern of the 5wt%Co/SiO_2:

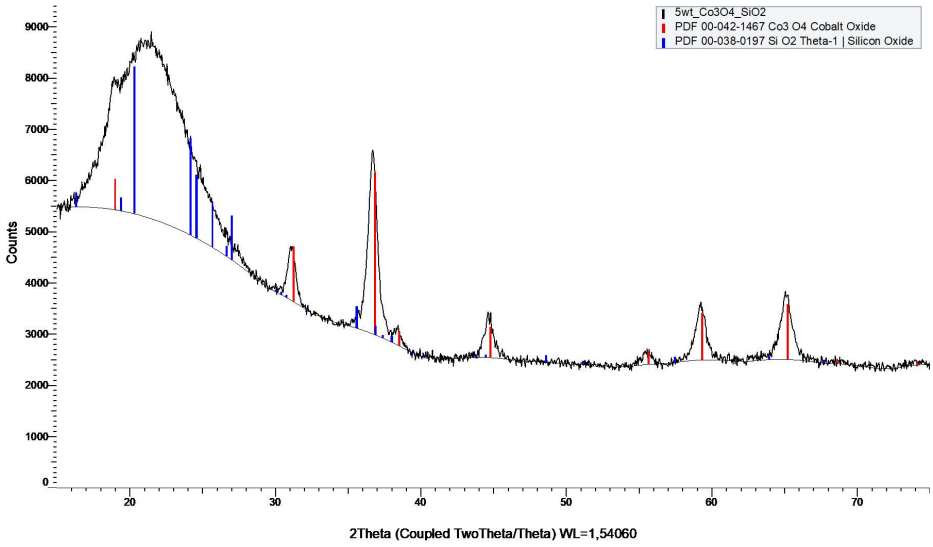

Figure D.9: The XRD pattern of the 5wt%Co/SiO_2

Figure D.10 shows the XRD pattern of the 10wt%Co/SiO_2:

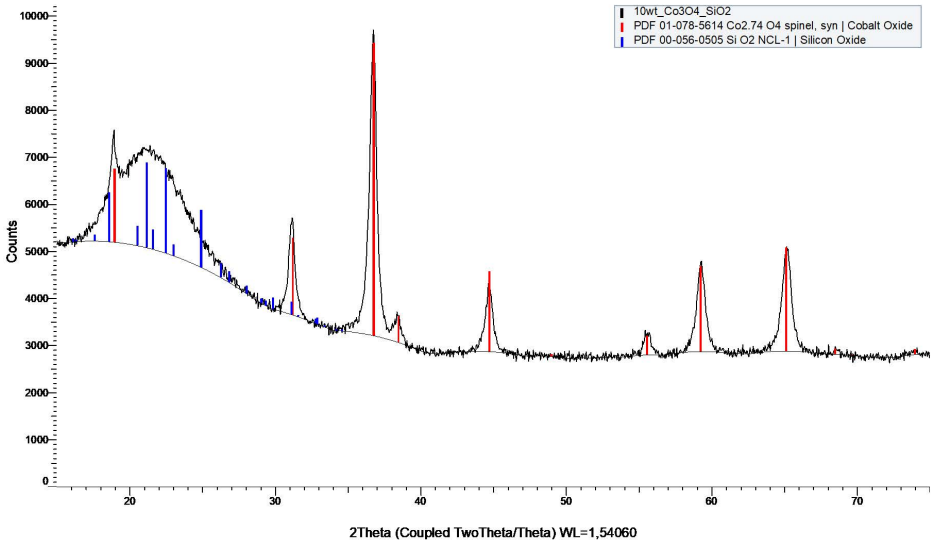

Figure D.10: The XRD pattern of the 10wt%Co/SiO_2

Figure D.11 shows the XRD pattern of the 20wt%Co/SiO_2:

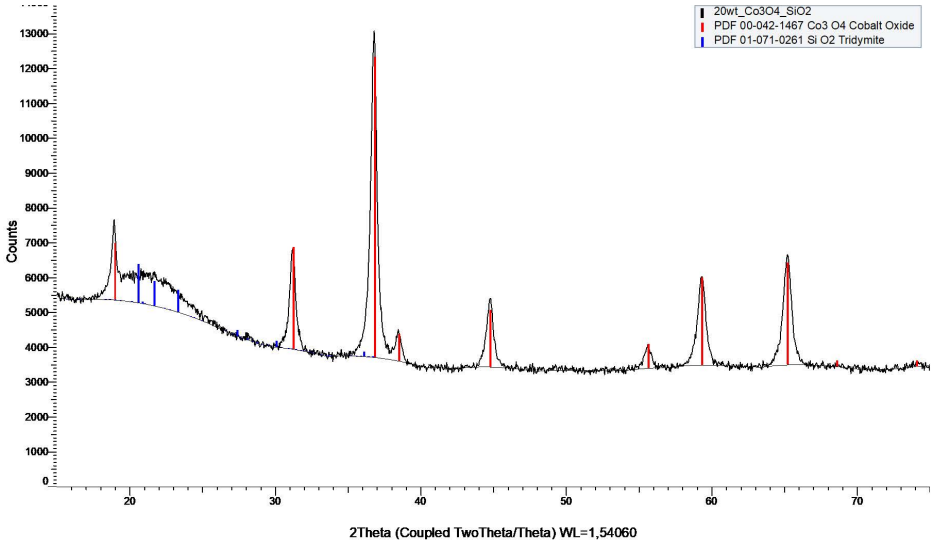

Figure D.11: The XRD pattern of the 20wt%Co/SiO_2

D.4 Ceria supported catalysts

Figure D.12 shows the XRD pattern of the 5wt%Co/CeO_2:

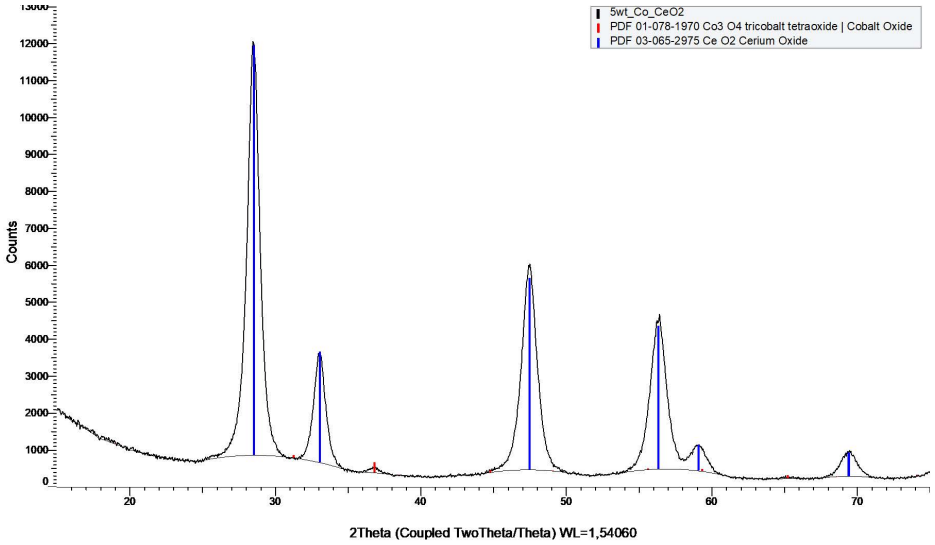

Figure D.12: The XRD pattern of the 5wt%Co/CeO_2

Figure D.13 shows the XRD pattern of the 10wt%Co/CeO_2:

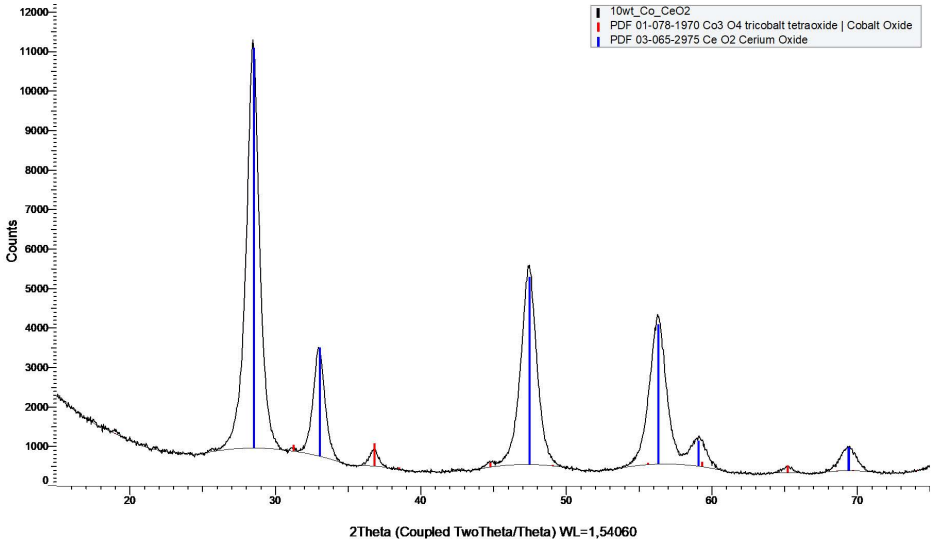

Figure D.13: The XRD pattern of the 10wt%Co/CeO_2

Figure D.14 shows the XRD pattern of the 20wt%Co/CeO_2:

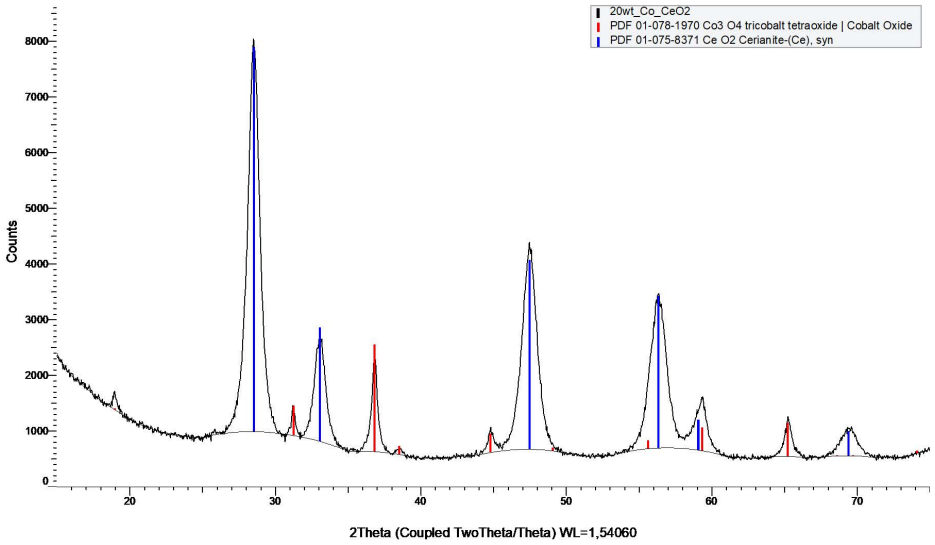

Figure D.14: The XRD pattern of the 20wt%Co/CeO_2

D.5 Zirconia supported catalysts

Figure D.15 shows the XRD pattern of the 5wt%Co/ZrO_2:

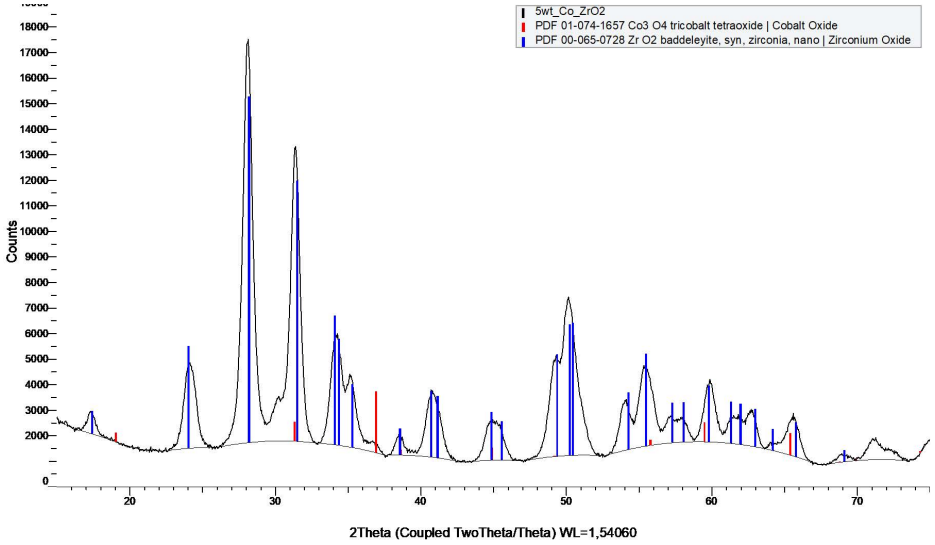

Figure D.15: The XRD pattern of the 5wt%Co/ZrO_2

Figure D.16 shows the XRD pattern of the 10wt%Co/ZrO_2:

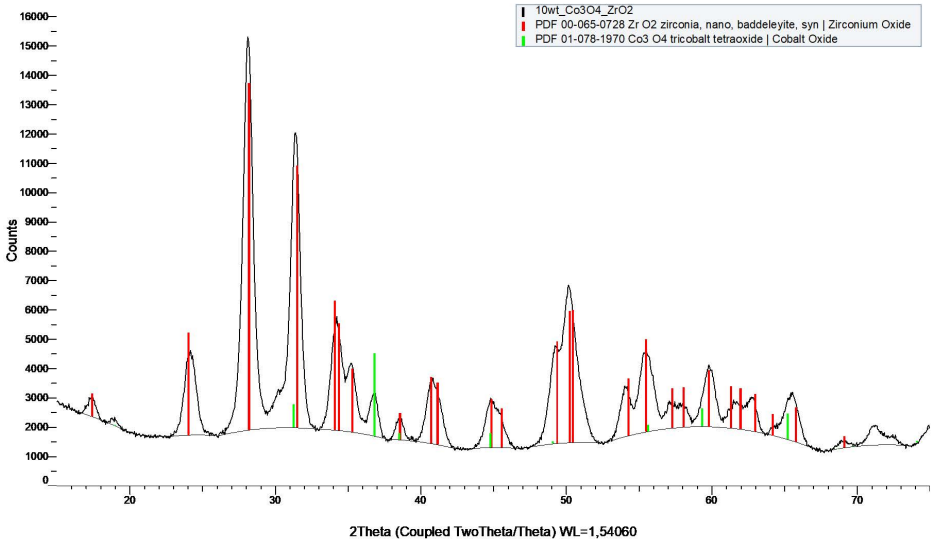

Figure D.16: The XRD pattern of the 10wt%Co/ZrO_2

Figure D.17 shows the XRD pattern of the 20wt%Co/ZrO_2:

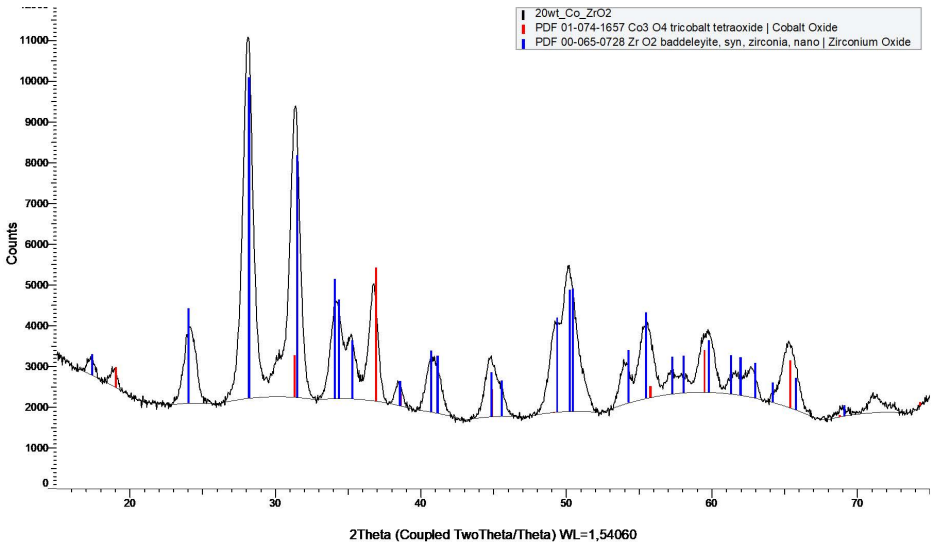

Figure D.17: The XRD pattern of the 20wt%Co/ZrO_2

Appendix E

Activity measurements

In this appendix the unaltered data of the activity measurements of NO oxidation are presented.

E.1 Alumina supported catalysts

Figure E.1 shows the activity measurements of NO oxidation over the cobalt oxides supported on Al_2O_3 with metal loading of 5, 10, and 20wt%Co in dry conditions:

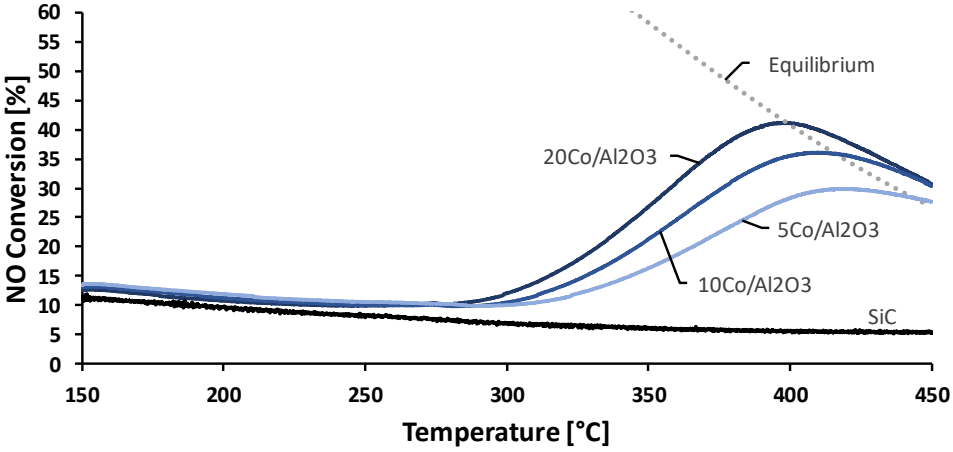

Figure E.1: The NO to NO_2 conversion over cobalt oxides supported on Al_2O_3 with metal loading of 5, 10, and 20wt%Co in dry conditions. GHSV = 43 400 h^{-1}. Feed: 10 % NO, 6 % O_2, rest Ar.

Figure E.2 shows the activity measurements of NO oxidation over the cobalt oxides supported on Al_2O_3 with metal loading of 5, 10, and 20wt%Co in wet conditions:

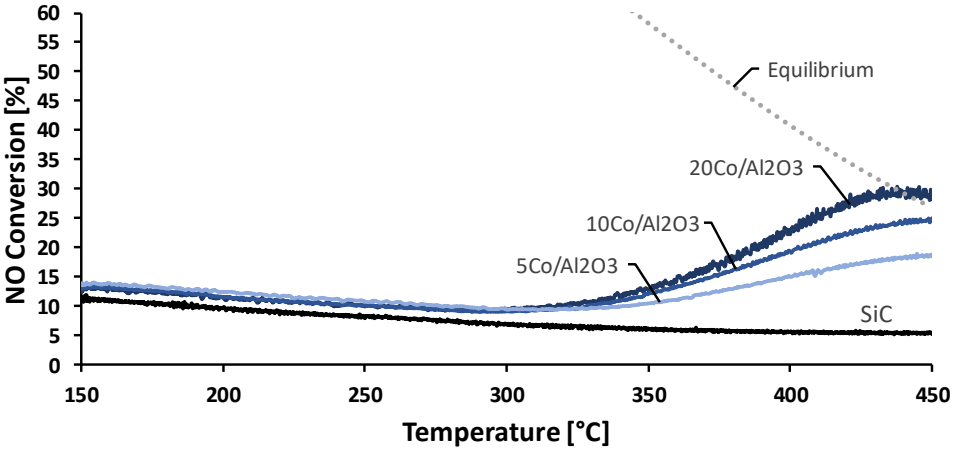

Figure E.2: The NO to NO_2 conversion over cobalt oxides supported on Al_2O_3 with metal loading of 5, 10, and 20wt%Co in wet conditions. GHSV = 43 400 h^{-1}. Feed: 10 % NO, 6 % O_2, rest Ar.

E.2 Promoted catalysts

Figure E.3 shows the activity measurements of NO oxidation over the promoted catalyst supported on Al_2O_3 with $20Co/Al_2O_3$ as a reference in dry conditions:

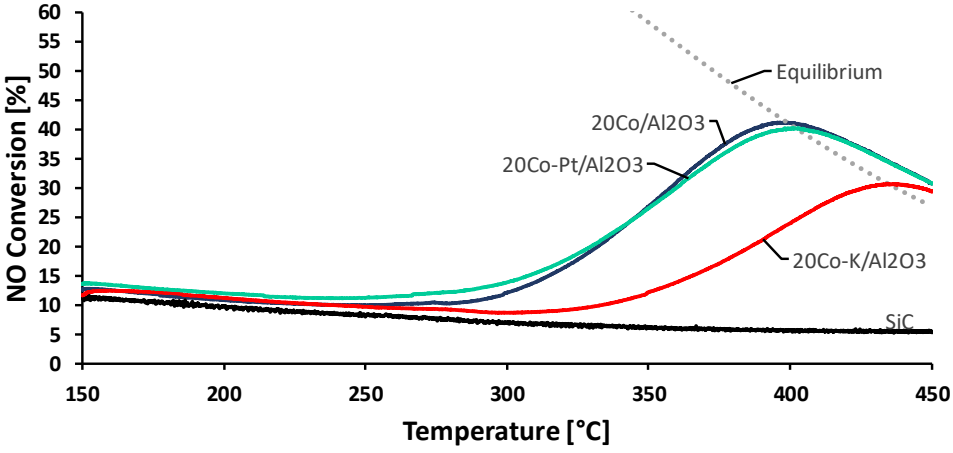

Figure E.3: The NO to NO_2 conversion over the promoted catalyst supported on Al_2O_3 with $20Co/Al_2O_3$ as a reference in dry conditions. GHSV = 43 400 h^{-1}. Feed: 10 % NO, 6 % O_2, rest Ar.

Figure E.4 shows the activity measurements of NO oxidation over the promoted catalyst supported on Al_2O_3 with $20Co/Al_2O_3$ as a reference in wet conditions:

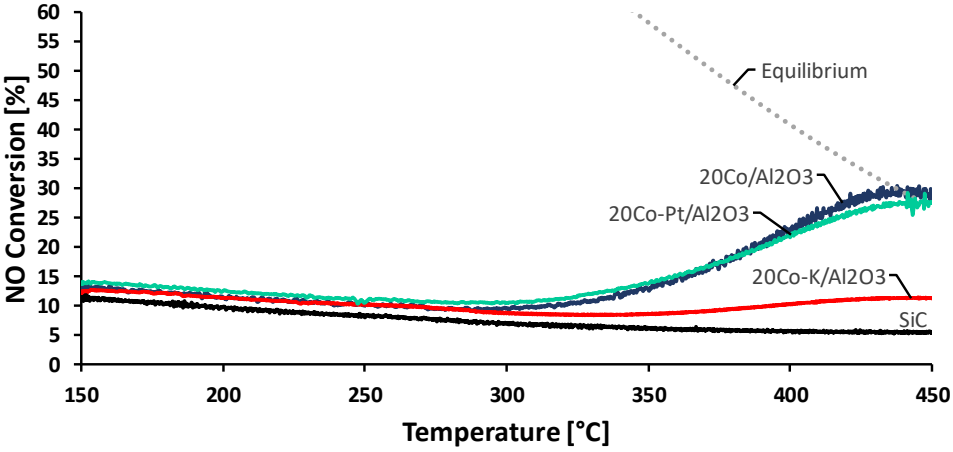

Figure E.4: The NO to NO_2 conversion over the promoted catalyst supported on Al_2O_3 with $20Co/Al_2O_3$ as a reference in wet conditions. GHSV = 43 400 h^{-1}. Feed: 10 % NO, 6 % O_2, 15 % H_2O, rest Ar.

E.3 Titania supported catalysts

Figure E.5 shows the activity measurements of NO oxidation over the cobalt oxides supported on TiO_2 with metal loading of 5, 10, and 20wt%Co in dry conditions:

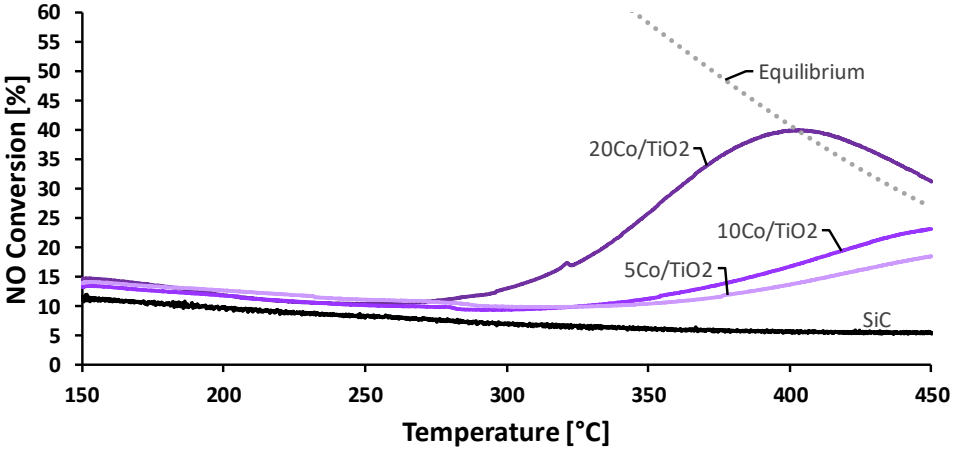

Figure E.5: The NO to NO_2 conversion over cobalt oxides supported on TiO_2 with metal loading of 5, 10, and 20wt%Co in dry conditions. GHSV = 43 400 h^{-1}. Feed: 10 % NO, 6 % O_2, rest Ar.

Figure E.6 shows the activity measurements of NO oxidation over the cobalt oxides supported on TiO_2 with metal loading of 5, 10, and 20wt%Co in wet conditions:

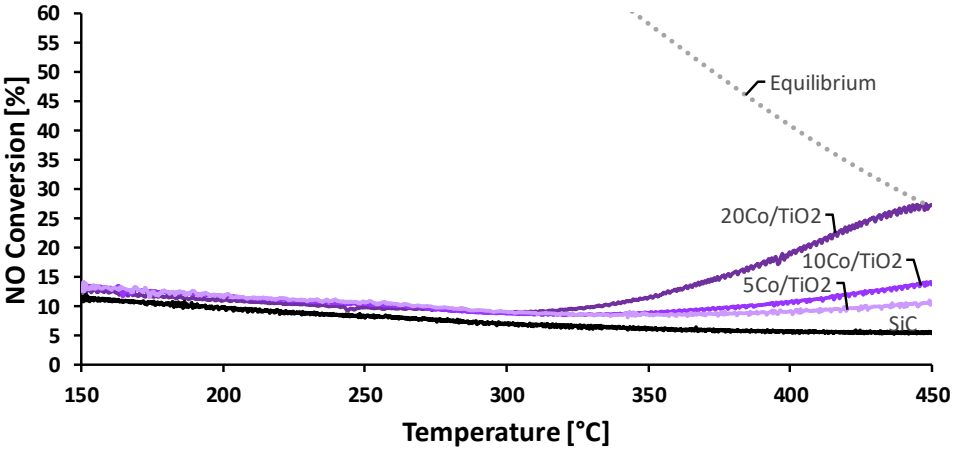

Figure E.6: The NO to NO_2 conversion over cobalt oxides supported on TiO_2 with metal loading of 5, 10, and 20wt%Co in wet conditions. GHSV = 43 400 h^{-1}. Feed: 10 % NO, 6 % O_2, rest Ar.

E.4 Silica supported catalysts

Figure E.7 shows the activity measurements of NO oxidation over the cobalt oxides supported on SiO_2 with metal loading of 5, 10, and 20wt%Co in dry conditions:

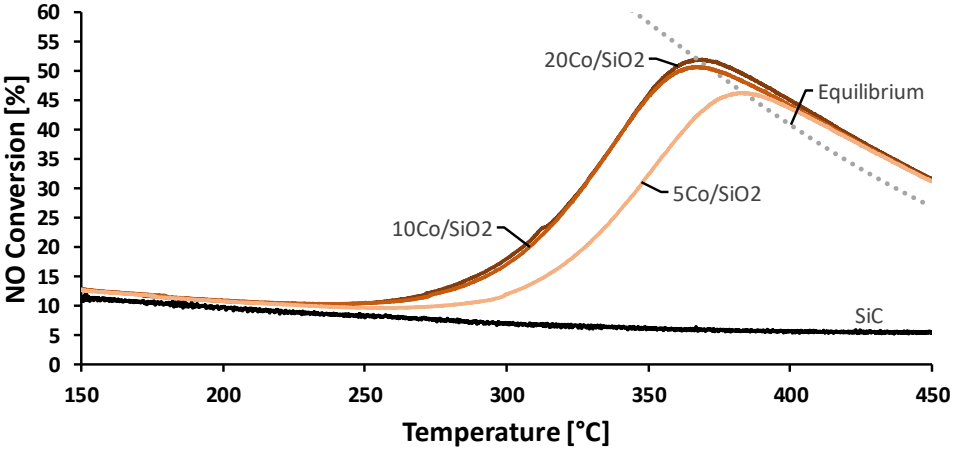

Figure E.7: The NO to NO_2 conversion over cobalt oxides supported on SiO_2 with metal loading of 5, 10, and 20wt%Co in dry conditions. GHSV = 43 400 h^{-1}. Feed: 10 % NO, 6 % O_2, rest Ar.

Figure E.8 shows the activity measurements of NO oxidation over the cobalt oxides supported on SiO_2 with metal loading of 5, 10, and 20wt%Co in wet conditions:

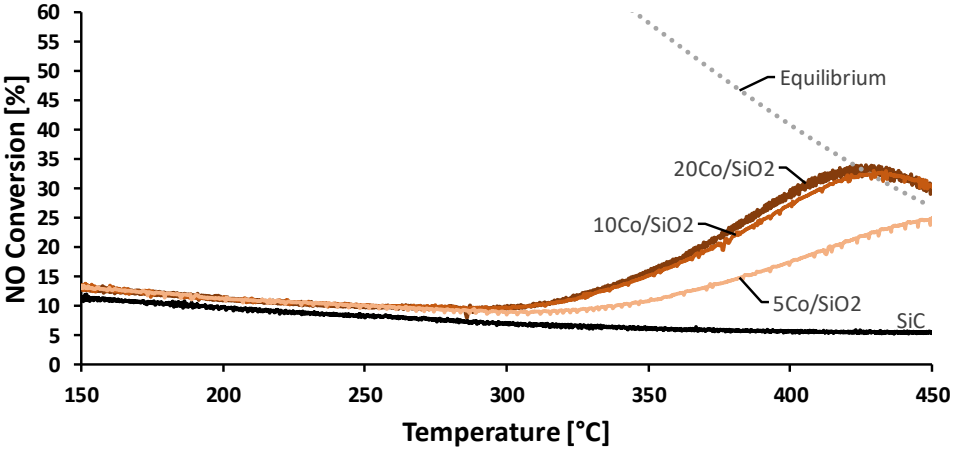

Figure E.8: The NO to NO_2 conversion over cobalt oxides supported on SiO_2 with metal loading of 5, 10, and 20wt%Co in wet conditions. GHSV = 43 400 h^{-1}. Feed: 10 % NO, 6 % O_2, rest Ar.

E.5 Ceria supported catalysts

Figure E.9 shows the activity measurements of NO oxidation over the cobalt oxides supported on CeO_2 with metal loading of 5, 10, and 20wt%Co in dry conditions:

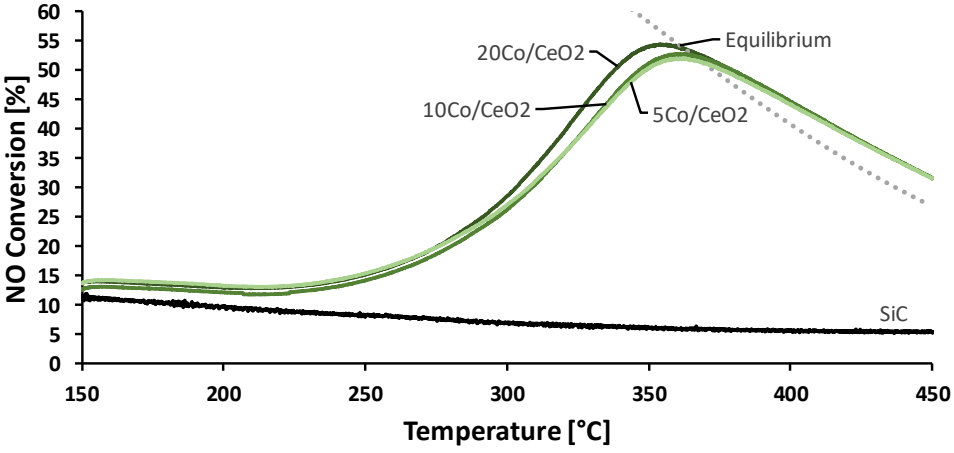

Figure E.9: The NO to NO_2 conversion over cobalt oxides supported on CeO_2 with metal loading of 5, 10, and 20wt%Co in dry conditions. GHSV = 43 400 h^{-1}. Feed: 10 % NO, 6 % O_2, rest Ar.

Figure E.10 shows the activity measurements of NO oxidation over the cobalt oxides supported on CeO_2 with metal loading of 5, 10, and 20wt%Co in wet conditions:

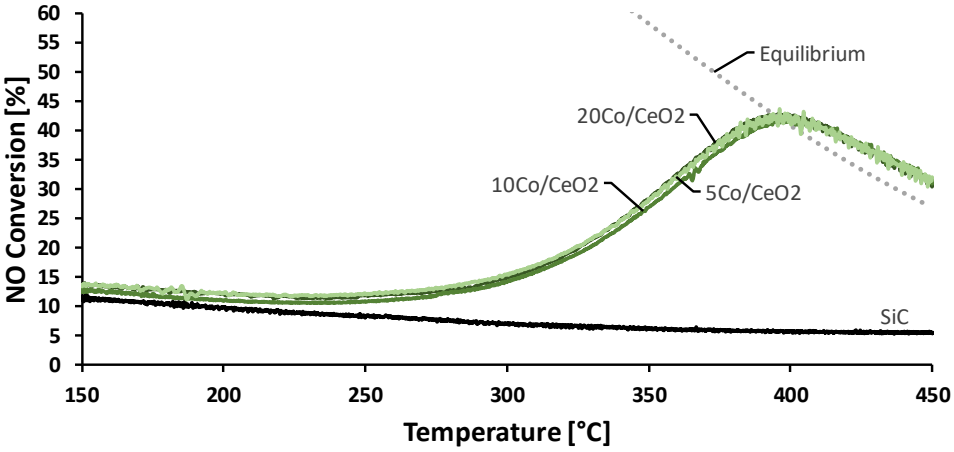

Figure E.10: The NO to NO_2 conversion over cobalt oxides supported on CeO_2 with metal loading of 5, 10, and 20wt%Co in wet conditions. GHSV = 43 400 h^{-1}. Feed: 10 % NO, 6 % O_2, rest Ar.

E.6 Zirconia supported catalysts

Figure E.11 shows the activity measurements of NO oxidation over the cobalt oxides supported on ZrO_2 with metal loading of 5, 10, and 20wt%Co in dry conditions:

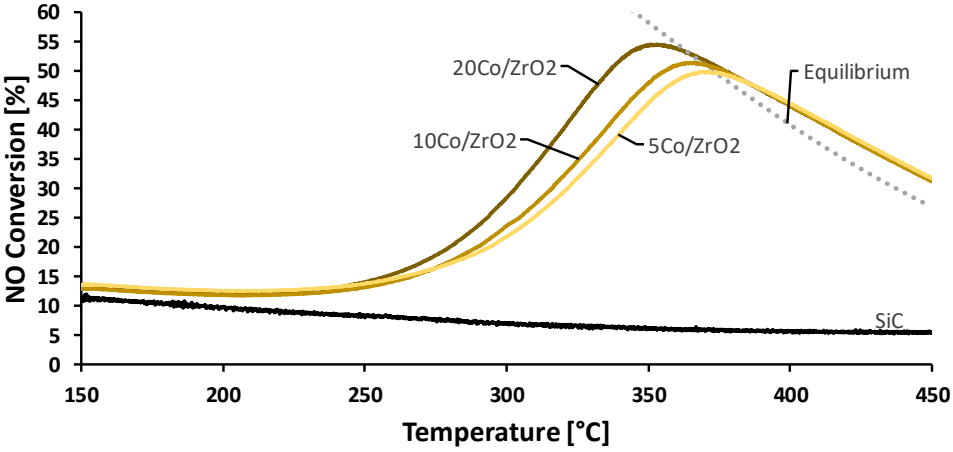

Figure E.11: The NO to NO_2 conversion over cobalt oxides supported on ZrO_2 with metal loading of 5, 10, and 20wt%Co in dry conditions. GHSV = 43 400 h^{-1}. Feed: 10 % NO, 6 % O_2, rest Ar.

Figure E.12 shows the activity measurements of NO oxidation over the cobalt oxides supported on ZrO_2 with metal loading of 5, 10, and 20wt%Co in wet conditions:

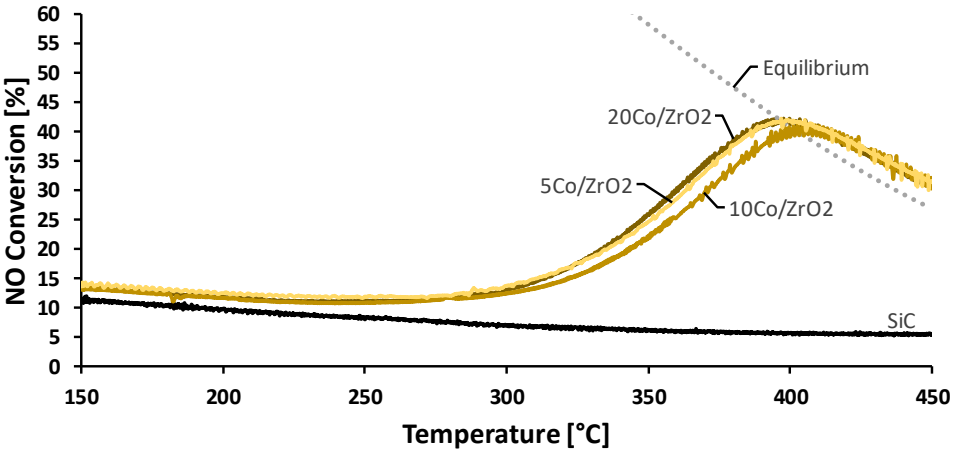

Figure E.12: The NO to NO_2 conversion over cobalt oxides supported on ZrO_2 with metal loading of 5, 10, and 20wt%Co in wet conditions. GHSV = 43 400 h^{-1}. Feed: 10 % NO, 6 % O_2, rest Ar.

E.7 Ceria support

Figure E.13 shows the activity measurements of the NO oxidation over 500 mg CeO_2 and 2.75 SiC in dry and wet conditions:

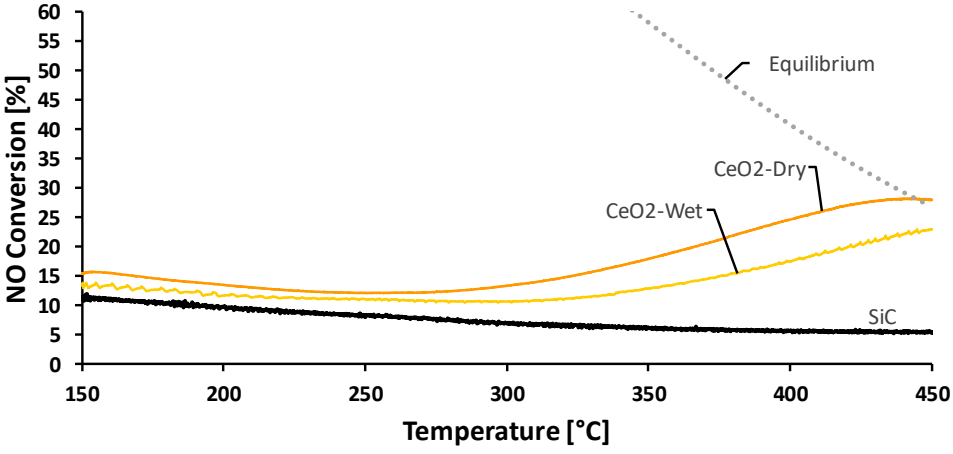

Figure E.13: The NO to NO_2 conversion over CeO_2 in dry and wet conditions. GHSV = 43 400 h^{-1}. Dry feed: 10 % NO, 6 % O_2, rest Ar. Wet feed: 10 % NO, 6 % O_2, 15 % H_2O, rest Ar.

E.8 Pure Cobalt Oxides

Figure E.14 shows the activity measurements of the NO oxidation over 500 mg Co_3O_4 and 2.75 g SiC in dry and wet conditions:

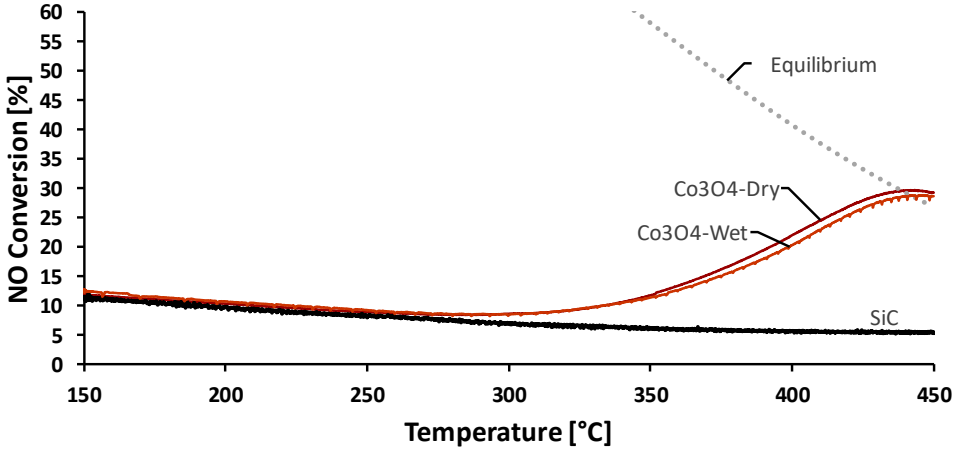

Figure E.14: The NO to NO_2 conversion over Co_3O_4 in dry and wet conditions. GHSV = 43400 h^{-1}. Dry feed: 10 % NO, 6 % O_2, rest Ar. Wet feed: 10 % NO, 6 % O_2, 15 % H_2O, rest Ar.

Appendix F

Risk Assessment

This appendix presents the risk assessment that was made for the specialization project and master thesis. In the risk assessment, not everything is assigned as it should be due to error in the internal system which makes it not possible to edit or remove certain elements.

ID	29640	**Status**	**Dato**
Risikoområde	Risikovurdering: Helse, miljø og sikkerhet (HMS)	Opprettet	05.09.2018
Opprettet av	Minadir Saracevic	Vurdering startet	05.09.2018
Ansvarlig	Magnus Rønning	Tiltak besluttet	05.09.2018
		Avsluttet	

Risikovurdering:

CAT, Master student, 2018, Minadir Saracevic

Gyldig i perioden:

9/5/2018 - 9/5/2021

Sted:

Kjemiblokk 5&2/ Kjemihall D 1.etg og 2.etg

Mål / hensikt

Preparation and synthesise supported cobalt oxide catalyst with γ-alumina, TiO_2, SiO_2, CeO_2 and ZrO_2 as the support. After that, the characterization and activity measurement of the prepared catalysts are performed.

Bakgrunn

The supported cobalt oxide catalysts will be used in oxidizing NO to NO_2 under Ostwald process conditions.

Beskrivelse og avgrensninger

The catalyst support could consist of aluminium oxide in gamma-phase (γ-alumina / γ-Al2O3), titanium dioxide (TiO2) , silicon dioxide (SiO2), cerium oxide (CeO2) and zirconium dioxide. The active phase of the catalyst will be cobalt, where the precursor CoN2O6*6H20 is used during the catalyst synthesis. There will also be made a catalyst which is promoted with Pt, where the Pt source is Pt(IV)(NO3)4 solution, Pt 15% w/w. Finally, one catalyst was promoted with potassium (K), where the K source is KNO3.

Prior to the synthesis procedure, the alumina is pre-calcined at 750 °C for 2h at a rate of 10 °C/min. The pre-calcined alumina is then sieved to get fraction 53-90 um. The incipient wetness impregnation will be used to synthesize the desired catalyst. This was also done for the other support materials but temperatures below 750 °C.

An amount of dried alumina is used to find the incipient wetness point, where it determines the pore volume of the material. This helps to calculate the required amount of deionized water needed for the impregnation method. The required amount of cobalt nitrate (and promoted sources) and deionized water is weighted to make the mixture used to impregnate the alumina. The mixture is added to the alumina using the drop by drop method. The catalyst is then dried overnight in a ventilated oven for at 120 °C, stirring it with a glass rod every 15 min for the first hour and subsequently every 30 min during the second hour. The newly made catalyst is stored in a glass container. This was also done for the other supported catalysts but with different supports.

After synthesis, the catalyst is calcined in a fixed bed quartz reactor under 0.7L/(g.h) airflow at 300 °C with a temperature ramp rate of 2 °C/min for 16h. Subsequently, increase the temperature to 500 °C at 10 °C/min for 2h. Sieve the obtained catalyst to get fraction 53-90 um.

For the characterization methods, the catalyst will be used to prepare a sample which is analyzed. This will include measuring the amount needed, placing inside U-tube reactors and making pellets. All of this risk the user to be exposed towards the catalyst material. For TPR and chemisorption, hydrogen is used to reduce the catalyst sample. TPR has a temperature analysis range of 40-850 °C and chemisorption has a temperature upwards of 400 °C.

The activity measurement has a packed bed reactor which is filled with 500 mg catalyst and 2.75 g inert packing material of SiC. The catalyst is placed between two plugs of quartz wool to keep it in place. The activity measurement used gases like NO, O2 and Ar. The activity measurement is performed in rig 2.1 at 2nd-floor Chemical Hall D. Reactor pressure is at atmospheric and temperature range is 150-450 °C. Pipes can have a temperature upwards of 200 °C.

List overall chemicals used:
Synthesis - CoN2O6*6H20, Al2O3, TiO2, SiO2, CeO2, ZrO2, H2O, KNO3, Pt(IV)(NO3)4 solution, Pt 15% w/w
Characterization and activity- H2, O2, Ar, NO, H3BO3

List of working locations:
Synthesis - ChemHallD 1st floor laboratory at the benches and fume hood
Calcination - ChemHallD apparatus 1.8, set-up 2&3

Characterization:
N2 adsorption/desorption - K5-425 at the working benches in the room and at the apparatus.
XRD - K2-113 at the XRD-lab bench
TPR - ChemHallD 2nd floor at working bench in the hall and at the apparatus
Chemisoprtion - K5-420 at the working bench and in the fume hood
XRF - K5-425 at the working benches in the room

Activity measurements:
ChemHallD 2nd floor at rig 2.1

Forutsetninger, antakelser og forenklinger

[Ingen registreringer]

Vedlegg

APPARATUSCARD[463].pdf
SDS_40%NO.pdf
SDS_O2.pdf
SDS-Cerium (IV) oksid.pdf
SDS-Potassium_nitrate.pdf
SDS-Pt(IV) nitrate solution, Pt 15 ww.pdf
SDS-Titanium (IV) oxide.pdf
SDS_Ar.pdf
SDS_H2.pdf
SDS_Boric acid.pdf
SDS_Cobalt.pdf
SDS_Alumina.pdf
SDS_SiO2.pdf
SDS_SiO2_2.pdf
SDS_ZrO2.pdf

Referanser

[Ingen registreringer]

Oppsummering, resultat og endelig vurdering

I oppsummeringen presenteres en oversikt over farer og uønskede hendelser, samt resultat for det enkelte konsekvensområdet.

Farekilde: **Use of CoN2O6 · 6H2O**

Uønsket hendelse: **Oxidizing by fire**

Konsekvensområde: Helse — Risiko før tiltak:  Risiko etter tiltak: 

Ytre miljø — Risiko før tiltak:  Risiko etter tiltak: 

Materielle verdier — Risiko før tiltak:  Risiko etter tiltak: 

Risikoreduserende tiltak	Ansvarlig	Registrert	Frist	Status
Fire extinguisher	Minadir Saracevic	05.09.2018	02.07.2019	Evaluert

Uønsket hendelse: **Spillage on skin**

Konsekvensområde: Helse — Risiko før tiltak:  Risiko etter tiltak: 

Risikoreduserende tiltak	Ansvarlig	Registrert	Frist	Status
Lab coat	Minadir Saracevic	05.09.2018	05.09.2018	Evaluert
Gloves	Minadir Saracevic	05.09.2018	02.07.2019	Evaluert

Uønsket hendelse: **Splash into the eyes**

Konsekvensområde: Helse — Risiko før tiltak:  Risiko etter tiltak: 

Risikoreduserende tiltak	Ansvarlig	Registrert	Frist	Status
Fume hood	Minadir Saracevic	05.09.2018	02.07.2019	Evaluert
Safety googles	Minadir Saracevic	05.09.2018	02.07.2019	Evaluert

Uønsket hendelse: **Inhalation to respiratory system and oral ingestion**

Konsekvensområde: Helse — Risiko før tiltak:  Risiko etter tiltak: 

Risikoreduserende tiltak	Ansvarlig	Registrert	Frist	Status
Lab coat	Minadir Saracevic	05.09.2018	05.09.2018	Evaluert
Fume hood	Minadir Saracevic	05.09.2018	02.07.2019	Evaluert
Gloves	Minadir Saracevic	05.09.2018	02.07.2019	Evaluert
Dust mask	Minadir Saracevic	08.01.2019	02.07.2019	Evaluert

Farekilde: **Use of γ-Al2O3**

Uønsket hendelse: **Irritating to respiratory system and skin**

Konsekvensområde: Helse — Risiko før tiltak: Risiko etter tiltak:

Risikoreduserende tiltak	Ansvarlig	Registrert	Frist	Status
Lab coat	Minadir Saracevic	05.09.2018	05.09.2018	Evaluert
Fume hood	Minadir Saracevic	05.09.2018	02.07.2019	Evaluert
Gloves	Minadir Saracevic	05.09.2018	02.07.2019	Evaluert

Farekilde: **Heated surfaces**

Uønsket hendelse: **Skin burns**

Konsekvensområde: Helse — Risiko før tiltak: Risiko etter tiltak:

Risikoreduserende tiltak	Ansvarlig	Registrert	Frist	Status
Lab coat	Minadir Saracevic	05.09.2018	05.09.2018	Evaluert
Heat protective gloves	Minadir Saracevic	05.09.2018	02.07.2019	Evaluert

Farekilde: **NOx gas formation**

Uønsket hendelse: **Inhalation to respiratory system**

Konsekvensområde: Helse — Risiko før tiltak: Risiko etter tiltak:
Ytre miljø — Risiko før tiltak: Risiko etter tiltak:

Risikoreduserende tiltak	Ansvarlig	Registrert	Frist	Status
Fume hood	Minadir Saracevic	05.09.2018	02.07.2019	Evaluert

Farekilde: **Use of Pt(IV)(NO3)4 solution, Pt 15% w/w**

Uønsket hendelse: **Oxidizing by fire**

Konsekvensområde: Helse — Risiko før tiltak: Risiko etter tiltak:
Ytre miljø — Risiko før tiltak: Risiko etter tiltak:
Materielle verdier — Risiko før tiltak: Risiko etter tiltak:

Risikoreduserende tiltak	Ansvarlig	Registrert	Frist	Status
Lab coat	Minadir Saracevic	05.09.2018	05.09.2018	Evaluert
Fire extinguisher	Minadir Saracevic	05.09.2018	02.07.2019	Evaluert

Farekilde: **Use of Pt(IV)(NO3)4 solution, Pt 15% w/w**

Uønsket hendelse: **Spillage on skin**

Konsekvensområde: Helse — Risiko før tiltak: Risiko etter tiltak:

Risikoreduserende tiltak	Ansvarlig	Registrert	Frist	Status
Lab coat	Minadir Saracevic	05.09.2018	05.09.2018	Evaluert
Gloves	Minadir Saracevic	05.09.2018	02.07.2019	Evaluert

Uønsket hendelse: **Splash into the eyes**

Konsekvensområde: Helse — Risiko før tiltak: Risiko etter tiltak:

Risikoreduserende tiltak	Ansvarlig	Registrert	Frist	Status
Fume hood	Minadir Saracevic	05.09.2018	02.07.2019	Evaluert
Safety googles	Minadir Saracevic	05.09.2018	02.07.2019	Evaluert

Uønsket hendelse: **Spillage on skin**

Konsekvensområde: Helse — Risiko før tiltak: Risiko etter tiltak:

Uønsket hendelse: **Oral ingestion**

Konsekvensområde: Helse — Risiko før tiltak: Risiko etter tiltak:

Risikoreduserende tiltak	Ansvarlig	Registrert	Frist	Status
Lab coat	Minadir Saracevic	05.09.2018	05.09.2018	Evaluert
Fume hood	Minadir Saracevic	05.09.2018	02.07.2019	Evaluert
Gloves	Minadir Saracevic	05.09.2018	02.07.2019	Evaluert

Farekilde: **Characterization by XRD**

Uønsket hendelse: **Inhalation to respiratory system and oral ingestion during preparation**

Konsekvensområde: Helse — Risiko før tiltak: Risiko etter tiltak:

Risikoreduserende tiltak	Ansvarlig	Registrert	Frist	Status
Lab coat	Minadir Saracevic	05.09.2018	05.09.2018	Evaluert
Gloves	Minadir Saracevic	05.09.2018	02.07.2019	Evaluert

Farekilde: **Characterization by XRD**

Uønsket hendelse: **Spillage on the skin**

Konsekvensområde: Helse — Risiko før tiltak: Risiko etter tiltak:

Risikoreduserende tiltak	Ansvarlig	Registrert	Frist	Status
Lab coat	Minadir Saracevic	05.09.2018	05.09.2018	Evaluert
Gloves	Minadir Saracevic	05.09.2018	02.07.2019	Evaluert

Uønsket hendelse: **Chemical exposure into the eyes**

Konsekvensområde: Helse — Risiko før tiltak: Risiko etter tiltak:

Risikoreduserende tiltak	Ansvarlig	Registrert	Frist	Status
Safety googles	Minadir Saracevic	05.09.2018	02.07.2019	Evaluert

Farekilde: **Characterization by XRF**

Uønsket hendelse: **Spillage on the skin**

Konsekvensområde: Helse — Risiko før tiltak: Risiko etter tiltak:

Risikoreduserende tiltak	Ansvarlig	Registrert	Frist	Status
Lab coat	Minadir Saracevic	05.09.2018	05.09.2018	Evaluert
Gloves	Minadir Saracevic	05.09.2018	02.07.2019	Evaluert

Uønsket hendelse: **Chemical exposure into the eyes**

Konsekvensområde: Helse — Risiko før tiltak: Risiko etter tiltak:

Risikoreduserende tiltak	Ansvarlig	Registrert	Frist	Status
Safety googles	Minadir Saracevic	05.09.2018	02.07.2019	Evaluert

Uønsket hendelse: **Inhalation to respiratory system and oral ingestion during preparation**

Konsekvensområde: Helse — Risiko før tiltak: Risiko etter tiltak:

Risikoreduserende tiltak	Ansvarlig	Registrert	Frist	Status
Lab coat	Minadir Saracevic	05.09.2018	05.09.2018	Evaluert
Gloves	Minadir Saracevic	05.09.2018	02.07.2019	Evaluert

Farekilde: **Use of boric acid (H3BO3)**

Uønsket hendelse: **Spillage on skin**

Konsekvensområde: Helse — Risiko før tiltak: Risiko etter tiltak:

Risikoreduserende tiltak	Ansvarlig	Registrert	Frist	Status
Lab coat	Minadir Saracevic	05.09.2018	05.09.2018	Evaluert
Gloves	Minadir Saracevic	05.09.2018	02.07.2019	Evaluert

Uønsket hendelse: **Chemical exposure into the eyes**

Konsekvensområde: Helse — Risiko før tiltak: Risiko etter tiltak:

Risikoreduserende tiltak	Ansvarlig	Registrert	Frist	Status
Fume hood	Minadir Saracevic	05.09.2018	02.07.2019	Evaluert
Safety googles	Minadir Saracevic	05.09.2018	02.07.2019	Evaluert

Uønsket hendelse: **Inhalation to respiratory system and oral ingestion during preparation**

Konsekvensområde: Helse — Risiko før tiltak: Risiko etter tiltak:

Risikoreduserende tiltak	Ansvarlig	Registrert	Frist	Status
Lab coat	Minadir Saracevic	05.09.2018	05.09.2018	Evaluert
Fume hood	Minadir Saracevic	05.09.2018	02.07.2019	Evaluert
Gloves	Minadir Saracevic	05.09.2018	02.07.2019	Evaluert

Farekilde: **Characterization by chemisorption and TPR**

Uønsket hendelse: **Spillage on skin**

Konsekvensområde: Helse — Risiko før tiltak: Risiko etter tiltak:

Risikoreduserende tiltak	Ansvarlig	Registrert	Frist	Status
Lab coat	Minadir Saracevic	05.09.2018	05.09.2018	Evaluert
Gloves	Minadir Saracevic	05.09.2018	02.07.2019	Evaluert

Uønsket hendelse: **Chemical exposure into the eyes**

Konsekvensområde: Helse — Risiko før tiltak: Risiko etter tiltak:

Risikoreduserende tiltak	Ansvarlig	Registrert	Frist	Status
Safety googles	Minadir Saracevic	05.09.2018	02.07.2019	Evaluert

Farekilde: **Characterization by chemisorption and TPR**

Uønsket hendelse: **Inhalation to respiratory system and oral ingestion during preparation**

Konsekvensområde: Helse — Risiko før tiltak: Risiko etter tiltak:

Risikoreduserende tiltak	Ansvarlig	Registrert	Frist	Status
Lab coat	Minadir Saracevic	05.09.2018	05.09.2018	Evaluert
Gloves	Minadir Saracevic	05.09.2018	02.07.2019	Evaluert

Farekilde: **Use of H2**

Uønsket hendelse: **Leaks and explosion**

Konsekvensområde: Helse — Risiko før tiltak: Risiko etter tiltak:
Ytre miljø — Risiko før tiltak: Risiko etter tiltak:
Materielle verdier — Risiko før tiltak: Risiko etter tiltak:

Risikoreduserende tiltak	Ansvarlig	Registrert	Frist	Status
Lab coat	Minadir Saracevic	05.09.2018	05.09.2018	Evaluert
Safety googles	Minadir Saracevic	05.09.2018	02.07.2019	Evaluert
Gloves	Minadir Saracevic	05.09.2018	02.07.2019	Evaluert
Fire extinguisher	Minadir Saracevic	05.09.2018	02.07.2019	Evaluert

Farekilde: **Use of NO**

Uønsket hendelse: **Explosion**

Konsekvensområde: Helse — Risiko før tiltak: Risiko etter tiltak:
Ytre miljø — Risiko før tiltak: Risiko etter tiltak:
Materielle verdier — Risiko før tiltak: Risiko etter tiltak:

Risikoreduserende tiltak	Ansvarlig	Registrert	Frist	Status
Lab coat	Minadir Saracevic	05.09.2018	05.09.2018	Evaluert
Safety googles	Minadir Saracevic	05.09.2018	02.07.2019	Evaluert
Gloves	Minadir Saracevic	05.09.2018	02.07.2019	Evaluert
Fire extinguisher	Minadir Saracevic	05.09.2018	02.07.2019	Evaluert

Uønsket hendelse: **Inhalation to respiratory system**

Konsekvensområde: Helse — Risiko før tiltak: Risiko etter tiltak:

Risikoreduserende tiltak	Ansvarlig	Registrert	Frist	Status
Lab coat	Minadir Saracevic	05.09.2018	05.09.2018	Evaluert

Farekilde: **Use of NO**

Uønsket hendelse: **Chemical burns on the skin and eyes**

Konsekvensområde: Helse — Risiko før tiltak:  Risiko etter tiltak: 

Risikoreduserende tiltak	Ansvarlig	Registrert	Frist	Status
Lab coat	Minadir Saracevic	05.09.2018	05.09.2018	Evaluert
Safety googles	Minadir Saracevic	05.09.2018	02.07.2019	Evaluert
Gloves	Minadir Saracevic	05.09.2018	02.07.2019	Evaluert

Farekilde: **Use of argon (Ar)**

Uønsket hendelse: **Explosion**

Konsekvensområde: Helse — Risiko før tiltak:  Risiko etter tiltak: 
Ytre miljø — Risiko før tiltak:  Risiko etter tiltak: 
Materielle verdier — Risiko før tiltak:  Risiko etter tiltak: 

Risikoreduserende tiltak	Ansvarlig	Registrert	Frist	Status
Lab coat	Minadir Saracevic	05.09.2018	05.09.2018	Evaluert
Safety googles	Minadir Saracevic	05.09.2018	02.07.2019	Evaluert
Gloves	Minadir Saracevic	05.09.2018	02.07.2019	Evaluert
Fire extinguisher	Minadir Saracevic	05.09.2018	02.07.2019	Evaluert

Farekilde: **Activity measurement of catalyst**

Uønsket hendelse: **Spillage on skin**

Konsekvensområde: Helse — Risiko før tiltak:  Risiko etter tiltak: 

Risikoreduserende tiltak	Ansvarlig	Registrert	Frist	Status
Lab coat	Minadir Saracevic	05.09.2018	05.09.2018	Evaluert
Gloves	Minadir Saracevic	05.09.2018	02.07.2019	Evaluert

Uønsket hendelse: **Inhalation to respiratory system and oral ingestion during preparation**

Konsekvensområde: Helse — Risiko før tiltak:  Risiko etter tiltak: 

Risikoreduserende tiltak	Ansvarlig	Registrert	Frist	Status
Lab coat	Minadir Saracevic	05.09.2018	05.09.2018	Evaluert
Gloves	Minadir Saracevic	05.09.2018	02.07.2019	Evaluert

Farekilde: **Activity measurement of catalyst**

Uønsket hendelse: **Heated surfaces**

Konsekvensområde: Helse — Risiko før tiltak:  Risiko etter tiltak: 

Risikoreduserende tiltak	Ansvarlig	Registrert	Frist	Status
Lab coat	Minadir Saracevic	05.09.2018	05.09.2018	Evaluert
Heat protective gloves	Minadir Saracevic	05.09.2018	02.07.2019	Evaluert

Uønsket hendelse: **Gas leaks**

Konsekvensområde: Helse — Risiko før tiltak:  Risiko etter tiltak: 
Ytre miljø — Risiko før tiltak:  Risiko etter tiltak: 

Risikoreduserende tiltak	Ansvarlig	Registrert	Frist	Status
Safety googles	Minadir Saracevic	05.09.2018	02.07.2019	Evaluert
Gloves	Minadir Saracevic	05.09.2018	02.07.2019	Evaluert

Uønsket hendelse: **Explosion**

Konsekvensområde: Helse — Risiko før tiltak:  Risiko etter tiltak: 
Ytre miljø — Risiko før tiltak:  Risiko etter tiltak: 
Materielle verdier — Risiko før tiltak:  Risiko etter tiltak: 

Risikoreduserende tiltak	Ansvarlig	Registrert	Frist	Status
Lab coat	Minadir Saracevic	05.09.2018	05.09.2018	Evaluert
Safety googles	Minadir Saracevic	05.09.2018	02.07.2019	Evaluert
Gloves	Minadir Saracevic	05.09.2018	02.07.2019	Evaluert
Fire extinguisher	Minadir Saracevic	05.09.2018	02.07.2019	Evaluert

Farekilde: **Use of O2**

Uønsket hendelse: **Explosion**

Konsekvensområde: Helse — Risiko før tiltak:  Risiko etter tiltak: 
Ytre miljø — Risiko før tiltak:  Risiko etter tiltak: 
Materielle verdier — Risiko før tiltak:  Risiko etter tiltak: 

Risikoreduserende tiltak	Ansvarlig	Registrert	Frist	Status
Lab coat	Minadir Saracevic	05.09.2018	05.09.2018	Evaluert
Safety googles	Minadir Saracevic	05.09.2018	02.07.2019	Evaluert
Gloves	Minadir Saracevic	05.09.2018	02.07.2019	Evaluert
Fire extinguisher	Minadir Saracevic	05.09.2018	02.07.2019	Evaluert

Farekilde: **Use of TiO2**

Uønsket hendelse: **Irritating to respiratory system, skin and eyes**

Konsekvensområde: Helse Risiko før tiltak: Risiko etter tiltak:

Risikoreduserende tiltak	Ansvarlig	Registrert	Frist	Status
Lab coat	Minadir Saracevic	05.09.2018	05.09.2018	Evaluert
Safety googles	Minadir Saracevic	05.09.2018	02.07.2019	Evaluert
Gloves	Minadir Saracevic	05.09.2018	02.07.2019	Evaluert
Dust mask	Minadir Saracevic	08.01.2019	02.07.2019	Evaluert

Farekilde: **Use of CeO2**

Uønsket hendelse: **Irritating to respiratory system, skin and eyes**

Konsekvensområde: Helse Risiko før tiltak: Risiko etter tiltak:

Risikoreduserende tiltak	Ansvarlig	Registrert	Frist	Status
Lab coat	Minadir Saracevic	05.09.2018	05.09.2018	Evaluert
Safety googles	Minadir Saracevic	05.09.2018	02.07.2019	Evaluert
Gloves	Minadir Saracevic	05.09.2018	02.07.2019	Evaluert
Dust mask	Minadir Saracevic	08.01.2019	02.07.2019	Evaluert

Uønsket hendelse: **Oral ingestion**

Konsekvensområde: Helse Risiko før tiltak: Risiko etter tiltak:

Risikoreduserende tiltak	Ansvarlig	Registrert	Frist	Status
Lab coat	Minadir Saracevic	05.09.2018	05.09.2018	Evaluert
Safety googles	Minadir Saracevic	05.09.2018	02.07.2019	Evaluert
Gloves	Minadir Saracevic	05.09.2018	02.07.2019	Evaluert
Dust mask	Minadir Saracevic	08.01.2019	02.07.2019	Evaluert

Farekilde: **Use of SiO2**

Uønsket hendelse: **Inhalation to respiratory system**

Konsekvensområde: Helse Risiko før tiltak: Risiko etter tiltak:

Risikoreduserende tiltak	Ansvarlig	Registrert	Frist	Status
Fume hood	Minadir Saracevic	05.09.2018	02.07.2019	Evaluert
Dust mask	Minadir Saracevic	08.01.2019	02.07.2019	Evaluert

Farekilde: **Use of ZrO2**

Uønsket hendelse: **Inhalation to respiratory system**

Konsekvensområde: Helse

Risiko før tiltak: Risiko etter tiltak:

Risikoreduserende tiltak	Ansvarlig	Registrert	Frist	Status
Fume hood	Minadir Saracevic	05.09.2018	02.07.2019	Evaluert
Dust mask	Minadir Saracevic	08.01.2019	02.07.2019	Evaluert

Endelig vurdering

The chemicals involved in this procedure are health hazardous and one should be careful to avoid any spillage or inhalation when handling these chemicals. Correct disposal is also an important factor, where one should be aware of the correct way to dispose of the chemical residues after the experiment. With the right safety measures during the synthesis procedure, characterization and activity measurements, these risks are minimized and the experiments can be performed. Due to lack of experience handling these specific chemicals, the risks may have been under- or overestimated during the risk evaluation.

Involverte enheter og personer

En risikovurdering kan gjelde for en, eller flere enheter i organisasjonen. Denne oversikten presenterer involverte enheter og personell for gjeldende risikovurdering.

Enhet /-er risikovurderingen omfatter

- Institutt for kjemisk prosessteknologi
- Institutt for materialteknologi

Deltakere

Minadir Saracevic

Lesere

Estelle Marie M. Vanhaecke
Anne Hoff
Hilde Johnsen Venvik
Karin Wiggen Dragsten
Gunn Torill Wikdahl
Hege Johannessen

Andre involverte/interessenter

[Ingen registreringer]

Følgende akseptkriterier er besluttet for risikoområdet Risikovurdering: Helse, miljø og sikkerhet (HMS):

Helse	Materielle verdier	Omdømme	Ytre miljø
			

Oversikt over eksisterende, relevante tiltak som er hensyntatt i risikovurderingen

I tabellen under presenteres eksisterende tiltak som er hensyntatt ved vurdering av sannsynlighet og konsekvens for aktuelle uønskede hendelser.

Farekilde	Uønsket hendelse	Tiltak hensyntatt ved vurdering
Use of CoN2O6 · 6H2O	Oxidizing by fire	Heat protective gloves
	Oxidizing by fire	Fire extinguisher
	Spillage on skin	
	Splash into the eyes	Fume hood
	Inhalation to respiratory system and oral ingestion	Fume hood
	Inhalation to respiratory system and oral ingestion	Dust mask
Use of γ-Al2O3	Irritating to respiratory system and skin	Dust mask
Heated surfaces	Skin burns	Heat protective gloves
NOx gas formation	Inhalation to respiratory system	Fume hood
Use of Pt(IV)(NO3)4 solution, Pt 15% w/w	Oxidizing by fire	Fire extinguisher
	Spillage on skin	
	Splash into the eyes	Fume hood
	Spillage on skin	
	Oral ingestion	
Characterization by XRD	Inhalation to respiratory system and oral ingestion during preparation	Dust mask
	Spillage on the skin	
	Chemical exposure into the eyes	
Characterization by XRF	Spillage on the skin	
	Chemical exposure into the eyes	
	Inhalation to respiratory system and oral ingestion during preparation	
Use of boric acid (H3BO3)	Spillage on skin	
	Chemical exposure into the eyes	
	Inhalation to respiratory system and oral ingestion during preparation	Dust mask
Characterization by chemisorption and TPR	Spillage on skin	
	Chemical exposure into the eyes	
	Inhalation to respiratory system and oral ingestion during preparation	
Use of H2	Leaks and explosion	
Use of NO	Explosion	
	Inhalation to respiratory system	
	Chemical burns on the skin and eyes	
Use of argon (Ar)	Explosion	

Activity measurement of catalyst	Spillage on skin	
	Inhalation to respiratory system and oral ingestion during preparation	Dust mask
	Heated surfaces	Heat protective gloves
	Gas leaks	
	Explosion	Heat protective gloves
	Explosion	Fire extinguisher
Use of O2	Explosion	
Use of TiO2	Irritating to respiratory system, skin and eyes	
Use of CeO2	Irritating to respiratory system, skin and eyes	
	Oral ingestion	
Use of SiO2	Inhalation to respiratory system	Fume hood
	Inhalation to respiratory system	Dust mask
Use of ZrO2	Inhalation to respiratory system	Fume hood
	Inhalation to respiratory system	Dust mask

Eksisterende og relevante tiltak med beskrivelse:

Lab coat
Preventing spills on body and clothing. Safety precautions for reducing skin burns due to hot equipment.

Fume hood
Prevent inhalation, spreading of volatiles and dust during the laboratory work

Safety googles
Avoid splashes of chemicals into the eyes, should be worn at all times.

Gloves
Wear nitril gloves during handling of the chemicals.

Heat protective gloves
The heat protective gloves are used when handling hot equipment.

Fire extinguisher
To prevent the fire from spreading and reduce the risk that the material oxides.

Lab coat
Preventing spills on body and clothing. Safety precautions for reducing skin burns due to hot equipment.

Safety googles
Avoid splashes of chemicals into the eyes, should be worn at all times.

Gloves
Wear nitril gloves during handling of the chemicals.

Lab coat
Preventing spills on body and clothing. Safety precautions for reducing skin burns due to hot equipment.

Safety googles
Avoid splashes of chemicals into the eyes, should be worn at all times.

Gloves
Wear nitril gloves during handling of the chemicals.

Lab coat
Preventing spills on body and clothing. Safety precautions for reducing skin burns due to hot equipment.

Safety googles
Avoid splashes of chemicals into the eyes, should be worn at all times.

Gloves
Wear nitril gloves during handling of the chemicals.

Dust mask
Reduces risk of inhalation of particles when exposed to the materials used

Risikoanalyse med vurdering av sannsynlighet og konsekvens

I denne delen av rapporten presenteres detaljer dokumentasjon av de farer, uønskede hendelser og årsaker som er vurdert. Innledningsvis oppsummeres farer med tilhørende uønskede hendelser som er tatt med i vurderingen.

Følgende farer og uønskede hendelser er vurdert i denne risikovurderingen:

- **Use of $CoN_2O_6 \cdot 6H_2O$**
  - Oxidizing by fire
  - Spillage on skin
  - Splash into the eyes
  - Inhalation to respiratory system and oral ingestion
- **Use of γ-Al_2O_3**
  - Irritating to respiratory system and skin
- **Heated surfaces**
  - Skin burns
- **NOx gas formation**
  - Inhalation to respiratory system
- **Use of $Pt(IV)(NO_3)_4$ solution, Pt 15% w/w**
  - Oxidizing by fire
  - Spillage on skin
  - Splash into the eyes
  - Spillage on skin
  - Oral ingestion
- **Characterization by XRD**
  - Inhalation to respiratory system and oral ingestion during preparation
  - Spillage on the skin
  - Chemical exposure into the eyes
- **Characterization by XRF**
  - Spillage on the skin
  - Chemical exposure into the eyes
  - Inhalation to respiratory system and oral ingestion during preparation
- **Use of boric acid (H_3BO_3)**
  - Spillage on skin
  - Chemical exposure into the eyes
  - Inhalation to respiratory system and oral ingestion during preparation
- **Characterization by chemisorption and TPR**
  - Spillage on skin
  - Chemical exposure into the eyes
  - Inhalation to respiratory system and oral ingestion during preparation
- **Use of H_2**
  - Leaks and explosion
- **Use of NO**
  - Explosion

- Inhalation to respiratory system
- Chemical burns on the skin and eyes

- **Use of argon (Ar)**
  - Explosion
- **Activity measurement of catalyst**
  - Spillage on skin
  - Inhalation to respiratory system and oral ingestion during preparation
  - Heated surfaces
  - Gas leaks
  - Explosion
- **Use of O2**
  - Explosion
- **Use of TiO2**
  - Irritating to respiratory system, skin and eyes
- **Use of CeO2**
  - Irritating to respiratory system, skin and eyes
  - Oral ingestion
- **Use of SiO2**
  - Inhalation to respiratory system
- **Use of ZrO2**
  - Inhalation to respiratory system

Detaljert oversikt over farekilder og uønskede hendelser:

Farekilde: Use of CoN2O6 · 6H2O

Uønsket hendelse: Oxidizing by fire

May intensify fire, oxidizer

Sannsynlighet for hendelsen (felles for alle konsekvensområder): **Lite sannsynlig (2)**

Kommentar:

The event of a fire is not very likely, results in a low probability. But there are electrical equipment(drying process) which produce heat that may be a source of fire.

Konsekvensområde: Helse ***Risiko:***

Vurdert konsekvens: **Stor (3)**

Kommentar: Depending on the severity of the fire, burns may results in a long recovery time.

Konsekvensområde: Ytre miljø ***Risiko:***

Vurdert konsekvens: **Stor (3)**

Kommentar: Fumes and damage resulting from the fire may lead to undesired gasses or liquids releasing into the environment.

Konsekvensområde: Materielle verdier ***Risiko:***

Vurdert konsekvens: **Stor (3)**

Kommentar: The equipment after the fire may be permanently damaged but does not contain any life threatening chemicals which could have been released due the fire.

Uønsket hendelse: Spillage on skin

May cause skin irritation and allergic reaction

Sannsynlighet for hendelsen (felles for alle konsekvensområder): **Sannsynlig (3)**

Kommentar:

Spillage may occur when working with chemicals

Konsekvensområde: Helse

Risiko:

Vurdert konsekvens: **Middels (2)**

Kommentar: Skin contact with the material may result to skin irritation and allergic reaction

Uønsket hendelse: Splash into the eyes

Acute toxicity and carcinogenic (may cause cancer)

Sannsynlighet for hendelsen (felles for alle konsekvensområder): **Lite sannsynlig (2)**

Kommentar:

The probability of getting chemicals into the eyes is not high due to no high pressures and the chemicals are stable during the synthesis.

Konsekvensområde: Helse

Risiko:

Vurdert konsekvens: **Svært stor (4)**

Kommentar: Acute toxicity in water and carcinogenic (may cause cancer) material may lead to high consequence if exposed to it.

Uønsket hendelse: Inhalation to respiratory system and oral ingestion

Acute toxicity and carcinogenic (may cause cancer)

Sannsynlighet for hendelsen (felles for alle konsekvensområder): **Lite sannsynlig (2)**

Kommentar:

The chemical is stable during normal conditions

Konsekvensområde: Helse

Risiko:

Vurdert konsekvens: **Svært stor (4)**

Kommentar: Acute toxicity in water and carcinogenic (may cause cancer) material may lead to high consequence if exposed to it.

Farekilde: Use of γ-Al2O3

Uønsket hendelse: Irritating to respiratory system and skin

The substance is not classified as health hazardous or dangerous for the environment.

Sannsynlighet for hendelsen (felles for alle konsekvensområder): **Sannsynlig (3)**

Kommentar:

Due the material being fine, it may more easily be exposed

Konsekvensområde: Helse

Risiko:

Vurdert konsekvens: **Liten (1)**

Kommentar: Not classified as health hazardous and is not environmentally dangerous.

Farekilde: Heated surfaces

Uønsket hendelse: Skin burns

Handling of hot equipment may lead to skin burns

Sannsynlighet for hendelsen (felles for alle konsekvensområder): **Sannsynlig (3)**

Kommentar:

Handling hot equipment may lead to severe burns if not protected

Konsekvensområde: Helse

Risiko:

Vurdert konsekvens: **Stor (3)**

Kommentar: May lead to burns and chemical spill on the skin. Calcination reactor will be close to 750 °C at highest temperature point, which may cause severe burns if touched unprotected.

Farekilde: NOx gas formation

Uønsket hendelse: Inhalation to respiratory system

Sannsynlighet for hendelsen (felles for alle konsekvensområder): **Sannsynlig (3)**

Kommentar:

There may be NOx formation(e.g during the calcination process), where the source is from the cobalt nitrate

Konsekvensområde: Helse

Risiko:

Vurdert konsekvens: **Stor (3)**

Kommentar: NOx gas is poisonous to inhale

Konsekvensområde: Ytre miljø

Risiko:

Vurdert konsekvens: **Middels (2)**

Kommentar: No significant danger considering small amounts

Farekilde: Use of Pt(IV)(NO3)4 solution, Pt 15% w/w

Uønsket hendelse: Oxidizing by fire

May intensify fire, oxidizer

Sannsynlighet for hendelsen (felles for alle konsekvensområder): **Lite sannsynlig (2)**

Kommentar:

The event of a fire is not very likely, results in a low probability. But there are electrical equipment(drying process) which produce heat that may be a source of fire.

Konsekvensområde: Helse

Risiko:

Vurdert konsekvens: **Stor (3)**

Kommentar: Depending on the severity of the fire, burns may results in a long recovery time.

Konsekvensområde: Ytre miljø

Risiko:

Vurdert konsekvens: **Stor (3)**

Kommentar: Fumes and damage resulting from the fire may lead to undesired gasses or liquids releasing into the environment.

Konsekvensområde: Materielle verdier

Risiko:

Vurdert konsekvens: **Stor (3)**

Kommentar: The equipment after the fire may be permanently damaged but does not contain any life threatening chemicals which could have been released due the fire.

Uønsket hendelse: Spillage on skin

May cause allergic reaction and skin corrosion

Sannsynlighet for hendelsen (felles for alle konsekvensområder): **Sannsynlig (3)**

Kommentar:

Spillage may occur when working with the chemical during the synthesis of the catalyst.

Konsekvensområde: Helse

Risiko:

Vurdert konsekvens: **Stor (3)**

Kommentar: This chemical contains nitric acid, which may lead to serious skin corrosion if the skin is exposed the acid.

Uønsket hendelse: Splash into the eyes

May cause severe eye damage

Sannsynlighet for hendelsen (felles for alle konsekvensområder): **Lite sannsynlig (2)**

Kommentar:

The probability of getting chemicals into the eyes is not high due to no high pressures and the chemicals are stable during the synthesis.

Konsekvensområde: Helse

Risiko:

Vurdert konsekvens: **Svært stor (4)**

Kommentar: Since the chemical contains nitric acid, if solution is splashed into the eyes it may cause severe or permanent damage.

Uønsket hendelse: Spillage on skin

May cause allergic reaction and skin corrosion

Sannsynlighet for hendelsen (felles for alle konsekvensområder): **Sannsynlig (3)**

Kommentar:

Spillage may occur when working with the chemical during the synthesis of the catalyst.

Konsekvensområde: Helse

Risiko:

Vurdert konsekvens: **Stor (3)**

Kommentar: This chemical contains nitric acid, which may lead to serious skin corrosion if the skin is exposed the acid.

Uønsket hendelse: Oral ingestion

Aquatic acute poisonous

Sannsynlighet for hendelsen (felles for alle konsekvensområder): **Lite sannsynlig (2)**

Kommentar:

No high pressure and it is a stable liquid under the experimental conditions

Konsekvensområde: Helse

Risiko:

Vurdert konsekvens: **Svært stor (4)**

Kommentar: It is aquatic acute poisonous and acidic, which can lead to severe damage

Farekilde: Characterization by XRD

Uønsket hendelse: Inhalation to respiratory system and oral ingestion during preparation

Acute toxicity and carcinogenic (may cause cancer)

Sannsynlighet for hendelsen (felles for alle konsekvensområder): **Lite sannsynlig (2)**

Kommentar:

The catalyst powder is stable during the preparation, no high pressure or heated surfaces are introduced during sample preparation.

Konsekvensområde: Helse

Risiko:

Vurdert konsekvens: **Svært stor (4)**

Kommentar: Acute toxicity in water and carcinogenic (may cause cancer) material may lead to high consequence if exposed to it.

Uønsket hendelse: Spillage on the skin

May cause skin irritation and allergic reaction

Sannsynlighet for hendelsen (felles for alle konsekvensområder): **Sannsynlig (3)**

Kommentar:

Spillage may occur when working preparing the sample holder with the catalyst. Steady hands are required to not spill any sample. Thus, the probability of spilling may be higher.

Konsekvensområde: Helse

Risiko:

Vurdert konsekvens: **Middels (2)**

Kommentar: Skin contact with the material may result to skin irritation and allergic reaction

Uønsket hendelse: Chemical exposure into the eyes

Acute toxicity and carcinogenic (may cause cancer)

Sannsynlighet for hendelsen (felles for alle konsekvensområder): **Lite sannsynlig (2)**

Kommentar:

The probability of getting chemicals into the eyes is not high due to no high pressures and the chemicals are stable during the preparation.

Konsekvensområde: Helse

Risiko:

Vurdert konsekvens: **Svært stor (4)**

Kommentar: Acute toxicity in water and carcinogenic (may cause cancer) material may lead to high consequence if exposed to it.

Farekilde: Characterization by XRF

Uønsket hendelse: Spillage on the skin

May cause skin irritation and allergic reaction.

Sannsynlighet for hendelsen (felles for alle konsekvensområder): **Sannsynlig (3)**

Kommentar:

Can spill powder on the skin when making the pellets for the XRF unit

Konsekvensområde: Helse

Risiko:

Vurdert konsekvens: **Stor (3)**

Kommentar: Due to the catalyst and boric acid, may get skin irritation

Uønsket hendelse: Chemical exposure into the eyes

The catalyst is carcinogenic (may cause cancer)

Sannsynlighet for hendelsen (felles for alle konsekvensområder): **Lite sannsynlig (2)**

Kommentar:

The chemicals are stable during the making of the pellets

Konsekvensområde: Helse

Risiko:

Vurdert konsekvens: **Svært stor (4)**

Kommentar: The catalyst is carcinogenic (may cause cancer), which may lead to permanent effects

Uønsket hendelse: Inhalation to respiratory system and oral ingestion during preparation

Sannsynlighet for hendelsen (felles for alle konsekvensområder): **Lite sannsynlig (2)**

Kommentar:

The chemicals are stable during the making of the pellets

Konsekvensområde: Helse

Risiko:

Vurdert konsekvens: **Svært stor (4)**

Kommentar: The catalysts is a carcinogenic (may cause cancer) material, may lead to high consequence if exposed to it.

Farekilde: Use of boric acid (H3BO3)

Used during sample preparation for the XRF unit.

Uønsket hendelse: Spillage on skin

Acid chemicals may lead skin corrosion and irritation

Sannsynlighet for hendelsen (felles for alle konsekvensområder): **Sannsynlig (3)**

Kommentar:

[Ingen registreringer]

Konsekvensområde: Helse

Risiko:

Vurdert konsekvens: **Stor (3)**

Kommentar: [Ingen registreringer]

Uønsket hendelse: Chemical exposure into the eyes

May cause severe eye damage

Sannsynlighet for hendelsen (felles for alle konsekvensområder): **Sannsynlig (3)**

Kommentar:

The pressure added when the samples is pressed may lead to exposure, but has a glass front to avoid sudden exposure if leaked. The chemical is stable during the preparation.

Konsekvensområde: Helse

Risiko:

Vurdert konsekvens: **Stor (3)**

Kommentar: [Ingen registreringer]

Uønsket hendelse: Inhalation to respiratory system and oral ingestion during preparation

May damage the reproductive capacity. May cause birth defects.

Sannsynlighet for hendelsen (felles for alle konsekvensområder): **Lite sannsynlig (2)**

Kommentar:

The catalyst powder is stable during the preparation. The pressure added when the samples is pressed may lead to exposure, but has a glass front to avoid sudden exposure if leaked.

Konsekvensområde: Helse

Risiko:

Vurdert konsekvens: **Svært stor (4)**

Kommentar: May damage the reproductive capacity and may cause birth defects.

Farekilde: Characterization by chemisorption and TPR

Uønsket hendelse: Spillage on skin

May cause skin irritation and allergic reaction.

Sannsynlighet for hendelsen (felles for alle konsekvensområder): **Lite sannsynlig (2)**

Kommentar:

Can spill powder on the skin when preparing the U-tube reactor

Konsekvensområde: Helse

Risiko:

Vurdert konsekvens: **Middels (2)**

Kommentar: Skin contact with the material may result to skin irritation and allergic reaction

Uønsket hendelse: Chemical exposure into the eyes

Acute toxicity and carcinogenic (may cause cancer)

Sannsynlighet for hendelsen (felles for alle konsekvensområder): **Lite sannsynlig (2)**

Kommentar:

The probability of getting chemicals into the eyes is not high due to no high pressures and the chemicals are stable during the preparation.

Konsekvensområde: Helse

Risiko:

Vurdert konsekvens: **Svært stor (4)**

Kommentar: Acute toxicity in water and carcinogenic (may cause cancer) material may lead to high consequence if exposed to it.

Uønsket hendelse: Inhalation to respiratory system and oral ingestion during preparation

Acute toxicity and carcinogenic (may cause cancer)

Sannsynlighet for hendelsen (felles for alle konsekvensområder): **Lite sannsynlig (2)**

Kommentar:

The catalyst powder is stable during the preparation, no high pressure or heated surfaces are introduced during sample preparation.

Konsekvensområde: Helse

Risiko:

Vurdert konsekvens: **Svært stor (4)**

Kommentar: Acute toxicity in water and carcinogenic (may cause cancer) material may lead to high consequence if exposed to it.

Farekilde: Use of H2

Used as a reducing agent in both during TPR and chemisorption

Uønsket hendelse: Leaks and explosion

Hydrogen as a gas under pressure, may explode upon heating

Sannsynlighet for hendelsen (felles for alle konsekvensområder): **Lite sannsynlig (2)**

Kommentar:

Possible leaks may occur due to faulty installation of valves, but the bottles are placed where they are not exposed to heat.

Konsekvensområde: Helse

Risiko:

Vurdert konsekvens: **Svært stor (4)**

Kommentar: In case of explosion and fires, severe burns and permanent damage may be a possibility

Konsekvensområde: Ytre miljø

Risiko:

Vurdert konsekvens: **Stor (3)**

Kommentar: Fire may lead to undesired gasses or liquids releasing into the environment.

Konsekvensområde: Materielle verdier

Risiko:

Vurdert konsekvens: **Svært stor (4)**

Kommentar: High material damage if explosion and fire occurs

Farekilde: Use of NO

Used in the activity measurement for NO oxidation over the catalyst in the packed bed reactor

Uønsket hendelse: Explosion

High pressure bottle

Sannsynlighet for hendelsen (felles for alle konsekvensområder): **Lite sannsynlig (2)**

Kommentar:

The gas is under pressure, may explode if the bottle is exposed to heat

Konsekvensområde: Helse

Risiko:

Vurdert konsekvens: **Svært stor (4)**

Kommentar: Acute poisonous if exposed to respiratory system and chemical burns to skin and eyes

Konsekvensområde: Ytre miljø

Risiko:

Vurdert konsekvens: **Svært stor (4)**

Kommentar: Poisonous gas and may react with exposed to other gases

Konsekvensområde: Materielle verdier

Risiko:

Vurdert konsekvens: **Svært stor (4)**

Kommentar: May lead to large material damage if the high pressure bottle explode

Uønsket hendelse: Inhalation to respiratory system

Acute poisonous

Sannsynlighet for hendelsen (felles for alle konsekvensområder): **Lite sannsynlig (2)**

Kommentar:

Gas is used from a bottle to send the gas to a reactor, low probability if all valves and pipes have been leaked proofed.

Konsekvensområde: Helse

Risiko:

Vurdert konsekvens: **Svært stor (4)**

Kommentar: Acute poisonous if it the gas is inhaled

Uønsket hendelse: Chemical burns on the skin and eyes

The gas may lead to chemical burn on the skin and eyes

Sannsynlighet for hendelsen (felles for alle konsekvensområder): **Lite sannsynlig (2)**

Kommentar:

Gas is used from a bottle to send the gas to a reactor, low probability if all valves and pipes have been leaked proofed.

Konsekvensområde: Helse

Risiko:

Vurdert konsekvens: **Svært stor (4)**

Kommentar: May lead to chemical burn on the skin and eyes

Farekilde: Use of argon (Ar)

Used as an inert gas in the activity measurement

Uønsket hendelse: Explosion

The bottle has high pressure and may explode if exposed to heat

Sannsynlighet for hendelsen (felles for alle konsekvensområder): **Lite sannsynlig (2)**

Kommentar:

The high pressure bottle is not exposed to heat, hence the low probability

Konsekvensområde: Helse

Risiko:

Vurdert konsekvens: **Stor (3)**

Kommentar: The explosion of the bottle may lead to cuts, hearing loss etc.

Konsekvensområde: Ytre miljø

Risiko:

Vurdert konsekvens: **Middels (2)**

Kommentar: The gas itself is inert and do not posses a high risk

Konsekvensområde: Materielle verdier

Risiko:

Vurdert konsekvens: **Svært stor (4)**

Kommentar: The explosion may lead to material damage of equipment etc.

Farekilde: Activity measurement of catalyst

Uønsket hendelse: Spillage on skin

May cause skin irritation and allergic reaction.

Sannsynlighet for hendelsen (felles for alle konsekvensområder): **Lite sannsynlig (2)**

Kommentar:

Can spill the catalyst powder on the skin when preparing the packed bed reactor

Konsekvensområde: Helse

Risiko:

Vurdert konsekvens: **Middels (2)**

Kommentar: Skin contact with the material may result to skin irritation and allergic reaction

Uønsket hendelse: Inhalation to respiratory system and oral ingestion during preparation

Acute toxicity and carcinogenic (may cause cancer)

Sannsynlighet for hendelsen (felles for alle konsekvensområder): **Lite sannsynlig (2)**

Kommentar:

The catalyst powder is stable during the preparation, no high pressure or heated surfaces are introduced during sample preparation.

Konsekvensområde: Helse

Risiko:

Vurdert konsekvens: **Svært stor (4)**

Kommentar: Acute toxicity in water and carcinogenic (may cause cancer) material may lead to high consequence if exposed to it.

Uønsket hendelse: Heated surfaces

The gas pipes and reactor in the chemical rig has heated surfaces

Sannsynlighet for hendelsen (felles for alle konsekvensområder): **Sannsynlig (3)**

Kommentar:

Handling hot equipment may lead to severe burns if not protected

Konsekvensområde: Helse

Risiko:

Vurdert konsekvens: **Stor (3)**

Kommentar: May lead to burns. Reactor will be close to 500 °C at highest temperature point, which may cause severe burns if touched unprotected.

Uønsket hendelse: Gas leaks

The NO gas may leak in the pipes and valves

Sannsynlighet for hendelsen (felles for alle konsekvensområder): **Lite sannsynlig (2)**

Kommentar:

The gases may leak in the valves and fittings, but are leak proofed before running an experiment and are in a closed cabinet.

Konsekvensområde: Helse

Risiko:

Vurdert konsekvens: **Svært stor (4)**

Kommentar: The gas is poisonous if inhaled and chemical burn on skin and eyes

Konsekvensområde: Ytre miljø

Risiko:

Vurdert konsekvens: **Svært stor (4)**

Kommentar: May react with other components to form unwanted products (e.g smog)

Uønsket hendelse: Explosion

The gas are stored in high pressure bottles and may explode if exposed to heat

Sannsynlighet for hendelsen (felles for alle konsekvensområder): **Lite sannsynlig (2)**

Kommentar:

The bottles are isolated from the rig and is not close to a heat source

Konsekvensområde: Helse

Risiko:

Vurdert konsekvens: **Svært stor (4)**

Kommentar: NO poisonous gas if exposed, explosion may lead to cuts, burn etc

Konsekvensområde: Ytre miljø

Risiko:

Vurdert konsekvens: **Svært stor (4)**

Kommentar: NO may react with other components (e.g smog)

Konsekvensområde: Materielle verdier

Risiko:

Vurdert konsekvens: **Svært stor (4)**

Kommentar: The explosion may damage the equipment permanently

Farekilde: Use of O2

Used both in chemisorption and activity measurements

Uønsket hendelse: Explosion

High pressure bottle

Sannsynlighet for hendelsen (felles for alle konsekvensområder): **Lite sannsynlig (2)**

Kommentar:

The bottle is not near a heat source, unlikely to explode due to heat exposure

Konsekvensområde: Helse

Risiko:

Vurdert konsekvens: **Stor (3)**

Kommentar: The oxygen may help to oxidize other gases if a fire erupts, leading to severe burns

Konsekvensområde: Ytre miljø

Risiko:

Vurdert konsekvens: **Stor (3)**

Kommentar: The gas has no significant consequences, but may help to contribute to oxidize other gases

Konsekvensområde: Materielle verdier

Risiko:

Vurdert konsekvens: **Svært stor (4)**

Kommentar: Permanent material damage may be expected due to bottle explosion or as a fire contributor

Farekilde: Use of TiO2

Uønsket hendelse: Irritating to respiratory system, skin and eyes

The substance is suspected of causing cancer

Sannsynlighet for hendelsen (felles for alle konsekvensområder): **Lite sannsynlig (2)**

Kommentar:

Pellet form and contains binder chemical, powder stable

Konsekvensområde: Helse

Risiko:

Vurdert konsekvens: **Stor (3)**

Kommentar: The material is suspected of causing cancer

Farekilde: Use of CeO2

Uønsket hendelse: Irritating to respiratory system, skin and eyes

The substance is classified to be toxic by oral ingestion

Sannsynlighet for hendelsen (felles for alle konsekvensområder): **Sannsynlig (3)**

Kommentar:

Due the material being fine, it may more easily be exposed

Konsekvensområde: Helse

Risiko:

Vurdert konsekvens: **Stor (3)**

Kommentar: Not classified as health hazardous by inhalation, skin contact or spillage into eyes but should be avoided

Uønsket hendelse: Oral ingestion

The substance is classified to be toxic by oral ingestion

Sannsynlighet for hendelsen (felles for alle konsekvensområder): **Lite sannsynlig (2)**

Kommentar:

The fine powder is stable under synthesis, but being fine powder may spread if dropped

Konsekvensområde: Helse

Risiko:

Vurdert konsekvens: **Stor (3)**

Kommentar: Classified as toxic by oral ingestion

Farekilde: Use of SiO2

Uønsket hendelse: Inhalation to respiratory system

May cause respiratory irritation

Sannsynlighet for hendelsen (felles for alle konsekvensområder): **Sannsynlig (3)**

Kommentar:

In dry powder form, risk of breathing dust

Konsekvensområde: Helse

Risiko:

Vurdert konsekvens: **Stor (3)**

Kommentar: May cause damage to organs through prolonged or repeated exposure

Farekilde: Use of ZrO2

Uønsket hendelse: Inhalation to respiratory system

May cause irritation to the respiratory system

Sannsynlighet for hendelsen (felles for alle konsekvensområder): **Sannsynlig (3)**

Kommentar:

Dry powder, may breathe in the dust.

Konsekvensområde: Helse

Risiko:

Vurdert konsekvens: **Liten (1)**

Kommentar: Classified as non-hazardous material

Oversikt over besluttede risikoreduserende tiltak:

Under presenteres en oversikt over risikoreduserende tiltak som skal bidra til å reduseres sannsynlighet og/eller konsekvens for uønskede hendelser.

- Lab coat
- Fume hood
- Safety googles
- Gloves
- Heat protective gloves
- Fire extinguisher
- Dust mask

Detaljert oversikt over besluttede risikoreduserende tiltak med beskrivelse:

Lab coat

Preventing spills on body and clothing. Safety precautions for reducing skin burns due to hot equipment.

Tiltak besluttet av: Minadir Saracevic

Ansvarlig for gjennomføring: Minadir Saracevic

Frist for gjennomføring: 9/5/2018

Fume hood

Prevent inhalation, spreading of volatiles and dust during the laboratory work

Tiltak besluttet av: Minadir Saracevic

Ansvarlig for gjennomføring: Minadir Saracevic

Frist for gjennomføring: 7/2/2019

Safety googles

Avoid splashes of chemicals into the eyes, should be worn at all times.

Tiltak besluttet av: Minadir Saracevic

Ansvarlig for gjennomføring: Minadir Saracevic

Frist for gjennomføring: 7/2/2019

Gloves

Wear nitril gloves during handling of the chemicals.

Tiltak besluttet av: Minadir Saracevic

Ansvarlig for gjennomføring: Minadir Saracevic

Frist for gjennomføring: 7/2/2019

Heat protective gloves

The heat protective gloves are used when handling hot equipment.

Tiltak besluttet av: Minadir Saracevic

Ansvarlig for gjennomføring: Minadir Saracevic

Frist for gjennomføring: 7/2/2019

Fire extinguisher

To prevent the fire from spreading and reduce the risk that the material oxides.

Tiltak besluttet av: Minadir Saracevic

Ansvarlig for gjennomføring: Minadir Saracevic

Frist for gjennomføring: 7/2/2019

Dust mask

Reduces risk of inhalation of particles when exposed to the materials used

Tiltak besluttet av: Minadir Saracevic

Ansvarlig for gjennomføring: Minadir Saracevic

Frist for gjennomføring: 7/2/2019

Detaljert oversikt over vurdert risiko for hver farekilde/uønsket hendelse før og etter besluttede tiltak

Farekilde: **Use of CoN2O6 · 6H2O**

Uønsket hendelse: **Oxidizing by fire**

Sannsynlighetsvurderinger (felles for alle konsekvensområder):

Opprinnelig sannsynlighet: Lite sannsynlig (2)

Begrunnelse: The event of a fire is not very likely, results in a low probability. But there are electrical equipment(drying process) which produce heat that may be a source of fire.

Sannsynlighet etter tiltak: Lite sannsynlig (2)

Begrunnelse:

Konsekvensvurderinger:

Konsekvensområde: **Helse** ***Risiko:***

Opprinnelig konsekvens: Stor (3)

Begrunnelse: Depending on the severity of the fire, burns may results in a long recovery time.

Konsekvens etter tiltak: Middels (2)

Begrunnelse: Less damage may be caused to the safety precautions.

Konsekvensområde: **Ytre miljø** ***Risiko:***

Opprinnelig konsekvens: Stor (3)

Begrunnelse: Fumes and damage resulting from the fire may lead to undesired gasses or liquids releasing into the environment.

Konsekvens etter tiltak: Middels (2)

Begrunnelse: Fire may be prevented

Konsekvensområde: **Materielle verdier** ***Risiko:***

Opprinnelig konsekvens: Stor (3)

Begrunnelse: The equipment after the fire may be permanently damaged but does not contain any life threatening chemicals which could have been released due the fire.

Konsekvens etter tiltak: Middels (2)

Begrunnelse: Fire may be prevented

Uønsket hendelse: **Spillage on skin**

Sannsynlighetsvurderinger (felles for alle konsekvensområder):

Opprinnelig sannsynlighet: Sannsynlig (3)

Begrunnelse: Spillage may occur when working with chemicals

Sannsynlighet etter tiltak: Sannsynlig (3)

Begrunnelse:

Konsekvensvurderinger:

Konsekvensområde: **Helse** ***Risiko:***

Opprinnelig konsekvens: Middels (2)

Begrunnelse: Skin contact with the material may result to skin irritation and allergic reaction

Konsekvens etter tiltak: Liten (1)

Begrunnelse: Lab coat and gloves prevent contact with the skin

Uønsket hendelse: **Splash into the eyes**

Sannsynlighetsvurderinger (felles for alle konsekvensområder):

Opprinnelig sannsynlighet: Lite sannsynlig (2)

Begrunnelse: The probability of getting chemicals into the eyes is not high due to no high pressures and the chemicals are stable during the synthesis.

Sannsynlighet etter tiltak: Lite sannsynlig (2)

Begrunnelse:

Konsekvensvurderinger:

Konsekvensområde: **Helse** ***Risiko:***

Opprinnelig konsekvens: Svært stor (4)

Begrunnelse: Acute toxicity in water and carcinogenic (may cause cancer) material may lead to high consequence if exposed to it.

Konsekvens etter tiltak: Middels (2)

Begrunnelse: Being protected by the fume hood and the safety gloves reduces the risk that there is chemical splash into the eyes.

Uønsket hendelse: **Inhalation to respiratory system and oral ingestion**

Sannsynlighetsvurderinger (felles for alle konsekvensområder):

Opprinnelig sannsynlighet: Lite sannsynlig (2)

Begrunnelse: The chemical is stable during normal conditions

Sannsynlighet etter tiltak: Lite sannsynlig (2)

Begrunnelse:

Konsekvensvurderinger:

Konsekvensområde: **Helse** ***Risiko:***

Opprinnelig konsekvens: Svært stor (4)

Begrunnelse: Acute toxicity in water and carcinogenic (may cause cancer) material may lead to high consequence if exposed to it.

Konsekvens etter tiltak: Middels (2)

Begrunnelse: Handling the chemicals in the fume hood and wearing safety equipment reduces the risk of the chemical exposure

Farekilde: Use of γ-Al2O3

Uønsket hendelse: Irritating to respiratory system and skin

Sannsynlighetsvurderinger (felles for alle konsekvensområder):

Opprinnelig sannsynlighet: Sannsynlig (3)

Begrunnelse: Due the material being fine, it may more easily be exposed

Sannsynlighet etter tiltak: Sannsynlig (3)

Begrunnelse:

Konsekvensvurderinger:

Konsekvensområde: Helse ***Risiko:***

Opprinnelig konsekvens: Liten (1)

Begrunnelse: Not classified as health hazardous and is not environmentally dangerous.

Konsekvens etter tiltak: Liten (1)

Begrunnelse: Not a dangerous chemical but still recommended to use the safety precautions to reduce risk of exposure.

Farekilde: Heated surfaces

Uønsket hendelse: Skin burns

Sannsynlighetsvurderinger (felles for alle konsekvensområder):

Opprinnelig sannsynlighet: Sannsynlig (3)

Begrunnelse: Handling hot equipment may lead to severe burns if not protected

Sannsynlighet etter tiltak: Lite sannsynlig (2)

Begrunnelse:

Konsekvensvurderinger:

Konsekvensområde: Helse ***Risiko:***

Opprinnelig konsekvens: Stor (3)

Begrunnelse: May lead to burns and chemical spill on the skin. Calcination reactor will be close to 750 °C at highest temperature point, which may cause severe burns if touched unprotected.

Konsekvens etter tiltak: Middels (2)

Begrunnelse: Using a lab coat decrease the exposure of the skin, reducing the area for burns

Farekilde: **NOx gas formation**

Uønsket hendelse: **Inhalation to respiratory system**

Sannsynlighetsvurderinger (felles for alle konsekvensområder):

Opprinnelig sannsynlighet: Sannsynlig (3)

Begrunnelse: There may be NOx formation(e.g during the calcination process), where the source is from the cobalt nitrate

Sannsynlighet etter tiltak: Sannsynlig (3)

Begrunnelse:

Konsekvensvurderinger:

Konsekvensområde: **Helse** ***Risiko:***

Opprinnelig konsekvens: Stor (3)

Begrunnelse: NOx gas is poisonous to inhale

Konsekvens etter tiltak: Liten (1)

Begrunnelse: NOx gas formation occurs in ventilated furnaces, reduces risk of exposure.

Konsekvensområde: **Ytre miljø** ***Risiko:***

Opprinnelig konsekvens: Middels (2)

Begrunnelse: No significant danger considering small amounts

Konsekvens etter tiltak: Liten (1)

Begrunnelse: NOx gas formation in ventilated furnaces.

Farekilde: **Use of Pt(IV)(NO3)4 solution, Pt 15% w/w**

Uønsket hendelse: **Oxidizing by fire**

Sannsynlighetsvurderinger (felles for alle konsekvensområder):

Opprinnelig sannsynlighet: Lite sannsynlig (2)

Begrunnelse: The event of a fire is not very likely, results in a low probability. But there are electrical equipment(drying process) which produce heat that may be a source of fire.

Sannsynlighet etter tiltak: Lite sannsynlig (2)

Begrunnelse:

Konsekvensvurderinger:

Konsekvensområde: **Helse** ***Risiko:***

Opprinnelig konsekvens: Stor (3)

Begrunnelse: Depending on the severity of the fire, burns may results in a long recovery time.

Konsekvens etter tiltak: Middels (2)

Begrunnelse: Layer of clothes over skin reduces the potential damage

Konsekvensområde: **Ytre miljø** ***Risiko:***

Opprinnelig konsekvens: Stor (3)

Begrunnelse: Fumes and damage resulting from the fire may lead to undesired gasses or liquids releasing into the environment.

Konsekvens etter tiltak: Middels (2)

Begrunnelse: Extinguishing the fire may reduce the potential to release gasses or liquids into the environment.

Konsekvensområde: **Materielle verdier** ***Risiko:***

Opprinnelig konsekvens: Stor (3)

Begrunnelse: The equipment after the fire may be permanently damaged but does not contain any life threatening chemicals which could have been released due the fire.

Konsekvens etter tiltak: Middels (2)

Begrunnelse: Less material damage can be a possibility if the fire is extinguished early.

Uønsket hendelse: **Splash into the eyes**

Sannsynlighetsvurderinger (felles for alle konsekvensområder):

Opprinnelig sannsynlighet: Lite sannsynlig (2)

Begrunnelse: The probability of getting chemicals into the eyes is not high due to no high pressures and the chemicals are stable during the synthesis.

Sannsynlighet etter tiltak: Lite sannsynlig (2)

Begrunnelse:

Konsekvensvurderinger:

Konsekvensområde: **Helse** ***Risiko:***

Opprinnelig konsekvens: Svært stor (4)

Begrunnelse: Since the chemical contains nitric acid, if solution is splashed into the eyes it may cause severe or permanent damage.

Konsekvens etter tiltak: Middels (2)

Begrunnelse:

Uønsket hendelse: **Oral ingestion**

Sannsynlighetsvurderinger (felles for alle konsekvensområder):

Opprinnelig sannsynlighet: Lite sannsynlig (2)

Begrunnelse: No high pressure and it is a stable liquid under the experimental conditions

Sannsynlighet etter tiltak: Lite sannsynlig (2)

Begrunnelse:

Konsekvensvurderinger:

Konsekvensområde: **Helse** ***Risiko:***

Opprinnelig konsekvens: Svært stor (4)

Begrunnelse: It is aquatic acute poisonous and acidic, which can lead to severe damage

Konsekvens etter tiltak: Middels (2)

Begrunnelse:

Farekilde: Characterization by XRD

Uønsket hendelse: Inhalation to respiratory system and oral ingestion during preparation

Sannsynlighetsvurderinger (felles for alle konsekvensområder):

Opprinnelig sannsynlighet: Lite sannsynlig (2)

Begrunnelse: The catalyst powder is stable during the preparation, no high pressure or heated surfaces are introduced during sample preparation.

Sannsynlighet etter tiltak: Lite sannsynlig (2)

Begrunnelse:

Konsekvensvurderinger:

Konsekvensområde: Helse ***Risiko:***

Opprinnelig konsekvens: Svært stor (4)

Begrunnelse: Acute toxicity in water and carcinogenic (may cause cancer) material may lead to high consequence if exposed to it.

Konsekvens etter tiltak: Middels (2)

Begrunnelse: Layer of protection and dust mask may results to lower consequence if event occurs

Uønsket hendelse: Spillage on the skin

Sannsynlighetsvurderinger (felles for alle konsekvensområder):

Opprinnelig sannsynlighet: Sannsynlig (3)

Begrunnelse: Spillage may occur when working preparing the sample holder with the catalyst. Steady hands are required to not spill any sample. Thus, the probability of spilling may be higher.

Sannsynlighet etter tiltak: Sannsynlig (3)

Begrunnelse:

Konsekvensvurderinger:

Konsekvensområde: Helse ***Risiko:***

Opprinnelig konsekvens: Middels (2)

Begrunnelse: Skin contact with the material may result to skin irritation and allergic reaction

Konsekvens etter tiltak: Liten (1)

Begrunnelse: Layer of protection may results to lower consequence if event occurs

Uønsket hendelse: **Chemical exposure into the eyes**

Sannsynlighetsvurderinger (felles for alle konsekvensområder):

Opprinnelig sannsynlighet: Lite sannsynlig (2)

Begrunnelse: The probability of getting chemicals into the eyes is not high due to no high pressures and the chemicals are stable during the preparation.

Sannsynlighet etter tiltak: Lite sannsynlig (2)

Begrunnelse:

Konsekvensvurderinger:

Konsekvensområde: **Helse** ***Risiko:***

Opprinnelig konsekvens: Svært stor (4)

Begrunnelse: Acute toxicity in water and carcinogenic (may cause cancer) material may lead to high consequence if exposed to it.

Konsekvens etter tiltak: Middels (2)

Begrunnelse: Layer of protection may results to lower consequence if event occurs

Farekilde: **Characterization by XRF**

Uønsket hendelse: **Spillage on the skin**

Sannsynlighetsvurderinger (felles for alle konsekvensområder):

Opprinnelig sannsynlighet: Sannsynlig (3)

Begrunnelse: Can spill powder on the skin when making the pellets for the XRF unit

Sannsynlighet etter tiltak: Sannsynlig (3)

Begrunnelse:

Konsekvensvurderinger:

Konsekvensområde: **Helse** ***Risiko:***

Opprinnelig konsekvens: Stor (3)

Begrunnelse: Due to the catalyst and boric acid, may get skin irritation

Konsekvens etter tiltak: Liten (1)

Begrunnelse: Layer of protection may results to lower consequence if event occurs

Uønsket hendelse: Chemical exposure into the eyes

Sannsynlighetsvurderinger (felles for alle konsekvensområder):

Opprinnelig sannsynlighet: Lite sannsynlig (2)

Begrunnelse: The chemicals are stable during the making of the pellets

Sannsynlighet etter tiltak: Lite sannsynlig (2)

Begrunnelse:

Konsekvensvurderinger:

Konsekvensområde: Helse ***Risiko:***

Opprinnelig konsekvens: Svært stor (4)

Begrunnelse: The catalyst is carcinogenic (may cause cancer), which may lead to permanent effects

Konsekvens etter tiltak: Middels (2)

Begrunnelse: Safety googles reduces the risk of exposure.

Uønsket hendelse: Inhalation to respiratory system and oral ingestion during preparation

Sannsynlighetsvurderinger (felles for alle konsekvensområder):

Opprinnelig sannsynlighet: Lite sannsynlig (2)

Begrunnelse: The chemicals are stable during the making of the pellets

Sannsynlighet etter tiltak: Lite sannsynlig (2)

Begrunnelse:

Konsekvensvurderinger:

Konsekvensområde: Helse ***Risiko:***

Opprinnelig konsekvens: Svært stor (4)

Begrunnelse: The catalysts is a carcinogenic (may cause cancer) material, may lead to high consequence if exposed to it.

Konsekvens etter tiltak: Middels (2)

Begrunnelse: Layer of protection and dust mask may results to lower consequence if event occurs

Farekilde: Use of boric acid (H3BO3)

Uønsket hendelse: Spillage on skin

Sannsynlighetsvurderinger (felles for alle konsekvensområder):

Opprinnelig sannsynlighet: Sannsynlig (3)

Begrunnelse:

Sannsynlighet etter tiltak: Sannsynlig (3)

Begrunnelse:

Konsekvensvurderinger:

Konsekvensområde: Helse ***Risiko:***

Opprinnelig konsekvens: Stor (3)

Begrunnelse:

Konsekvens etter tiltak: Liten (1)

Begrunnelse: With lab coat and gloves, the consequence are minimized.

Uønsket hendelse: Chemical exposure into the eyes

Sannsynlighetsvurderinger (felles for alle konsekvensområder):

Opprinnelig sannsynlighet: Sannsynlig (3)

Begrunnelse: The pressure added when the samples is pressed may lead to exposure, but has a glass front to avoid sudden exposure if leaked. The chemical is stable during the preparation.

Sannsynlighet etter tiltak: Sannsynlig (3)

Begrunnelse:

Konsekvensvurderinger:

Konsekvensområde: Helse ***Risiko:***

Opprinnelig konsekvens: Stor (3)

Begrunnelse:

Konsekvens etter tiltak: Liten (1)

Begrunnelse: Fume hood and safety googles reduces the consequence if spillage occurs.

Uønsket hendelse: **Inhalation to respiratory system and oral ingestion during preparation**

Sannsynlighetsvurderinger (felles for alle konsekvensområder):

Opprinnelig sannsynlighet: Lite sannsynlig (2)

Begrunnelse: The catalyst powder is stable during the preparation. The pressure added when the samples is pressed may lead to exposure, but has a glass front to avoid sudden exposure if leaked.

Sannsynlighet etter tiltak: Lite sannsynlig (2)

Begrunnelse:

Konsekvensvurderinger:

Konsekvensområde: **Helse** ***Risiko:***

Opprinnelig konsekvens: Svært stor (4)

Begrunnelse: May damage the reproductive capacity and may cause birth defects.

Konsekvens etter tiltak: Middels (2)

Begrunnelse: Protective layers and dust mask reduces the risk of exposure.

Farekilde: **Characterization by chemisorption and TPR**

Uønsket hendelse: **Spillage on skin**

Sannsynlighetsvurderinger (felles for alle konsekvensområder):

Opprinnelig sannsynlighet: Lite sannsynlig (2)

Begrunnelse: Can spill powder on the skin when preparing the U-tube reactor

Sannsynlighet etter tiltak: Lite sannsynlig (2)

Begrunnelse:

Konsekvensvurderinger:

Konsekvensområde: **Helse** ***Risiko:***

Opprinnelig konsekvens: Middels (2)

Begrunnelse: Skin contact with the material may result to skin irritation and allergic reaction

Konsekvens etter tiltak: Middels (2)

Begrunnelse:

Uønsket hendelse: **Chemical exposure into the eyes**

Sannsynlighetsvurderinger (felles for alle konsekvensområder):

Opprinnelig sannsynlighet: Lite sannsynlig (2)

Begrunnelse: The probability of getting chemicals into the eyes is not high due to no high pressures and the chemicals are stable during the preparation.

Sannsynlighet etter tiltak: Lite sannsynlig (2)

Begrunnelse:

Konsekvensvurderinger:

Konsekvensområde: **Helse** ***Risiko:***

Opprinnelig konsekvens: Svært stor (4)

Begrunnelse: Acute toxicity in water and carcinogenic (may cause cancer) material may lead to high consequence if exposed to it.

Konsekvens etter tiltak: Middels (2)

Begrunnelse: Layer of protection may results to lower consequence if event occurs

Uønsket hendelse: **Inhalation to respiratory system and oral ingestion during preparation**

Sannsynlighetsvurderinger (felles for alle konsekvensområder):

Opprinnelig sannsynlighet: Lite sannsynlig (2)

Begrunnelse: The catalyst powder is stable during the preparation, no high pressure or heated surfaces are introduced during sample preparation.

Sannsynlighet etter tiltak: Lite sannsynlig (2)

Begrunnelse:

Konsekvensvurderinger:

Konsekvensområde: **Helse** ***Risiko:***

Opprinnelig konsekvens: Svært stor (4)

Begrunnelse: Acute toxicity in water and carcinogenic (may cause cancer) material may lead to high consequence if exposed to it.

Konsekvens etter tiltak: Middels (2)

Begrunnelse: Layer of protection may results to lower consequence if event occurs

Farekilde: Use of H2

Uønsket hendelse: Leaks and explosion

Sannsynlighetsvurderinger (felles for alle konsekvensområder):

Opprinnelig sannsynlighet: Lite sannsynlig (2)

Begrunnelse: Possible leaks may occur due to faulty installation of valves, but the bottles are placed where they are not exposed to heat.

Sannsynlighet etter tiltak: Lite sannsynlig (2)

Begrunnelse:

Konsekvensvurderinger:

Konsekvensområde: Helse ***Risiko:***

Opprinnelig konsekvens: Svært stor (4)

Begrunnelse: In case of explosion and fires, severe burns and permanent damage may be a possibility

Konsekvens etter tiltak: Middels (2)

Begrunnelse: Layer of protection may results to lower consequence if event occurs

Konsekvensområde: Ytre miljø ***Risiko:***

Opprinnelig konsekvens: Stor (3)

Begrunnelse: Fire may lead to undesired gasses or liquids releasing into the environment.

Konsekvens etter tiltak: Middels (2)

Begrunnelse: Layer of protection and fire extinguisher may results to lower consequence if event occurs

Konsekvensområde: Materielle verdier ***Risiko:***

Opprinnelig konsekvens: Svært stor (4)

Begrunnelse: High material damage if explosion and fire occurs

Konsekvens etter tiltak: Middels (2)

Begrunnelse: Fire extinguisher may contribute to reduce the damage caused by the fire

Farekilde: **Use of NO**

Uønsket hendelse: **Explosion**

Sannsynlighetsvurderinger (felles for alle konsekvensområder):

Opprinnelig sannsynlighet: Lite sannsynlig (2)

Begrunnelse: The gas is under pressure, may explode if the bottle is exposed to heat

Sannsynlighet etter tiltak: Lite sannsynlig (2)

Begrunnelse:

Konsekvensvurderinger:

Konsekvensområde: **Helse** ***Risiko:***

Opprinnelig konsekvens: Svært stor (4)

Begrunnelse: Acute poisonous if exposed to respiratory system and chemical burns to skin and eyes

Konsekvens etter tiltak: Middels (2)

Begrunnelse: Layer of protection may results to lower consequence if event occurs

Konsekvensområde: **Ytre miljø** ***Risiko:***

Opprinnelig konsekvens: Svært stor (4)

Begrunnelse: Poisonous gas and may react with exposed to other gases

Konsekvens etter tiltak: Middels (2)

Begrunnelse: Layer of protection may results to lower consequence if event occurs

Konsekvensområde: **Materielle verdier** ***Risiko:***

Opprinnelig konsekvens: Svært stor (4)

Begrunnelse: May lead to large material damage if the high pressure bottle explode

Konsekvens etter tiltak: Middels (2)

Begrunnelse: Layer of protection may results to lower consequence if event occurs

Uønsket hendelse: **Inhalation to respiratory system**

Sannsynlighetsvurderinger (felles for alle konsekvensområder):

Opprinnelig sannsynlighet: Lite sannsynlig (2)

Begrunnelse: Gas is used from a bottle to send the gas to a reactor, low probability if all valves and pipes have been leaked proofed.

Sannsynlighet etter tiltak: Lite sannsynlig (2)

Begrunnelse:

Konsekvensvurderinger:

Konsekvensområde: **Helse** ***Risiko:***

Opprinnelig konsekvens: Svært stor (4)

Begrunnelse: Acute poisonous if it the gas is inhaled

Konsekvens etter tiltak: Middels (2)

Begrunnelse: Sensors placed in the chemical rig detects small ppm levels of leaked gasses and the lines are leak proofed before usage.

Uønsket hendelse: **Chemical burns on the skin and eyes**

Sannsynlighetsvurderinger (felles for alle konsekvensområder):

Opprinnelig sannsynlighet: Lite sannsynlig (2)

Begrunnelse: Gas is used from a bottle to send the gas to a reactor, low probability if all valves and pipes have been leaked proofed.

Sannsynlighet etter tiltak: Lite sannsynlig (2)

Begrunnelse:

Konsekvensvurderinger:

Konsekvensområde: **Helse** ***Risiko:***

Opprinnelig konsekvens: Svært stor (4)

Begrunnelse: May lead to chemical burn on the skin and eyes

Konsekvens etter tiltak: Middels (2)

Begrunnelse: Layer of protection may results to lower consequence if event occurs

Farekilde: **Use of argon (Ar)**

Uønsket hendelse: **Explosion**

Sannsynlighetsvurderinger (felles for alle konsekvensområder):

Opprinnelig sannsynlighet: Lite sannsynlig (2)

Begrunnelse: The high pressure bottle is not exposed to heat, hence the low probability

Sannsynlighet etter tiltak: Lite sannsynlig (2)

Begrunnelse:

Konsekvensvurderinger:

Konsekvensområde: **Helse** ***Risiko:***

Opprinnelig konsekvens: Stor (3)

Begrunnelse: The explosion of the bottle may lead to cuts, hearing loss etc.

Konsekvens etter tiltak: Middels (2)

Begrunnelse: Layer of protection may results to lower consequence if event occurs

Konsekvensområde: **Ytre miljø** ***Risiko:***

Opprinnelig konsekvens: Middels (2)

Begrunnelse: The gas itself is inert and do not posses a high risk

Konsekvens etter tiltak: Middels (2)

Begrunnelse:

Konsekvensområde: **Materielle verdier** ***Risiko:***

Opprinnelig konsekvens: Svært stor (4)

Begrunnelse: The explosion may lead to material damage of equipment etc.

Konsekvens etter tiltak: Middels (2)

Begrunnelse: Layer of protection may results to lower consequence if event occurs

Farekilde: **Activity measurement of catalyst**

Uønsket hendelse: **Spillage on skin**

Sannsynlighetsvurderinger (felles for alle konsekvensområder):

Opprinnelig sannsynlighet: Lite sannsynlig (2)

Begrunnelse: Can spill the catalyst powder on the skin when preparing the packed bed reactor

Sannsynlighet etter tiltak: Lite sannsynlig (2)

Begrunnelse:

Konsekvensvurderinger:

Konsekvensområde: **Helse** ***Risiko:***

Opprinnelig konsekvens: Middels (2)

Begrunnelse: Skin contact with the material may result to skin irritation and allergic reaction

Konsekvens etter tiltak: Middels (2)

Begrunnelse:

Uønsket hendelse: **Inhalation to respiratory system and oral ingestion during preparation**

Sannsynlighetsvurderinger (felles for alle konsekvensområder):

Opprinnelig sannsynlighet: Lite sannsynlig (2)

Begrunnelse: The catalyst powder is stable during the preparation, no high pressure or heated surfaces are introduced during sample preparation.

Sannsynlighet etter tiltak: Lite sannsynlig (2)

Begrunnelse:

Konsekvensvurderinger:

Konsekvensområde: **Helse** ***Risiko:***

Opprinnelig konsekvens: Svært stor (4)

Begrunnelse: Acute toxicity in water and carcinogenic (may cause cancer) material may lead to high consequence if exposed to it.

Konsekvens etter tiltak: Middels (2)

Begrunnelse: Layer of protection may results to lower consequence if event occurs

Uønsket hendelse: Heated surfaces

Sannsynlighetsvurderinger (felles for alle konsekvensområder):

Opprinnelig sannsynlighet: Sannsynlig (3)

Begrunnelse: Handling hot equipment may lead to severe burns if not protected

Sannsynlighet etter tiltak: Sannsynlig (3)

Begrunnelse:

Konsekvensvurderinger:

Konsekvensområde: Helse ***Risiko:***

Opprinnelig konsekvens: Stor (3)

Begrunnelse: May lead to burns. Reactor will be close to 500 °C at highest temperature point, which may cause severe burns if touched unprotected.

Konsekvens etter tiltak: Liten (1)

Begrunnelse: Heat protective gloves and lab coat reduces risk of skin exposure to heated surfaces

Uønsket hendelse: Gas leaks

Sannsynlighetsvurderinger (felles for alle konsekvensområder):

Opprinnelig sannsynlighet: Lite sannsynlig (2)

Begrunnelse: The gases may leak in the valves and fittings, but are leak proofed before running an experiment and are in a closed cabinet.

Sannsynlighet etter tiltak: Lite sannsynlig (2)

Begrunnelse:

Konsekvensvurderinger:

Konsekvensområde: Helse ***Risiko:***

Opprinnelig konsekvens: Svært stor (4)

Begrunnelse: The gas is poisonous if inhaled and chemical burn on skin and eyes

Konsekvens etter tiltak: Middels (2)

Begrunnelse: Layer of protection may results to lower consequence if event occurs

Konsekvensområde: **Ytre miljø** ***Risiko:***

Opprinnelig konsekvens: Svært stor (4)

Begrunnelse: May react with other components to form unwanted products (e.g smog)

Konsekvens etter tiltak: Middels (2)

Begrunnelse: Sensor and ventilated spaces reduces risk of exposure.

Uønsket hendelse: **Explosion**

Sannsynlighetsvurderinger (felles for alle konsekvensområder):

Opprinnelig sannsynlighet: Lite sannsynlig (2)

Begrunnelse: The bottles are isolated from the rig and is not close to a heat source

Sannsynlighet etter tiltak: Lite sannsynlig (2)

Begrunnelse:

Konsekvensvurderinger:

Konsekvensområde: **Helse** ***Risiko:***

Opprinnelig konsekvens: Svært stor (4)

Begrunnelse: NO poisonous gas if exposed, explosion may lead to cuts, burn etc

Konsekvens etter tiltak: Middels (2)

Begrunnelse: Layer of protection may results to lower consequence if event occurs

Konsekvensområde: **Ytre miljø** ***Risiko:***

Opprinnelig konsekvens: Svært stor (4)

Begrunnelse: NO may react with other components (e.g smog)

Konsekvens etter tiltak: Middels (2)

Begrunnelse: Sensor and ventilated spaces reduces risk of exposure.

Konsekvensområde: **Materielle verdier** ***Risiko:***

Opprinnelig konsekvens: Svært stor (4)

Begrunnelse: The explosion may damage the equipment permanently

Konsekvens etter tiltak: Middels (2)

Begrunnelse: Layer of protection and fire extinguisher may results to lower consequence if event occurs

Farekilde: **Use of O2**

Uønsket hendelse: **Explosion**

Sannsynlighetsvurderinger (felles for alle konsekvensområder):

Opprinnelig sannsynlighet: Lite sannsynlig (2)

Begrunnelse: The bottle is not near a heat source, unlikely to explode due to heat exposure

Sannsynlighet etter tiltak: Lite sannsynlig (2)

Begrunnelse:

Konsekvensvurderinger:

Konsekvensområde: **Helse** ***Risiko:***

Opprinnelig konsekvens: Stor (3)

Begrunnelse: The oxygen may help to oxidize other gases if a fire erupts, leading to severe burns

Konsekvens etter tiltak: Middels (2)

Begrunnelse: Layer of protection may results to lower consequence if event occurs

Konsekvensområde: **Ytre miljø** ***Risiko:***

Opprinnelig konsekvens: Stor (3)

Begrunnelse: The gas has no significant consequences, but may help to contribute to oxidize other gases

Konsekvens etter tiltak: Middels (2)

Begrunnelse: Layer of protection and fire extinguisher may results to lower consequence if event occurs

Konsekvensområde: **Materielle verdier** ***Risiko:***

Opprinnelig konsekvens: Svært stor (4)

Begrunnelse: Permanent material damage may be expected due to bottle explosion or as a fire contributor

Konsekvens etter tiltak: Middels (2)

Begrunnelse: Fire extinguisher may contribute to reduce damage due to fires.

Farekilde: **Use of TiO2**

Uønsket hendelse: **Irritating to respiratory system, skin and eyes**

Sannsynlighetsvurderinger (felles for alle konsekvensområder):

Opprinnelig sannsynlighet: Lite sannsynlig (2)

Begrunnelse: Pellet form and contains binder chemical, powder stable

Sannsynlighet etter tiltak: Lite sannsynlig (2)

Begrunnelse: Less likely to inhale small dust particles

Konsekvensvurderinger:

Konsekvensområde: **Helse** ***Risiko:***

Opprinnelig konsekvens: Stor (3)

Begrunnelse: The material is suspected of causing cancer

Konsekvens etter tiltak: Middels (2)

Begrunnelse: Material is quite stable under handling. In case spill happens, protective layers prevent inhalation and external contact with the material

Farekilde: Use of CeO2

Uønsket hendelse: Irritating to respiratory system, skin and eyes

Sannsynlighetsvurderinger (felles for alle konsekvensområder):

Opprinnelig sannsynlighet: Sannsynlig (3)

Begrunnelse: Due the material being fine, it may more easily be exposed

Sannsynlighet etter tiltak: Sannsynlig (3)

Begrunnelse:

Konsekvensvurderinger:

Konsekvensområde: Helse ***Risiko:***

Opprinnelig konsekvens: Stor (3)

Begrunnelse: Not classified as health hazardous by inhalation, skin contact or spillage into eyes but should be avoided

Konsekvens etter tiltak: Liten (1)

Begrunnelse: Not classified as health hazardous

Uønsket hendelse: Oral ingestion

Sannsynlighetsvurderinger (felles for alle konsekvensområder):

Opprinnelig sannsynlighet: Lite sannsynlig (2)

Begrunnelse: The fine powder is stable under synthesis, but being fine powder may spread if dropped

Sannsynlighet etter tiltak: Lite sannsynlig (2)

Begrunnelse:

Konsekvensvurderinger:

Konsekvensområde: Helse ***Risiko:***

Opprinnelig konsekvens: Stor (3)

Begrunnelse: Classified as toxic by oral ingestion

Konsekvens etter tiltak: Middels (2)

Begrunnelse: The protective layers will prevent oral ingestion if spillage occurs

Farekilde: Use of SiO2

Uønsket hendelse: Inhalation to respiratory system

Sannsynlighetsvurderinger (felles for alle konsekvensområder):

Opprinnelig sannsynlighet: Sannsynlig (3)

Begrunnelse: In dry powder form, risk of breathing dust

Sannsynlighet etter tiltak: Svært lite sannsynlig (1)

Begrunnelse: Small risk of exposure when using a mask and/or fume hood

Konsekvensvurderinger:

Konsekvensområde: Helse ***Risiko:***

Opprinnelig konsekvens: Stor (3)

Begrunnelse: May cause damage to organs through prolonged or repeated exposure

Konsekvens etter tiltak: Middels (2)

Begrunnelse: Having protective gear reduces the risk of consequence if the dust is in the air

Farekilde: Use of ZrO2

Uønsket hendelse: Inhalation to respiratory system

Sannsynlighetsvurderinger (felles for alle konsekvensområder):

Opprinnelig sannsynlighet: Sannsynlig (3)

Begrunnelse: Dry powder, may breathe in the dust.

Sannsynlighet etter tiltak: Svært lite sannsynlig (1)

Begrunnelse: Small risk of exposure when using a mask and/or fume hood

Konsekvensvurderinger:

Konsekvensområde: Helse ***Risiko:***

Opprinnelig konsekvens: Liten (1)

Begrunnelse: Classified as non-hazardous material

Konsekvens etter tiltak: Middels (2)

Begrunnelse: Having protective gear reduces the risk of consequence if the dust is in the air

Minadir Saracevic

NO to NO2 oxidation over Supported Cobalt Oxides Catalysts

NTNU
Norwegian University of
Science and Technology